Investigating the Link between Southern African Droughts and Global Atmospheric Teleconnections using Regional Climate Models

Arlindo Oliva Meque

Thesis Presented for the Degree of

DOCTOR OF PHILOSOPHY
In the Department of Environmental and Geographical Science

University of Cape Town

Supervisor: Dr Babatunde J. Abiodun

September 2015

Declaration I

I know the meaning of plagiarism and declare that all the work in the thesis, except for that which is properly acknowledged, is my own.

Signed by candidate

Signature Removed

_____

Arlindo Oliva Meque

Declaration II

Parts of this thesis have been published. The text of this thesis includes material from the paper entitled “Simulating the Link between ENSO and Summer Drought in Southern Africa using Regional Climate Models", Published in the Climate Dynamics Journal. The co-author of the manuscript publication directed and supervised the research that forms the basis for the thesis.

Abstract

Drought is one of the natural hazards that threaten the economy of many nations, especially in Southern Africa, where many socio-economic activities depend on rain-fed agriculture. This study evaluates the capability of Regional Climate Models (RCMs) in simulating the Southern African droughts. It uses the Standardized Precipitation-Evapotranspiration Index (SPEI, computed using rainfall and temperature data) to identify 3-month droughts over Southern Africa, and compares the observed and simulated drought patterns. The observation data are from the Climate Research Unit (CRU), while the simulation data are from 10 RCMs (ARPEGE, CCLM, HIRHAM, RACMO, REMO, PRECIS, RegCM3, RCA, WRF, and CRCM) that participated in the Regional Climate Downscaling Experiment (CORDEX) project. The study also categorizes drought patterns over Southern Africa, examines the persistence and transition of these patterns, and investigates the roles of atmospheric teleconnections on the drought patterns.

The results show that the drought patterns can occur in any season, but they have preference for seasons. Some droughts patterns may persist up to three seasons, while others are transient. Only about 20% of the droughts patterns are induced solely by El Niño Southern Oscillation (ENSO), other drought patterns are caused by complex interactions among the atmospheric teleconnections. The study also reveals that the Southern Africa drought pattern is generally shifting from a wet condition to a dry condition, and that the shifting can only be captured with a drought monitoring index that accounts for temperature influence on drought. Only few CORDEX RCMs simulate the Southern African droughts as observed. In this regard, the ARPEGE model shows the best simulation. The best performance may be because the stretching capability of ARPEGE helps the model to eliminate boundary condition problems, which are present in other RCMs. In ARPEGE simulations, the stretching capability would allow a better interaction between large and small scale features, and may lead to a better representation of the rain producing systems in Southern Africa. The results of the study may be applied to improve monitoring and prediction of regionally-extensive drought over Southern Africa, and to reduce the socio-economic impacts of drought in the region.

Acknowledgements

There are many people who made this journey possible. First, I would like to thank my supervisor Dr Babatunde J. Abiodun, for his support and guidance during the course of these four years. I found in him a friend, older brother, and a role model in every aspects of life.

I am very thankful to Professor Bruce Hewitson, the Director of the Climate System Analysis Group (CSAG), for creating an environment suitable for research. Despite his busy schedule, Professor Hewitson is always approachable and ready to help students with their needs. I also thank him for hosting me as a Visiting Scientist prior to the commencement of my PhD program, to be familiar to CSAG environment and culture before embarking on the hard task of PhD thesis.

I would like to extend my gratitude to the Mozambican Government for allowing me to come to South Africa on a study leave. I thank the Applied Centre for Climate and Earth Systems Science (ACCESS), the Southern African Development Community (SADC) Climate Services Centre and the Mozambican Ministry of Science and Technology for the financial support. I thank the Centre for High Performance Computing (CHPC) in Cape Town for the computational resources.

I would like to acknowledge the UK Met Office and the UK Department for International Development (DFID) for the support through the fellowship scheme of the Climate Science Research Partnership (CSRP). My special thanks to my mentors in the project, namely, Mark Tadross, Alberto Arribas, Andrew Colman, Richard Graham and Michael Vellinga. The CSRP project allowed my interaction with several scientists around the World and created the foundations of the present work.

I sincerely thank all the staff members and students from the Department of Environmental and Geographical Science (EGS) for their cordiality and collaborative spirit, more especially to my officemates (Lawal, Sabina, Sarah, Teboho, Nkulumo,Tich and Zakky) for the jokes and lively debates on a wide range of topics. I am very grateful to Phillip Mukwenha for his invaluable help on several computer glitches I faced during this long journey.

I am most appreciative to the Mozambican friends and all other friends I made during my stay in Cape Town, for their support and lots of fun we had. This made me forget the pain of being away from home.

I am deeply grateful to my parents Oliva and Marieta, for their unconditional love and for their early understanding of the value of Education. I thank also my nephews for renewing my joy of being alive. I am much indebted to my Fiancée, Rumbidzayi Machiridza, for her presence and support during my darkest moments. When everything seemed to fall apart she uplifted me with her unshaken faith.

I Thank the Almighty God for being always by my side and for doing exceedingly, abundantly, above and beyond all I ask for.

Dedication

To my Parents:

Oliva and Marieta

Table of Contents

List of Figures

List of Tables

List of Abbreviations

AAO Antarctic Oscillation

CMIP5 Coupled Model Intercomparison Project Phase 5

CORDEX Coordinated Regional Climate Downscaling Experiment

DMI Dipole Mode Index

ENSO El Niño Southern Oscillation

EOF Empirical Orthogonal Functions

GCM Global Climate Model

IOD Indian Ocean Dipole

MEI Multivariate ENSO Index

ONI Ocean Niño Index

PCA Principal Component Analysis

PDSI Palmer Drought Severity Index

PET Potential Evapotranspiration

RCM Regional Climate Model

SAM Southern Annular Mode

SASD South Atlantic Subtropical Dipole

SIOD Subtropical Indian Ocean Dipole

SOMs Self Organizing Maps

SPEI Standardized Precipitation-Evapotranspiration Index

SPI Standardized Precipitation Index

WMO World Meteorological Organization

1 : Introduction

1.1 What is Drought?

Drought, a very popular concept among Governments around the world including the laypeople, has no universal scientific definition (Benages, 2014). As a result of this, more than 150 definitions concerning drought hazard can be found in the literature (Boken et al., 2005). For instance, the Intergovernmental Panel on Climate Change (IPCC, 2007) defines drought as "a prolonged absence or marked deficiency of precipitation", a "deficiency of precipitation that results in water shortage for some activity or for some group", or a "period of abnormally dry weather sufficiently prolonged for the lack of precipitation to cause a serious hydrological imbalance". On the other hand, the encyclopaedia of World Climatology (Oliver, 2005) defines drought as an "insidious natural hazard that results from a deficiency of precipitation from expected or normal that, when extended over a season or longer period of time, is insufficient to meet the demands of human activities". From these two definitions one can conclude that the deficiency of precipitation is the root cause of any drought event. However, different flavours of drought definitions are found in the literature because drought is a relative concept. Different stakeholders have different perceptions of drought (Rossi et al. 2007). For example, there is no agreed threshold of precipitation by which all the stakeholders can declare onset of drought (Botterill and Cockfield, 2013). Therefore, what might be considered as drought episode in one region, can represent normal conditions in a different region or even to a different group of people in the same region. For example, a water management practitioner notices a drought event when water levels in the reservoir or river start to decrease, whereas for a farmer a drought can be a concern when plants start to wither. For this reason, any drought definition must always incorporate its impact on the society (Rossi et al., 2007).

However, drought is different from aridity. Drought is in general any abnormal and ephemeral situation, in which rainfall is below normal conditions, whereas aridity is more of a perennial situation, i.e., there is always a deficit in precipitation (Wilhite, 2005; Lake, 2011). In arid regions, the net balance between precipitation and potential evapotranspiration is negative, the insolation is strong and temperatures are high (Mainguet, 1999).

1.2 Types of Drought

Droughts can be clustered into four main types: meteorological drought, agricultural drought, hydrological drought and socio-economical drought. The latter three types of drought result as a consequence of a prolonged meteorological drought and are defined according to their impacts on society (Lake, 2011). As shown in Fig.1.1, droughts start with precipitation deficit accompanied by high temperatures, strong winds and less cloud cover. If this situation prevails, it may lead to agricultural drought and eventually to hydrological drought.

1.2.1 Meteorological Drought

The meteorological drought is characterized by a deficiency of precipitation (including snow fall) for a long period of time such as a season or a year (Lake, 2011). This definition can vary from region to region according to stakeholder's need or application and, to the drought triggers (WMO, 2006). Moreover, different regions have different rainfall characteristics. For example, 100 millimetres of precipitation in a semi-arid region of Namibia does not have the same effect as in northern Mozambique. The atmospheric conditions that bring about dry conditions in these two regions are completely different.

1.2.2 Agricultural Drought

The Agricultural drought occurs when the available soil moisture is not enough to sustain the crops and forage (Wilhite, 2005). As a result, there is a decrease in agricultural productivity. This type of drought is also associated with losses in livestock production due to the reduction in grazing. The crop failure and reduction in livestock lead to other negative impacts such as famine and malnutrition (Rojas et al., 2011).

1.2.3 Hydrological Drought

This type of drought is said to occur when there's a lack in surface and subsurface waters (Wilhite, 2005). The hydrological drought affects the hydropower sector with power outages, load shedding and problems in dam operations (Calzi, 2013). Other sectors of activity such as

transportation and irrigation are also affected due to a dwindling stream flow. The scarcity of water affects the domestic and industrial water supply processes, which may in turn lead to outbreak of water-borne diseases such as cholera, diarrhoea and tuberculosis (Jain et al., 2007). The hydrological drought can also inflict damages on tourism due to less recreation and it has also impact on the environment due to the stress of many endangered species (UNSDIR, 2009).

1.2.4 Socio-economical Drought

The socio-economical drought happens when the above drought types start affecting on the economy of a nation or region, mainly due to the imbalance between supply and demand of goods (Wilhite, 2005). This may lead to economic inflation and to the crippling of many household's income. When the economy collapses other factors such as poverty, riots and war can take place (Boken et al., 2005). Due to the water scarcity, the electricity tariffs are raised in order to offset the high cost of its production. Additional impacts of drought includes staff turnover in the industries through the migration of people.

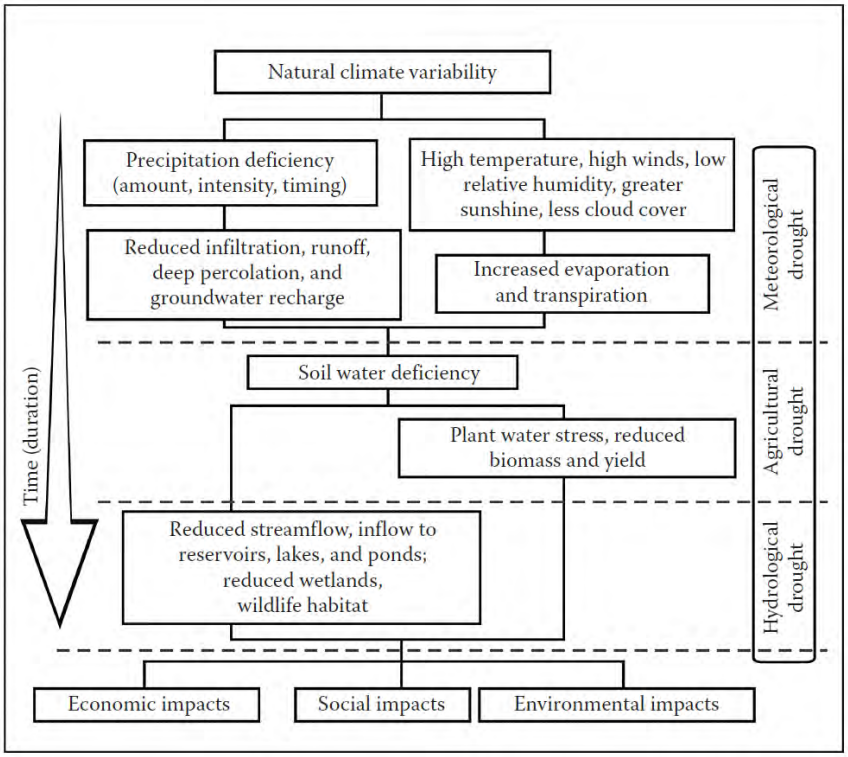

Figure 1.1: Different types of drought and their associated impacts. Source: Wardlow et al. (2012).

1.3 Drought characteristics

Describing the characteristics of drought is not a straightforward process. Unlike other natural hazards (e.g., tropical cyclones), it is challenging to notice the commencement of a drought event and more often a drought event is declared when its impacts are already taking place. Furthermore, drought characteristics can vary depending on the type of drought and the intended application (Sheffield and Wood, 2011). However, there are four important and common drought characteristics:

- Drought Duration (L): refers to the number of consecutive months (or weeks) in which the precipitation (or soil moisture or runoff) is below the chosen threshold (Andreadis et al., 2005). The duration is highly dependent on the chosen threshold for the declaration of the start and end of the drought episode.
- Drought magnitude (M): it is the deficit below the threshold. It measures the cumulative precipitation deficit during the drought event (Santos, 2011).
- Drought intensity (I): is the ratio between M and L, i.e., magnitude divided by the duration of the drought event.
- Drought Severity (S): refers to either the value of precipitation (or any other drought indicator) at a given month during the drought event or the minimum of precipitation during the event (Thompson 1999; Vidal et al., 2010).

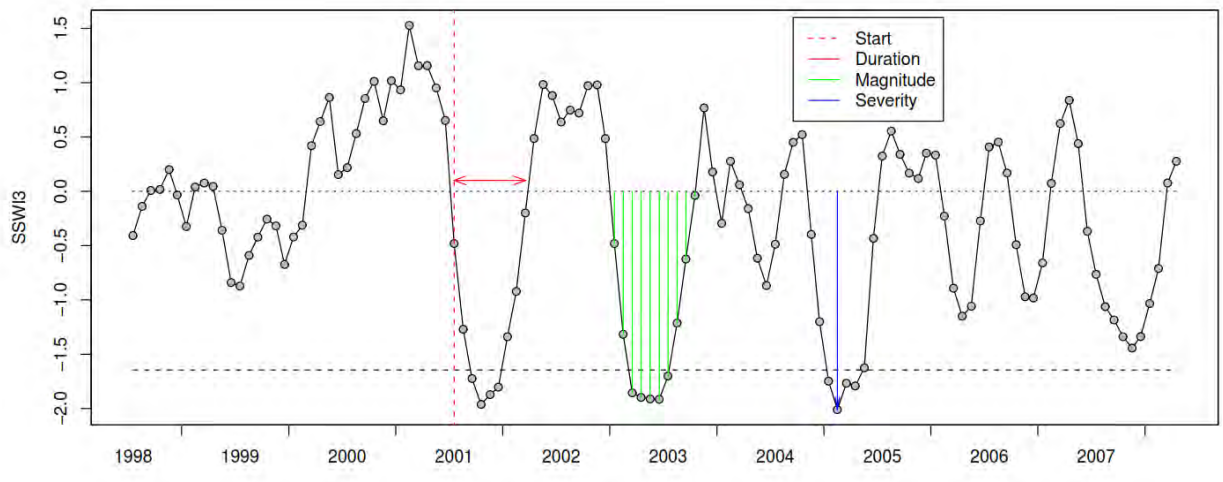

Figure 1.2: Drought characteristics. Source: Vidal et al. (2010).

1.4 Impacts of droughts in Southern Africa

Droughts are a recurrent phenomenon in most of the Southern African countries. The most drought prone countries in the region are Zimbabwe and Mozambique, where more than 10 drought events have been recorded during the 1970-2004 period (Fig.1.3). During the 1980-2000 period, four severe droughts (1982/83, 1987/88, 1991/92 and 1994/95) impacted the region (FAO, 2004). The two worst droughts in the region were reported in 1982/83 and 1991/92 rainy seasons. These two droughts threatened the livelihoods of rural people who have the rain-fed agriculture as their main source of income.

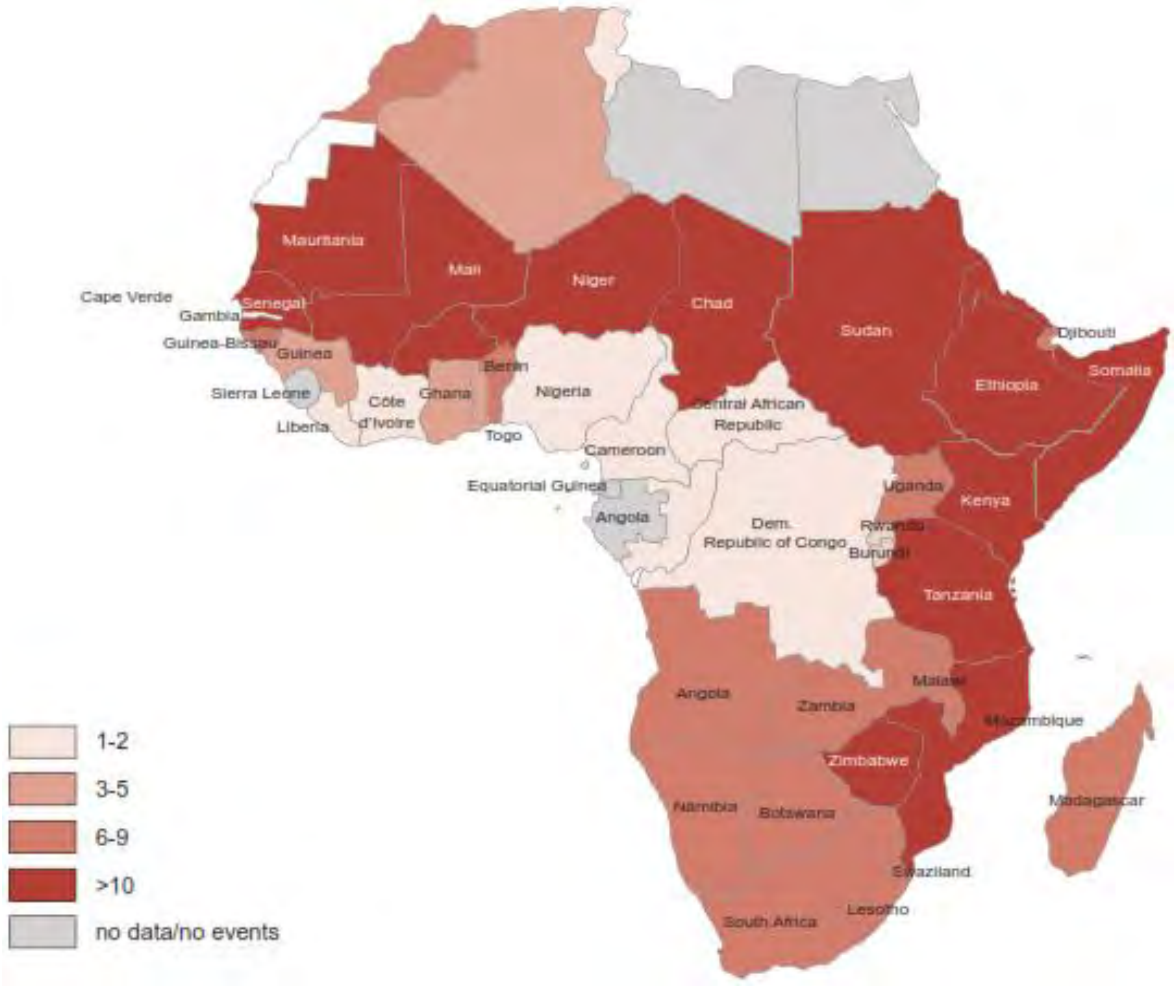

Figure 1.3: Number of drought events per country during the period 1970-2004. Source: Economic Commission for Africa (ECA, 2008).

1.4.1 Impacts of drought on food security

Drought is the primary natural disaster in Africa. It affects the population in the continent more than any other type of hazard. As shown in Fig.1.4, 80% of the African population is vulnerable to drought and consequently more affected by its impact. During the period 1900-2013, 291 drought events were reported in the African continent, affecting more than 300 million people (Masih et al. 2014).

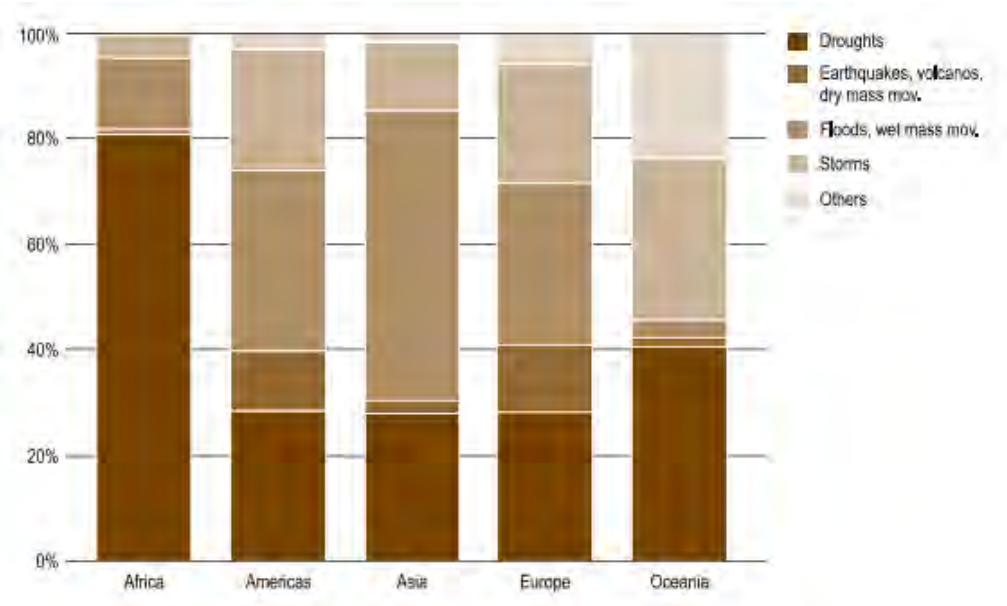

Figure 1.4: Proportion of persons affected by different natural disasters in Africa, Americas, Asia, Europe and Oceania for the period 1970-2008. Source: UNISDR (2009).

The major impact of drought in Southern Africa is on food supply as the livelihood of the people in the region is highly dependent on rain-fed agriculture. Droughts in the region cause crop failure which leads to food insecurity. For example, the 1991/92 drought caused famine, and deepened poverty in many Southern African countries. To combat the drought impacts on food security, the region imported more than 11 million tons of cereal (Calliham et al. 1994; FAO, 2004). The food shortage has a negative impact on the health of the population due to the malnutrition (Calow et al. 2010). For instance, the protracted drought of 1982/83 season claimed 100 thousands lives in Mozambique (WMO, 2014). As shown in Fig.1.5, Lesotho, Mozambique,

Zimbabwe, Zambia, Tanzania and Angola have the highest mortality rate resulting from severe drought events.

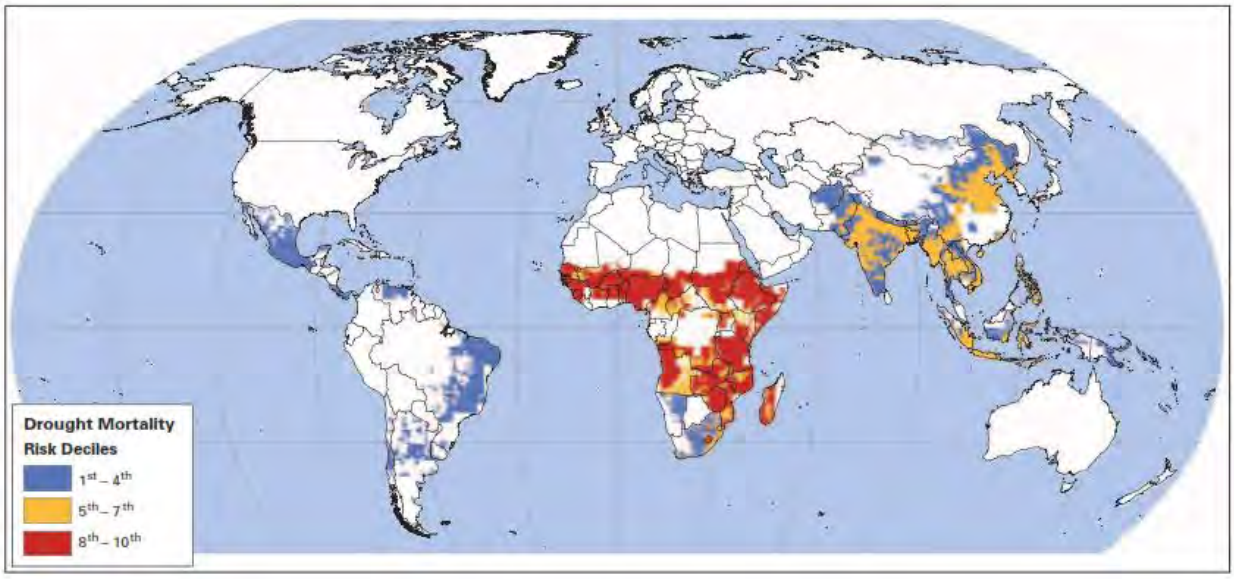

Figure 1.5: Mortality associated with drought events. Source: The World Bank (2005).

1.4.2 Drought Impacts on Water and Energy

During the 1991/92 rainy season, the summer rainfall reduced by 50% below the normal value and the water level in reservoirs dropped by 50% in Botswana, South Africa, Zimbabwe, Namibia and Lesotho (Unganai and Kogan, 1998; Jury and Mwafulirwa, 2002). More than three million people in Malawi had no access to clean water and several municipalities in Zimbabwe imposed restriction in water usage (Benson and Clay, 1998; Calow et al. 2010). The decline in rainfall also caused problems in the generation of electricity in the region as many countries rely on the hydropower. Problems in electricity supply caused load shedding in Zambia and Zimbabwe where US$102 million losses in GDP as well as job losses were reported (Benson and Clay, 1998). As a way of coping with the lack of water, people in rural areas were forced to excavate wells and boreholes in order to fulfil the household activities. The consumption of contaminated water from these boreholes led to outbreak of diseases such as diarrhoea, cholera and dysentery in Malawi (Calow et al. 2010).

1.4.3 Drought impacts on the economy

Droughts cause serious damages in any nation where they occur, especially in Southern Africa where agriculture is the mainstay of the economy. For instance, the food import during the 1991/92 drought cost more than $4 billion (Calliham et al. 1994; FAO, 2004). In South Africa alone the cost was estimated to be US$ 1.7 billion (WMO, 2014). The drought caused economic inflation in the region and as a consequence, the projected economic growth did not materialize since a big portion of the budget was diverted to drought relief funds (Dube and Jury, 2000). For example the gross domestic product (GDP) of Zimbabwe dropped by 8% during the 1991/92 season while the decline in Zambian GDP was 2.8% (ECA, 2008). In Malawi, droughts and dry spells are associated with one percent annual GDP loss (World Bank, 2005). The unforeseen expenditures resulting from droughts can force governments to borrow money from domestic or international institutions, or introduce new taxes and charges for goods and services. For instance, the government of Zimbabwe was forced to introduce drought levies on company taxes during the 1984/85 and 1986/87 seasons (Benson and Clay, 1998). In addition, the Zimbabwean government got a US$ 150 million loan from the World Bank and US$18 million from the United Kingdom (Benson and Clay, 1998). Table 1.1 summarizes all the drought impacts in the Southern Africa sub-region.

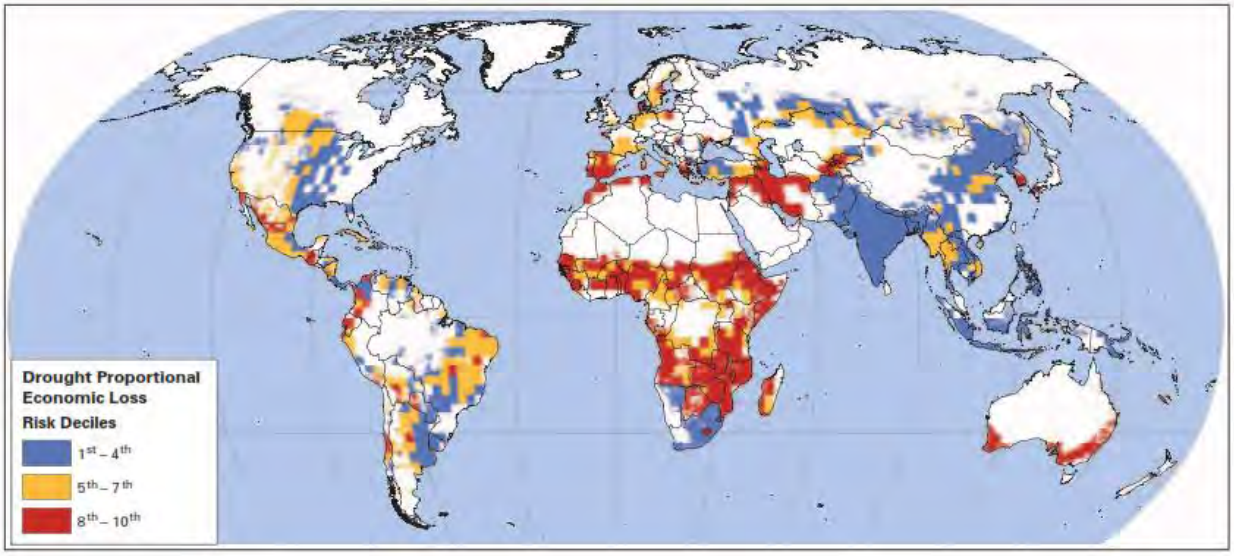

Figure 1.6: Economic loss caused by drought as a proportion of GDP density. Source: The world Bank (2005).

Table 1.1: Impacts of drought in Southern Africa. Adapted from FAO (2004).

Primary Impacts	Secondary Impacts
	SOCIAL
Disrupted distribution of water resources	Migration, resettlement, conflicts between water users
Increased quest for water	Increased conflicts between water users
Marginal lands become unsustainable	Poverty, Unemployment
Reduced grazing quality and crop yields	overstocking, reduced quality of living
Employment lay-offs	Reduced or no income
Increased food insecurity	Malnutrition and famine, civil strife and conflict
Increased pollutant concentrations	Public health risks
Inequitable drought relief	Social unrest, distrust
Increased forest and range fires	Increased threat to human and animal life
Increased urbanization	Social pressure, reduced safety
	ENVIRONMENTAL
Increased damage to natural habitats	Loss of biodiversity
Reduced forest, crop and range land productivity	Reduced income and food shortages
Reduced water levels	Lower accessibility to water
Reduced cloud cover	Plant scorching
Increased daytime temperature	Increased fire hazard
Increased evapotranspiration	Crop withering and dying
More dust and sandstorms	Increased soil erosion, increased air pollution
Decreased soil productivity	Desertification and soil degradation (topsoil erosion)
Decreased water resources	Lack of water for feeding and drinking
Reduced water quality	More waterborne diseases
	ECONOMIC
Reduced business with retailers	Increased prices for farming commodities
Food and energy shortages	Drastic price increases, expensive imports/substitutes
Loss of crops for food and income	Increased expense of buying food, loss of income
Reduction of livestock quality	sale of livestock at reduced market price
Water scarcity	Increased transport costs
Loss of jobs, income and property	Deepening poverty, increased unemployment
Less income from tourism and recreation	Increased capital shortfall
Forced financial loans	Increased debt, increased credit risk for financial institutions

1.5 Ocean-Atmospheric Teleconnections

Since the beginning of the 20th Century, scientists around the World have been fascinated by the idea of identifying areas in the world that are geographically separated but are climatically related, so that weather changes in one region can be related to weather changes in other region (Glantz, 2001). For instance, it was found that drought conditions in South Africa and India occur at the same time (Bridgman and Olivier, 2006). This relationship between climate anomalies from non-contiguous regions is referred as teleconnection (Glantz, 2001; Bridgman and Olivier, 2006). The climate in Southern Africa is known to be related to different oceanic and atmospheric patterns. The prominent oceanic patterns having effect on climate over Southern Africa are El Niño Southern Oscillation (ENSO), Indian Ocean Dipole (IOD), the Indian Ocean Subtropical Dipole (IOSD), the South Atlantic Subtropical Atlantic Dipole (SASD), the Benguela Niño and the Southern Annular Mode (SAM). Below we describe succinctly each of the oceanic modes.

1.5.1 El Niño Southern Oscillation (ENSO)

El Niño is a term coined by the Peruvian Sailors to a warm ocean current moving southwards along the Peruvian coast every 2 to 7 years (Glantz, 2001). This invasion of warm waters happens in general during the Christmas time, hence the name El Niño, which in Spanish means the child Jesus (Caviedes, 2001). Conversely, La Niña, which is a Spanish word for female child, refers to an anomalous cooling of surface waters in the eastern and central Pacific Ocean. The collective oceanic and atmospheric impacts of El Niño and La Niña conditions form the so-called El Niño Southern Oscillation (ENSO), which plays a prominent role in the rainfall variability in Southern Africa and worldwide (Glantz, 2001; Trujillo and Thurman, 2011). Sea Level Pressure (SLP) is another parameter used to understand the ENSO phenomenon. In general, ENSO is associated with changes in the SLP values over the Pacific Ocean. In some occasions the SLP values are higher over the eastern Pacific Oceans than over the western side and vice-versa. This fluctuation of the SLP values in the Pacific Ocean is commonly referred as Southern Oscillation (Rosenzweig and Hillel, 2008; Barry and Chorley, 2003). The Southern Oscillation is quantified by the Southern Oscillation Index (SOI), which is calculated as the standardized difference between SLP values from Tahiti (Central Pacific) and Darwin (western Pacific). Positive values

of the SOI represent a normal or high phase, which is characterized by high SLP values over the Tahiti region, hence strengthening of the easterly trade winds in the Pacific Ocean. On the other hand, negative values of SOI represent a low phase, which is characterized by high SLP values over the western Pacific than the eastern side leading to the weakening of the easterly trade winds.

ENSO causes different impacts worldwide. While in some regions of the world rainfall is inhibited, in other places ENSO is associated with floods (Glantz, 2001). For example, the 1982-83 El Niño was associated with severe droughts in Indonesia, Peru, Bolivia, Australia including Southern Africa. In contrast, some other regions of world such as Southern Brazil and United Sates, suffered with floods. The drought and floods from the El Niño caused widespread negative impacts on the affected areas. For instance, there was a considerable reduction in agricultural outputs (e.g., corn, soybean and rice) in the United States, Indonesia and Southern Africa (Rosenzweig and Hillel, 2008). Furthermore, the floods triggered damage of infrastructures in Brazil, Argentina and Paraguay. Fig.1.7 summarizes the atmospheric conditions associated to the ENSO event.

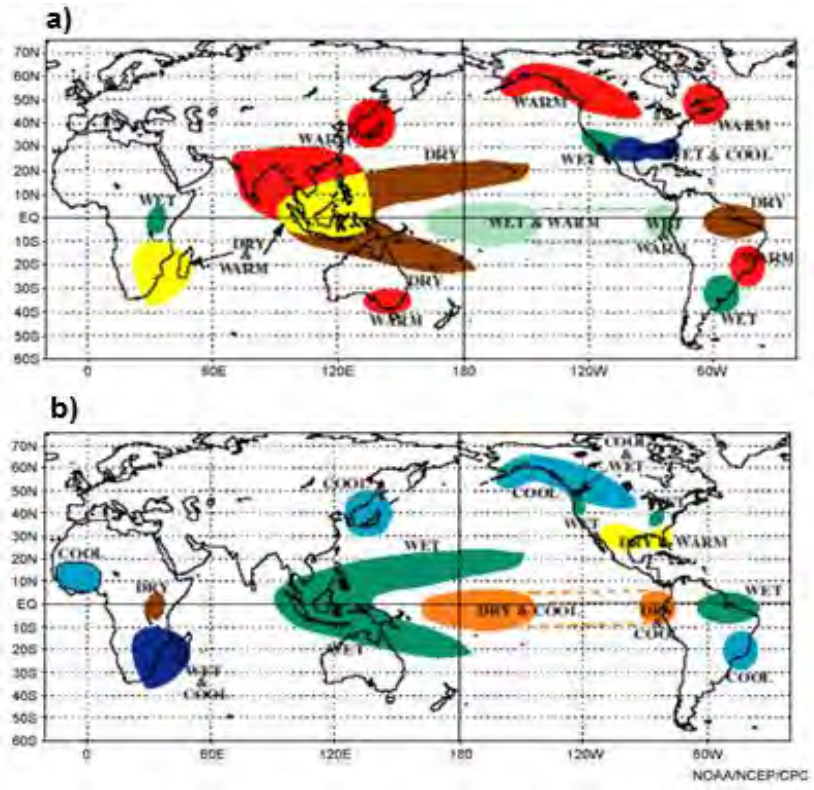

Figure 1.7: Impact of El Niño (a) and La Niña (b) during the austral summer. Source: NOAA.

1.5.2 The Southern Annular mode

The Southern Annular Mode (SAM), also called Antarctic Oscillation (AAO), is the primary mode of variability in the high latitudes of the Southern Hemisphere (Thompson and Wallace, 2000). It is characterized by changes in atmospheric pressure between the mid-latitudes and South Pole. The SAM is generally represented by the Southern Annular Mode Index (SAMI) or Antarctic Oscillation Index (AAOI), which can be computed using two different approaches. In the first approach, SAMI is represented by the leading Empirical Orthogonal Function (EOF) mode of the 850 hPa height anomalies around south of 20˚S (Reason and Rouault, 2005). In the second approach (Fig.1.8), SAMI is calculated as the normalized difference of the zonal SLP between Antarctic (65˚S) and Southern Hemisphere mid-latitude (40˚S). The negative phase of the SAM is characterized by high SLP anomalies around the Southern Polar region and low pressure values over the Southern hemisphere mid-latitude region (Reason and Roualt,2005; Bridgman and Oliver,2006). A reversed situation is reported during the positive phase of the SAM.

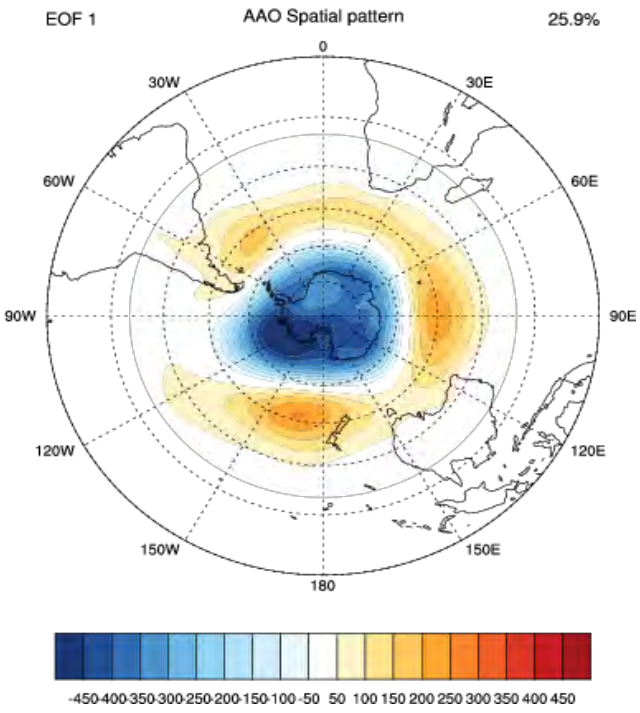

Figure 1.8: Leading EOF mode (25.9%) of monthly anomalies of sea level pressure for the period 1981-2011. Source: National Oceanic and Atmospheric Administration (NOAA).

1.5.3 The Indian Ocean Dipole

The Indian Ocean Dipole (IOD), which is also known as the Indian Ocean Zonal Model (IOZM), is characterized by anomalous fluctuation of SSTs in the Indian Ocean (Saji et al., 1999). The positive phase of IOD is characterized by anomalous low SST off the Coast of Sumatra Island in Indonesia and abnormal high SST values around Somalia, in the western Indian Ocean side (Fig.1.9). This situation leads to droughts over the maritime continent and downpours over Eastern Africa. A reversed scenario is observed during the negative phase, with atypical high SSTs off Sumatra and abnormal low SSTs over the western Indian Ocean. As a result, droughts are reported over eastern Africa while heavy rains are recorded over Indonesia.

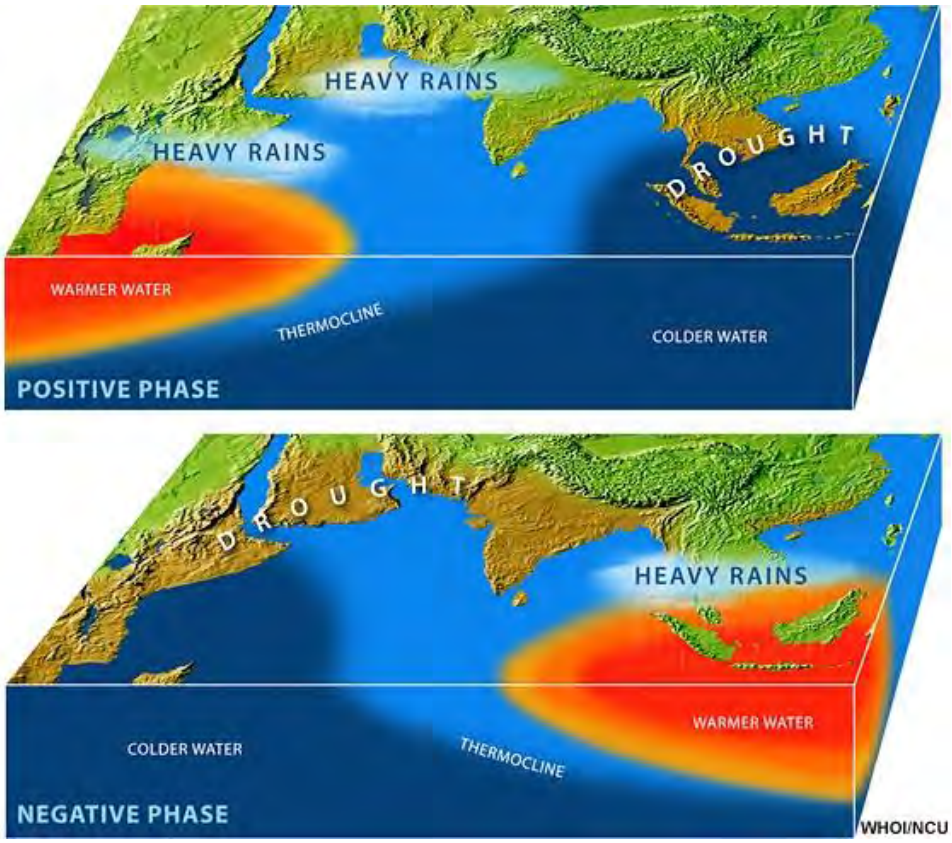

Figure 1.9: Positive and negative phases of the IOD. Source: www.meted.ucar.edu.

1.5.4 The Indian Ocean Subtropical Dipole

The Indian Ocean Subtropical Dipole (IOSD) or Subtropical Indian Ocean Dipole (SIOD) is another mechanism affecting the Southern African climate, particularly during the austral summer (Behera and Yamagata 2001, Reason 2001, Hansingo and Reason 2009). A positive (negative) IOSD is characterized by warm (cold) SST anomalies south of Madagascar and negative (positive) anomalies off the northwestern coast of Australia (Morioka et al., 2010). The Position of the Mascarene High pressure centre was reported to exert an Impact on the development of the SIOD. For example, a positive SIOD phase is always associated with a strengthened Mascarene subtropical High pressure centre, which leads to a stronger south-easterly flow pattern and consequent moisture flux inland (Morioka et al.,2010). The SIOD index can be calculated as the difference between western (55˚E-65˚E; 37˚S-27˚S) and north-eastern (90˚E-100˚E; 28˚S-18˚S) SST anomalies as shown in Fig.1.10.

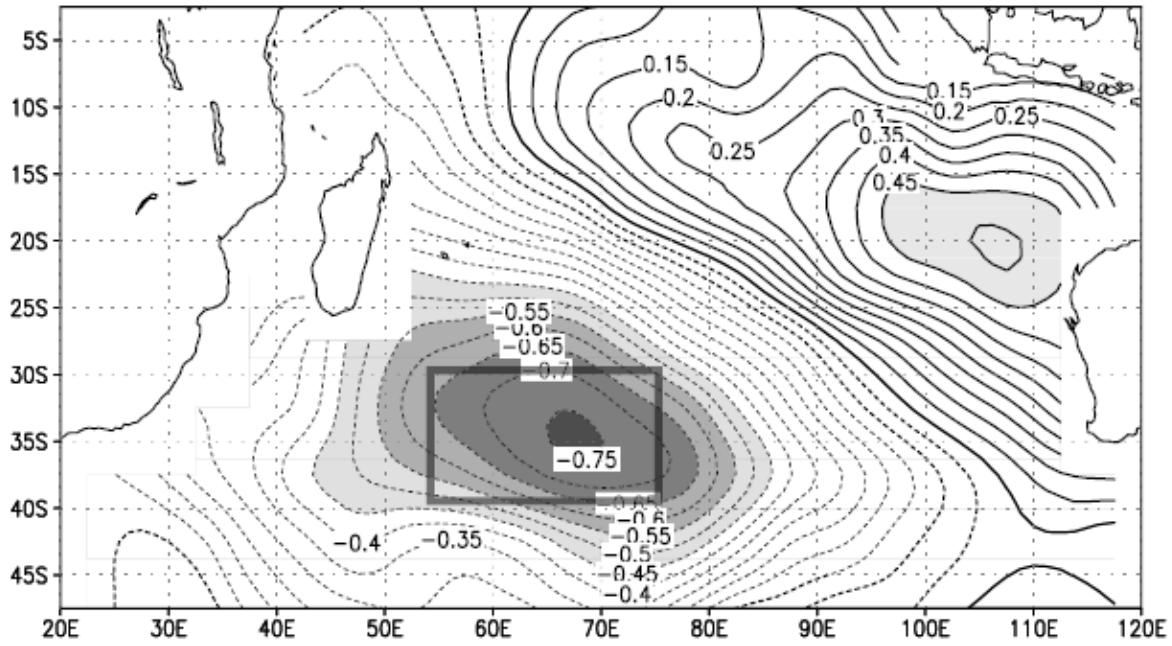

Figure 1.10: Spatial pattern of the second singular value (SVD) mode of sea surface temperature anomalies in the Indian Ocean during the period 1950-1999. This configuration corresponds to a negative phase of the IOSD. Source: Fauchereau et al. (2003).

1.5.5 South Atlantic Subtropical Dipole

The South Atlantic Subtropical Dipole (SASD) is another dipole mode, which is found in the Atlantic Ocean (Venegas et al. 1997, Fauchereau et.al 2003, Hermes and Reason 2005, Morioka et al. 2011, Morioka et al. 2012). As described by Hermes and Reason (2005), a positive event of SASD occurs when there are warm SST anomalies on the western side of the subtropical basin in the Atlantic Ocean. The reverse is valid for the negative phase. The SASD mechanism is very similar to the one of IOSD, it is dependent on the strengthening or weakening of the St Helena subtropical high and is common during the austral summer when it reaches its mature phase. The SASD is always identified by leading mode of either Empirical Orthogonal Function analysis (Fig.1.11) or Singular Value Decomposition (SVD). The SASD index is usually calculated as a difference between southwestern (30˚W-10˚W, 40˚S-30˚S) and north-eastern (0-20˚W; 25˚S-15˚S) boxes as shown in Fig.1.11.

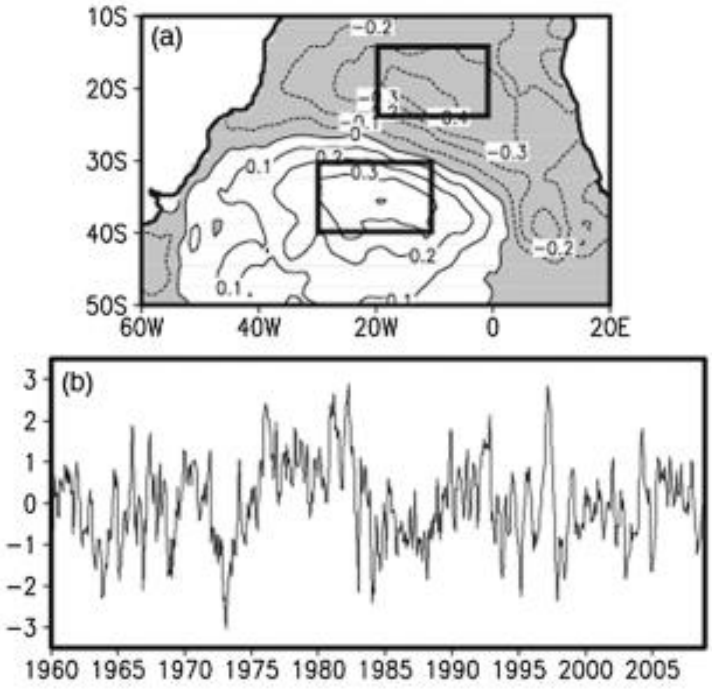

Figure 1.11: First EOF mode of sea surface temperature in the Atlantic Ocean (a) and its associated principal component (b). The boxes represent positive and negative poles. Source: Morioka et al. (2011).

1.5.6 Benguela Niño

Benguela Niño is an El Niño-like feature in the Atlantic Ocean (Shannon et al., 1986; Florenchie et al., 2003). It is characterized by an unusual warming of SSTs off the coast of Angola and Namibia (Grim and Reason, 2010). Unlike the El Niño in the Pacific Ocean, Benguela Niño is a sporadic phenomenon in the Atlantic Ocean, which is originated by the propagation of the equatorial warm water towards the west coast of Africa (Rouault et al., 2003). The invasion of warm waters affects the Benguela current, hence the coastal upwelling, which in turn leads to loss in fisheries due to the low availability of nutrients in the ocean (Florenchie et al., 2003; Rouault et al., 2007). The Benguela Niño is very common during the austral summer and reaches its peak around January-February-March (Grim and Reason, 2010). Anomalously cold event can also happen over the same region and it is generally called by Benguela Niña (Florenchie et al., 2004; Reason et al., 2006).

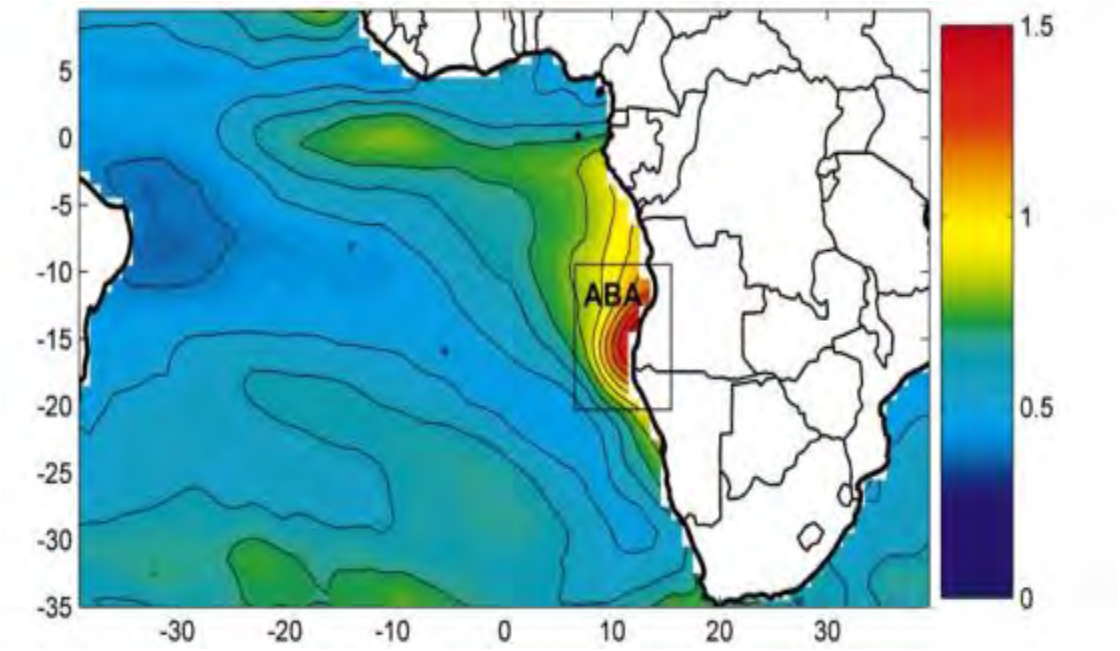

Figure 1.12: Standard deviation of SST anomalies (^{0}C) over the South Atlantic Ocean for the period 1982-2000. ABA stands for Angola-Benguela Area. Source: Florenchie et al. (2004).

1.6 Southern African Climate

Southern Africa (Africa South of the Equator) is a semi-arid region, which is characterized by a high degree of rainfall variability with recurrent floods and droughts. The rainfall over south of 10˚S occurs during the summer period (from October to April) with the late summer (January to March) contributing 40% of the annual rainfall (Richard et al., 2001; Cretat et al., 2012). However, over the southwestern portion (the southwestern Cape) the climate is Mediterranean, with the rain occurring mainly during the winter season due to the occurrence of cold fronts, extratropical cyclones and cut-off lows (Reason et al., 2001; Reason et al.,2006; Blamey and Reason,2007; Philippon et al., 2011). Generally, the rainfall shows meridional and zonal variations. It shows a South-north gradient, with the rain increasing from the South to north. In a similar way, the rain decreases from the eastern to western coasts (Fig.1.13).

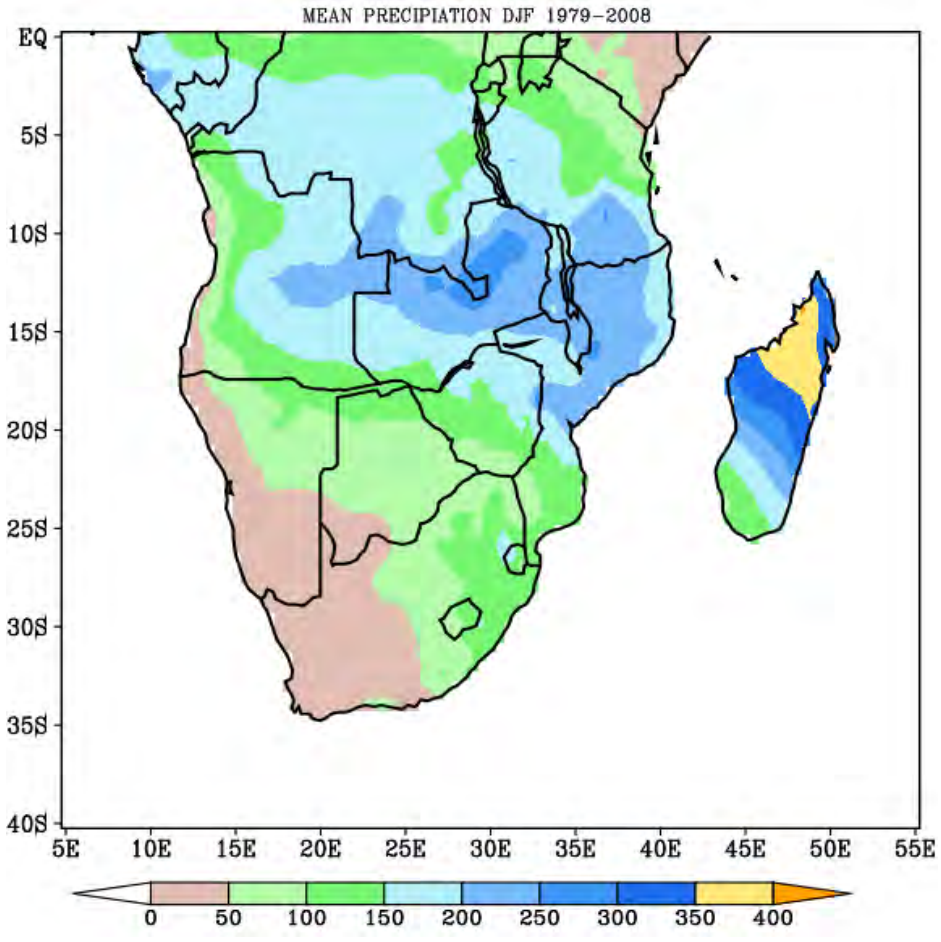

Figure 1.13: Austral summer (DJF) mean rainfall (mm) over the 1979-2008 period.

1.6.1 Dominant synoptic features in Southern Africa

The Southern African climate is controlled by different factors including orography, subtropical high pressure centres in the Atlantic and Indian Oceans, the Intertropical Convergence Zone (ITCZ) and the Angola low. One of the key players shaping the climate of the region is orography, which has the ability of creating microclimates and impact on rainfall pattern at a given location (Fig.1.14). The orography can trigger the so-called rain shadow, which happens over mountainous regions where the elevation uplifts the airflow. The raising of the air causes convection to take place and rainfall is favoured on the windward side of the mountain, while on the lee side of the mountain the rainfall is scarce due to the sinking of the air (Nicholson, 2011). For example, the Drakensberg Mountains in Lesotho are the highest mountains south of 10˚S. Around the Drakensberg Mountains, precipitation is irregular with some locations recording about 1400 mm annual rainfall while others recording precipitation less than 800 mm (Nel, 2009). Similar scenario is observed in the Cape Folded Mountains of Western Cape (South Africa) where the precipitation is abundant over the windward side of the escarpment and scarce on the lee side of the Mountains (Phillipon et al., 2011).

The region is dominated by two semi-permanent anticyclone cells, one in the Atlantic Ocean and the other one in the Indian Ocean (Van Heerden and Taljaard, 1998). The high pressure centre in the Atlantic is commonly known by South Atlantic High (SAH) or St. Helena high pressure centre, while the one in the Indian Ocean is referred as the South Indian High (SIH) or Mascarene high pressure Centre (Nicholson, 2011). The position of these two subtropical highs has impact on the rains in the region. For example, during the summer period, the two cells are completely located in their respective oceans, creating favourable conditions for moisture transport inland and associated rainfall. In contrast, during the winter period, the two centres unite forming a huge high pressure centre from the Atlantic Ocean all the way into the Indian Ocean. This situation causes a subsidence over the bulk Southern Africa and inhibits occurrence of precipitation since the atmosphere is relatively stable (Nicholson, 2011).

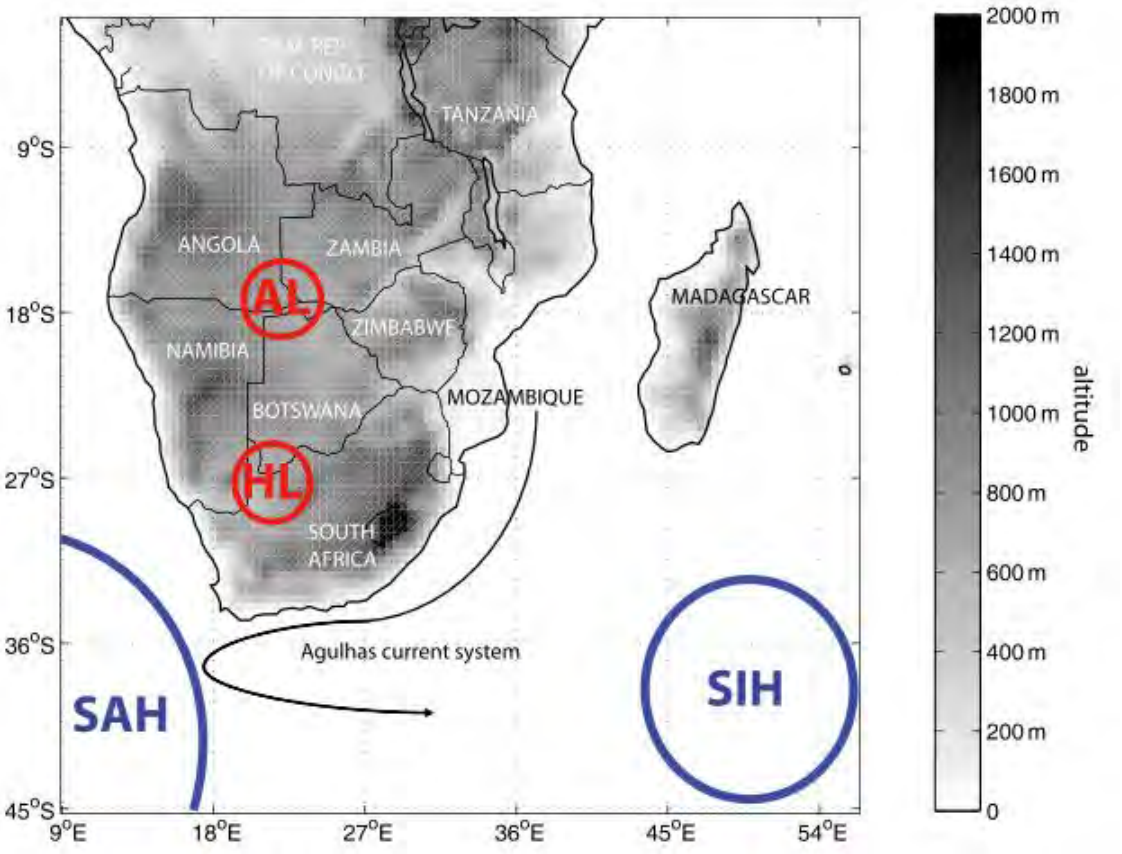

Figure 1.14: Dominant synoptic patterns over Southern Africa during austral summer: Angola Low (AL), Kalahari Heat Low (HL), South Atlantic High (SAH) and South Indian Ocean High (SIH). Source: Macron et al. (2014).

Another mechanism having impact on the Southern African Climate is the Intertropical Convergence Zone (ITCZ), which is a region of cloud band and heavy rainfalls originated by the convergence between the southeastern and northeastern trade winds (Fig.1.15). The ITCZ moves seasonally following the thermal Equator. During the Austral winter (June to August) the ITCZ is situated in Northern Hemisphere while in austral summer (December to February) the ITCZ moves far South over the continental Southern Africa reaching South-eastern Zambia and Central Mozambique (Reason et al., 2006).

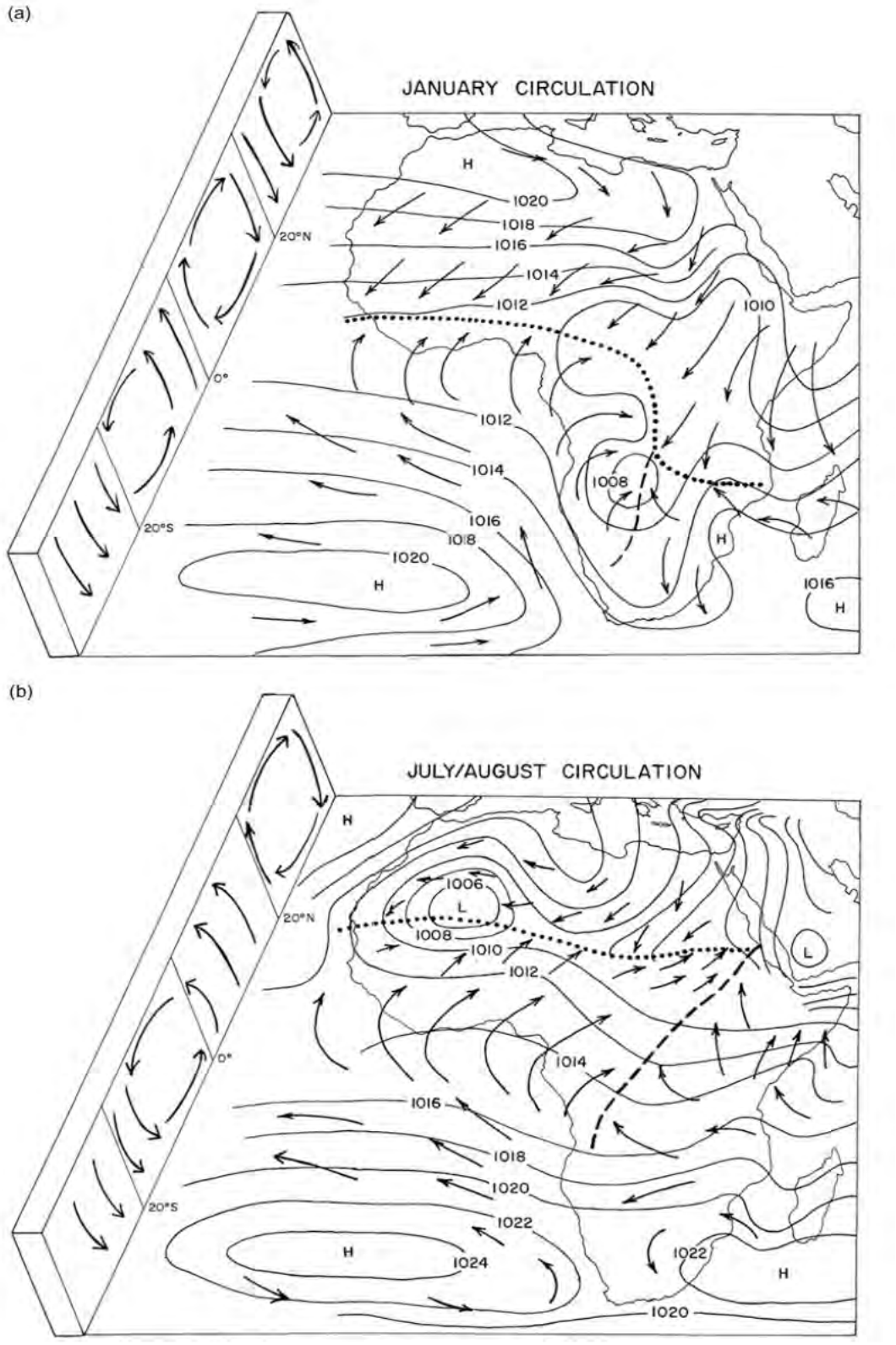

Figure 1.15: Circulation features over Africa during summer (a) and winter (b). Source: Nicholson (2011).

1.7 Climate Modelling

Different characteristics of the atmosphere and ocean, such as motion, obey the laws of physics. Therefore, the behaviour of the atmosphere and oceans can be represented in terms of equations, which the scientific community tries to solve using some approximations (Neelin, 2011). With the increase in the computation power there are multiple efforts worldwide of climate modelling experiments using either Global Climate Models or Regional Climate Models. In this section we provide an overview of these two approaches.

1.7.1 Global Climate Models (GCMs)

Global Climate Models or General Circulation Models (GCMs) are a very important tool for investigating climate variability and change (Rummukainen, 2010). Based on the laws governing the atmosphere, GCMs are used for weather prediction as well as climate studies at a global scale. In the GCMs, the atmosphere is divided into small three-dimension boxes or grids (Dahan, 2010). Each grid point represents the average conditions of the atmosphere at a specific location (Fig.1.16). The division of the atmosphere into grid points and layers is done in order to reduce the computational costs.

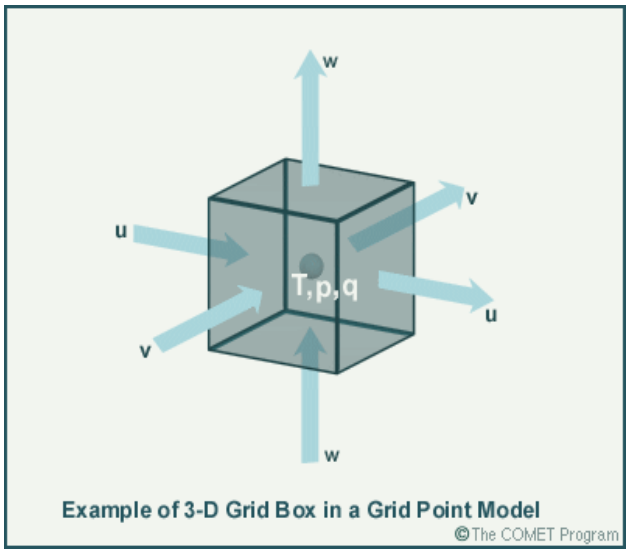

Figure 1.16: Example of a grid point. All the meteorological variables, i.e, Temperarute (T), pressure(p), moisture (q), zonal wind(u), meridional wind and the vertical motion (w) represent average condtions at this specific grid point. Source: The COMET Program: **www.metedu.ucar.edu.**

GCM were originally developed for the study of the climate through the understanding of the beahviour of atmosphere. In recent years, more complex GCMs were built, incorpotating more components of the climate system such as the ocean, sea ice and land. These improvements in the GCMs capabilities were achieved as result of the increase in the computational resources, which afforded a better storage capacity of the GCM outputs as well as improvement in the sharing of huge amount of the datasets among the reseach institutes. With the advent of the climate change issue, new projects of data sharing and model intercomparison emerged. For example the Program for Climate Model Diagnosis and Intercomparison (PMCDI) was created in early 1990s under the umbrella of the World Climate Research Project (WRCP). More recently,Coupled Model Intercompasion Projects (CMIP), named CMIP3 and CMIP5 were created for further data sharing and model evaluations (Meehl , 2007; Taylor et al. 2012).

Despite the reasonable skills of GCMs in reproducing global and hemispheric features, they have limitations, especially with their horizontal resolution which is typical of 300 Kilometres (predominantly in the CMIP3 models). This coarse resolution cannot capture small scale features that happen at local scale and play a crucial role in the rainfall producing systems (McGregor 1997; Wilby and Wigley 1997). For this reason, the future climate projections from the IPCC are of no great use for specific sectors such agriculture and hydrology, which require a finer resolution (less than 50 km). To overcome this limitation, a process termed Downscaling is usually performed onto GCMs outputs in order to bridge the gap between the GCM grid resolution and resolution of interest to decision-makers. The downscaling process can be either statistic or dynamic (Benestad, 2008)

1.7.2 Statistical downscaling

Statistical downscaling (SD) is referred to the process of linking large scale features to small scale climate conditions through the use of advanced statistical methods (Wilby et al.,2004, Benestad,2008). The large scale feature is generally from a GCM while the small scale feature comes from a specific grid point or meteorological station. There are three main assumptions behind the statistical downscaling approach (Wilby et al.,2004):

a) There is a strong relationship between the predictors and predictands and the GCM skillfully simulates the predictors. In other words, if the GCM cannot capture the large scale phenomenon then the downscaling effort is not worthy.

b) The relationship between the predictor (large scale variable) and the predictand (regional Varaible) is stationary. This means that the association between the large and local scale variables remains the same even under climate change conditions.

c) The identified predictors can realistically reproduce the climate change signal. That's to say that if the predictor suffers a perturbation, similar magnitude of pertubation must be also reflected in the predictand.

Three main statistical downscaling techniques are currently in use: Linear methods (Wilks,2011), weather classification methods (e.g.,Wilby et al.,2004; Hewiston et al. 2014), and weather generator methods (e.g.,Wilks, 2010; Semenov and Barrow,2002).

1.7.2.1 Linear methods

The linear methods are based on the historical relationship between the large and local scale variables. These methods require a very long time serie in order to estabilish a robust relationship between predictors and predictands. The most common methods in this category include, simple and multiple regression (MLR), Canonical Correlations Analysis (CCA) and Singular Value Decomposition (SVD). The simple linear regression (SLR) summarizes the relationship between the predictor field and the predictand through a straight line (Wilks,2011). In fact, the SLR seeks to minimize the root mean square of predicting the local scale variable, given the large scale field (Benestad, 2008). The MLR is very similar to the SLR, the main difference between the two approaches is the number of predictors. While the SLR deals with only one predictor, the MLR involves the use of at least two predictor fields (Wilks, 2011).
CCA is a statistical technique that identifies pairs of patterns (predictor and predictand) having the highest correlation (Storch and Zwiers,1999; Benestad, 2008). The result from this multivariate statistical method is a spatial map showing the maximum correlation between the

predictor and predictand. The SVD approach is very similar to the CCA, instead of finding the maximum correlation between predictor and predictand, the SVD methods searches for pair of patterns that maximize the covariance. The SVD method is also commonly known as Maximum Covariance Analysis (MCA, Storch and Zwiers, 1999; Wilks, 2011). In general, results from the CCA are similar to those obtained using the MCA method (e.g., Van den Dool,2007; Wilks, 2011).

1.7.2.2 Weather Classification Methods

In this method, synoptic patterns are grouped based on their similarity (Wilby et al.,2004). The groups, which are also known as states, are organized in such a way that they represent one type of precipitation or temperature. For instance, frontal systems can be considered as a group because they are generally associated with a specific type of precipitation in Southern Africa. These methods can be appropriate for downscaling climate variables that exihibt a non-Gaussian distribution such as daily precipitation (USAID, 2014). Examples of these methods include analogue approaches, Cluster Analysis, hidden Markov models and neural networks. Compared with the linear methods, the weather classification methods require substantial computational resources and are relatively complex.

1.7.2.3 Weather Generators

Weather Generators use stochastic techniques to create synthetic data of weather variables (e.g., rainfall, maximum and minimum temperature, radiation, etc.) on a daily and sub-daily timescales (Wilby et al., 2004; USAID,2014). While the linear methods are frequently used for spatial downscaling, weather generators are mostly used for temporal downscaling which makes them suitable for climate variability and change at a much localized point such as catchment areas (USAID, 2014). Several Weather Generators have been developed during recent years. The Long Ashton Research Station Weather Generator (LARS-WG, Semenov and Barrow,2002), MarkSim GCM (Jones and Thornton,2013) and Nonhomogenous Hidden Markov Models are but few examples of different Weather Generators currently in use. LARS-WG is a semi-parametric type of Weather Generator normally used for generating weather data at a single point. Similar to

LARS-WG, MarkSim-GCM is also a single site Weather Generator used for creating synthetic weather data. It is a web-based weather generator and it uses the third-order Markov chains to simulate the rainfall. Some advantages and disadvantages of the three empirical statistical downscaling approaches are summarized in Table 1.2.

Table 1.2: Main statistical downscaling methods and their advantages and disadvantages. Source: adapated from Wilby et al. (2004) and USAID (2014).

Method	Strengths	Weakness
Linear Methods(e.g., simple and linear multiple regression, CCA,SVD)	• Relatively straightforward to apply • Employs full range of available predictor variables	• Require normality of data(e.g., monthly temperature) • Not suitable for non-normal data distributions (e.g., daily rainfall) • Poor representation of extreme events
Weather Classification (e.g., analogue method, cluster analysis, neural networks)	• Yields physically interpretable linkages to surface climate • Versatile, i.e., can be applied to both normally and non-normally distributed data (e.g., surface climate, air quality, flooding, erosion, etc.)	• Requires additional step of weather type classification • Requires large amount of data and some computational resources • Incapable of predicting new values that are outside the range of the historical data
Weather Generators (e.g., LARS-WG, MarkSim GCM, NHMM)	• Can generate sub-daily information • Able to simulate the length of wet and dry spells • Produces large number of series, which is valuable for uncertainty analysis • Production of novel scenarios	• Data-intensive • Sensitive to missing or erroneous data in the calibration set • Only some Weather Generators can check for the coherence between multiple variables (e.g., high insolation should not be predicted on a rainy day) • Requires generation of multiple time series and statistical post-processing of results

1.7.3 Dynamical Downscaling

Dynamical downscaling (DD) entails nesting a Limited Area Model (LAM) or Regional Climate Model (RCM) within a GCM (Giorgi, 1990; Giorgi and Mearns, 1999; Coffier, 2011). The atmospheric variables from either a GCM or Reanalysis dataset serve as the boundary conditions for the RCM, which is run at a much higher resolution than the driving GCM (Giorgi and Mearns, 1999). Typically, the horizontal resolution of a RCM is equal to or less than 50km, which is relatively a good resolution for capturing small scales features such as orography and water bodies that affect the rainfall producing systems at a local scale. However, if the RCM is hydrostatic, there is a limit to how the resolution can be increased (Jacobson, 2005). A very high resolution would compromise the non-hydrostatic effect, because as the resolution increases the non-hydrostatic behaviour becomes very important (Abiodun et al., 2008; Abiodun et al. 2011). In the hydrostatic approximation, vertical accelerations are ignored by neglecting the total derivative in the vertical momentum equation (Kalnay, 2003; Jacobson, 2005). Neglecting the vertical acceleration has an advantage of discarding the acoustic waves which in turn avoid the need of a shorter timestep for resolving the momentum equation (Kalnay, 2003; Jacobson, 2005).

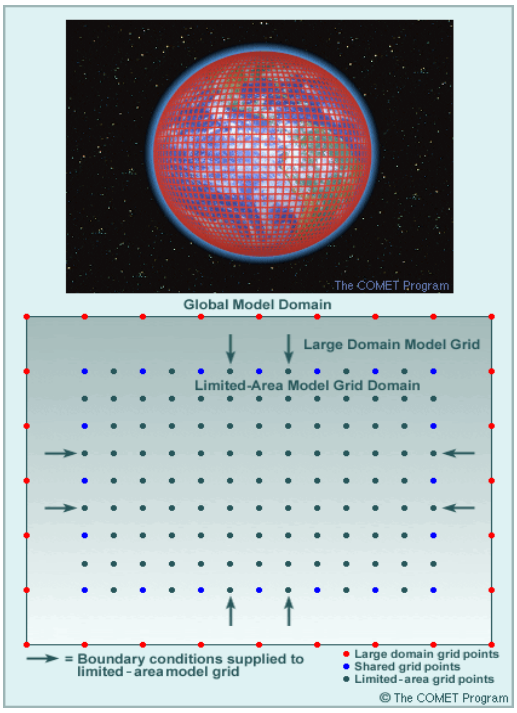

Figure 1.17: Example of a nested regional climate model. Source: The COMET Progam.

While RCMs are good in representing local-scale features, they are sensitive to the quality of data used for the lateral boundary conditions (Hewitson and Crane, 1996; Denis et al., 2002). Lateral boundary conditions (LBC) play a crucial role in the dynamic downscaling process. A minor error in the LBC can quickly propagate into the RCM domain and cause the model to produce unrealistic simulations (Zhong et al., 2010). Therefore, LBC must meet the following criteria (e.g., Kalnay, 2003; Warner, 2011):

a) Allow a free propagation of meteorological fields (e.g., waves) from the GCM to the RCM
b) Prevent the reflected short waves at the outflow boundaries to re-enter into the domain of interest
c) Eliminate artificial feedbacks between grids that may pose model integration problems

There are two approaches for formulating LBC (Kalnay, 2003; Warner, 2011). In the first approach, the GCM, which possesses the lower grid resolution, supplies the RCM with the required LBC. This approach is commonly known as one-way or parasitic nesting (Jacobson, 2005). This is the approach used by the majority of RCMs because it allows the RCMs to develop freely and the host GCM is not affected by the solutions from the RCM (Warner, 2011). In the second approach, the interaction between the GCM and RCM is allowed, i.e., the information from the RCM affects the host GCM and vice-versa. This approach is known as two-way interactive nesting (Kalnay, 2003; Warner, 2011). In theory, this approach should yield good results but care must be taken, in some cases the information from the RCM can be distorted and impact the entire simulation (Jacobson, 2005). Generally, the two-way interactive boundary condition requires more computational resources than the one-way nesting (Coiffier, 2011; Warner, 2011).

In recent years enormous efforts have been carried out in order to provide regional and accurate climate information through the dynamical downscaling approach. Table 1.3 summarizes some of those efforts.

Table 1.3: Dynamical Downscaling inicitatives around the World. Source: USAID (2014).

Project	Region	Purpose	Method
PRUDENCE (Prediction of Regional Scenarios and Uncertainties for Defining European Climate Change Risks and effects) (2001-2004)	Europe	Provide High-resolution Climate change scenarios for 21st century	8 RCMs
ENSEMBLES (ENSEMBLE-Based Predictions of Climate Change and their impacts) (2004-2009)	Europe	Develop and ensemble prediction system to construct integrated scenarios of future climate change for quantitative risk assessment	RCM ensemble
CLARIS (climate Change Assessment and impact studies) (2008-present)	South America	Predict climate changes and their socio-economic impacts	5 RCMs
NARCCAP (North American Regional Climate Change Assessment Program) (2006-present)	North America	• Provide climate change scenario information for the United states, Canada and Mexico • Explore the separate and combined uncertainties in regional climate simulations that result from the use of different GCMs and RCMs	6 RCMs
AMMA (African Monsoon Multidisciplinary Analyses)	West Africa	• Improve understanding and ability to predict the West African Monson (WAM) • Relate variability of the WAM to various sectors • Integrate multidisciplinary	Multi-RCM Comparison

(2009-present)		research with prediction and decision making	
STARDEX (Statistical and Regional Dynamical Downscaling of Extremes for Europeans Regions) (2002-2005)	Europe	Identify robust downscaling methods to produce future scenarios of extremes for the end of the 21st century	Dynamical and statistical
CORDEX (Coordinated Regional Climate Downscaling Experiment) (2009-present)	Africa	• Promote international downscaling coordination • Facilitate easier analysis by scientists and end-user communities at the local level of regional climate changes	10 RCMs

1.7.3.1 The CORDEX project

The aim of the CORDEX project is to downscale Climate projections from the CMIP5 GCMs. The GCMs from the CMIP5 have a resolution ranging from 100 to 200km, which is still coarse for reliable climate change information and consequent design of adaptation strategies (Jones et al., 2011). The need for local scale and tailored climate change information led to a proliferation of isolated downscaling efforts around the World. With the increased number of downscaling initiatives, there was a risk of producing wrong information for the policymakers and other stakeholders. Aware of this problem, the World Climate Research Program (WRCP) created a group whose mission was (Jones et al., 2011):

a) To assess and improve the existing climate downscaling techniques
b) To generate improved regional climate change information worldwide
c) To encourage interaction and knowledge exchange between the modelling community and end-users

The main recommendation from the WRCP task team was the creation of the CORDEX project. Under the CORDEX project multi-model regional climate change information is made available for different stakeholders around the World including Africa (Fig1.18).

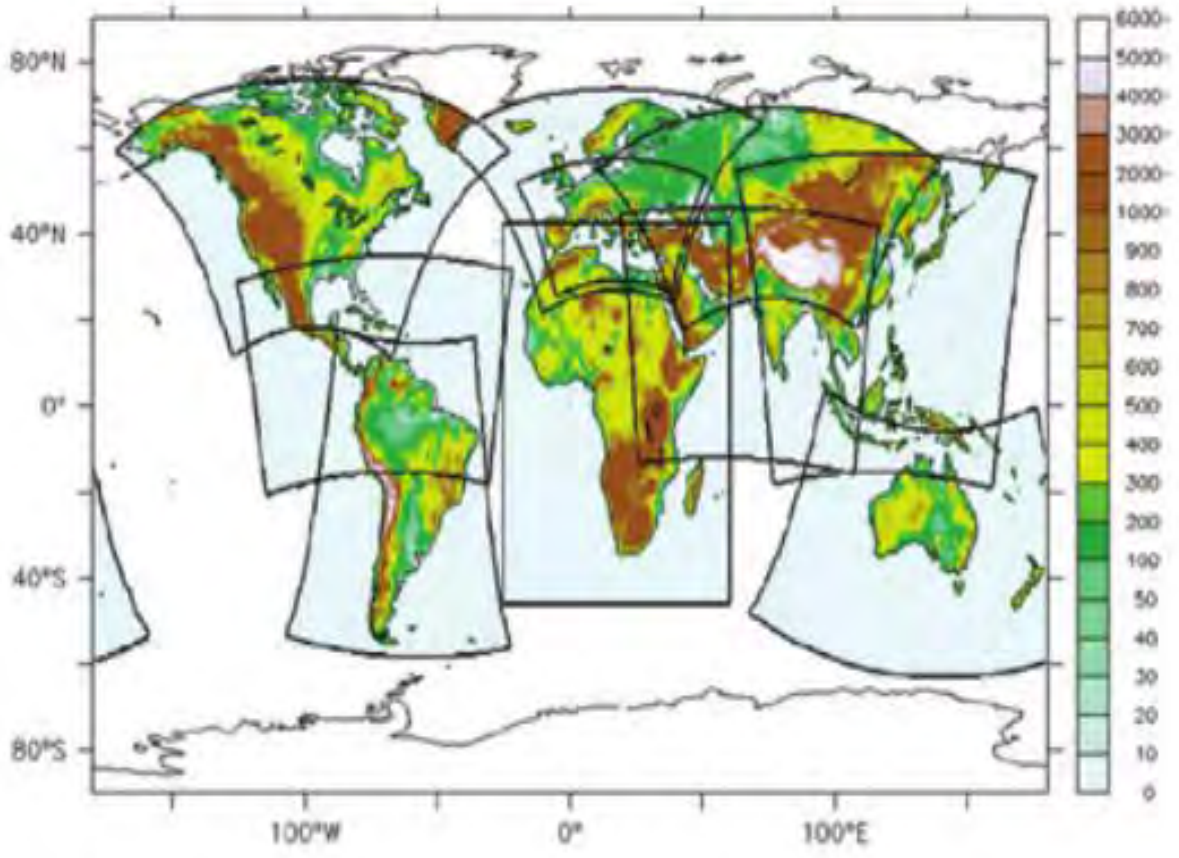

Figure 1.18: Different domains of the CORDEX RCMs. Source: Jones et al. (2011).

1.8 Motivation for this study

Several studies (e.g., Meadows 2006, Shongwe et al., 2009) have shown that Southern Africa is likely to experience even more frequent and more severe droughts in the future because of global warming. For instance, Meadows (2006) projected that the future increase in temperature over Southern Africa will be accompanied by a decrease in precipitation, hence more frequent and more severe droughts. Yet, Burke et al. (2006) investigated the evolution of global droughts and reported a net global drying trend and an increase of dry areas from 1% to 30% by the end of the 21st century. Sheffield and Wood (2008) examined the changes in drought occurrence using soil moisture data and found that long-term droughts will be more frequent in the future. Furthermore, the latest report from the Intergovernmental Panel on Climate Change (IPCC, 2013) projects a warming scenario for Southern Africa towards the end of the 21st century; hence more extreme weather events such as droughts and heat waves are expected to be more recurrent phenomena in future. In light of those projected events, governments in the region need to be better equipped with reliable climate information in order to tackle the shocks resulting from droughts and minimize their impacts. Therefore, there is a keen interest in monitoring and understanding the dynamics of droughts in Southern Africa.

In Southern Africa, only few drought events are short-lived (occurring in only one season), most droughts persist more than a season or a year and affect large areas in Southern Africa (Rouault and Richard 2005). Moreover, the devastating impacts of drought may persist longer than the drought duration, not allowing the drought affected area to fully recover before another event occurs. For instance, the 1982/1983 drought persisted for 19 months with devastating effects on food security and loss of livestock and other associated impacts. Despite the impacts of drought on the economy of the region, no study has attempted to investigate how a single drought event (occurring in one season) can persist and become a multi-year drought or transit from one type of drought to another. An improvement in the understanding of drought persistence and transition can enable communities to become more resilient to drought shocks and to develop a better response capacity. This can also help decision-makers and resource managers (agriculture and water) to make better plans under institutional constraints and limited financial resources.

1.9 Aim of the study

The aim of this study is to examine the ability of Regional Climate Models (RCMs) in simulating Drought characteristics in Southern Africa. The RCMs under scrutiny are part of the Coordinated Regional Climate Downscaling Experiment (CORDEX, Jones et al., 2011). The assessment of the capability of these climate models in reproducing past and present drought characteristics in Southern Africa is fundamental because the CORDEX RCMs are being used worldwide for downscaling of climate change projections to the regional scale. Therefore, a good performance of the RCMs in simulating the past and present climate will increase our reliability on the climate change projection resulting from them. To successfully achieve our endeavour we propose to attain the following objectives:

- Quantify the relationship between the El Niño Southern Oscillation (ENSO) and droughts over Southern Africa in observation and in CORDEX RCMs;
- Examine the sensitivity of the simulated link between ENSO and droughts, to RCM boundary conditions;
- Identify major drought patterns in southern Africa and examine their characteristics (focusing on their persistence and transition);
- Investigate the dynamics associated with the major drought patterns in Southern Africa;
- Assess the ability of the CORDEX RCMs in realistically simulating the persistence and transition of droughts in Southern Africa;

1.10 Thesis outline

The present thesis is organized into 7 chapters, including this one (Chapter 1), which introduces the concept of drought and its impacts over Southern Africa. The chapter also describes the main air-sea interaction mechanisms that have impact of rainfall distribution over Southern Africa and presents the aim and objectives of the study.

Chapter 2 provides an overview of the main drought indices currently in use across the World for monitoring and investigation of droughts. It also reviews the efforts in the Southern African

region to understand droughts and their precursors. The multivariate statistical methods for grouping large climate data are also presented, including their advantages and limitations. Various climate modelling efforts at global and regional scales are also discussed in this chapter.

Chapter 3 describes the datasets as well as the methodology used in order to achieve the objectives of the study. It gives more detail about the Standardized Precipitation-Evapotranspiration Index (SPEI), which is the chosen drought index in the study. The Potential Evapotranspiration, which is an important element for calculating the SPEI, is also explained in details. All the climate indices used in the study are presented including the methodology for their calculation.

Chapter 4 reports the results on the performance of Regional Climate Models in simulating the link between ENSO and droughts in Southern Africa. The chapter also presents the results on the sensitivity of the simulated link between ENSO and Southern Africa droughts to different lateral boundary conditions. The added value afforded by downscaling global climate features to local scale climate is also discussed.

Chapter 5 shows the 12 most dominant drought patterns in Southern Africa and their characteristics, which include the persistence and transition. The circulation anomalies associated with the drought patterns are presented. Composite analyses of precipitation, temperature and sea surface temperatures for each drought pattern are presented in this chapter.

Chapter 6 discusses how well the regional climate models simulate the drought patterns created in the previous chapter. Different methods are used in order to assess the model's performance in capturing the frequency of occurrence of the drought patterns and their probability of persisting or transiting to a different drought pattern.

Chapter 7 summarizes the findings from the study. It also presents the caveats of the study and provides some recommendations on how to improve the study and the way forward.

2 : Literature Review

This chapter presents an overview of the main drought indices used worldwide to characterize drought events. It also summarizes previous work on drought over Southern Africa, including the efforts carried out in order to improve our understanding of droughts in Southern Africa and their triggering mechanisms. It also presents the multivariate statistical methods in use for clustering climate data as well as their advantages and limitations.

2.1 Measuring Droughts

Owing to the complex nature of drought, several indices have been developed in order to be able to assess and quantify drought (Heim, 2002). Some of developed drought indices include Percent of Normal (PN), deciles (Gibbs and Maher, 1967), Palmer Drought Severity Index (PDSI; Palmer, 1965), standardized precipitation Index (SPI, Mckee et al., 1993), and Standardized Precipitation-Evapotranspiration Index (SPEI, Vicente-Serrano et al., 2010). The existence of multiple droughts indices is due to the fact that no single drought index is suitable for all purposes. For instance, precipitation is a key element for meteorological drought while an index that takes into account soil moisture is more suitable for a farmer, and one that has stream flow in its computation is more likely to be adopted by a person in the water sector (Quiring, 2001; Dai, 2011). There are many other drought indices described in the literature which have a limited application. Details of some of the well-known drought indices and their usefulness are presented below.

2.1.1 Palmer Drought Severity Index (PDSI)

The PDSI was originally developed by Palmer (1965) and is widely used in the United States of America (e.g., Karl, 1982). It is based on the water balance equation and incorporates precipitation, temperature and soil moisture. PDSI values typically range from -4.0 to 4.0 with negative values indicating deficiency in water (see Table 2.1). The main advantages of the PDSI is that it considers both precipitation and temperature, making the index sensitive to the changes in these two parameters, hence suitable for climate change studies (Mishra and Singh, 2010).

Some shortcomings and imprecision have been detected in the PDSI (Alley, 1984, Mishra and Singh, 2010):

- Compared to other indices, PDSI was reported to be complex to calculate.
- There is a problem with the portability of the index. PDSI was originally conceived for arid and semiarid regions of the United Sates; therefore, the index doesn't perform well in other regions of the globe.
- The index considers only liquid precipitation, i.e., it doesn't account for snow and ice. This assumption makes the index to underestimate the runoff.
- PDSI can be only computed for a timescale of 9 and 12 months, which might not be suitable for short-term droughts. Short-term droughts have more impact on sectors of activity such as water resources and agriculture.

Some of the limitations observed in the PDSI were eliminated with the development of the self-calibrated PDSI (SC-PDSI; Wells et al. 2004, Vicente-Serrano et al. 2010). The SC-PDSI improved the original PDSI by dynamically adjusting the empirical constants that were previously fixed for the Midwest United States climate. This calibration of the PDSI allows the index to be easily comparable at two different locations. The SC-PDSI resolved just part of the problems because the index has still a fixed timescale ranging from 9 to 12 months.

The original PDSI has been barely used over Southern Africa. However, some studies (e.g., Dai, 2011, 2013; Zhao and Dai, 2015) have used the SC-PDSI to investigate droughts worldwide including Southern Africa. For example, Zhao and Dai (2015) reported an increasing trend in agricultural droughts over the region under the low-moderate emission scenario. The increase is projected to be up to 100% for moderate drought and 200% for severe droughts. They also reported reduced evapotranspiration due to decrease in soil moisture.

Table 2.1: PDSI classification. Source: Fuchs et al.(2014).

PDSI	Drought Classification
4.0 or more	Extremely wet
3.0 to 3.99	Very wet
2.0 to 2.99	Moderately wet
1.0 to 1.99	Slightly wet
0.5 to 0.99	Incipient wet spell
0.49 to -0.49	Near normal
-0.5 to -0.99	Incipient dry spell
-1.0 to -1.99	Mild droughts
-2.0 to -2.99	Moderate droughts
-3.0 to -3.99	Severe droughts
-4.0 to less	Extreme severe drought

2.1.2 Standardized Precipitation Index (SPI)

The index was developed by Mckee et al. (1993) as an alternative to the PDSI. It has different categories that define drought intensities ranging from -2 (and less) to 2 (and above), with negative values indicating deficiency in water (see Table 2.2). SPI was recently considered by the World Meteorological Organization (WMO) as the reference drought index and is the most used drought index worldwide (Hayes et al. 2011; Potop et al., 2012). The main advantage of SPI is that it is based solely on precipitation making it very easy to compute. Opposed to PDSI, the SPI can be calculated for different time-scales making the index attractive in other sectors such as meteorology and hydrology. Since the index is standardized, two different regions can be now compared in terms of dryness or wetness. The main disadvantage of the SPI is that it does not include some other variables (e.g., temperature, evapotranspiration, wind speed and soil water holding capacity) having influence on drought. Furthermore, the index assumes that other variables are stationary (Vicente-Serrano et al., 2010). Although precipitation is the main driver of drought hazards, recent studies have shown the importance of including temperature in characterizing drought over any region (i.e. Vicente-Serrano et al. 2010, 2011; Abiodun et al. 2012). Vicente-Serrano et al. (2011) showed that drought severity is not only related to

precipitation, but to other variables such as potential evapotranspiration (PET, through temperature), which may play a more crucial role under the warming climate.

Table 2.2: SPI Classification. Source: Fuchs et al. (2014).

SPI	Drought classification
2.0 and above	Extremely wet
1.5 to 1.99	Very wet
1.0 to 1.49	Moderately wet
-0.99 to 0.99	Near normal
-1.0 to -1.49	Moderately dry
-1.5 to -1.99	Severely dry
-2.0 and less	Extremely dry

2.1.3 Standardized Precipitation-Evapotranspiration Index (SPEI)

The SPEI was recently developed by Vicente-Serrano et al. (2010) as a way of improving the capabilities of SPI. Unlike the SPI which is based upon precipitation only, the SPEI requires precipitation and mean temperature for its calculation. The index is based on monthly differences between precipitation and potential evapotranspiration (PET). The PET can be generated using less data demanding methods such as Thornthwaite (1948) or more physically based methods such as Penman-Monteith (PM) equation. The SPEI is believed to combine the sensitivity of the PDSI to changes in evaporation demand (caused by temperature fluctuations and trends) with the simplicity of calculation and the multi-temporal nature of the SPI (Vicente-Serrano et al. 2010; Ma et al., 2013). This index is particularly suited to detecting, monitoring, and exploring the consequences of global warming on drought conditions. Critics of the SPEI (e.g., Ma et al. 2013) pointed out that its spatial comparability is not guaranteed due to the fact that the index relies heavily on temperature. For example, under very warm conditions the index was reported to produce an increased water deficit and consequently increased PET. The SPEI has a same classification as the SPI. The SPEI is currently being used in different places around the world (e.g., Abiodun et al., 2013; McEvoy et al. 2012), including our study area (e.g., Ujeneza and

Abiodun, 2014; Araujo et al., 2014; Edossa et al., 2014; Trambauer et al., 2014 and Naumann et al., 2014). For instance, Trambauer et al. (2014) used several drought indices including SPEI and SPI, to investigate hydrological droughts over the Limpopo river basin during the period 1979-2010. They found that the majority of the drought indices were in phase. Furthermore, their study indicated that in case the actual evapotranspiration and soil moisture data are not available, the SPEI can be used in place of agricultural drought indices such as Evapotranspiration Deficit Index (ETDI) and Root Stress Anomaly Index (RSAI).

Table 2.3: SPEI classification scale. Source: Wang et al. (2014).

SPEI	Drought category		Probability (%)
≥2	Extreme wet		2.3
1.5 to 1.99	severe wet		4.4
1 to 1.49	Moderate wet		9.2
0 to 0.99	Mild wet	near-normal	34.1
0 to -0.99	Mild drought	near-normal	34.1
-1.0 to -1.49	Moderate drought		9.2
-1.5 to -1.99	Severe drought		4.4
≤-2.0	Extreme drought		2.3

2.2 Drought monitoring and estimation in Southern Africa

Traditionally, the dry and wet periods in the region are identified using the percent of normal method (Unganai and Bandason, 2005). This method involves the calculation of a rainfall index, which is then expressed as a departure from long-term mean (e.g., Jury and Mwafulirwa, 2002; Mulenga et al., 2003; Nicholson et al., 2001; Reason et al., 2005). This method is very useful when computed for a homogenous region or a particular season, but may give spurious results when comparing drought conditions from two different locations, mainly due to the differences in the long-term mean from the two regions (GAR, 2011).

A considerable number of previous studies on drought over Southern Africa have used the SPI, which is officially endorsed by the WMO. For instance, Rouault and Richard (2005) used SPI to examine the intensity and spatial extent of droughts over Southern Africa; Manatsa et al. (2008)

used SPI to investigate how the Darwin sea level pressure anomalies can be used as predictors for Southern African droughts. In addition, Manatsa et al. (2010) used SPI to assess the multidimensional aspects of agricultural drought in Zimbabwe; Unganai et al. (2013) used SPI to tailor the seasonal climate forecast for climate risk management in the rain-fed farming system in Zimbabwe. The weighted SPI (Lyon 2004) was used by Lyon (2009) to study droughts and heat waves in Southern Africa. More recently, Dutra et al. (2014) used the index to investigate a probabilistic methodology for near-real-time meteorological drought monitoring. Furthermore, they also examined the feasibility of seasonal forecast of drought in four African basins including the Limpopo basin, which falls under our region of study.

Other drought indices have been also explored in the region. Some studies (e.g., Grist et al., 1997; Unganai and Kogan, 1998; Richard and Poccard, 1998; Anyamba et al., 2002) used the Normalized Difference Vegetation Index (NDVI). The NDVI was found to be a good proxy for droughts in Southern Africa and correlates well with ENSO (Anyamba et al., 2002, Phillipon et al., 2014). Although not common, agricultural drought indices have been also used in the region. For instance, Moeletsi and Walker (2012) used the Water Requirement Satisfaction Index (WRSI) to investigate the agricultural droughts over the Free State Province in South Africa.

More recently, some studies employed the newly developed drought index, the SPEI, to understand the characteristics of droughts in the region. For example, Ujeneza and Abiodun (2014) used the index to investigate to what extent GCMs simulate the drought regimes in Southern Africa. Subsequently, Araujo et al. (2014) employed the SPEI to study drought impacts on grape Yields in Western Cape, in South Africa. Edossa et al. (2014) have also used SPEI to investigate the impact of ENSO on drought over a catchment in central South Africa. The present study will also employ the SPEI method to characterize the droughts in Southern Africa.

2.3 Statistical techniques used for categorizing climate data

2.3.1 Empirical Orthogonal Functions

Empirical Orthogonal Functions (EOFs), also known as Principal Components Analysis (PCA, Jollife, 2002; Wilks, 2011), are one of the most common methods in use for interrogating climate data. They are mainly used for reducing large number of variables to smaller one (the principal components), which still retain most of the variability from the original dataset. EOFs are also used as a first step for other types of exploratory data analysis methods such as canonical correlation (CCA, Wilks, 2011). One of the main properties of the EOF methods is that the resulting principal components are orthogonal, i.e., they are uncorrelated and they are generated in a such way that the first principal component (PC) accounts for the large variance in the dataset, the second PC accounts for the second largest variance in the dataset, and so on.

The EOF method has been used for studying the Southern African climate (e.g., Richard et al., 2000; Manatsa and Mukwada, 2012; Ujeneza and Abiodun, 2014). For example, Manatsa and Mukwada (2012) used the PCA to identify rainfall homogenous regions over Zimbabwe and concluded that the first mode of the PCA was enough to represent the major rainfall patterns affecting the Zimbabwe. Ujeneza and Abiodun (2014) applied the PCA method to categorize droughts into different regimes. The Authors found that four modes of PCA, representing 50% of SPEI, were enough to capture the main drought regimes in Southern Africa. However, the EOF method doesn't perform very well in every situation. For instance, in the study by Ujeneza and Abiodun (2014), the remaining 50% percent of the SPEI variance over Southern Africa is not accounted for in the study. This may result in discarding an exceptional drought episode or categorizing it into a much broader EOF pattern, which is not representative of the unusual drought conditions. In fact, some studies (e.g., Skific et al. 2009; Bezeau et al., 2014) have reported that EOF analysis has problems in capturing rare events or accounting for new emerging patterns, mainly because EOF analysis is primarily a linear multivariate statistical method. Therefore, there is need for classifying droughts in Southern Africa using exploratory data analysis methods with no previous assumptions. This study is in that direction.

2.3.2 Cluster Analysis

Cluster Analysis (CA) is another popular method used for grouping datasets with some degree of similarity (Everitt et al., 2011). The technique seeks to group datasets or objects in such a way that the difference within a group is minimized while the difference among the groups is maximized (Hewitson and Crane, 2002; Everitt et al., 2011). There are two main algorithms used in order to perform the CA, namely hierarchical and partitioning algorithms (Rencher, 2002; Aggarwal and Reddy, 2014). In the hierarchical algorithm, all the objects are considered as different clusters, and then similar clusters are joined together gradually. The resulting cluster can be visualized in a structure with a shape of tree named dendrogram (Rencher, 2002, Wehrens, 2011). Examples of the hierarchical include the single linkage, complete linkage, average linkage and ward method, which are very common methods used in the climate data analysis. On the other hand, the partitioning algorithms involve choosing first a number of clusters. Examples of partitioning methods include K-means and K-medoids (Wehrens, 2011).
The CA has been used in a number of climate studies over Southern Africa (e.g., Landman and Mason,1999; Tennant and Hewitson, 2002; Fauchereau et al.,2009; Manhique et al.,2011; Cretat et al.,2012; Ash and Matyas,2012 ; Cretat et al., 2015; Favre et al.,2015). For instance, Landman and Mason (1999) employed the Ward's method to divide South Africa into eight homogenous regions while Ash and Matyas (2012) used the CA to group tropical cyclones in the Southwest Indian Ocean according to their trajectories.

2.3.3 Self Organizing Maps

Self Organizing Maps (SOMs), aka Kohonen Maps are a type of unsupervised artificial neural network used for a multitude of applications such as data clustering and reduction, data visualization, ordering multidimensional data and sampling (Kohonen 2001; Lobo, 2009). Generally, the algorithm compresses any multidimensional data into a 2D array of nodes that can also be called as neurons or units. The structure of the array is commonly rectangular but other shapes such as hexagonal and toroidal can also be used. The nodes resulting from the SOM analysis are organized in such a way that similar patterns are kept close to each other while non-resembling patterns are placed far from each other (Hewitson and Crane,2002; Sheridan and

Lee, 2011). The training of SOMs can be summarized in three fundamental steps (Lobo, 2009; Resta, 2012): first, for each input pattern "y" the algorithm calculates the Euclidian distance between "y" and all the neurons of the SOM array, and then it selects the neuron having the shortest distance from "y". This closest neuron is called winning neuron or Best Matching Unit (BMU). Finally, the algorithm adjusts the position of the nodes so that the topology of the SOMs array is preserved. These steps can be repeated many times.

The SOMs algorithm has an advantage over the traditional multivariate techniques such as Empirical Orthogonal Functions (EOF) or K-means clustering technique because of its intrinsic property of non-linearity as well as its topological order (Skific et al. 2009; Bezeau et al., 2014). For instance, node (4) in the SOMs algorithm is very close to nodes (3) and (5) showing a clear transition between them, but the same notion is not valid in the k-means clustering where the relationship between different clusters is not indicated (Agarwal and Skupin 2008; Wehrens 2011). SOMs are also superior to the EOF method (Bezeau et al., 2014). The EOF analysis accounts only for a certain percentage of variability in the dataset, whereas the SOMs analysis accounts for the full range of variability in the dataset.

SOMs analysis has been extensively used over Southern Africa (Tennant 2003; Tadross et al. 2005; Tennant and Reason 2005; Tumbo et al. ,2010; Mackellar et al. 2010; Tozuka et al., 2013; Maure,2013; Oettli et al.,2013; Engelbrecht et al. 2015; Abiodun et al.,2015). For example, Maure (2013) employed SOM to investigate the relevant synoptic patterns affecting the aerosol concentration in Southern Africa during the biomass burning season, whereas Abiodun et al. (2015) applied the algorithm to classify widespread rainfall events over Western Cape (South Africa). However, to our knowledge no one has used the algorithm to categorize drought patterns in Southern Africa. Given the above reasons, the present study will employ the SOMs algorithm.

2.4 Impact of remote and local sea surface temperatures on Southern African droughts

2.4.1 Impact of El Niño Southern Oscillation (ENSO)

Earlier studies (e.g., Richard et al. 2000; Richard et al., 2001) have devoted their attention to identifying drought triggers in Southern Africa. In this regard, ENSO was reported as being the chief cause of drought events in the region. For example, Rouault and Richard (2005) investigated the intensity and spatial extent of droughts in Southern Africa for a period of 99 years (1901-1999) and concluded that over 66 percent of severe droughts in the region are ENSO-related. In addition, they found that this link between ENSO and droughts in the sub-region was stronger after 1970s. In fact, prior to 1970s the summer droughts in Southern Africa were strongly linked to regional SSTs, more specifically with SSTs over the southwestern Indian Ocean (Richard et al., 2000; Richard et al., 2001; Fauchereau et al., 2003). Although the relationship between ENSO and precipitation in Southern Africa is not linear, different studies have established that La Niña years are generally associated with wet conditions, whereas El Niño years are associated with dry conditions over the region (e.g., Ropelewski and Halpert, 1987; Kruger, 1999; McHug and Rodgers, 2000; Camberlin et al., 2001; Reason and Jagadheesha, 2005).

During the El Niño years, a continental high pressure centre dominates over Southern Africa and suppresses convection and rainfall in the region, due to the changes in the Walker Circulation (Reason et al., 2000; Mulenga et al., 2003). Walker Circulation is an east-west overturning circulation pattern originated by a zonal distribution of heat in the continent and oceans around the tropics (Sandeep et al. 2014). In austral summer, during non-ENSO conditions, Southern Africa is dominated by a rising branch of the Walker Circulation. As result, convection takes place and rain-bearing clouds are created (Glantz, 2001). However, during El Niño events, the Walker Circulation suffers mutation; the zonal flow towards west in the Pacific Ocean weakens, allowing warm waters in the west to shift eastwards along the equatorial belt. As a consequence, the African Walker cell is characterized by a divergence at low level and convergence aloft, hence inhibition of precipitation over Southern Africa (Ratnam et al., 2012).

During La Niña events, the oceanic and atmospheric conditions resemble the ones observed during normal conditions, with exception that they are now stronger (Trujillo and Thurman, 2011). The intensification of the Walker branch over Africa enhances moisture convergence inland and favours the formation of Tropical Temperate Troughs (TTTs, Harrison 1984; Todd and Washington, 1999; Washington and Todd, 1999; Todd et al., 2004, Fauchereau et al., 2009; Pohl et al., 2009; Manhique et al., 2011; Hart 2010). TTTs are Northwest-Southeast oriented cloud bands which are formed as a result of interaction between tropical and mid-latitude systems and they are responsible for most of the convection and summer rainfall over Southern Africa (Vigaud et al., 2012; Macron et al., 2014). The TTTs systems generally develop inside the South Indian Convergence Zone (SICZ, cook, 2000, Vigaud et al., 2012). As defined by Cook (2000), SICZ is a Land-Based Convergence Zone (LBCZ) which extends from the southeastern coast of Southern Africa all the way into the Indian Ocean, and it is associated with profuse rainfall over the region. According to Manhique et al. (2011), the SICZ is located over the coterminous Southern Africa during the La Niña events, hence heavy downpours are favoured. For instance, an active SICZ in January 2013 accompanied by La Niña conditions caused heavy rainfall and flooding conditions in Central and Southern Mozambique, claiming at least 100 lives and displacing about 200 thousand people (Manhique et al., 2015).

It has been also recognized that ENSO impacts on Tropical Cyclone activities in the southwest Indian Ocean (SWIO). ENSO exerts an impact on the genesis and trajectories of tropical cyclones in the SWIO (Vitart et al., 2003; Ash and Matyas, 2012; Kuleshov, 2012, Malherbe et al., 2013). For instance, Kuleshov (2012) suggested that during El Niño years the tropical cyclone genesis is above normal over the western side of the SWIO (west of 85˚E) and below normal over the eastern side of the basin (east of 85˚E), while during the La Niña years the reverse is generally observed. The frequency of tropical cyclones has an impact on drought, for example a landfall of a tropical cyclone can terminate or ameliorate a drought situation because of the associated rainfall (Maxwell et al., 2013).

In recent decades, two different “flavours” of El Niño have been discovered in the Pacific Ocean (Ashok et al., 2007; Yeh et al., 2009). During the typical El Niño, the SST anomalies are anomalously warm in the eastern side of the Pacific Ocean and anomalously cold in the western

side of the Pacific Ocean. This type of El Niño event is referred as canonical El Niño or Eastern Pacific El Niño (Yeh et al., 2009; Ashok and Yamagata, 2009). However, there are moments when the SST anomalies are warm over the central Pacific and extremely cold in western and eastern Pacific Ocean. This type of El Niño is known as Central Pacific El Niño (CP), dateline El Niño, warm pool El Niño or El Niño Modoki (Yeh et al., 2009; Ashok and Yamagata, 2009). Modoki is a Japanese expression for "a similar but different thing" (Ashok et al., 2007). Indeed, these two types of El Niño are similar but are associated with different impacts. For example, El Niño Modoki was reported to cause different impacts in different countries around the World (Ratnam et al., 2011). Over Southern Africa, the canonical El Niño triggers more severe droughts than the El Niño Modoki (Ratnam et al., 2014). This less impact of the Modoki it is due to its weak impact on the Walker circulation (Ratnam et al., 2014). This classification of ENSO in the Pacific Ocean was reported to not account for all the ENSO-related SST features. Consequently, a further classification of the ENSO events was proposed by Johnson (2013), who categorized ENSO signatures into four El Niño and Four La Niña groups. Among the four El Niño types classified by Johnson (2013), only one matches the canonical El Niño event, namely El Niño type 4 (EN4), while other three (EN1, EN2 and EN3) represent different flavours of the Modoki Niño (Hoell et al., 2014). With regard to the four La Niña types, two exhibit EP features (LN1 and LN4) while others (LN3 and LN4) show CP features (Hoell et al., 2014). Hoell et al. (2014) found that the impacts of the four types of El Niño over Southern Africa are also distinct. For example EN4, the EP El Niño, is associated with widespread dry condition over the region while EN1 is associated with above rainfall conditions over a large area of Southern Africa (Hoell et al., 2014). With respect to La Niña types, the Authors found that all La Niña flavours induce wet conditions south of 10˚S, though less evidence with the LN3 event.

2.4.2 Impact of the Antarctic Oscillation (AAO)

The Antarctic Oscillation is the leading mode of climate variability south of 20˚S in Southern Hemisphere (Thompson and Wallace, 2000; Reason and Rouault 2005; Pohl et al., 2010). The physical mechanisms involved on the manifestation of the AAO have been investigated by Lorentz and Hartman (2001) and Codron (2005), who found that interactions of eddy-mean flows are at the origin of this seesaw behaviour of seal level pressure in the Southern

Hemisphere. Studies (e.g., Reason and Rouault 2005; Reason et al.,2006) have linked the AAO with rainfall over Southern Africa, especially over the Western Cape Province of South Africa during the austral winter (JJA) season. For example, Reason and Rouault (2005) found that in general a positive phase of AAO is likely to induce wet conditions over western South Africa while a negative phase is likely to provoke dry conditions over the same area. In recent studies, scientists have pointed out that the AAO is exhibiting a marked positive trend since the late 1950s (e.g., Bridgman and Oliver, 2006). With this scenario, one could expect more wet winters over the Western Cape, however some other studies (e.g., Pohl et al. 2010) have argued that the AAO doesn't act in isolation. For instance, Pohl et al. (2010) reported that AAO is intrinsically tied to the ENSO phenomenon in the Pacific Ocean. The Authors found that the impact of AAO on the Southern Africa rainfall is negligible when the impact of ENSO is removed. In fact they found that the positive phase of the AAO is more likely to produce wet conditions over Southern Africa when it co-occurs with La Niña conditions. Similarly, the negative phase of AAO is likely to produce below normal rainfall conditions over Southern Africa if it occurs in conjunction with the El Niño. However, there is still some controversy about the Impact of ENSO on rainfall over the Western Cape Province of South Africa. Some studies (e.g., Reason and Rouault, 2005; Blamey and Reason, 2007) have found no relationship between ENSO and winter rainfall over Western Cape, while a recent study by Philippon et al. (2011) concluded that there is a link between ENSO and rainfall. The Authors reported that there is indeed a significant positive correlation between ENSO and rainfall since 1976/77 during the May-June-July (MJJ) season. According to these Authors, during the El Niño episodes the Western Cape region of South Africa experiences above normal seasonal rainfall totals accompanied by longer wet spells and high frequency and intensity of rains. As opposed to that, La Niña events are associated with a deficit in rainfall total as well as shorter wet spells and lower intensity of the rain.

2.4.3 Impact of local sea surface temperatures

Previous research efforts (e.g., Rocha and Simmonds, 1997; Washington and Preston,2006; Williams et al.,2010) have also focused on understanding the role played by the Atlantic and Indian Oceans in triggering or terminating drought events in Southern Africa. A comprehensive understanding of the behaviour of these surrounding waters was believed to improve the seasonal

forecast of the rains in the region (e.g., Jury, 1996; Makarau and Jury, 1997; Jury, 1998; Jury et al., 1999). In this section we present the impact exerted by both Atlantic and Indian Oceans on the climate variability over Southern Africa.

2.4.3.1 Atlantic Ocean

Unlike in the Pacific Ocean, which has ENSO as the dominant mode of variability, it is difficult to single out a leading mode in the Atlantic Ocean. However, some studies (e.g., Morioka et al., 2011; Wainer et al., 2014) have identified the Benguela Niño and the South Atlantic Subtropical dipole (SASD) as important variations of SST having impact over Southern Africa. Although the nature of the Benguela Niño variability is not yet fully understood, previous research work has established a link between this phenomenon and the precipitation over Southern Africa including Brazil (Shannon et al., 1986; Florenchie et al., 2003; Reason et al., 2006; Hansingo and Reason, 2009; Grim and Reason, 2011). As opposed to the El Niño events in the Pacific Ocean, a Benguela Niño episode is associated with above normal rainfall conditions in Angola and Namibia, which in some occasions creates floods and negative impacts on the socio-economic activities in these countries (Reason et al.,2006; Rouault et al., 2007). For example, Benguela Niños have been reported to impact negatively on fishery activities (Rouault et al., 2003; Reason et al., 2006).

The SASD has been also a subject of study in the Atlantic Ocean (Venegas et al., 1997; Fauchereau et al., 2003; Hermes and Reason, 2005; Morioka et al., 2011). The study by Venegas et al. (1997) was among the first one recognizing the existence and the importance of the SASD. Venegas et al. (1997) used both Empirical Orthogonal Functions (EOF) and Singular Value Decomposition techniques (SVD) to investigate SSTs and SLP in the Atlantic Ocean and concluded that the strengthening and weakening of the St Helena high pressure centre was responsible for a dipole-like structure of SSTs in the Atlantic Ocean. They also reported that the dipole-like pattern in SST had a northeast-southwest orientation and was stronger during the austral summer period. Further studies (e.g., Fauchereau et al., 2003, Hermes and Reason, 2005; Morioka et al., 2011) confirmed the previous work and reported that the positive phase of the SASD is generally associated with above normal rainfall conditions over Southern Africa while the negative phase of the SASD is more likely to bring about droughts in the region.

2.4.3.2 Indian Ocean

Indian Ocean dipole (IOD, Saji et al., 1999) and the Indian Ocean Subtropical Dipole (IOSD, Hermes and Reason, 2005; Kataoka et al., 2012) are the dominant modes of SST in the Indian Ocean that have impact on Southern African Climate. Previous research work conducted by Behera et al. (2000) and by Behera and Yamagata (2001) found that the IOSD generally develops during the summer period and it is associated with a modification of the Mascarene high pressure centre in the Indian Ocean. Subsequent studies (Fauchereau et al., 2003; Hermes and Reason, 2005) agreed with the findings from Behera and Yamagata (2001) and suggested that the large-scale forcing of the IOSD is similar to a wavenumber 3 or 4 spatial structure in the Southern Hemisphere. More recently, some other studies (e.g., Morioka et al., 2012) highlighted the importance of the mixed-layer in modulating the IOSD. For instance, during the positive phase of the IOSD, which is characterized by warm SST anomalies over the southwestern Indian Ocean, the Mascarene high reduces the latent heat flux loss resulting in a thinner layer thickness over the southwestern side of the dipole (Morioka et al., 2012; Kataoka et al., 2012). In general, the positive phase of the IOSD is associated with wet summers over Southern Africa due to enhanced convective activities over the region (Kataoka et al., 2012).

Indian Ocean dipole is another dominant mode over the Indian Ocean. It was identified by Saji et al. (1999), who using 40 years of observations found that IOD was the second leading mode of SST variability in the Indian Ocean, accounting for 12% of variability. The IOD is observed over the Tropical Indian Ocean and was reported to develop during the austral winter and reach its mature phase during the austral spring (Liu et al., 2014; Weller et al., 2014). More recently, Guo et al. (2015) classified the IOD into three types. The first IOD type is ENSO-related and is triggered by the anomalous walker circulation. The second type of IOD occurs a year after an El Niño or La Niña event. The third type of IOD is completely independent of ENSO. However, there is still an ongoing discussion about the independence of the IOD from the ENSO phenomenon. Some studies (e.g., Behera et al 1999; Webster et al,1999; Yamagata et al.,2003) suggested that IOD is indeed independent from ENSO, while other studies (e.g., Chamber et al.,1999; Dommenget and Latiff 2002; Dommenget, 2007, 2011) refute this theory. For instance, Dommenget and Lattif (2002) suggested that the dipole mode found by Saji et al. (1999) could be a result of poor interpretation of EOF analysis. Furthermore, Dommenget (2011) advocated

that the Dipole Mode Index (DMI) used as a proxy for the IOD doesn't represent any teleconnection. Zhao and Nigam (2015) also drew a similar conclusion. These authors question the idea of independence of IOD from ENSO mainly because the DMI is partially correlated (r ≈0.7) with the Principal Component analysis timeseries from the second EOF mode and it is also correlated (r ≈0.35) with Niño3.4 timeseries.

2.5 Performance of Climate Models in Simulating the Southern African Climate

2.5.1 Global Climate Models

The first climate modelling efforts in the region were reported in early 1990s (e.g., Hewitson and Crane 1994; Joubert, 1995, 1997; Joubert and Mason, 1996; Joubert and Tyson, 1996). Several research studies focused on improving the rainfall seasonal forecast over the region (e.g., Tennant, 1999; Landman et al., 2009; Landman et al., 2012; Landman and Beraki, 2012) while others attempted to investigate the impact of climate change over Southern Africa (e.g., Joubert, 1997; Joubert and Hewitson, 1997; Mason and Joubert 1997; Lyon; 2009). GCMs experiments have been also performed in order to understand the impact of SST on the Southern African Climate (e.g., Rocha and Simmonds, 1997; Reason and Jagadheesha 2005; Hansingo and Reason, 2009). For example, Rocha and Simmonds (1997) carried out a series of sensitivity tests, forcing a GCM with different SST anomalies associated with drought conditions in Southern Africa. The Authors confirmed the effect of ENSO on droughts over Southern Africa but found no link between SSTs in the Atlantic and droughts over Southern Africa. Hansingo and Reason (2009) also modelled the atmospheric response of the Southern African region to different SST anomalies associated with Benguela Niños. Reason and Jagadheesha (2005) investigated the recent impacts of ENSO over Southern Africa using a GCM and concluded that the model had problem in capturing the impacts of ENSO over Southern Africa. More recently, Klutse et al. (2015) examined the capability of two GCMs in simulating rainfall and circulation patterns during the ENSO years. The Authors found that both GCMs don't agree entirely with the observations, the models were capable of simulating the relationship between ENSO and rainfall in Southern Africa only for some areas of the domain (e.g., southwest Democratic Republic of Congo and Northern Angola), whereas for other sub-regions (e.g., Tanzania and Northern Mozambique) the models showed discrepancies with the observations. Tanzania and Northern

Mozambique fall under the region where the Pacific SSTs are highly correlated with rainfall, therefore the poor performance of both GCMs over this region is symptomatic of problems with GCMs. The present study tries to understand how the same link between ENSO and rainfall over Southern Africa can be represented in the RCMs.

2.5.2 Regional Climate Models

As stated in previous sections, the GCM predictions and projections of regional scale features are subject to biases, mainly because of their low horizontal grid resolution. As a way of enhancing the skill of GCM results, Regional Climate Models (RCMs) with higher resolution are usually used to downscale the global scale from the GCM simulations to regional scale. Various studies have successfully used this approach over Southern Africa (e.g. Joubert et al., 1999; Hudson and Jones, 2002; Tadross et al., 2005; Tadross et al.,2006; Kgatuke et al., 2008; Mackellar et al.,2010; Haensler et al., 2011; Engelbrecht et al., 2002, 2009, 2013; Ratnam et al., 2012, 2013, Diallo et al.,2014). However, there has been a controversy on the capability of RCMs in faithfully representing the link between ENSO and the Southern Africa rainfall (Hudson and Jones, 2002; Boulard et al., 2013; Ratnam et al., 2013). For instance, Boulard et al. (2013) used the Weather Research and Forecasting (WRF) model, driven by a global reanalysis dataset, to examine the capability of the model in reproducing the influence of El Niño conditions over Southern Africa in the 1971-1998 period and found that the model performed poorly in downscaling the influence of ENSO on rainfall. Using the same WRF model, forced by the same global reanalysis dataset, Ratnam et al. (2013) argued that the model performs well in simulating the ENSO-induced interannual variability of rainfall over Southern Africa in 1991-2011. All these studies represent customized and isolated efforts of studying the influence of ENSO on drought over Southern Africa, and are based on a single model realization of one RCM and single lateral boundary-forcing. Hence, owing to differences in model physics, there is a need to study the link between ENSO and Southern African droughts using a set of RCMs forced with the same boundary condition. Recently, a Coordinated Regional Climate Downscaling Experiment (CORDEX; Jones et al., 2011) that meets this criterion was released by the World Climate Research Programme (WCRP). CORDEX provides a unique and new set of climate

projections dynamically downscaled, using different RCMs over different domains around the world, including Africa. Hence, the present study explores this unique opportunity to investigate how the RCMs simulate the link between ENSO and droughts over Southern Africa.

2.5.2.1 CORDEX RCMs

Several studies have been conducted in order to assess to what extent the CORDEX Models simulate the regional climate details around the designated domains. Over Africa, studies have been also carried out at continental scale (Nikulin et al.,2012; Laprise et al.,2012; Panitz et al., 2014; Kim et al., 2014; Dosio et al.,2015; Dosio and Panitz,2015) as well as at regional level (Kalognomou et al.,2013; Gbobaniyi et al., 2013; Endris et al., 2013; Shongwe et al. 2014; Klutse et al., 2014; Favre et al., 2015, Abiodun et al. 2015; Endris et al. 2015; Haile and Rientjes,2015; Mounkaila et al.,2015). Overall, the results from the CORDEX RCMs simulations are very encouraging. All the studies confirm that the CORDEX RCMs simulate well the temporal and spatial distributions of precipitation over the African domain. However, some biases can be found in some sub-regions as well as during some seasons. All the studies also agree on the fact that the multimodel ensemble mean outperforms any individual RCM in the CORDEX set.

There is an ongoing debate on how different Lateral Boundary Conditions (LBC) can impact the quality RCM outputs. For example, Laprise et al. (2012) examined the added value introduced by the downscaling process over the African CORDEX domain. They examined the performance of the Canadian Regional Climate Model forced by ERA-Interim reanalysis and by two GCMs, and found that errors in the LBC had an impact on the RCM's skill in simulating some of the regional-scale features. Similar conclusion was drawn by Endris et al. (2015), who investigated the ability of CORDEX models in simulating the teleconnection responses over Eastern Africa. The authors found that when RCMs were forced by perfect lateral boundary conditions (Reanalysis dataset) they reproduced a very similar pattern as in the observations. However when the RCMs were forced with different GCMs they yielded different results. More recently, Abiodun et al. (2015) investigated how climate models simulate extreme rainfall events over

Western Cape (South Africa) and found that different GCM boundary conditions did not have a great impact on the spatial pattern of the extreme rainfall threshold over Western Cape. Furthermore, Dosio and Panitz (2015) used the COSMO RCM driven by four GCMs to understand climate change projections over the African Domain. They found that in some regions of Africa, the rainfall trend between the RCM and the four GCMs where diverging. The present study also investigates how the quality of LBC condition may affect the capability of a RCM in simulating the link between ENSO and droughts over Southern Africa.

3 : Data and Methods

This chapter describes in detail the datasets and methodologies applied to achieve the objectives of the study. Section 3.1 provides the details of the datasets from the observations, reanalysis and models. It also describes the several climate indices used to investigate the link between the atmospheric teleconnections and droughts in Southern Africa. Section 3.2 gives an overview of differente techniques used in the study in order to cluster Southern Africa droughts into different groups and assess the performance of the CORDEX RCMs in capturing those drought patterns.

3.1 Data

3.1.1 Observations

3.1.1.1 Climate Research Unit (CRU)

We employed monthly precipitation (PRE) and mean temperature (TMP) from the Climate Research Unit Time Series 3.22 (CRU TS3.22, Harris et al. 2014). CRU TS3.22 is a high-resolution (0.5˚X0.5˚grid resolution) dataset which covers the entire globe excluding the oceans. It is based upon information from meteorological rain gauge stations and span from January 1901 to December 2013. This dataset include other variables such as minimum temperature (TMN), maximum temperature (TMX), vapour pressure (VAP), cloud cover (CLD), rain days (WET), frost days and potential evapotranspiration (PET). The PET was generated using the Penman-Monteith formula. Here, we used CRU dataset to generate SPEI values for two different periods, namely 1950-2013 and 1989-2008. CRU TS.322 can be freely downloaded from the British Atmospheric Data Centre (BADC) website: http://badc.nerc.ac.uk/data/cru.

3.1.1.2 University of Delaware (UDEL)

We also used monthly precipitation and mean temperature gridded data from University of Delaware (UDEL), version 3.01. Similar to the CRU dataset, the UDEL dataset covers land only, with a grid resolution of 0.5˚X0.5, spanning from 1900-2010 (Legates and Willmott, 1990). UDEL dataset is mainly sourced from the Global Historical Climatology Network (GHCN) and Global Summary of the Day (GSOD) records. In this study, the UDEL dataset was used to

calculate SPEI values, which were compared against the SPEI from CRU. The UDEL data can be downloaded at http://www.esrl.noaa.gov/psd/data/gridded/data.UDel_AirT_Precip.html.

3.1.1.3 Extended Resconstructed Sea Surafce Temperatures (SST)

Extended reconstructed SSTs (ERSST, Smith et al., 2008) are monthly SST values based on the International Comprehensive Ocean-Atmosphere Data (ICOADS) SST. The dataset uses statistical methods for filling in the missing values. It spans from January 1854 to present and has 2˚x2˚ horizontal grid spacing. However, because of the very sparse data, the first 26 years from dataset are generally discarded. Here, we used the version 3b (v3b) of the dataset. The main difference between this version and the previous one is that v3b doesn't include satellite inputs which were reported to affect negatively the observations. In the present study, ERSST data were used to calculate different climate indices and to generate composite analyses. The ERSST data can be freely sourced from the USA National Oceanic and Atmospheric Administration (NOAA) website: http://www.esrl.noaa.gov/psd/data/gridded/data.noaa.ersst.html.

3.1.2 Reanalysis

We used two different reanalyzes data for this study. The first dataset is the European Centre for Medium-Range Weather Forecasts (ECMWF) ERA-Interim reanalysis data (ERAINT; Dee et al., 2011). ERA-interim is a global atmospheric reanalysis dataset originally created to replace the ERA40 reanalysis dataset, which was reported to have problems with the satellite information (Dee et al., 2011). Initially, ERAINT was generated from January 1989 up until present but, currently it encompasses the period 1979-present. It has a 0.75˚X0.75˚ grid resolution and 60 vertical levels. For the consistence of the fields in the ERAINT, the system utilizes a 4-dimensional variational analysis (4D-var) technique for data assimilation. In the present study, ERAINT dataset was used to drive the 10 CORDEX RCMs under scrutiny. The ERAINT dataset can be freely obtained from http://apps.ecmwf.int/datasets/data/interim-full-daily/.

The second reanalysis dataset was sourced from the 20th Century Reanalysis project (20CR, Compo et al. 2011). 20CR is a global atmospheric circulation dataset which assimilates only surface pressure and uses monthly SST and sea-ice as boundary conditions. Unlike the ERAINT,

20CR uses Ensemble Kalman Filter approach (EKF) for data assimilation and covers the period 1871-2011, which provides a lengthy record for the assessment of Global climate models. This dataset has 2˚x2˚ grid spacing and was reported to be the best reanalysis product over Southern Africa (Zhang et al. 2012). In this thesis, we used 20CR dataset to investigate the circulation anomalies associated with each drought pattern. This data set is freely available for download at http://www.esrl.noaa.gov/psd/data/gridded/data.20thC_ReanV2.html.

3.1.3 Climate Indices

For predictive purpose, we examined the relationship between atmospheric teleconnections and drought patterns in Southern Africa. In the examination, we focused on austral summer (DJF), because it is the rainy season for most part of Southern Africa. The different climate indices used in the study are described below. Apart from the Antarctic oscillation that is based on Sea Level Pressure, all other indices are based on SST. Therefore, all SST-based indices were calculated using the ERSST dataset.

3.1.3.1 Oceanic Niño Index (ONI)

The Ocean Niño Index is one of the most common indices employed to monitor ENSO. It measures the the departure of SST anomalies from their normal in the equatorial eastern Pacific Ocean. The index is calculated as as a 3-moth running mean of SST anomalies in the Niño 3.4 region (Fig.3.1). El Niño (La Niña) situation is declared when the ONI is above (below) +0.5˚(-0.5˚) for five consecutive months. In this work, we calculated our own ONI, which was used to investigate the link between ENSO and droughts in Southern Africa.

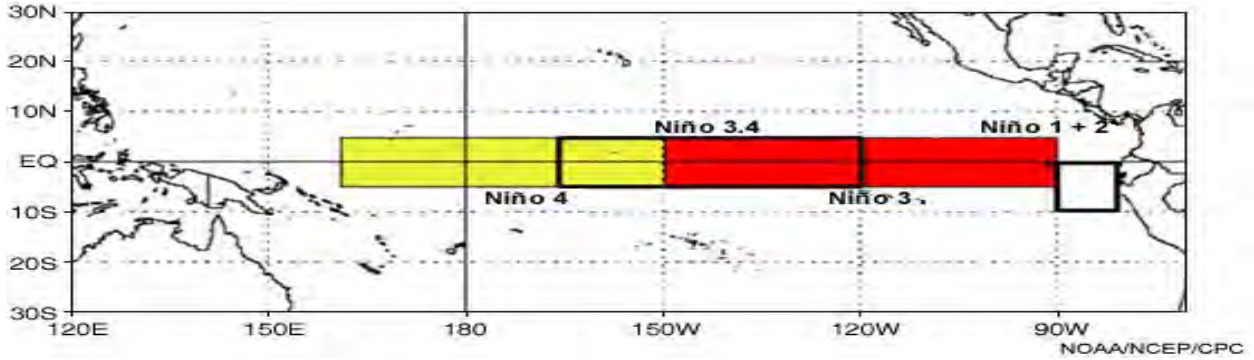

Figure 3.1: Schematic representation of the Niño regions in the Pacific Ocean. Source **www.meted.edu.com.**

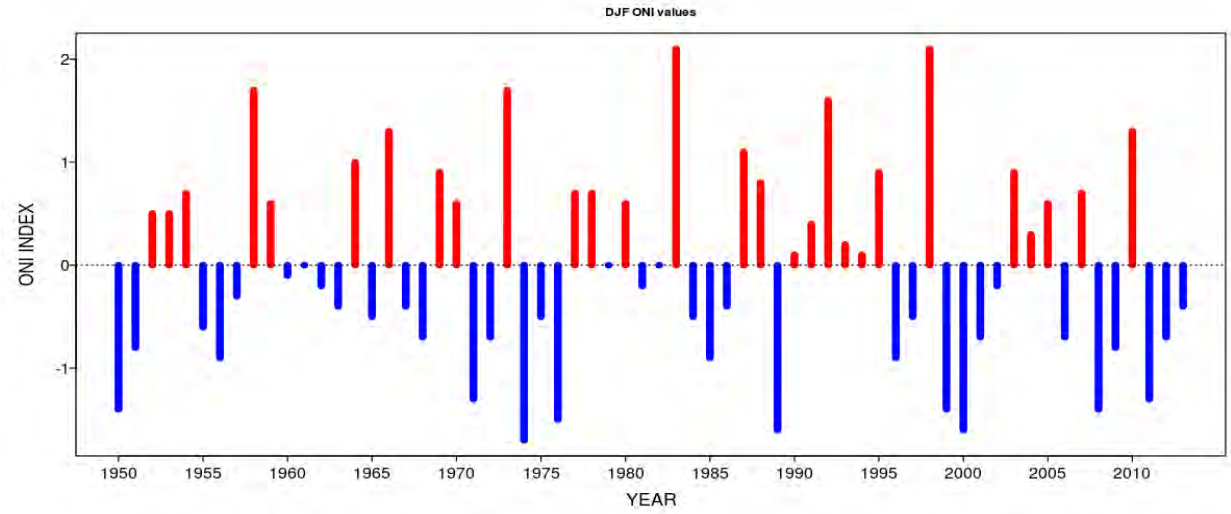

Figure 3.2: ONI values during the austral summer (December-January-February) period. Positive values represent warm phase of ENSO while negative values represent negative phase of ENSO phenomenon.

3.1.3.2 Multivariate ENSO Index (MEI)

The Multivariate ENSO index (MEI) is another index used for monitoring ENSO conditions in the Pacific Ocean. It is a bimonthly (e.g., February-March, March-April,…, November-December) ENSO index based on six variables (sea level pressure, zonal and meridional surface winds, sea surface temperatures, surface air temperature and total cloudiness fraction of the sky) observed over the tropical Pacific region. The MEI is represented by the first unrotated principal component analysis performed on the six meteorological variables. Positive MEI values represent El Niño conditions, while negative MEI values indicate La Niña conditions.

The MEI has been previously applied to study the connection between ENSO and drought in many parts of the world (e.g., Andrews et al., 2004; Hallack-Alegria et al., 2012) including our study region (e.g., Fauchereau et al., 2009; Boulard et al., 2012). In this study, we also used the MEI to investigate the link between ENSO and droughts in Southern Africa. The MEI data for the 1989-2008 period were obtained from the NOAA Earth System Research Laboratory website (http://www.esrl.noaa.gov/psd/enso/mei/table.html). An example of MEI time series is shown in Fig. 3.3.

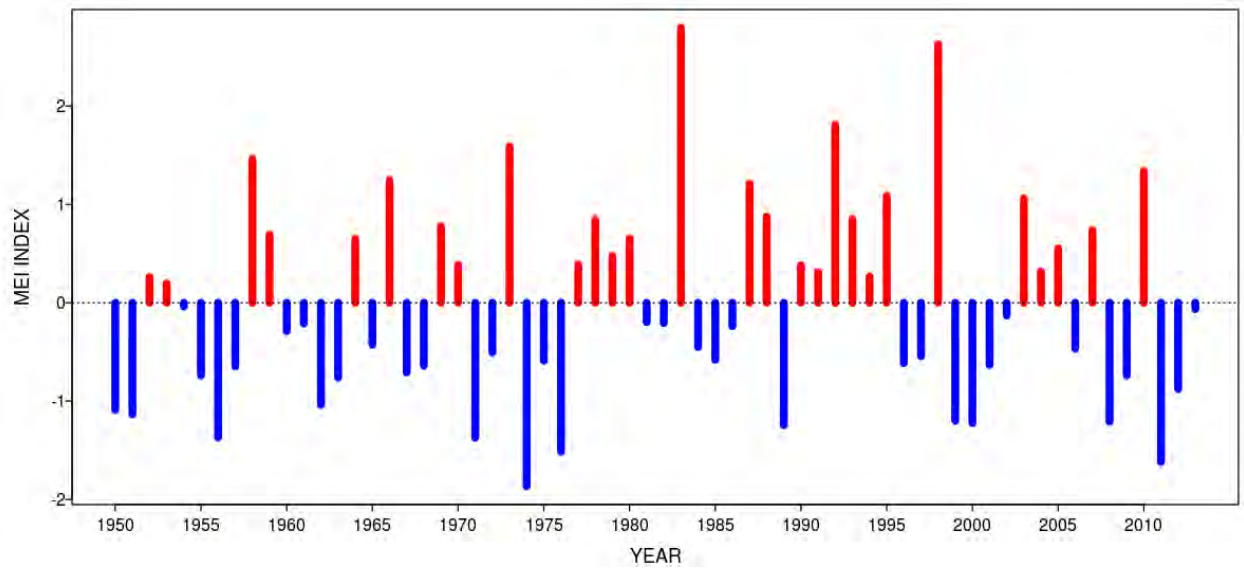

Figure 3.3: MEI time series for the austral summer period. Red colour shows positive values (El Niño conditions) while blue colour represents negative values which can lead to La Niña conditions in the eastern equatorial Pacific Ocean.

In this study, we used both ONI and MEI to investigate the impact of ENSO on droughts in Southern Africa. There is a good agreement between the two indices. In fact, the correlation between them is r=0.97 (Fig.3.4).

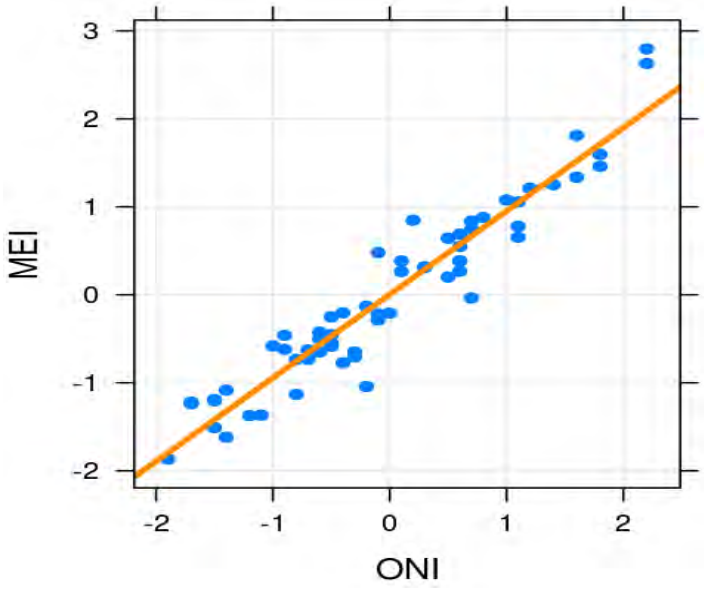

Figure 3.4: Scatter plot of ONI and MEI indices. The dark orange line represents the line of best fit .

3.1.3.3 The Dipole Mode Index(DMI)

The Dipole Mode Index is used to monitor the Indian Ocean dipole mode. It is calculated as the difference between the western (50˚E-70˚E,10˚S-10˚N) and the eastern(90˚E-110˚E,10˚S-Equator) indian equatorial SST anomalies (Fig.3.5). Positive DMI values reprent a positive IOD while negative DMI indicates a negative phase of the IOD (Fig.3.6).

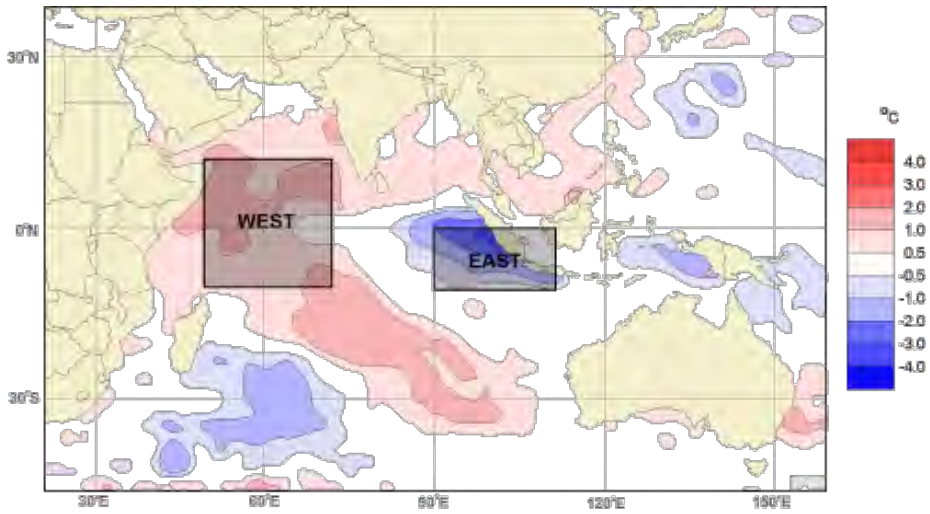

Figure 3.5: SST anomalies during a positive IOD event in 1997. Western and Eastern regions in the Indian Ocean used to generate the DMI are represented in boxes. Source: The Australian Bureau of Meteorology: http://www.bom.gov.au/climate/IOD/about_IOD.shtml.

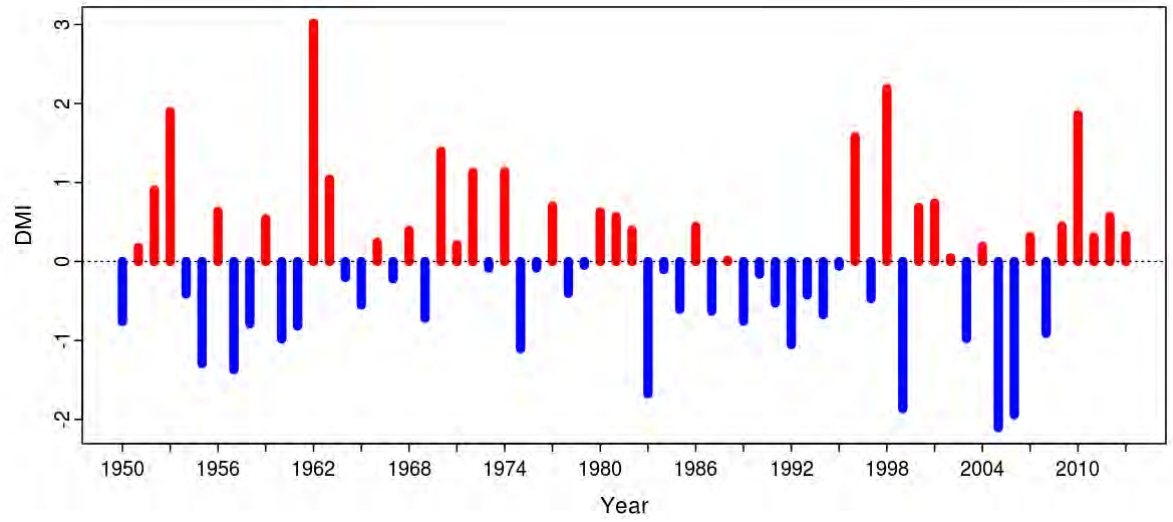

Figure 3.6: DMI timeseries for the austral summer. Red values represent positive phase while blue values represent negative phase of the index.

3.1.3.4 Benguela Niño Index (BNI)

The Benguela Niño Index (BNI) was calculated as in Grim and Reason (2011). Using the ERSST dataset we calculated the SST anomalies over a box (10˚-28˚S,8˚-15˚E), which is located off the coast of Angola. Positive phases of the BNI are identified when the SST anomalies are equal to or greater than one standar deviation, whereas the negative events of BNI are identified when the index is equal to or less than minus one standard deviation.

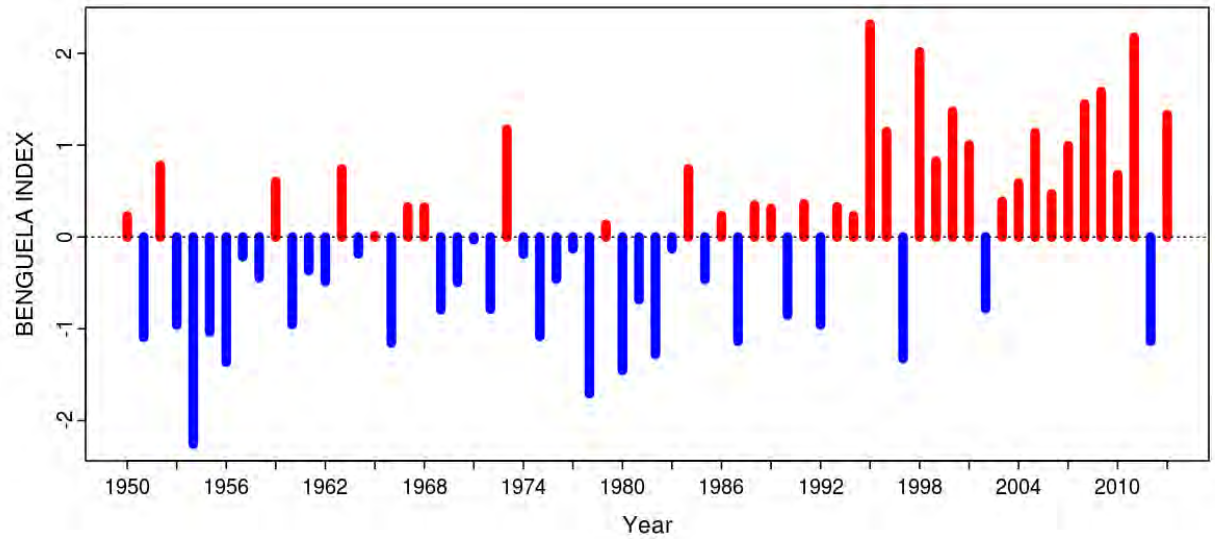

Figure 3.7: Summer Benguela Niño timeseries. Red colour shows a positive values while blue colour represents negative values of the BNI.

3.1.3.5 The Antartic Oscillation (AAO)

The Antartic Oscilaltion index was taken from the NOAA's Earth System Laboratory (http://www.esrl.noaa.gov/psd/data/20thC_Rean/timeseries/monthly/AAO/). It is generated by the leading mode of principal component analysis of monthly sea level pressure over south of 20˚S, in the Southern Hemisphere. Prior to the calculation of the AAO index, the monthly Sea level Pressure values are weighted using the the square root of the cosine of latitude and then are projected back onto the loadings and standardized in order to create timeseries of principal component analysis (Thompson and Wallace,2000).

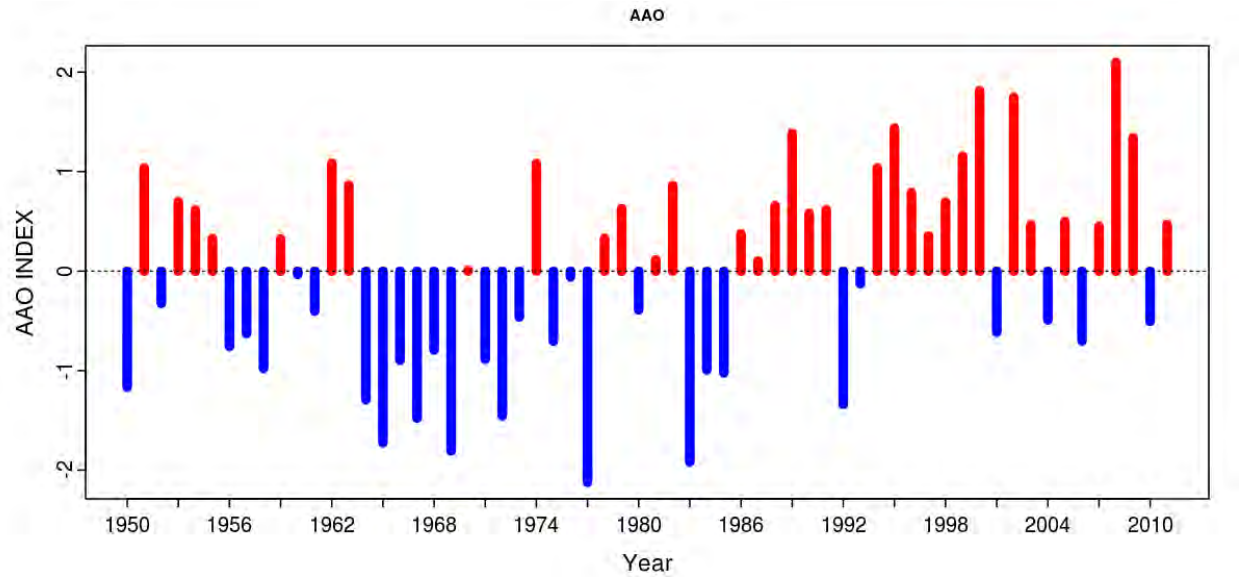

Figure 3.8: Summer AAO timeseries. Red colour represents positive events while negative colour represents negative events.

Using the ERSST data we also generated the South Atlantic Subtoprical Index (SASDI) and the Indian Ocean Subtropical Dipole Index (IOSDI). The SASDI was calculated as the difference between southwestern (30˚W-10˚W, 40˚S-30˚S) and north-eastern (0-20˚W; 25˚S-15˚S) poles in the Atlantic Ocean. On the other hand, IOSDI was calculated as the difference between western (55˚E-65˚E; 37˚S-27˚S) and north-eastern (90˚E-100˚E; 28˚S-18˚S) SST anomalies in the Indian Ocean.

3.1.4 Models

The simulation data are results of ten RCMs that participate in the CORDEX Project. The CORDEX RCMs used in the present study (Table 3.1) were driven by ERA-Interim reanalysis data and cover the entire African domain (Fig.3.9) with a horizontal grid spacing of 0.44^{o}. The RegCM3 model uses the National Oceanic and Atmospheric Administration (NOAA) weekly optimum interpolated sea surface temperature (Reynolds et al. 2007) while the CRCM model uses sea surface temperature (SST) from the Atmospheric Model Intercomparison project, phase 2 (AMIP2). The remaining RCMs in the CORDEX set use SST from ERAINT as the ocean boundary conditions (Nikulin et al., 2012). The study domain of the present study is Southern

Africa (Fig.3.9). The simulated data cover a period of 19 years (1989-2008). We also analysed seasonal precipitation and temperature data from seven GCMs (Table 3.2) that participated in the Fifth Phase of Coupled Model Inter-comparison Project (CMIP5; Taylor et al., 2012; http://cmip-pcmdi.llnl.gov). The historical simulations of these GCM were downscaled to 0.44˚ using the Rossby Centre (SMHI) regional climate model (RCA4; Samuelsson et al., 2011). The historical simulations of the GCMs extend from 1951 to 2005, but the present study focuses on 1989-2005 period.

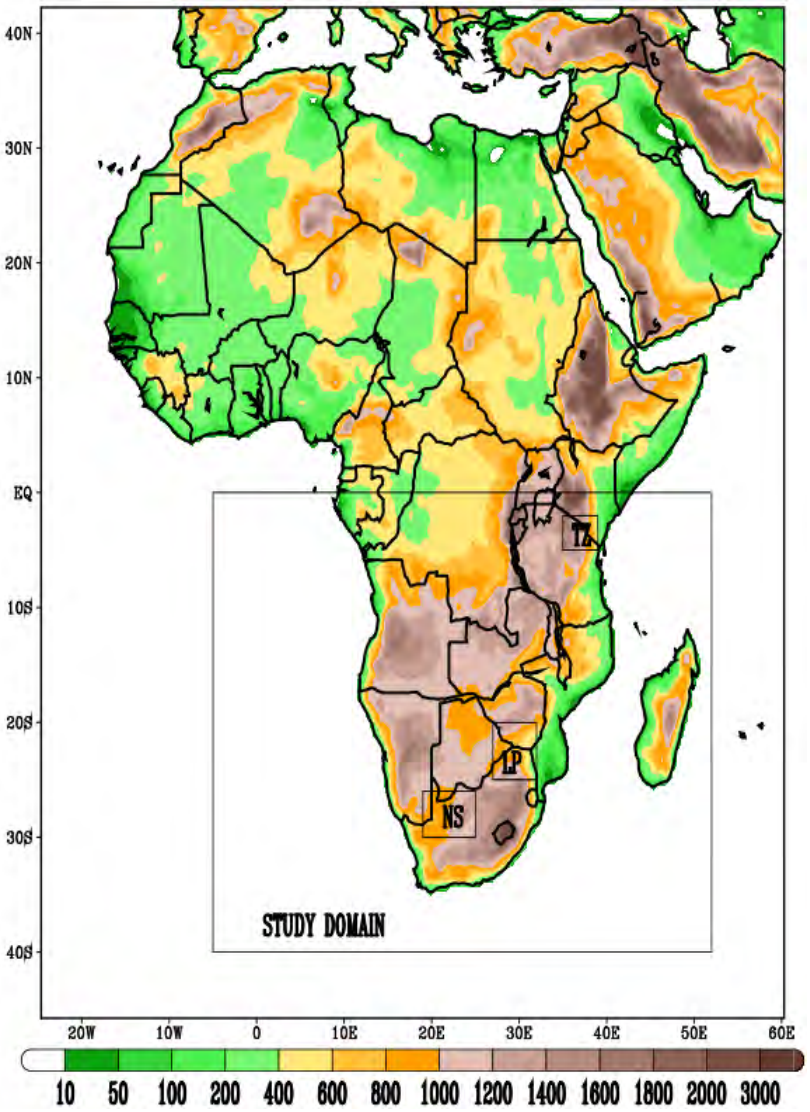

Figure 3.9: The simulation domain of CORDEX-Africa showing the African topography (meters) and the Southern African domain used in this study. The boxes inland (LP, NT and NS) indicate the three sub-regions in which time series data are investigated.

Table 3.1: List of the CORDEX regional climate models used in the study. All models have a common grid resolution of 0.44˚x0.44˚

Modelling Centre	Institute ID	Model Name	Projection
Centre National de Recherches Meteorologiques	CNRM	ARPEGE5.1	Polar, stretching
Danmarks Meterologiske Institut	DMI	HIRHAM	Rotated pole
Abdus Salam International Centre for Theoretical Physics	ICTP	RegCM3	Mercator
CCLM Community	CCLMcom	CCLM	Rotated pole
Koninklijk Nederlands Meteorologisch Instituut	KNMI	RAMCO	Rotated pole
Max Planck Institute for Meteorology	MPI-M	REMO	Rotated pole
Sveriges Meteorologiska och Hydrologiska Inistitut	SMHI	RCA3	Rotated pole
University of Cape Town	UCT	PRECIS	Rotated pole
Universidad de Cantabria	UC	WRF3.1	Mercator
Université du Québec á Montréal	UQAM	CRCM	Rotated pole

Table 3.2: List of the CMIP5 models used in the study

Modelling Centre	Institute ID	Model Name	Resolution
Canadian Centre for climate Modeling and Analysis	CCMA	CanESM2	2.8˚X2.8˚
NOAA Geophysical Fluid Dynamic Laboratory	NOAA GFDL	GFDL_ESM2M	2.5˚X2.0˚
Max Planck Institute for Meteorology	MPI-M	MPI-ESM-LR	1.8˚X1.8˚
Norwegian Climate Centre	NCC	NorESM1-M	1.5˚X1.9˚
Atmosphere and Ocean Research Institute (University of Tokyo), National Institute for Environmental studies and Japan agency for Marine-Earth Science and Technology	MIROC	MIROC5	2.8˚X2.8˚
Centre National de Recherches Meteorolo-Giques /Centre Europeen de Recherche et Formation Avancees en calcul scientifique	CNRM-CERFACS	CNRM-CM5	1.4˚X1.4˚
UK Met Office Hadley centre	MOHC	HadGEM2-ES	1.875˚X1.25˚

3.2 Methods

3.2.1 Drought identification

In this study, we used SPEI to quantify droughts in Southern Africa. There are three main steps one needs to take in order to compute the SPEI. The first step is the estimation of the Potential Evapotranspiration (PET). PET can be obtained via three methods, namely, Thornthwaite, Penman-Monteith (PM) and Hargreaves equation. In the present work, PET was generated using the Thornthwaite method. The main advantage of the Thornthwaite method over others is that it requires only temperature and the latitude of the location where we need to compute it. This simplicity of the Thornthwaite method makes it eligible for places such as Southern Africa where Meteorological observations are scanty. The PET using the Thornthwaite method is calculated as follows:

$$PET = 16K(\frac{10T}{I})^m \quad (3.1)$$

Where T is the monthly mean temperature (˚C), m and I are heat index coefficients, and K is a correction coefficient.

The second step in the computation of the SPEI entails the calculation of the difference between monthly precipitation (P) and the estimated PET. This difference is commonly known as climatic water balance and is given as follows:

$$D_i = P_i - PET_i \quad (3.2)$$

Where “i” is the month

Finally, the calculated differences (D) are aggregated at different time-scales and fitted to a theoretical three-parameter log-logistic (LLG) distribution, which seems to yield good results than other statistical distributions such as Pearson III, Lognormal and General Extreme Value (Begueria et al., 2013).

The Log-logistic distribution employed for the standardization of the difference (D) can be expressed as follows:

$$F(x) = [1 + (\frac{\alpha}{x-\gamma})^{\beta}]^{-1} \quad (3.3)$$

Where, α is the scale, β the shape and γ the origin parameters for the D time series. The parameters α, β and γ can be computed using the L-moment method (Ahmad et al., 1988).

The SPEI values can then be calculated using the Abramowitz and Stegun (1965) approximation as follows:

$$SPEI = W - \frac{c_0+c_1W+c_2W^2}{1+d_1W+d_1W^2+d_3W^3} \quad (3.4)$$

Where, $W = \sqrt{-2\ln(P)}$ for ≤ 0.5 , with P being the probability of exceeding a determined value of D.

C_0,C_1, C_2 , d_1 , d_2 , and d_3 are constants expressed as follows:

$C_0 = 02.515517$, C_1 =0.80853, $C_2 = 0.010328$, d_1 =1.432788, d_2 =0.189269 and d_3=0.001308

For being a standardized value, the average of SPEI is always zero and its standard deviation is 1. This important characteristic of SPEI allows the comparison of drought severity over two different regions.

In this study, the 3-month SPEI was calculated for both Observations (CRU and UDEL) and simulations (CORDEX RCMs and CMIP5 GCMs), using the SPEI package in the R software environment (www.R-project.org). We compared the SPEI values calculated using Thornthwaite equation (SPEI_TH) with the SPEI values computed using Penman-Monteith equation (SPEI_PM) and the results are shown in Fig.3.10. The SPEI_PM data

(1950-2013) were sourced from the Spanish National Research Council (http://sac.csic.es/spei/database.html). Overall, there is a good agreement between the two datasets, which is confirmed by the high correlation coefficient (r=0.70). However, the SPEI_TH values seem to be slightly higher than the SPEI_PM values. These small discrepancies between SPEI_TH and SPEI_PM are expected, because unlike the Thornthwaite equation, the PM equation incorporates more meteorological parameters such as solar radiation, temperature, wind speed and humidity (Begueria et al., 2013). In the present study, we used the SPEI_TH since our goal is to evaluate the CORDEX models and, not all the variables required to calculate SPEI_PM are available for the models in the CORDEX archive.

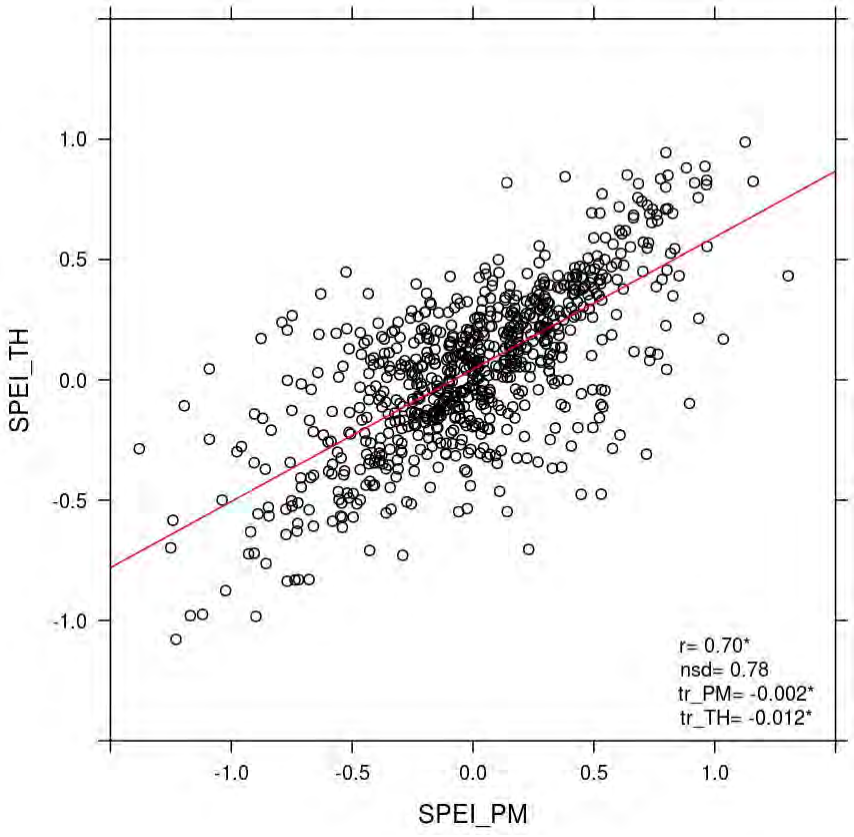

Figure 3.10: Comparison between SPEI_TH and SPEI_TH. Both SPEI_TH and SPEI_PM were computed using CRU dataset. The red line represents the line of best fit. tr_PM is the annual trend for the SPEI_PM while tr_TH is the annual trend for the SPEI_TH. The normalized standard deviation (nsd) between SPEI_TH and SPEI_PM is equal to 0.78. The star symbol (*) represents significant values at 95% level.

3.2.2 Understanding the link between ENSO and Droughts over Southern Africa

To investigate the link between ENSO and Southern African droughts we used composite and correlation analyses (Van den Dool, 2007; Wilks, 2011). Composite analysis, also known as superimposed epoch analysis, is a very simple but effective technique for isolating a signal from atmospheric fields. Based on the MEI time series we identified El Niño and La Niña years. The Warm and cold ENSO years were selected whenever the MEI was above +0.5 or below -0.5, respectively, during the whole summer period. We then grouped the observed and simulated SPEI, precipitation and temperature according to these two ENSO phases and calculated their mean and variance. We used the Student's t-test to assess whether the created composites are statistically different or not.

We also employed the Pearson Correlation analysis, which is another straightforward and powerful method for investigating links between two atmospheric fields (Wilks, 2011). The correlation analysis was performed between the ENSO index and the SPEI and our focus is on the austral summer season (December-January-February), which is the rainy season in most parts of Southern Africa. Therefore, any rainfall deficit during this season may lead to drought, crop failure and famine. Furthermore, previous studies have shown that seasonal climate anomalies for this season have high predictability during ENSO years, as the season is the mature period for El Niño and La Niña events (Reason et al. 2000; Landman and Beraki, 2012; Boulard et al. ,2013;Manatsa et al,2015).

3.2.3 Influence of lateral boundary conditions

To investigate the impact of RCM boundary conditions on the simulated link between ENSO and Southern African droughts, we used sensitivity experiments in which RCA simulations were forced with seven GCM simulations (Table 3.2). For the sensitivity experiments, ENSO was represented by ONI values. We also assessed the added value afforded by the downscaling of the simulated link between ENSO and droughts. The added value (δ), which is a measure of difference between GCM and RCM errors, was computed according to Di Luca et al. (2012 and 2013) as:

$$\delta = (r_{GCM} - r_{OBS})^2 - (r_{RCM} - r_{OBS})^2 \quad \text{(3.5)}$$

Where, $r_{OBS,}$ r_{GCM} and r_{RCM} represents the correlation between ENSO and SPEI in observation, GCM, and RCM, respectively.

A positive value of δ means that the RCA downscaling improves the simulated link, while a negative value indicates that the RCM downscaling does not improve the simulated link.

3.2.4 Classification of drought patterns

For the classification of droughts into different groups we employed the SOMs analysis using the SOM_PAK 3.2 software (Kohonen et al., 1995), which was freely obtained from the Helsinki University of Technology (http://www.cis.hut.fi/research/som_pak/). Although the choice of the number of SOMs nodes is subjective (Cavos 1999; Brown et al. 2010), we reasoned that 12 SOM archetypes (4X3) were adequate to describe the main drought patterns in Southern Africa and, moreover, the same array was previously used for the same area of study by Tadross et al. (2005), Mackellar et al. (2010) and Maure (2013). We performed two experiments with the SOMs analysis. In the first experiment, SPEI values from the CRU data spanning from 1950 to 2013 were used as the input data into the SOMs analysis. This experiment aimed at categorizing droughts from the observation perspective.

In the second experiment, we intended to assess how RCMs from the CORDEX project simulate the drought patterns obtained in the first experiment. With this in mind, SPEI values from CRU dataset were blended with those from the 10 RCMs and ERAINT reanalysis. The resulting array of 126x92x12 dimension was subjected to the SOM analysis. This approach is very effective and has been used extensively in previous studies (e.g., Cassano et al., 2007; Finnis et al. 2009; Schuenemann and Cassano, 2009) including our region of study (Abiodun et al., 2015). To investigate the synoptic conditions associated with each drought state, composite analysis was performed on SST, rainfall, temperature and the dynamic fields for each node and season.

3.2.5 Performance of the RCMs in simulating drought patterns

We used different metrics in order to assess how well the CORDEX RCMs simulate the drought patterns over Southern Africa. These metrics include Taylor Diagram, phase synchronization and correlation analysis between the simulated and observed frequency of occurrence of the 12 drought patterns. Taylor Diagrams are graphical diagrams used to summarize the performance of climate models against observations (Taylor, 2001). The diagrams are based on several statistical metrics, namely the Pearson's correlation coefficients, root-mean-square error (RMSE) and standard deviation. In the present study, the SPEI values from the 10 RCMs and the ERAINT reanalysis data were averaged over the entire domain of study and compared against the area-averaged SPEI values from the CRU dataset, which was used as the reference data. Taylor Diagrams have been used over Southern Africa to assess the performance of the CORDEX RCMs in reproducing the monthly as well as the seasonal mean rainfall (Kalognomou et al., 2013; Shongwe et al., 2014).

Phase synchronization (η) is another method used for evaluating how well the patterns in the CORDEX RCMs match those from the observations. Phase synchronization is calculated as follows (Misra, 1991):

$$\eta = \left(\frac{n-n'}{n}\right) x100\% \tag{3.6}$$

Where n is the total number of seasons and n' is the number of seasons in which model and observations show opposite signs of SPEI values. If a model simulates perfectly the patterns as in the observation η will be 100%, whereas a η=0 means that model and observations are out of phase during the entire period of study. Phase synchronization has been already used over Southern Africa to gauge the skill of climate and crop models (Tozuka et al., 2013; Araujo et al., 2014).

4 : The link between ENSO and summer drought in Southern Africa

This chapter evaluates the capability of the RCMs in simulating the link between ENSO and Southern African droughts. Here we used the SPEI, computed using rainfall and temperature data to identify 3-month drought over Southern Africa, and compares the observed and simulated correlation between ENSO and SPEI. The observation data are from the Climate Research Unit (CRU), while the simulation data are from 10 RCMs from the CORDEX project. The chapter analysed the austral summer season (December-February) data for 19 years (1989-2008).

4.1 The relationship between ENSO and drought (SPEI)

This section evaluates how well the CORDEX RCMs simulate the link between ENSO and droughts (SPEI) over Southern Africa. Fig. 4.1 shows a strong correlation between ENSO and droughts over Southern Africa for both observations and simulations. In the CRU data (Fig 4.1a), the correlation between ENSO and SPEI shows a marked dipole pattern over Southern Africa with positive values ($r \geq 0.6$) over the eastern part of the tropical area (north of 15^{o}S) and negative values ($r \leq -0.6$) over the sub-tropical area (south of 15^{o}S). The correlation is weak ($r = \pm 0.3$) over Western part of the tropical area. It is also weak over the south-western tip of Southern Africa, possibly because this area experiences an Austral winter regime (Reason et al., 2002; Reason and Jagadheesha, 2005; Reason and Rouault, 2005; Philippon et al., 2011; Vigaud et al., 2012). When compared to CRU data, ERAINT replicates the dipole pattern very well, except that it shows a weaker positive correlation ($r \approx 0.5$) over the eastern part of the tropical area than in CRU data, and extends the positive correlation westwards into Angola, making the area of positive correlation wider than in CRU data. The biases in the ERAINT results may be attributed to the low resolution and the convective parameterization scheme used in the reanalysis.

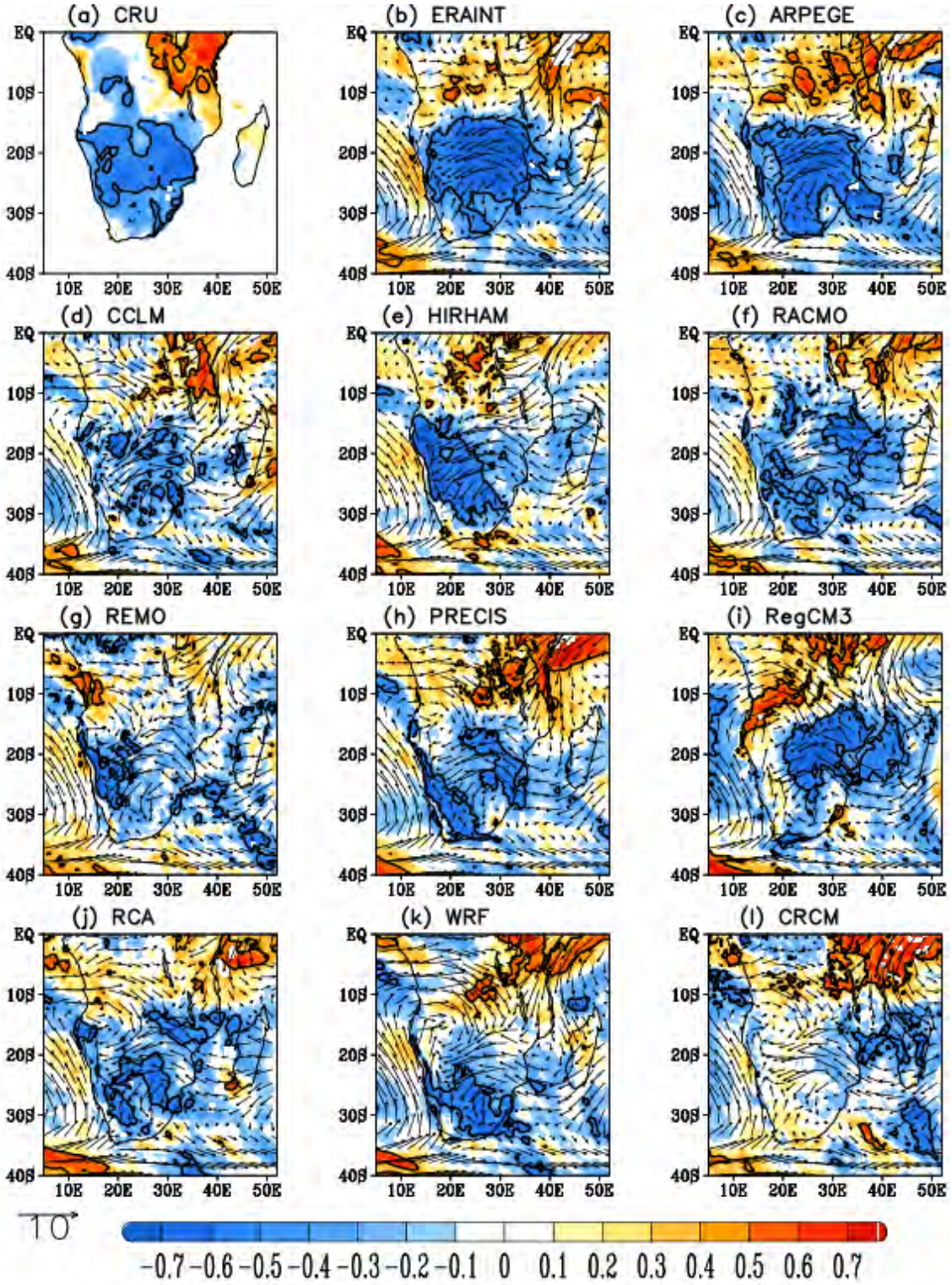

Figure 4.1: The coefficient of correlation between ENSO and drought (SPEI) over Southern Africa in summer (DJF, 1989-2008), as observed (CRU and ERAINT) and simulated (CORDEX RCMs). The contours show areas where the correlation is significant at 95% using the t-test. The corresponding 850 hpa winds are shown in the background; the arrow at lower left corner indicates 10 m/s wind speed.

The RCM simulations show different patterns of the correlation between the ENSO and Southern African droughts (Fig 4.1). In some RCMs (i.e. ARPEGE), the simulated correlation pattern is close to the observed (or ERAINT) pattern, but in other RCMs (i.e. CRCM) the pattern is different. Among the RCMs, ARPEGE simulates the best correlation pattern, although it is closer to the ERAINT pattern than it is to the CRU pattern. The main shortcoming in the ARPEGE correlation pattern is that it shows a stronger correlation than observed over the entire Southern Africa, even over the south-west, where CRU shows no correlation. However, the best performance of ARPEGE here is consistent with Kalognomou et al. (2013), who show that ARPEGE consistently outperforms all CORDEX RCMs over Southern Africa in all the seasons. The good performance of ARPEGE in simulating the link between ENSO and Southern African droughts may be due to its capability of being a global stretch-grid model. This may help the model yield a better simulation of the Walker circulation, and to experience no shock at the lateral boundaries between the driving data (ERAINT) and RCM dynamics. RegCM3 also captures the general pattern of the observed correlation between ENSO and droughts, but its area of significant correlation is confined to the central area of Southern Africa. The model fails to reproduce the negative correlation over Namibia and southern Angola, where it shows a positive correlation. Only HIRHAM and REMO show a good correlation over Namibia and southern Angola; other RCMs (including ARPEGE) either show a weaker correlation or show opposite correlation when compared to the observed pattern. Nevertheless, HIRHAM and REMO simulate poor correlation patterns elsewhere, especially over the eastern side of Southern Africa. This agrees with a previous study (Haensler et al., 2011) that showed that the REMO model has a better skill in drier areas (i.e. the south-west) than in more humid areas (south-east and north-east) of Southern Africa. In RCA model, the areas of significant correlation are scattered over Southern Africa, but in WRF the area of significant correlation is displaced south with few patches over southern Namibia and Botswana. CRCM portrays the most striking correlation pattern; it shows no-correlation to weak-correlation over the entire Southern Africa. Hence, among the CORDEX RCMs, CRCM shows the lowest capability in linking ENSO with the Southern African droughts. Hernandez-Diaz et al. (2013) also reported that CRCM has cold biases over most areas in Southern Africa.

There is a very good agreement between ERAINT and RCM 850hPa mean winds over Southern Africa in DJF (Fig.4. 1). South of 15^{o}S, the wind pattern is characterized with strong anti-cyclonic wind over the Southern Atlantic Ocean (i.e. west of Southern Africa) and strong easterlies transporting warm, moist air from the Indian Ocean to the sub-continent. North of 15^{o}S, the wind pattern is characterized by strong north-easterlies in the east and westerlies in the west, producing convergence flow at the centre. The major difference between ERAINT and RCM wind patterns is that the westerlies are stronger in the RCM (except HIRHAM) than in ERAINT. It is difficult to link the wind pattern with the ENSO-drought correlation pattern, but generally, in the ERAINT and RCM (except in CRCM), the area of negative correlation experiences easterly winds (from Indian Ocean), while the area of positive correlation experiences north-easterly or westerly flow.

4.2 The influence of ENSO on precipitation and temperature

Since precipitation and temperature are the two variables used in computing the drought index (SPEI), it is of interest to examine how well the models simulate the relationship between ENSO and each of these variables. The correlation between ENSO and precipitation over the study area shows a good resemblance with that of ENSO and drought (compare Fig.4.1 and Fig. 4.2). The general pattern shows positive correlations ($r \approx 0.5$) over the tropical region and negative correlation ($r \approx -0.6$) over the sub-tropical region. The significant negative correlation over central parts of Southern Africa suggests that a warm ENSO event will induce lower rainfall over Southern Africa, while a cold ENSO event will produce above-normal rainfall conditions, which is consistent with the findings from previous studies over the region. As in CRU data, ERAINT and most RCMs show negative correlation over central parts of Southern Africa. The ARPEGE model best captures this well-known feature over Southern Africa. In line with Fig.4.1, the HIRHAM and REMO models show a strong correlation over Namibia. The weakness of the CRCM in capturing the link between ENSO and droughts is also reflected in capturing the link between ENSO and rainfall.

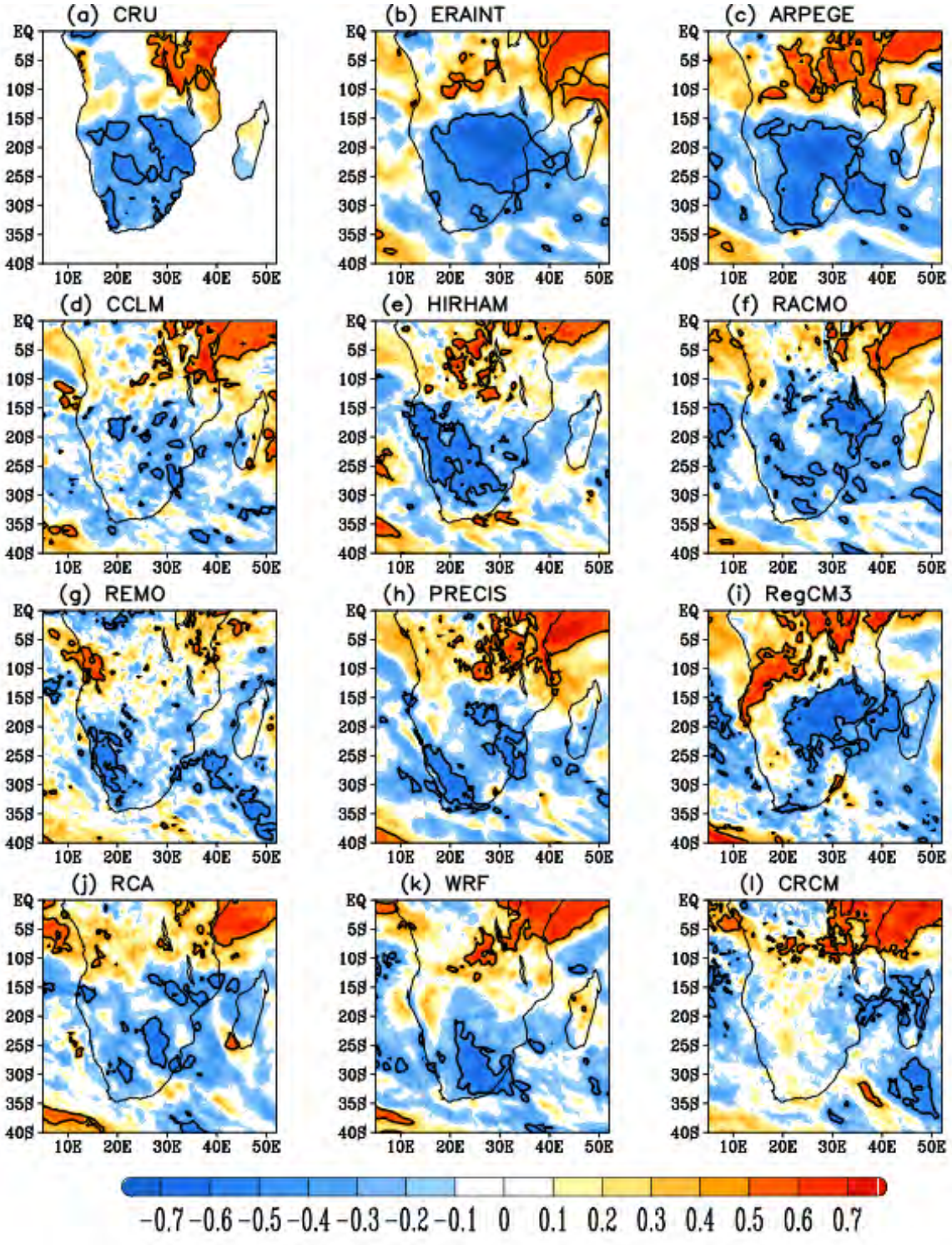

Figure 4.2: The coefficient of correlation between ENSO and precipitation over Southern Africa in summer (DJF, 1989-2008), as observed (CRU and ERAINT) and simulated (CORDEX RCMs). The contours show areas where the correlation is significant at 95% using the t-test.

The CRU data show a significant positive correlation between ENSO and temperature in DJF over the bulk of Southern Africa (Fig. 4.3). This is also a well-known feature that strong abnormally high temperatures and sometimes heat-waves are recorded over most of the Southern African sub-continent during El Niño years (Richard et al., 2001; Lyon, 2009). During El Niño years, the convergence zone that normally reaches 20˚S in January, during the Austral summer, is weakened and shifted to the east and north, resulting in dry conditions over the sub-continent (Mason, 2001). The resemblance between the CRU data and ERAINT patterns is noticeable. Both show positive correlation over sub-tropical areas and negative correlation values over the tropical areas, but they show contrary correlations over a large part of the Democratic Republic of Congo (DRC), where ERAINT shows positive correlation coefficients. In comparison to the observations, the ARPEGE model continues to show a high reliability in simulating the relationship between ENSO and temperature over Southern Africa, but performs poorly over Angola, where ERAINT does not perform well either.

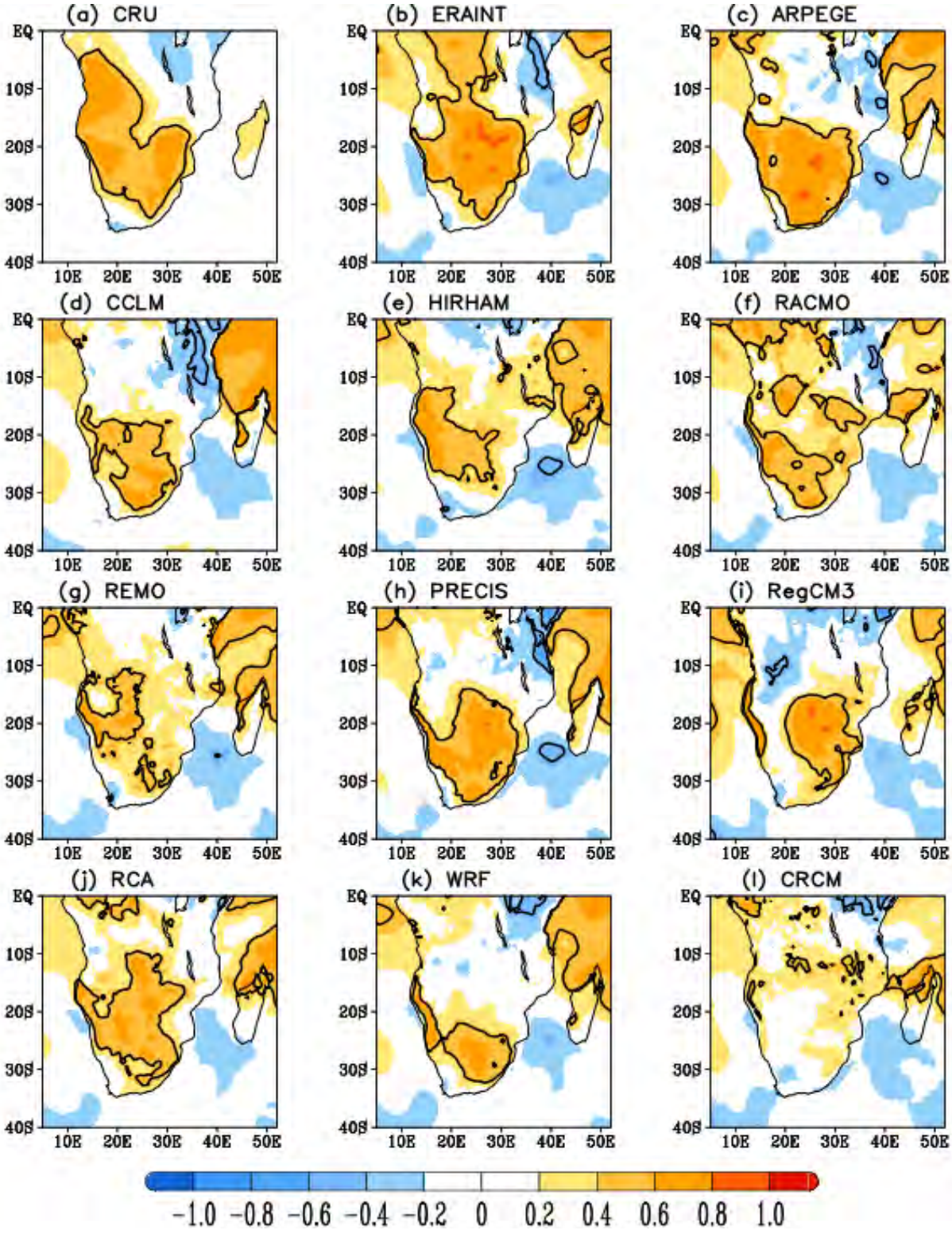

Figure 4.3: The coefficient of correlation between ENSO and temperature over Southern Africa in summer (DJF, 1989-2008), as observed (CRU and ERAINT) and simulated (CORDEX RCMs). The contours show areas where the correlation is significant at 95% using the t-test.

Fig.4.4 compares the influence of ENSO on rainfall, temperature, and drought over the three selected areas (see Fig.3.9): Limpopo area (LP: 27˚-32˚E, 20˚-25˚S), North-eastern South Africa (NS: 19˚-25˚E, 30˚-26˚S) and over north-eastern highlands of Tanzania (TZ: 35˚-39˚E, 5˚-2˚S). The LP area is usually considered as the drought corridor in Southern Africa (Usman and Reason, 2004) because of the high dry-spell frequencies over this area in DJF. Reason et al. (2005) found a good relationship between ENSO and dry-spell frequencies over this area. However, Fig.4.4a shows that, over this area, the correlation between ENSO and temperature ($r \approx 0.7$) is stronger than the correlation between ENSO and rainfall ($r \approx -0.5$); the same is true over the NS (Fig.4.4b), but the reverse is the case over TZ (Fig. 4.4c). This suggests that the influence of ENSO on drought ($r \approx 0.6$) over LP and NS areas may be more associated with enhanced evapotranspiration (i.e. warming) than with reduced rainfall; but over TZ, the influence is more associated with the reduced rainfall than with enhanced evapotranspiration. In other words using only rainfall to quantify, predict, or monitor the influence of ENSO on drought over LP and NS areas may underestimate the influence on the drought. ERAINT results also show that the influence of ENSO on temperature (or on SPEI) is stronger than on rainfall over the two areas. All RCMs (except HIRHAM) simulate this characteristic. However, most RCMs (i.e. CCLM, HIRHAM, RACMO, REMO, RCA, CRCM and WRF) grossly underestimate the link between ENSO and drought (rainfall and temperature) over the three areas (LP, NS and TZ).

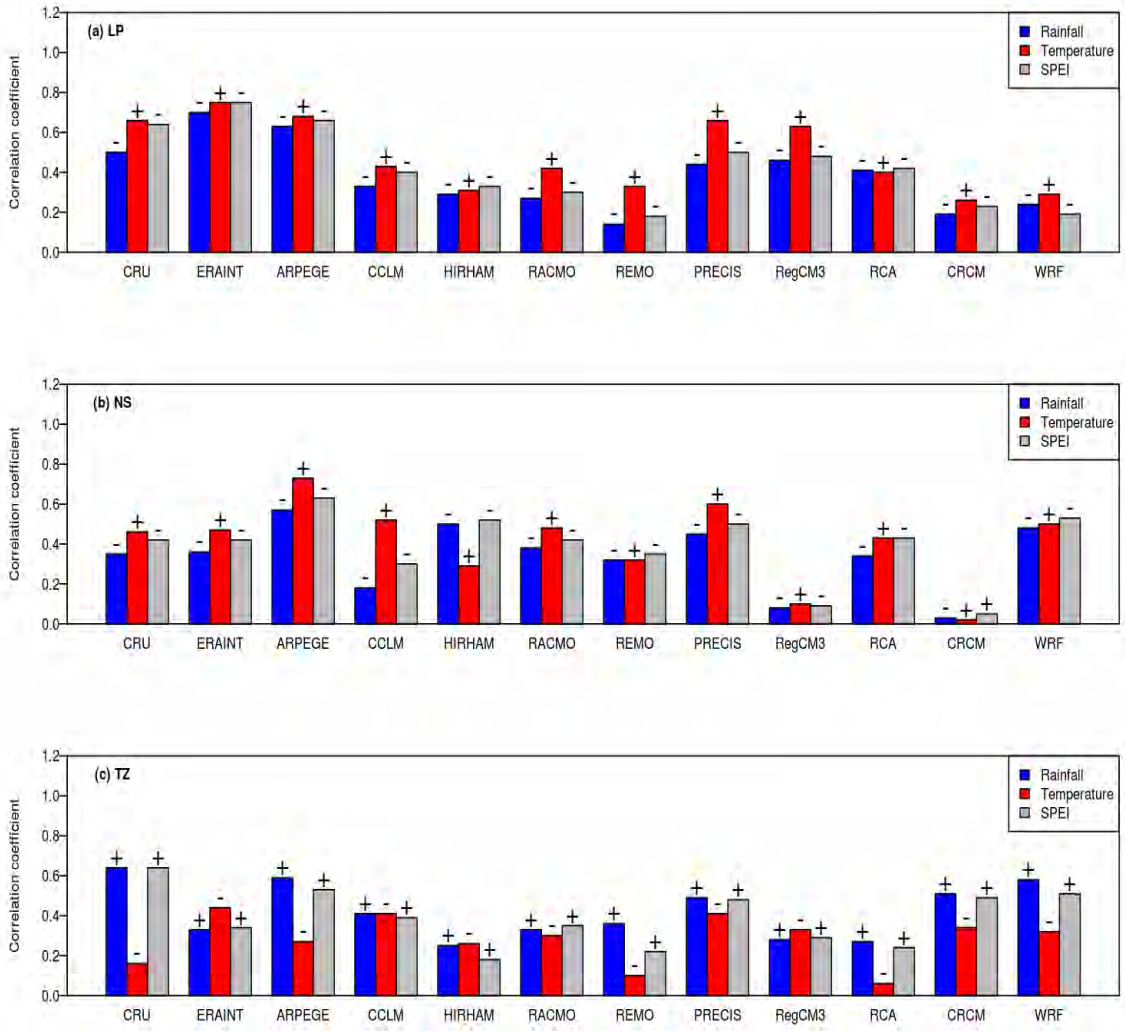

Figure 4.4: The coefficient of correlation between ENSO and climate variables (rainfall, temperature and SPEI) over (a) Limpopo (LP), (b) North-western South Africa (NS), and (c) North-eastern Tanzania (TZ). The signs of the correlation coefficients are indicated on the bars.

4.3 Composite of SPEI and temperature during El Niño and La Niña events

For a better understanding of the impact of ENSO on Southern African droughts, we present the composites of SPEI, precipitation, and temperature during El Niño and La Niña conditions. Within our study period (1989-2008), there were six El Niño events (1991/92, 1994/95, 1997/98, 2002/03, 2004/05 and 2006/07) and six La Niña events (1995/96, 1998/99, 1999/2000, 200/01, 2005/06 and 2007/08). Fig.4.5 shows the

composite of SPEI for the La Niña events. The figure shows that the cold phase of ENSO (La Niña) is associated with positive SPEI (wet conditions) over the sub-tropical Southern Africa and negative SPEI (dry conditions) over the north-eastern tropical area. This is consistent with Fig.4.2 and is in agreement with previous studies that explored the composite of rainfall during La Niña events. La Niña events are associated with the occurrence of Tropical Temperate Troughs (TTTs; Harrison 1984; Todd and Washington, 1999; Washington and Todd, 1999; Todd et al., 2004), which are NW-SE oriented cloud bands. They are more common during the November-February period and are associated with an increase in the intensity of the African Walker Cell, which in turn enhances moisture convergence over Southern Africa (Ratnam et al., 2013). The ERAINT and RCMs simulate that during La Niña years, the anti-cyclonic flow over the Atlantic Ocean is weaker and shifts westward (i.e. off the sub-continent). This will enhance more low level convergence and precipitation. The cold ENSO events are also associated with lower temperature over the bulk of Southern Africa and higher temperature over northern Mozambique, Tanzania, north-eastern Zambia and southern DRC (not shown). However, the reverse is the case with the warm phase of the ENSO condition (El Niño). El Niño event favours widespread dry conditions in the region, except over northern Mozambique, southern Tanzania, north-eastern Zambia and eastern DRC, where El Niño events produce wet conditions (Fig.4.6). The anti-cyclonic flow shifts eastward over the sub-continent, consequently inhibiting precipitation over the region. The warm ENSO produces higher temperatures over most parts of Southern Africa and lower temperatures in the sub-tropical regions.

The RCMs (except CRCM) show similar patterns as the observations, but the magnitude of the SPEI anomalies during the La Niña and El Niño events are weaker than the observed; only ARPEGE produces the magnitude of SPEI anomalies that is comparable with observation. Contrary to observation, some RCMs (e.g. REMO, PRECIS and RegCM3) simulate no changes in SPEI over the Drakensberg Mountains (around the Kingdom of Lesotho) during the La Niña and El Niño conditions. High elevation areas, such as the Drakensberg Mountains, usually experience higher precipitation with lower temperatures (i.e. lower PET) than the surroundings; this might reduce the severity of

drought over the mountains, and some models might find it difficult to simulate this process.

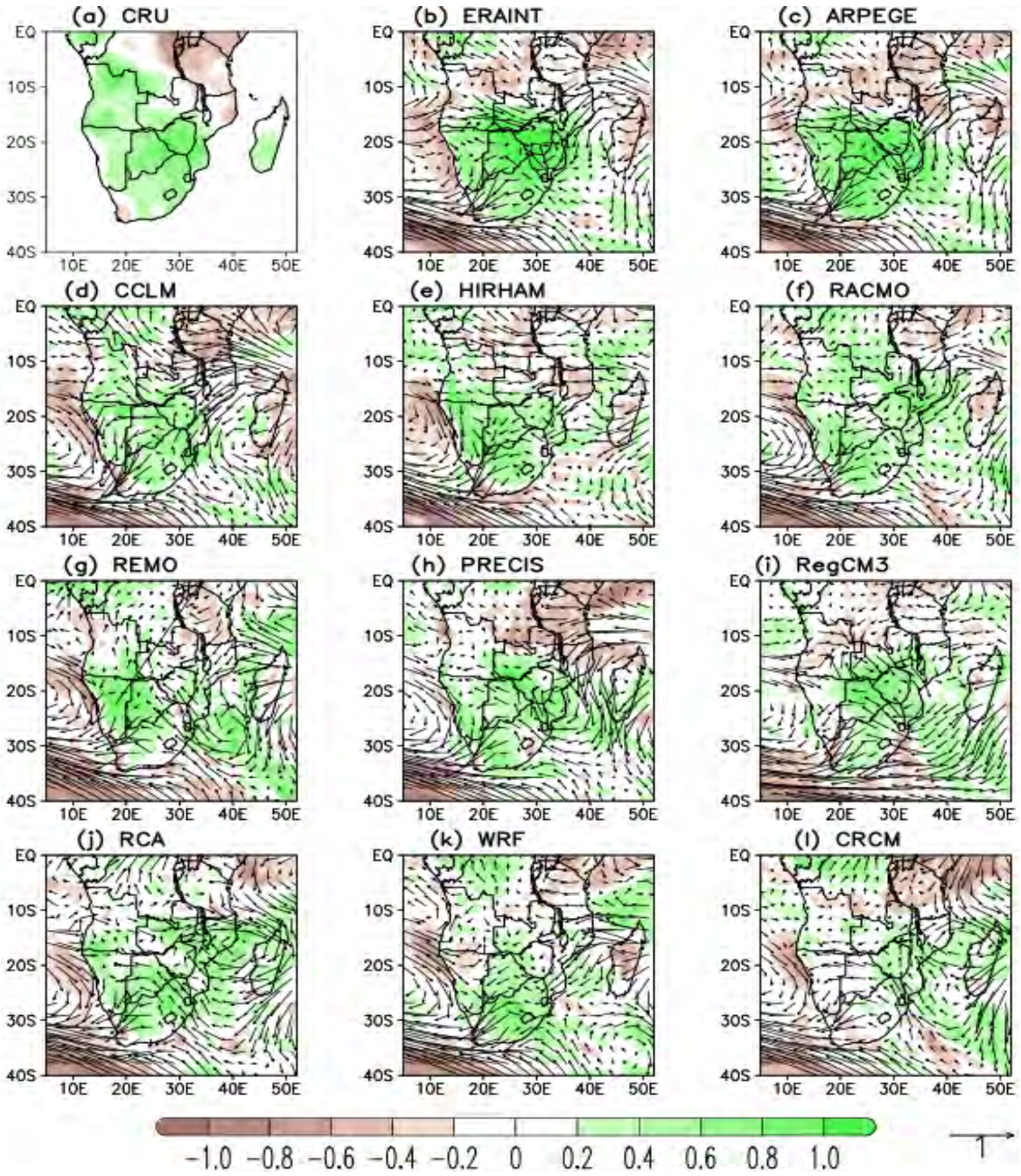

Figure 4.5: The composite of drought index (SPEI) and wind anomalies (in m/s) at 850 hPa in December– January of La Niña years.

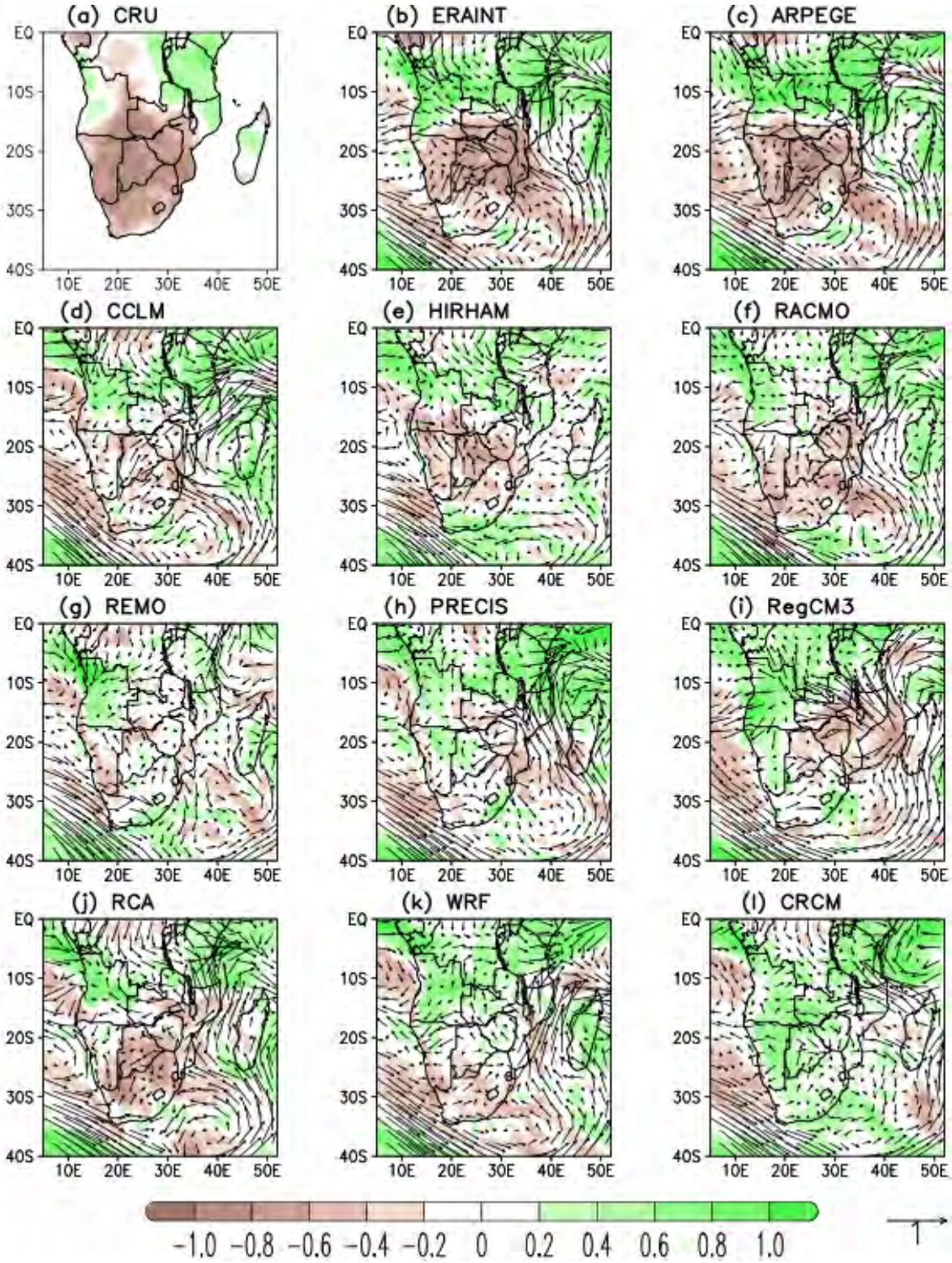

Figure 4.6: The composite of drought index (SPEI) and wind anomalies (in m/s) at 850 hPa in December– January of El Niño years.

4.4 The influence of boundary conditions

This section investigates the sensitivity of the simulated link between ENSO and Southern African drought to the GCM simulations used as boundary forcing. We used the RCA model to examine the influence of boundary conditions. The RCA was chosen because it was the only model available with different GCM forcing. However, as shown in the previous section, RCA also gives a credible simulation of the link when forced with ERAINT; hence the model is also suitable for the sensitivity experiment. Fig.4.7 represents the GCM simulated links between ENSO and SPEI, Fig.4.8 shows the link after the GCM simulations are dynamically downscaled with RCA, while Fig.4.9 gives the added value of the downscaling to the simulated link when compared with observation.

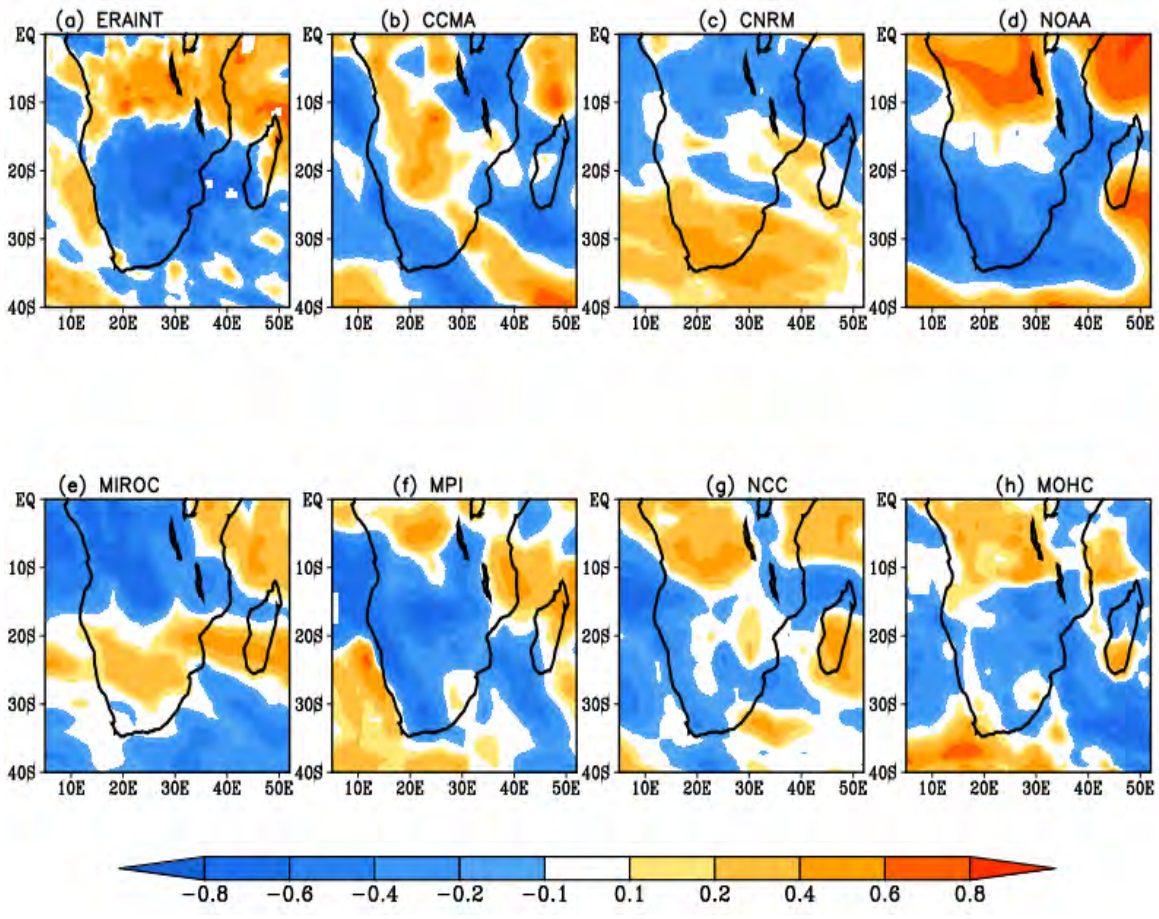

Figure 4.7: The coefficient of correlation between ENSO (i.e. Niño3.4) and drought index in ERAINT and GCM simulations.

With or without the downscaling, the correlation patterns for ERAINT are the same (Figs. 4.7a and 4.8a) and the added value of the downscaling is negative over most areas in Southern Africa (Fig.4.9a), except over a small area in the northern part of Angola. Hence, downscaling ERAINT results with RCA adds no value to the simulated link between ENSO and Southern African droughts. While the downscaling improves the simulated link for some GCM (i.e. CCMA, CNRM and MIROC), it adds no substantial value to the simulated link for other GCM (i.e. NOAA, MPI, NCC and MOHC). Without downscaling, CCMA simulation fails to simulate the negative correlation over the central part of Southern Africa and over the north-eastern part of South Africa, and fails to reproduce the positive correlation in the north-eastern part of Southern Africa (Fig. 4.7b).

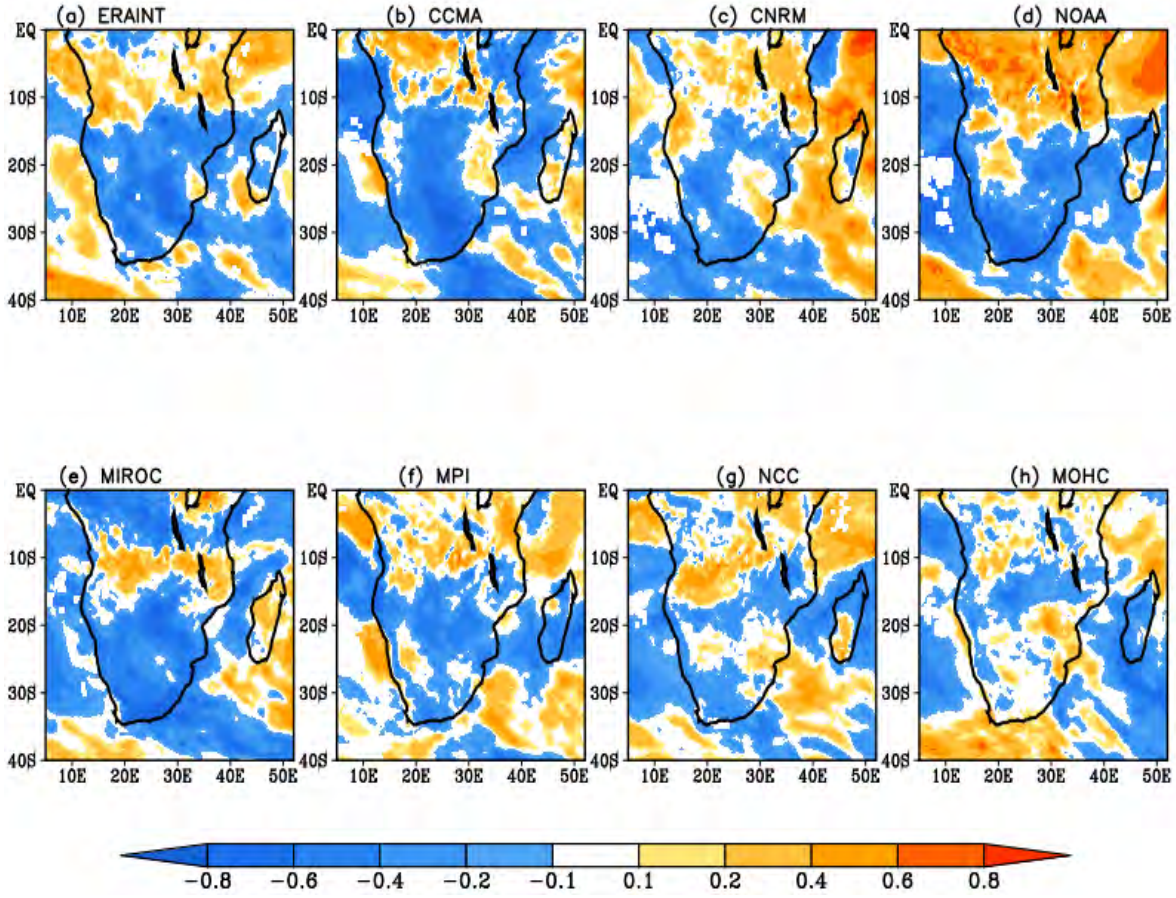

Figure 4.8: The coefficient of correlation between ENSO (i.e. Niño3.4) and drought index in RCA simulations forced with ERAINT and GCM datasets.

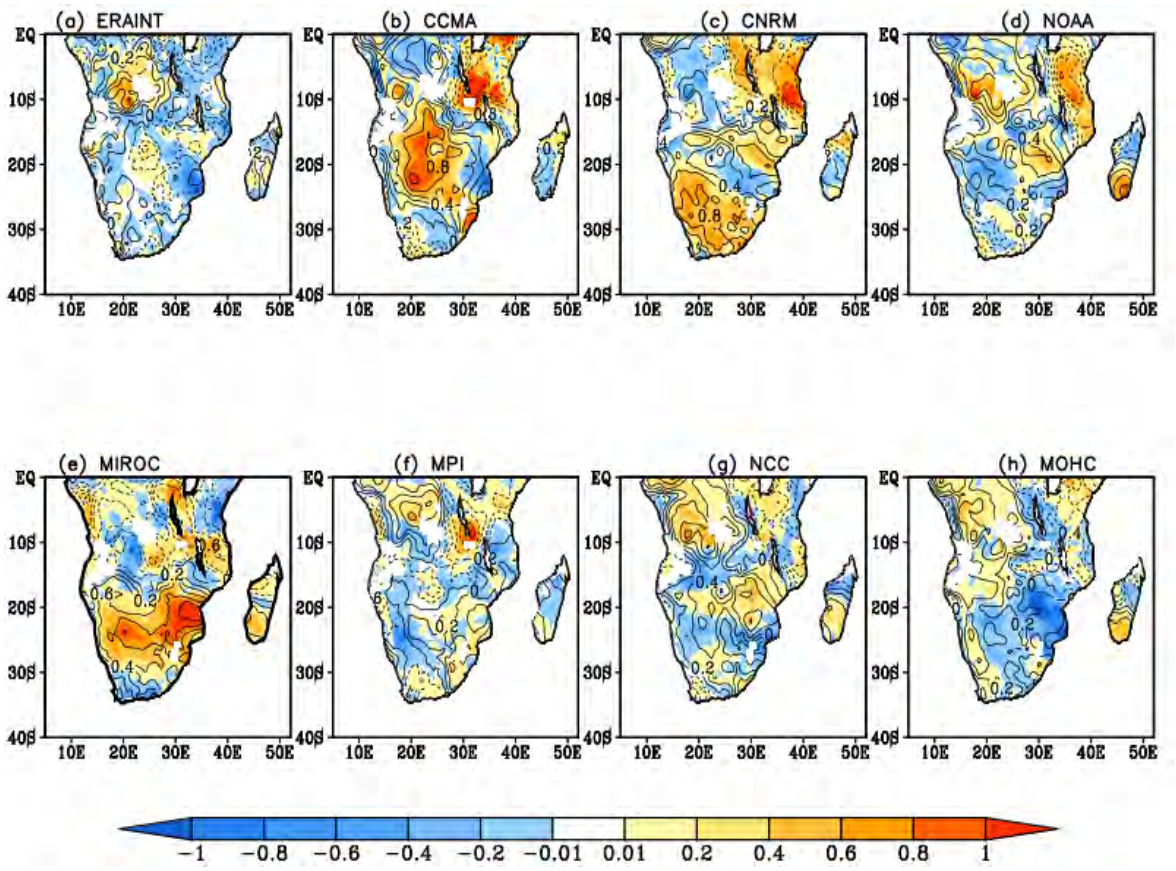

Figure 4.9: The added value (shaded) of the RCA dynamical downscaling to the simulated link between ENSO and droughts in Southern Africa. The GCM biases in simulating the link are indicated with contours; the contour interval is 0.2.

The RCA downscaling corrects these biases (Fig.4.8b) and provides an added value of more than 0.5 over the areas (Fig.4.9b). CNRM simulation, on the other hand, fails to simulate the negative correlation pattern over the southern part of South Africa and over Mozambique (Fig.4.7c). It also fails to simulate the positive correlation over the north-eastern part of Southern Africa (Fig.4.7c). Unfortunately, we don't have the necessary data to diagnose the reason for the poor performance of CNRM in simulating the link; however, it may be due to the boundary conditions or the convective parameterization schemes used in the model. The RCA downscaling corrects the shortcoming to an extent and provides an added value up to 0.2 over South Africa and up to 0.6 over Tanzania (Fig. 4.9c). MIROC fails to simulate negative correlation in the 20^{o} – 30^{o}S zone and the positive correlation over Tanzania (Fig.4.7e). While the RCA downscaling corrects the

MIROC bias in the 20^o – 30^oS zone (with up to 0.8 added value), it does not improve the simulated link over Tanzania (Fig.4.9e). For the simulations of the remaining four GCM, the RCA downscaling only provides added values over small areas, i.e., over Tanzania in NOAA (Fig.4.9d), over the border of Zambia and Tanzania in MPI (Fig.4.9f), and the northern part of Angola in NCC (Fig. 4.9g). However, it is important to note that the added value of RCA to GCM results decreases as the GCM bias ($bs = r_{GCM} - r_{OBS}$) in simulating the ENSO-drought decreases. For instance, ERAINT is already very good in representing the link ($bs < 0.2$, except over Congo) because of data assimilation; hence, RCA is not adding value ($\delta \approx -0.4$). On the other hand, CNRM is poor in simulating the link ($bs > 0.6$), the RCA added value is substantial ($bs > 0.8$).

Focusing on the drought corridor area in Southern Africa, the RCA downscaling improves the simulated ENSO-drought link over the area in some cases and worsens it in other cases (Fig.4.10). However, none of the RCA downscaling reproduces the magnitude of the observed link. With ERAINT, the RCA downscaling weakens the simulated link, because it reduces the influence of ENSO on both rainfall and temperature (Fig.4.10). In two cases (CNRM and MOHC), the downscaling produces a wrong sign of the correlation between ENSO and the drought index, even though the GCM produce the right sign. This occurs because the RCM compromises the sign of the correlation between ENSO and the rainfall over the area. In some cases, the downscaling improves the simulated correlation between ENSO and the drought index. This is because the RCM improves the simulation between ENSO and rainfall, or between ENSO and temperature, or both. However, downscaling MIROC and NOAA simulations gives the best ENSO-drought link over LP (Fig.4.10a) and NS (Fig.4.11a), while downscaling MPI and NOAA simulations gives the best ENSO-drought link over TZ (Fig.4.12a).

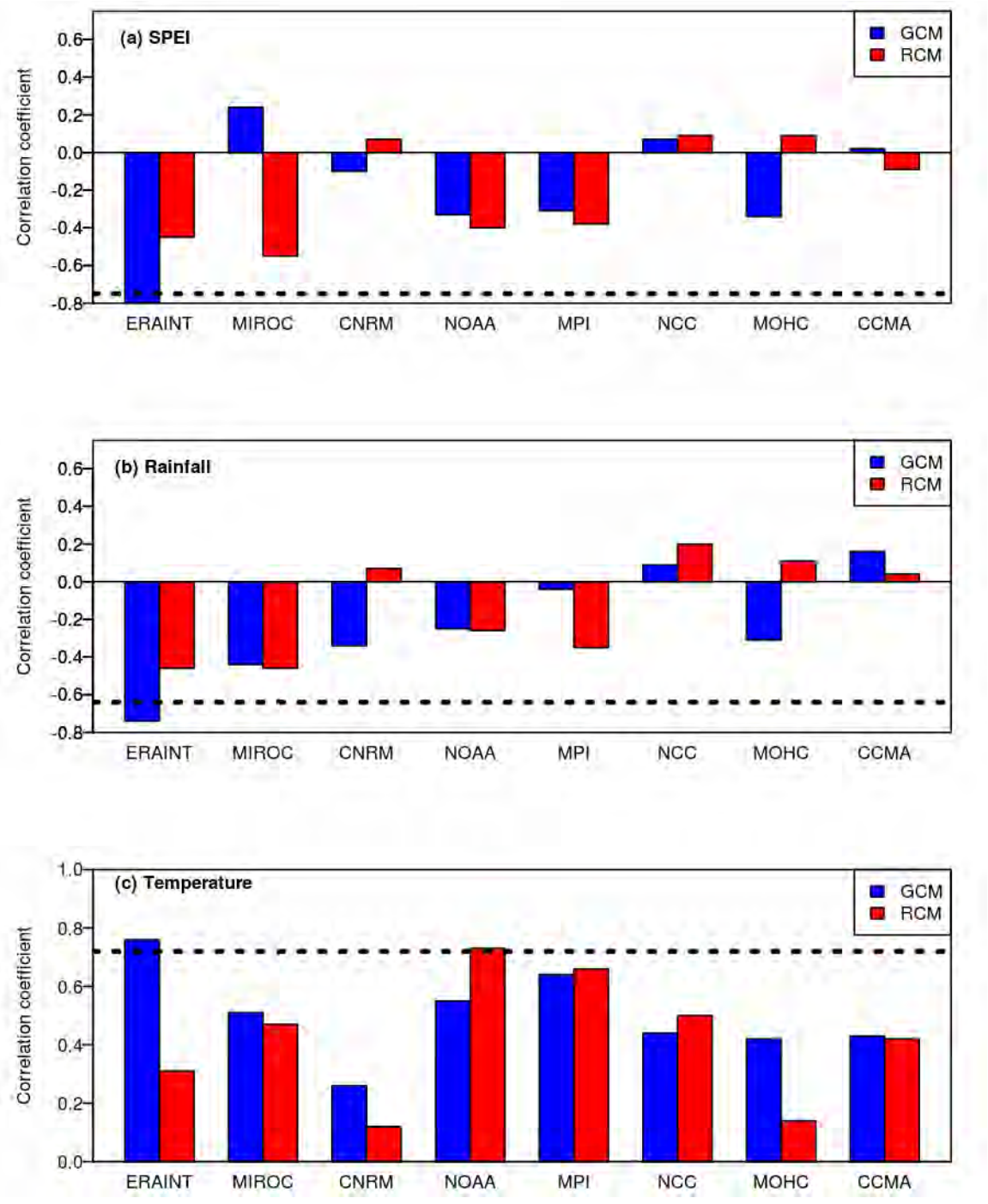

Figure 4.10: The correlation between ENSO and (a) SPEI, (a) rainfall and (c) temperature (c) over the drought corridor (LP) in Southern Africa for both GCM and RCA4. The dotted line represents the value of the CRU data.

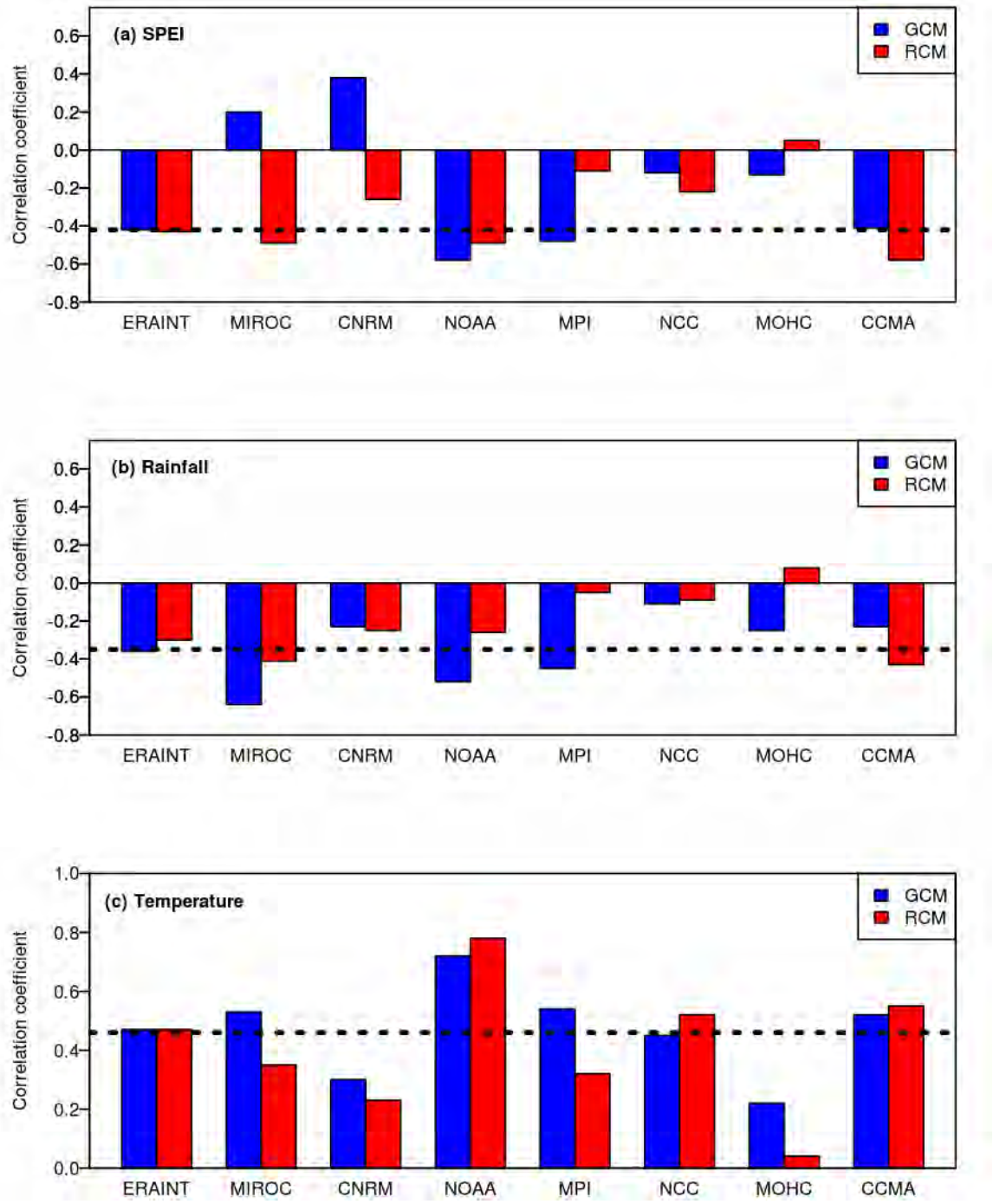

Figure 4.11: The correlation between ENSO and (a) SPEI, (a) rainfall and (c) temperature (c) over North-western South Africa (NS) in Southern Africa for both GCM and RCA4. The dotted line represents the value of the CRU data.

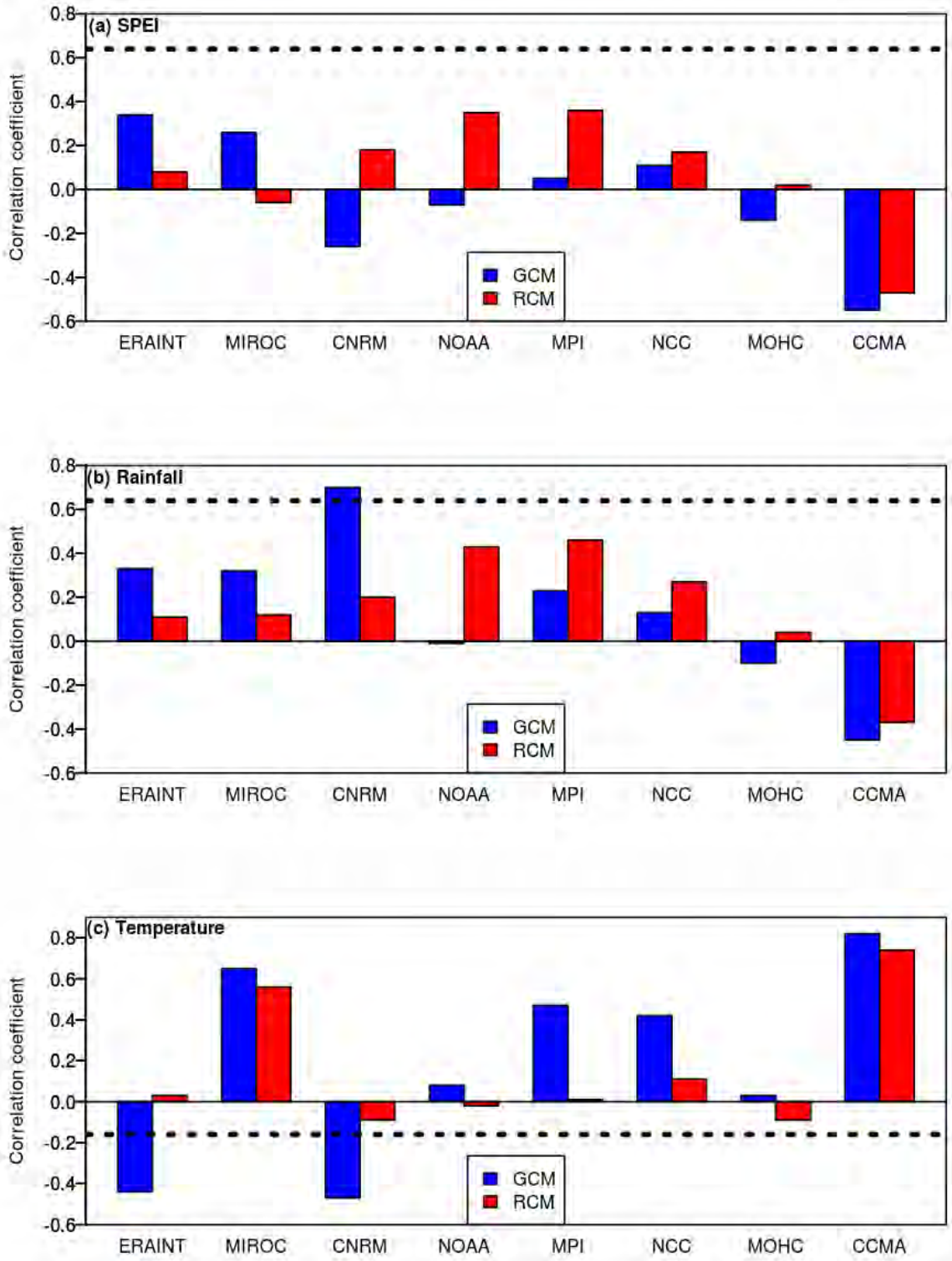

Figure 4.12: The correlation between ENSO and (a) SPEI, (a) rainfall and (c) temperature (c) over in North-eastern Tanzania (NT) for both GCM and RCA4. The dotted line represents the value of the CRU data.

4.5 Summary

This chapter assessed the ability of RCMs in simulating the relationship between ENSO and Southern African droughts by using a 3-month SPEI from CRU data and RCM outputs from CORDEX project for austral summer period (1989-2008). Correlations and composite analyses were used to examine the link between ENSO and droughts in Southern Africa. We also investigated the sensitivity of this link in RCM simulations to different lateral boundary conditions. The results confirm the strong correlation between ENSO and droughts over Southern Africa. In CRU data and ERAINT, the drought index shows a dipole pattern over Southern Africa, with positive (up to +0.6) values over the tropical area and negative values (up to -0.6) over the sub-tropical area. In agreement with previous studies, El Niño years are associated with widespread drought conditions during the Austral summer in Southern Africa, while La Niña years are more in favour of wet conditions. Some RCMs simulate the correlation pattern as in observation. Among the CORDEX RCMs, ARPEGE simulates the best link between ENSO and droughts. The best performance may be because the stretching capability of ARPEGE helps the model to eliminate boundary condition problems, which are present in other RCMs. In ARPEGE simulations, the stretching capability would allow a better interaction between large and small scale features, and may lead to a better representation of the rain producing systems in Southern Africa. On the other hand, the CRCM exhibits the least capability in simulating the link. The study shows that the link between ENSO and droughts is owing to the influence of ENSO on both temperature and rainfall fields. The link between ENSO and temperature is more statistically significant than the link between ENSO and rainfall. Our results suggest that errors in lateral boundary conditions have an impact on the simulated relationship between ENSO and Southern African drought. Despite their coarse resolution, some GCM are capable of reproducing the link between ENSO and droughts. In general, different lateral boundary conditions can improve or degrade the simulated link. The RCA model adds little skill when it is driven by the MPI global model, because of its already good performance in representing the link. On the contrary, the high resolution of RCA simulation improves the link between ENSO and drought substantially when it is driven by MIROC5, CNRM and CanESM2 global models. In

general, the added value of RCA to the simulated ENSO-drought link decreases as the capability of a GCM in simulating the link increases.

5 : The persistence and transition of droughts in Southern Africa

This chapter categorizes drought patterns over Southern Africa, examines the persistence and transition of the drought patterns, and investigates the roles of atmospheric teleconnections on the drought patterns. The 3-month SPEI was used to identify droughts during the period 1950-2013 while SOMs algorithm was applied to categorize the drought patterns. In this chapter we also test the sensitivity of the drought patterns to different datasets and different drought indices.

5.1 The drought patterns

Fig.5.1 presents the SOMs classification (3x4 nodes array) of SPEI distribution over Southern Africa depicting the major drought patterns over the sub-continent. As expected of any SOM result, the nodes at the four edges of the array (i.e. nodes 1, 4, 9 and 12) show the most extreme patterns, while other nodes feature patterns that provide a continuous transition among the four extreme patterns. Node (1) shows a widespread dry condition (negative SPEI) over the entire Southern Africa, except along the tropical eastern coast (north-eastern Mozambique and eastern Tanzania) and south-western tip of South Africa. However, the core of the dry conditions (SPEI < -1.0) is over the Caprivi Strip (Northern Botswana, north-eastern Namibia, south-eastern Angola and south-western Zimbabwe). In contrast to node (1), Node (12) shows a wet condition (positive SPEI) over the entire southern Africa, and the core of the wet condition (SPEI > 1.0) is located over northern Botswana. Node (9) shows a dipole pattern, with dry conditions located north of 20˚S and the wet condition located south of 20˚S. The core of the dry condition extends from northern Mozambique to southern DRC, while the core of the wet condition is over the Drakensberg mountain ranges (in Lesotho). Node (4) is a mirror image of Node (9), except that the core of the wet condition extends from Mozambique to Tanzania while the core of the dry condition is over the northern part of South Africa. The most frequent drought patterns are Nodes (3) and (12); each accounts for about 11%

of the dataset. The driest drought pattern is Node (1) (i.e. the mean SPEI = -0.53) while the wettest drought pattern is Node (12) (i.e. mean SPEI = +0.53). In general, the drought patterns may also be broadly classified into three conditions: the all-dry patterns (Nodes 1, 2, 5, and 6), the all-wet patterns (Nodes 7, 8, 11 and 12), and the dipole patterns (Nodes 3, 4, 9 and 10).

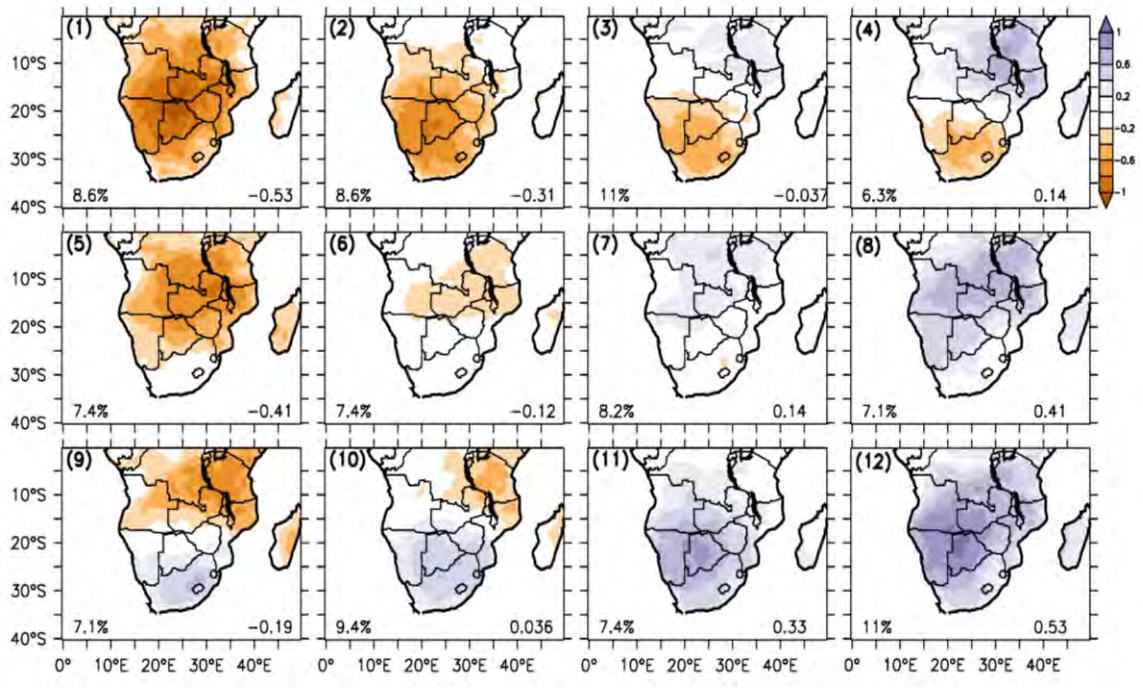

Figure 5.1: The SOM array (3 x 4 nodes) of the seasonal SPEI (3-month scale). Each node represents a drought pattern over Southern Africa in 1950 - 2013. Negative SPEI corresponds to a dry condition while the positive values correspond to a wet condition. In each panel, the node tag is on the upper left corner of the panel, the frequency of occurrence (%) of the node is on the lower left corner, and the mean SPEI (over Southern Africa) is on the lower right corner.

There is a good agreement between the SOM drought patterns (Fig. 5.1) and those obtained by Ujeneza and Abiodun (2014; hereafter, UA2014) using the rotated Principal Component Analysis (PCA). All the four drought patterns (PF1, PF2, PF3, and PF4) in UA2014 appear in Fig.5.1. For instance, PF1 roughly corresponds to Nodes (2) and (11), PF2 to Nodes (5) and (8), PF3 to Nodes (4) and (9), and PF4 to Nodes (6) and (7). Nevertheless, some of the drought patterns in Fig.5.1 are missing in the UA2014 classification. For instance, Nodes (1) and (12) patterns, which depict dry and wet conditions (respectively) over the entire Southern Africa, are not in UA2014. In addition,

Node (7) that features wet/neutral condition is also missing in UA2014 results. This may be because the PCA classification of UA2014 only accounts for 50% of the SPEI variations over Southern Africa. Hence, since the SOMs analysis used in the present study accounts for all the SPEI variations, the drought classification in Fig.5.1 may provide a more robust and more extensive classification than the one in UA2014. To further investigate the robustness of the drought patterns, we repeated the SOM analysis separately for each season, i.e., December-January-February (DJF), March-April-May (MAM), June-July-August (JJA) and September-October-November (SON). The classification of the drought patterns for each season (not shown) roughly remains the same as in Fig.5.1, especially the nodes at the four edges of the array (Nodes 1, 4, 9, and 12).

5.2 Seasonal and decadal distribution of the drought patterns

Fig. 5.2 shows the seasonal variation of the drought patterns (displayed in Fig.5.1) and reveals that the drought patterns (except Node 5) can occur in any season; however, each drought pattern has preference for a season. Node (1) has preference for austral autumn (MAM; 8 events), while Node (12) has preference for austral winter (JJA; 12 events). Node (10) has its highest frequency in austral spring (SON; 10 events), while Node (4) and (9) mostly occur in summer (DJF; 6 and 8 events, respectively). Conversely, Node (5) does not occur in summer (DJF), Node (6) rarely occurs in autumn MAM (1 event), while Node (10) and (11) hardly feature in austral winter (JJA; 1 event each). The reason for the seasonal preference of the drought patterns is not clear and remains a subject of future study.

The decadal frequency of the drought patterns (Fig.5.3) suggests a general shift in the Southern African drought pattern, from all-wet patterns (in the earlier three decades, i.e. 1950 – 1970) to all-dry patterns (in the last three decades., 1990 – 2010). For instance, there has been a positive trend (increase) in decadal frequency of Nodes (2), (5) and (6) since 1960, but a negative trend (decrease) in the decadal frequency of Nodes (2), (8) and

(12). While Nodes (2) and (6) have been the most dominant drought pattern since 1990, Nodes (8) and (12) have not occurred since 1990. However, there is no distinct trend in the decadal frequency of the dipole patterns. Fig.5.3 also shows that the drought patterns have their maximum decadal frequency in different periods. For example, Nodes (1) and (9) feature their maximum decadal frequency in 1990 (9 and 6 events, respectively), Node (11) in 1950 (9 events), and Node (3) in 1980 (9 events).

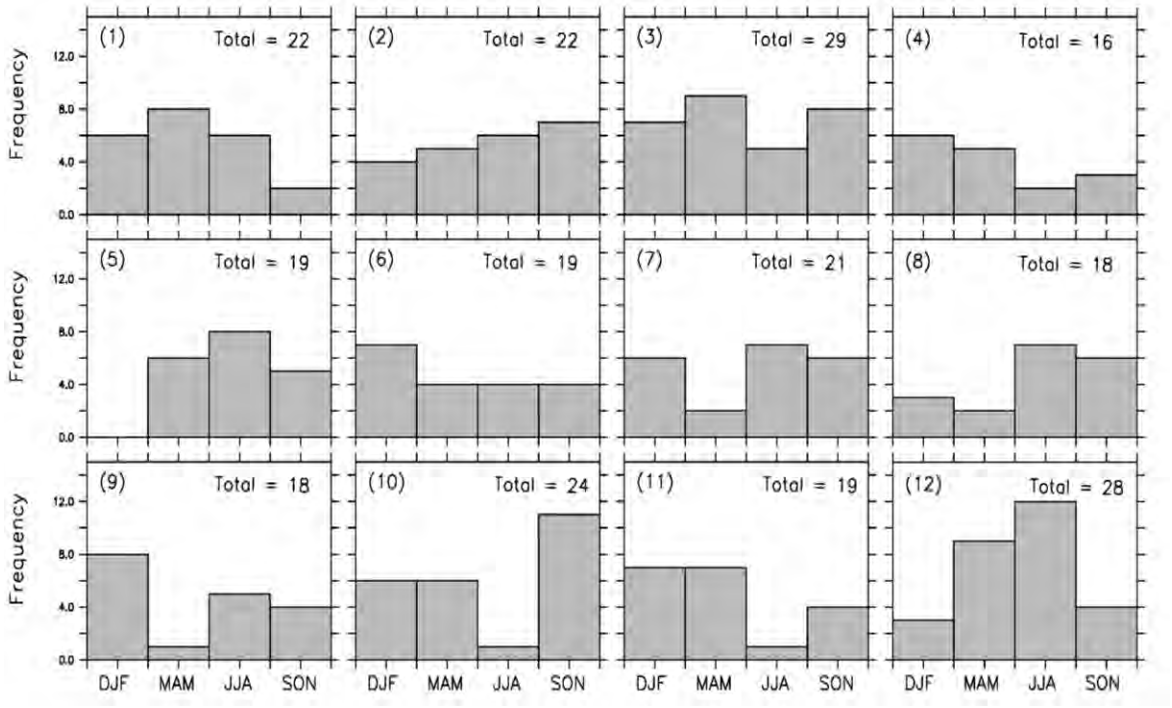

Figure 5.2: The seasonal variation of the drought patterns (shown in Fig. 5.1). The total number of events for each drought pattern is indicated in the panel.

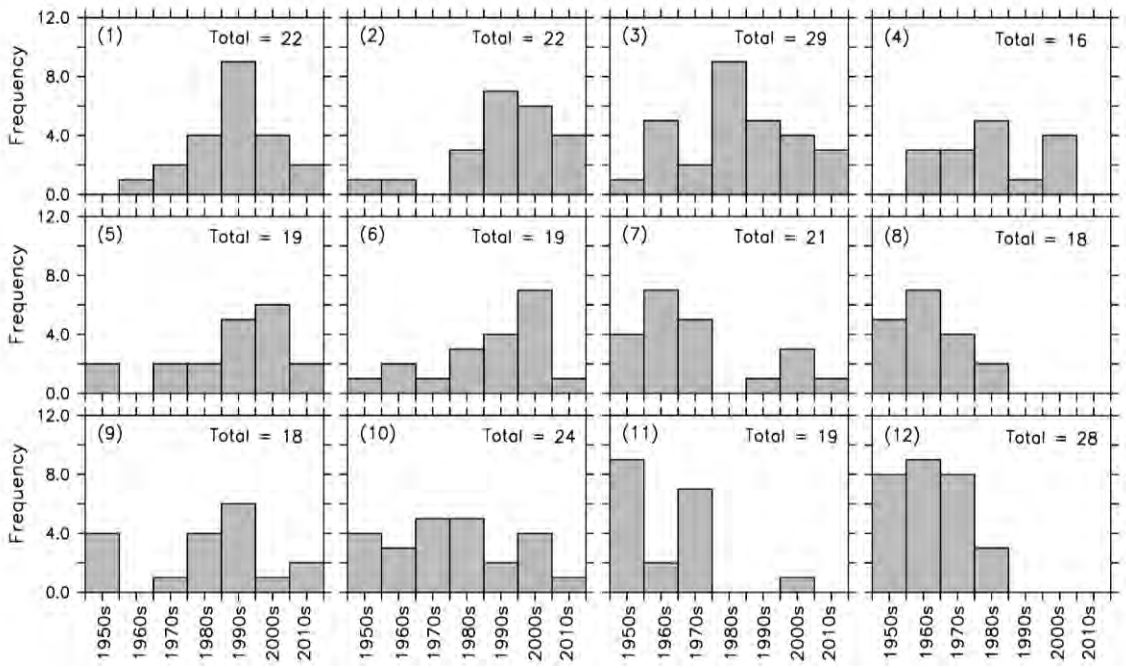

Figure 5.3: The decadal variation of the drought patterns (shown in Fig 5.1). The total number of events for each drought pattern is indicated in the panel.

5.3 Sensitivity of the drought patterns to different datasets and different drought indices

To investigate the sensitivity of the drought patterns and their characteristics to datasets, we repeated the SOMs analysis with another observation dataset from the University of Delaware (hereafter, UDEL). The results of the analysis (shown in Fig.5. 4) are generally the same as for CRU dataset. For instance, the spatial distribution of the extreme drought patterns are the same as in CRU (except for the different arrangement of the patterns), and the percentage frequency of the patterns is comparable with the corresponding patterns in CRU. More importantly, UDEL agrees with CRU on the shift of Southern African drought patterns, from all-wet patterns (in the earlier three decades, i.e. 1950 – 1970) to all-dry patterns (in the last three decades, 1990 – 2010). For instance, UDEL shows that while Node (12) has been the dominant since 1990, Node (1) has not featured since 1990. The few differences between UDEL and CRU results might be due to the difference the time coverage; while UDEL covers 1950 – 2010, CRU covers 1950-2013.

We also tested the sensitivity of the drought pattern and characteristics to different drought indices, by repeating the SOM analysis with SPI, which uses only rainfall to monitor droughts; CRU rainfall data was used for SPI calculation. The results (Fig.5.5) show that SPI produces similar droughts as of SPEI, but the decadal variability of the SPI drought patterns differs from that of SPEI, at least in three ways. First, the SPI does not reproduce the general shift in the Southern African drought patterns, from all-wet patterns to all-dry patterns. Second, in contrast to the SPEI, SPI shows that the all-wet patterns (Node 9 and 10; Fig.5.5) have occurred more than 10 times in the last decades. Third, SPI has not featured the driest drought pattern (Node 4; Fig.5.5) since 2000, whereas, SPEI has featured it seven times. However, the comparison of SPEI and SPI results suggest that the general shift in Southern African drought pattern, from all-wet patterns to all-dry patterns, is due to the temperature influence on the drought identification, and the shift is consistent with the impact of global warming on Southern Africa climate (i.e., Tadross et al., 2005). Hence, the comparison further provides compelling evidence that inclusion of temperature in drought monitoring (i.e. in drought index) may give a better understanding of the characteristics and dynamics of Southern African droughts.

(a)

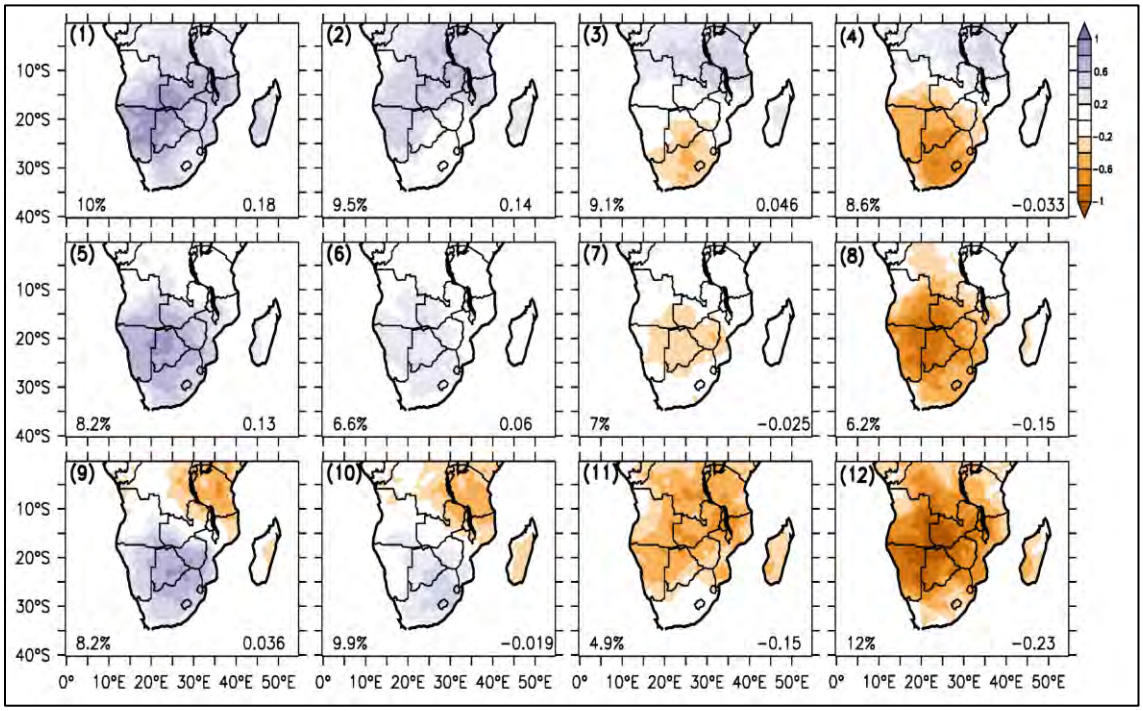

(b)

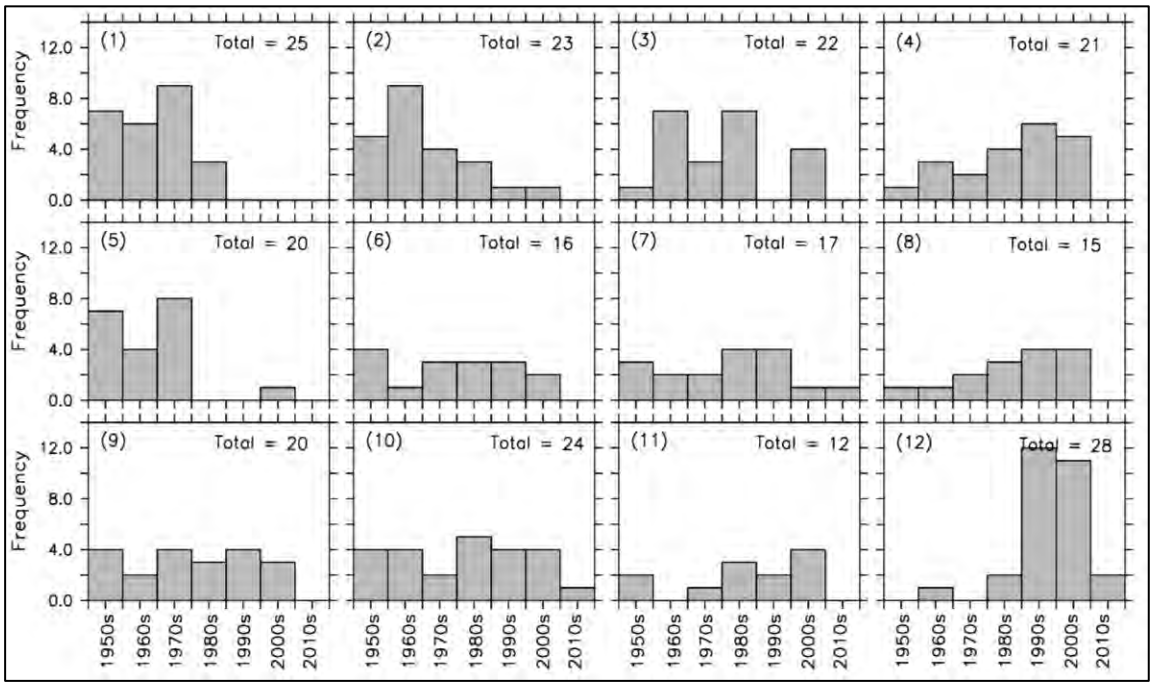

Figure 5.4: (a) The SOM classification of drought patterns obtained with the UDEL dataset (upper panel); and (b) the corresponding decadal frequency of the drought patterns. The labels are as in figures (5.1) and (5.3), respectively.

(a)

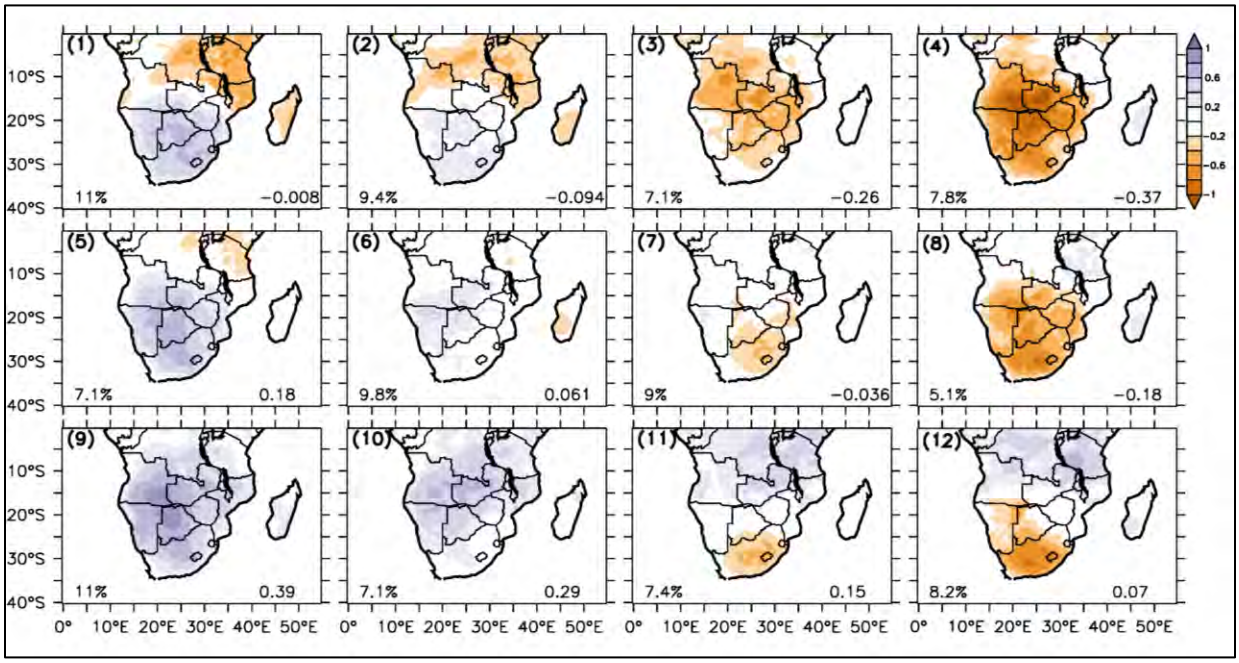

(b)

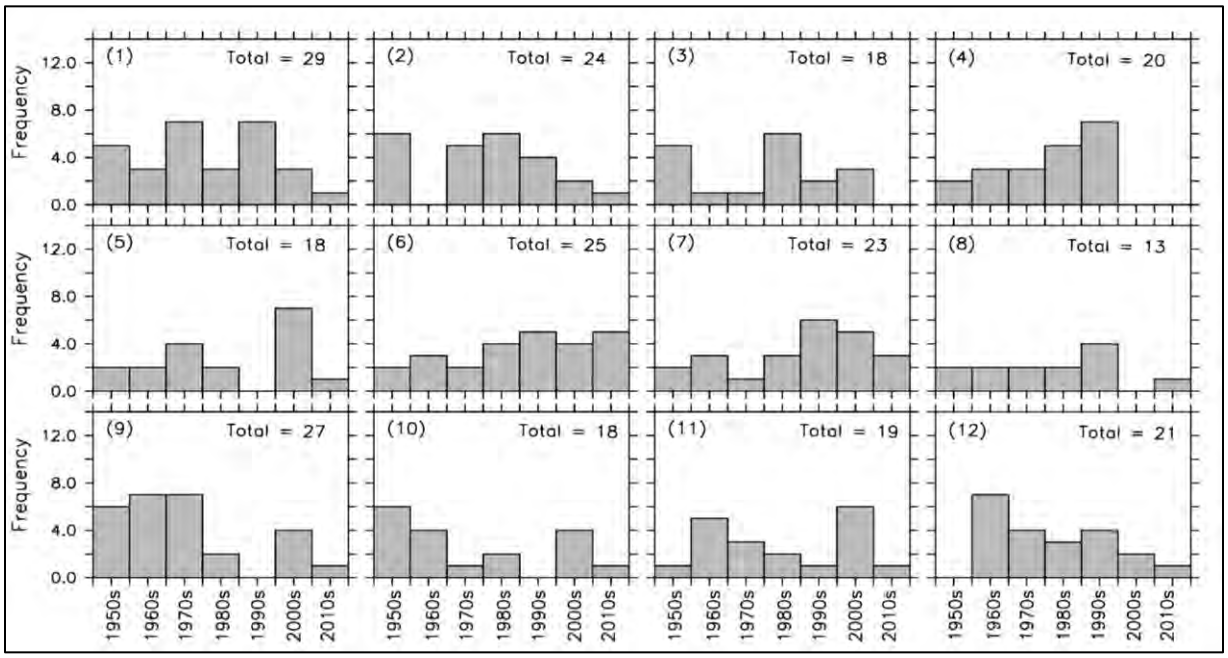

Figure 5.5: (a) the SOM classification of drought patterns obtained with SPI; and (b) the corresponding decadal frequency of the drought patterns. The labels are as in figures (5.1) and (5.3), respectively.

5.4 Sensitivity of the drought patterns to different formulation of PET

To investigate the sensitivity of the results to changes in methods of obtaining PET for SPEI calculation, we repeated the SOMs analysis but using SPEI_PM, which was obtained using the Penman-Monteith method. The result shows that the general structure of the new drought patterns (Fig.5.6) is similar to the one generated when using the Thornthwaite method (SPEI_TH). The only difference is that node (1) in the two approaches is slightly different. Dry conditions in node 1 cover the whole Southern Africa when using the Thornthwaite, whereas with the PM method some areas such as Tanzania and Northern Mozambique are drought-free. Furthermore, the magnitude of the dryness/wetness is less pronounced when using the PM method. For example, the area-average SPEI in node (1) for the Thornthwaite method is -0.53 while for the PM method, the same node shows area-average SPEI of -0.15. Despite these differences, the two approaches converge in reporting the drought shift over Southern Africa from all-wet patterns to all-dry patterns since 1990s. The two methods also agree that node (1), which represents dry conditions over almost the entire Southern Africa, was very common during the 1990s.

(a)

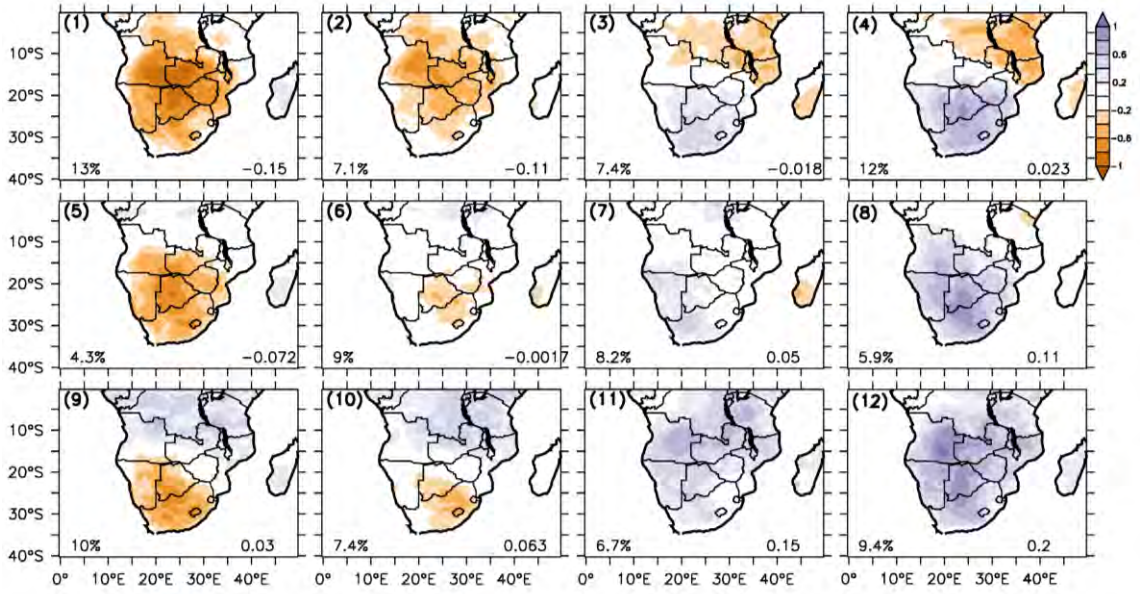

(b)

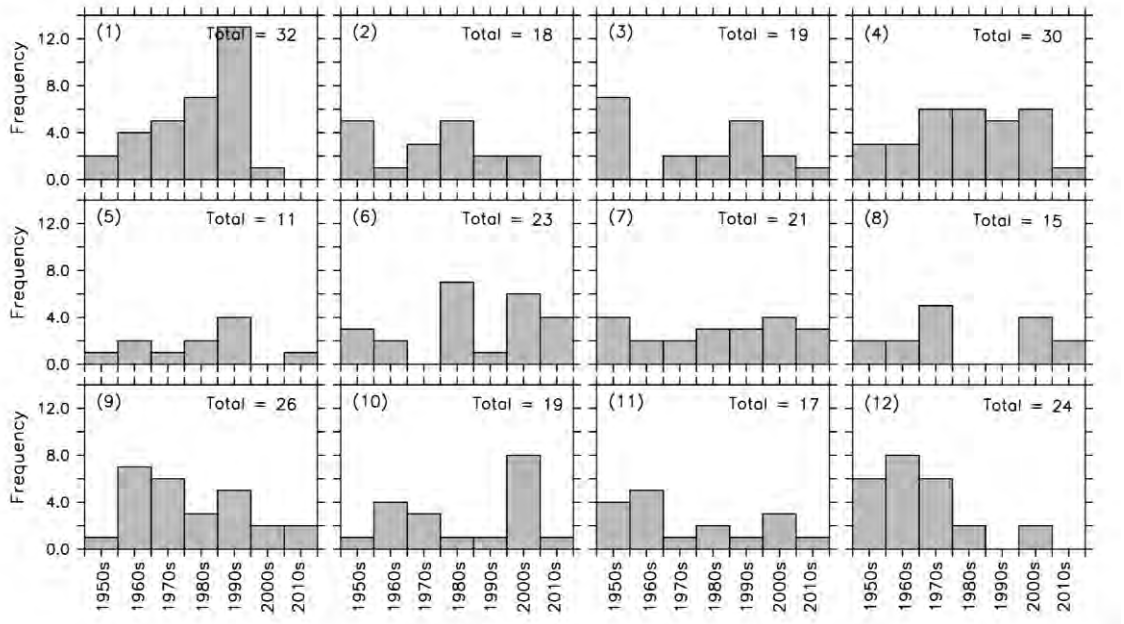

Figure 5.6: (a) The SOM classification of droughts in Southern Africa obtained with the CRU dataset using the Penman-Montheith method for the calculation of PET (upper panel); and (b) the corresponding decadal frequency of the drought patterns. The labels are as in figures (5.1) and (5.3), respectively.

5.5 The persistence and transition of the drought patterns

Figure (5.7a) shows that the general shift in the Southern Africa drought patterns (i.e. from all-wet to all-dry patterns) features in all the seasons, although it is most remarkable in austral winter (JJA) and least notable in austral summer (DJF). No season featured all-wet pattern in the last three years (2011 - 2013), therefore each season has experienced either a persistently dry condition or dipole condition, or a transition between the two conditions during this period. This suggests that the sub-continent has been experiencing a net drying condition over the period.

At the inter-seasonal scale (Fig. 5.7a & b), some drought patterns have persisted for more than a season (Fig.5.7a), although no drought pattern has persisted for a whole year. In this regard, Nodes (7) and (4) have the longest length of persistence; they persisted for three seasons (DJF, MAM and JJA) in 1966 and 1986, respectively. However, Node (12) has the highest number of persistence; it persisted 8 times (i.e. about 30% of its total occurrences). On the other hand, Node (10) has the smallest number of persistence (only once), making it the most transient drought pattern. However, each drought pattern has particular drought patterns it can transit to and those it may not transit to (Fig. 5.7b). The most common transition is from Node (10) to Node (11) and from Node (11) to Node (12). Each of these transitions occurred 7 times in the past. Hence, there is a 30% possibility that Node (10) will always transit to Node (11), and about a 40% probability that Node (11) will always transit to Node (12). However, Node (10) has never transited to Node (4) or to Node (8), while Node (11) has never transited to Node (1), (2), (4), (6) or (9). In addition, there is a possibility for a two-way transition between two extreme drought patterns. For instance, there is one case of Node (1) transiting to Node (12) and five cases of Node (12) transiting to Node (1).

At inter-annual scale (Fig 5.7a & c), Node (12) still has the highest number of persistence (6 cases), but five nodes (Nodes 5, 8, 10, 11, and 12) have the longest period of persistence. Nodes (10) persisted for three austral spring periods (1953 – 1955), Nodes (12) and (5) persisted for three austral winter periods (1953 – 1955 and 2001 – 2003, respectively), while Node (11) lingered for three austral autumn periods (1953 – 1955).

Among the drought patterns, only Node (4) never featured any inter-annual persistence. However, the inter-annual transition among the drought patterns is less organised than that of the seasonal transition. The most common inter-annual transition is from Node (5) to Node (12); it has occurred 6 times in the past. The dynamic behind the transition and persistence of the drought pattern is not yet clear and is beyond the scope of present study, but a good understanding and application of the persistency and transitioning may help improve the seasonal and inter-annual forecasts of droughts over Southern Africa.

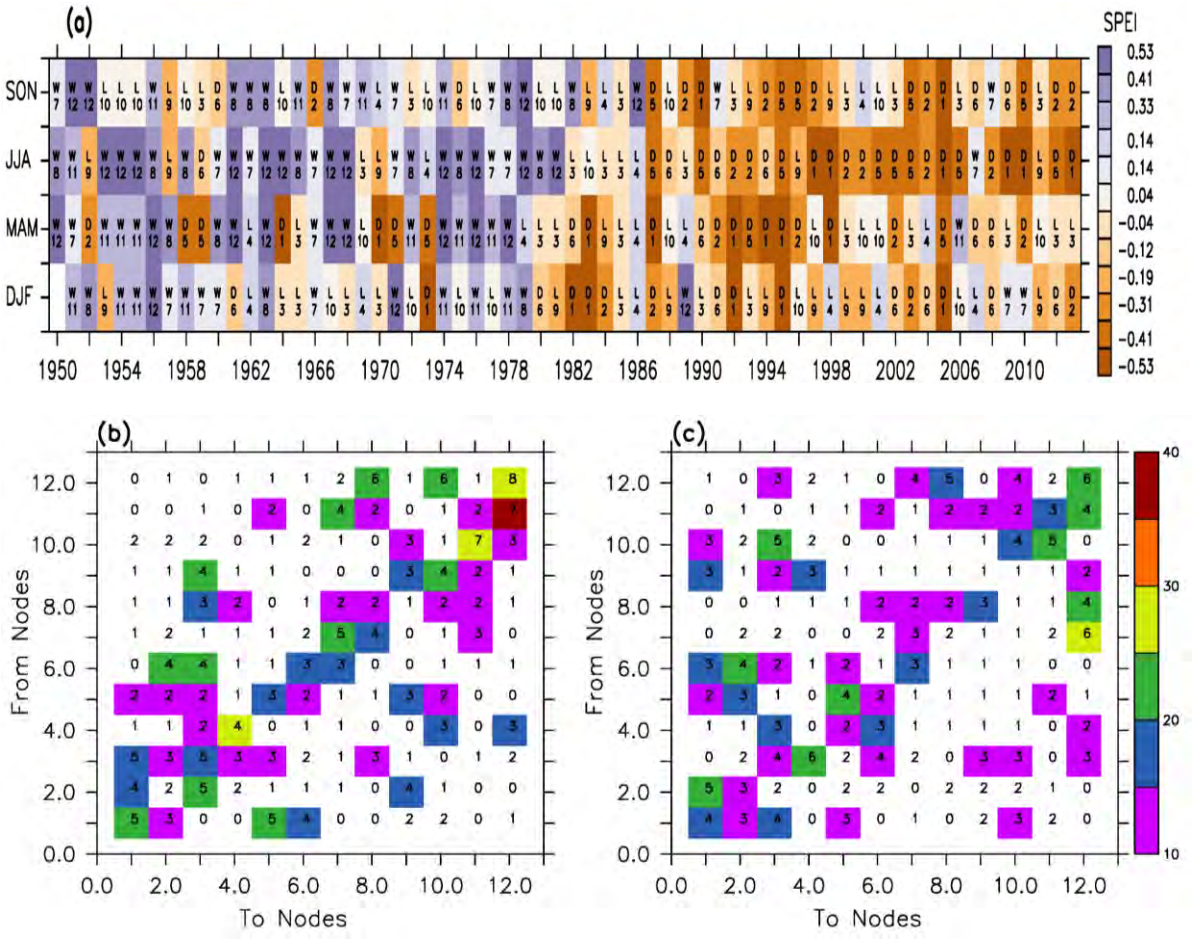

Figure 5.7: The persistence and transition of the drought patterns: (a) the seasonal and yearly occurrences of the drought patterns; (b) the inter-seasonal statistics; and (c) inter-annual statistics. In panel (a), the numbers (1 - 12) indicate the tags of the drought patterns; the letters (W, D and L) indicate the general description of the drought patterns (W = All-wet; D = All-dry; L = Dipole); and the colours show the spatial mean SPEI for the drought patterns. In panel (b) and (c), the numbers indicate the number of time drought patterns on y-axis transit to drought patterns on the x-axis; and the colours indicate the percentage of the transition.

5.6 The relationship between atmospheric teleconnection and the drought patterns in austral summer (DJF)

In this section we examine the impact of the atmospheric teleconnection on the drought patterns during the austral summer. The atmospheric teleconnections considered in this section are ENSO, AAO, Benguela Niño, SASD, SIOD and IOD. All the SST-based indices were calculated based on non-detrended SST from the ERSST dataset. Positive phases of the indices are identified when the SST anomalies are equal to or greater than one standard deviation, whereas the negative events of the indices are identified when the SST anomalies are equal to or less than minus one standard deviation.

As an indication of the relationship between the drought pattern and atmospheric teleconnections, Fig.5.8 presents the frequency of overlapping between the drought patterns and the active phases of the teleconnections in summer. Node (1) and (12) show a substantial and consistent relationship with ENSO, but not with other teleconnections (IOD, AAO, and BEN). For instance, 67% (4 events) of Node (1) occurrences coincides with the positive phase of ENSO (EL- Niño), while 100% (3 events) of Node (12) occurrences happens during the negative phase of ENSO (La Niña). Although Node (1) also shows a substantial relationship with other teleconnections, this relationship is not consistent. For example, the pattern features well during the active phases of BEN (67%), but occurs in both positive (50%) and negative (17%) modes of the teleconnection. It also features well during the active phases of IOD (50%), but mainly during the negative (50%) phases. Node (12), on the other hand, shows no relationship with IOD, weak relationship with BEN (< 34%), and an inconsistent relationship with AAO (< 34% in positive modes). No other drought pattern shows substantial and consistent relationship with ENSO or with other teleconnections. In some cases, two opposite drought patterns feature in the same phase of a teleconnection (i.e. Nodes 4 and 9 in positive IOD; Node 1 and Node 12 in positive and negative AAO). This makes it difficult to relate any of these patterns with the teleconnection. Hence, the most consistent message from the discussion is that Nodes (1) and (2) are the only drought patterns solely induced by ENSO events. However, this does not indicate that all ENSO events will produce Node (1) or Node

(12). Table 5.1 shows the frequency of occurrence of ENSO, AAO, SASD, BEN, IOD and SIOD for each drought pattern.

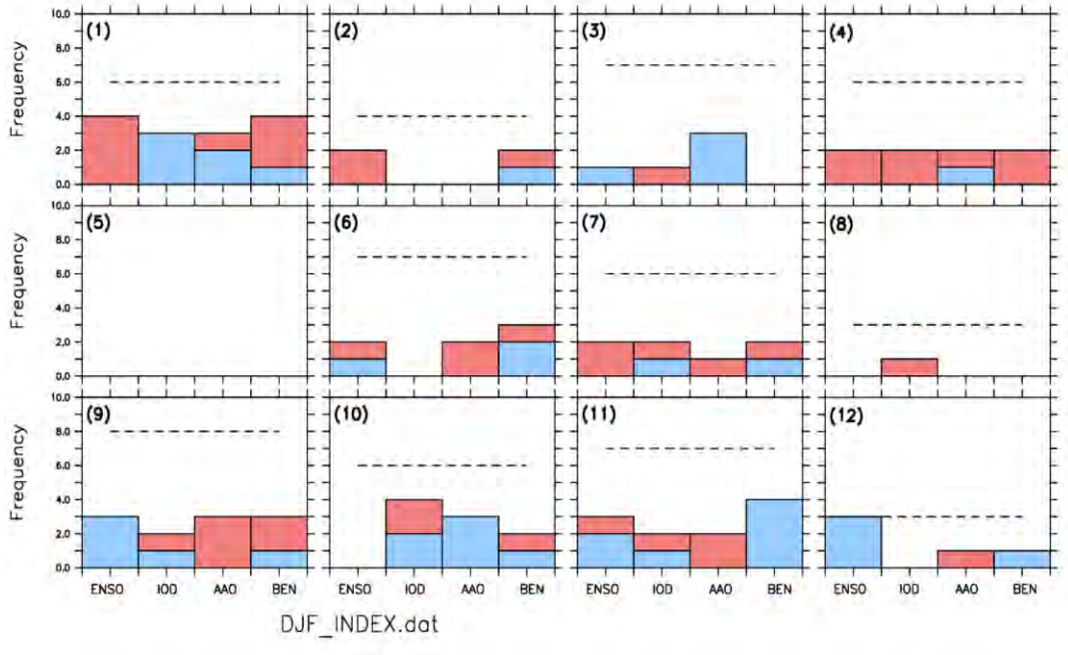

Figure 5.8: The frequency of overlapping between the drought patterns and the active phases (positive: red; negative: blue) of atmospheric teleconnections (i.e. climate indices: ENSO, IOD, AAO and BEN) in DJF. The total number each drought event is indicated with a dash line.

We used the Fisher Exact Test to investigate the association between the climate indices and the drought patterns over Southern Africa. The results of the Fisher Exact Test are to reject the null hypothesis of no association between the climate indices and the drought patterns. The Fisher Exact Test results reveal that ENSO (p-value = 0.003696) and Antarctic Oscillation (p-value=0.01977) have strong association with all the drought patterns over Southern Africa. For instance, when ENSO is in a cool phase (La Niña conditions) and the Antarctic Oscillation is positive, drought pattern 9 has more chances to occur. Drought pattern (1) is associated with El Niño and a negative phase of IOD while drought pattern (12) is significantly linked to la Niña conditions. The results suggest that drought pattern (11) is frequently originated by the co-occurrence of la Niña conditions and negative Benguela Niño.

Table 5.1: Interaction between the 12 nodes (N1…N12) and several climate indices during the austral summer period. ENSO+ represents El Niño events, ENSO- represents La Niña events and ENSO~ represents neutral conditions. The positive and negative signs in each climate indices represent positive and negative phases, respectively.

	N1	N2	N3	N4	N5	N6	N7	N8	N9	N10	N11	N12	Total
ENSO+	4	2	0	2	0	1	2	0	0	0	1	0	**12**
ENSO-	0	0	1	0	0	1	0	0	3	0	3	3	**11**
ENSO~	2	2	6	4	0	5	4	3	5	6	4	0	**41**
IOD+	0	0	1	2	0	0	1	1	1	2	1	0	**9**
IOD-	3	0	0	0	0	0	1	0	1	2	1	0	**8**
AAO+	1	0	0	1	0	2	1	0	3	0	2	1	**11**
AAO-	2	0	3	1	0	0	0	0	0	3	1	1	**11**
BEN+	3	1	0	2	0	1	1	0	2	1	0	0	**11**
BEN-	1	1	0	0	0	2	1	0	1	1	4	1	**12**
SASD+	1	0	0	1	0	1	0	0	2	1	2	0	**8**
SASD-	3	3	1	1	0	0	1	1	0	1	1	0	**12**
SIOD+	1	0	1	0	0	0	1	0	0	1	3	1	**8**
SIOD-	0	0	2	1	0	0	1	1	3	1	1	0	**10**
Total	**21**	**9**	**15**	**15**	**0**	**13**	**14**	**6**	**21**	**19**	**24**	**7**	**164**

Figure (5.9) presents the composite of DJF SST anomalies for each drought pattern. For Node (1), the SST pattern features positive anomalies over both central and eastern Pacific Ocean. In agreement with Hoell et al. (2014), the SST pattern is characterized by warm Indian and tropical Atlantic SST. This SST pattern has been identified as El Niño type 3 (hereafter, EN3; Johnson 2013 and Hoell et al., 2014). Similar SST configuration was found by Ratnam et al (2014), who associated this SST pattern with below-normal rainfall conditions over a bulk of Southern Africa. Node (4) is also associated with warm pool (positive SST anomalies) over the Pacific Ocean, but the warming is confined to the equatorial eastern Pacific Ocean. This SST pattern, which is usually called the eastern Pacific El Niño or Canonical El Niño, is classified as El Niño type 4 (EN4) by Hoell et al., (2014). It is accompanied with warm SST over the tropical Atlantic and tropical Indian Ocean. Hence, Node (1) and Node (4) drought patterns are caused by different 'flavours' of El Niño events.

In contrast, the SST anomaly pattern for Node (12) features cold SST over the equatorial and central Pacific (i.e. La Niña event). This SST pattern, which features cold tropical Atlantic and Indian oceans, is called La Niña type 1 (LN1) in Hoell et al. (2014). Node (9) is also characterised with SST anomalies that shows maximum cooling over the central Pacific Ocean, and features maximum warming over the Southern Atlantic and Southern Indian Oceans. The SST pattern corresponds to La Niña type 4 (LN4) in Hoell et al (2014). Many authors (i.e. Hoell et al., 2014; Johnson 2013) have shown that LN1 dominated the La Niña pattern prior to 1990 while LN4 dominated afterwards. This is consistent with the shifting of Southern African droughts (from all-wet drought patterns to all-dry patterns; Fig.5.3), in that, Node (12) that is associated with LN1 dominated prior to 1990, but has not featured since 1990. Meanwhile Node (6) that is associated with LN4 is becoming more frequent since 1990.

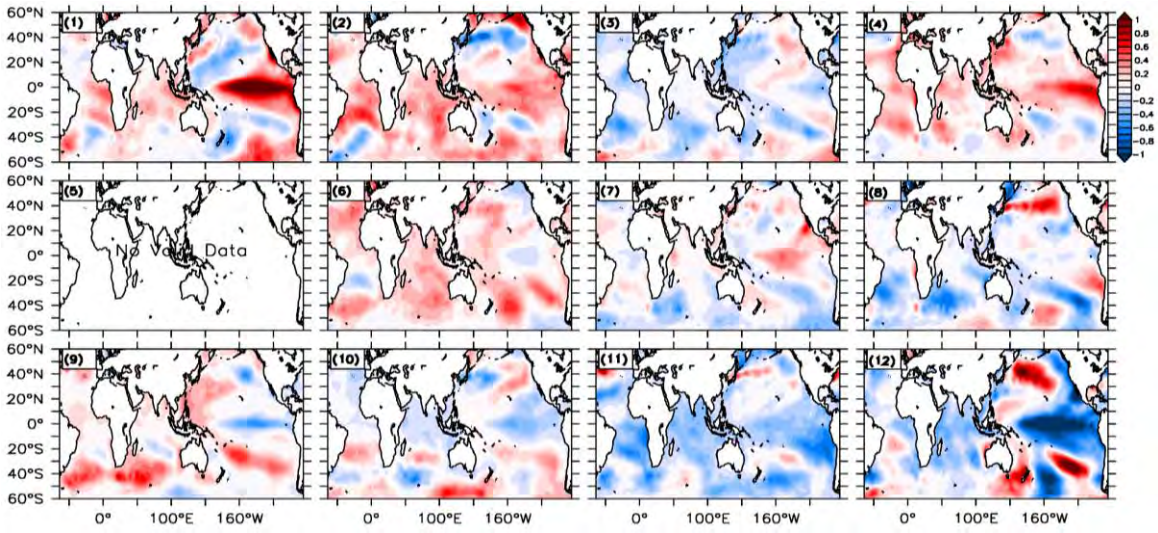

Figure 5.9: Composite of sea surface temperature (SST, ^{o}C) anomalies for the drought patterns during Summer (DJF) in 1950 -2013.

5.7 Composites of rainfall, temperature and dynamic fields

Figure (5.10) presents the composites of DJF rainfall and temperature fields for the extremely different drought pattern (Nodes 1, 4, 9 and 12). A comparison of figures (5.1) with (5.10) shows that, in general, dry conditions (i.e. SPEI < 0) are associated with warming and rainfall deficit, while wet conditions (i.e. SPEI> 0) are induced by cooling and rainfall surplus. This agrees with the general relationship between rainfall and land surface temperature that an increase in rainfall will lower soil temperature (e.g. Trenberth and Shea 2005; Lyon, 2009). However, there are conditions that deviate from this norm. For example, Node (1) shows areas of surplus rainfall with dry condition (SPEI < 0) because of the associated warming. The warming (possibly caused by higher insolation or advection of warmer dry air) produces higher evapotranspiration that exceeds the rainfall surplus and thereby causes a water balance deficits (SPEI < 0) over the areas. For a similar reason, Node (12) features some areas of rainfall deficit with wet condition (SPEI > 0) due to the associated cooling, which reduces the evapotranspiration and causes a water balance surplus (SPEI > 0) over the areas. For a better understanding of the dynamics behind the rainfall and temperature changes that induce the drought patterns, figures (5.10) and (5.11) present the composite of anomalies in vertical wind, moisture transport, and moisture flux convergence for the extremely different drought patterns (Nodes 1, 4, 9 and 12) during DJF.

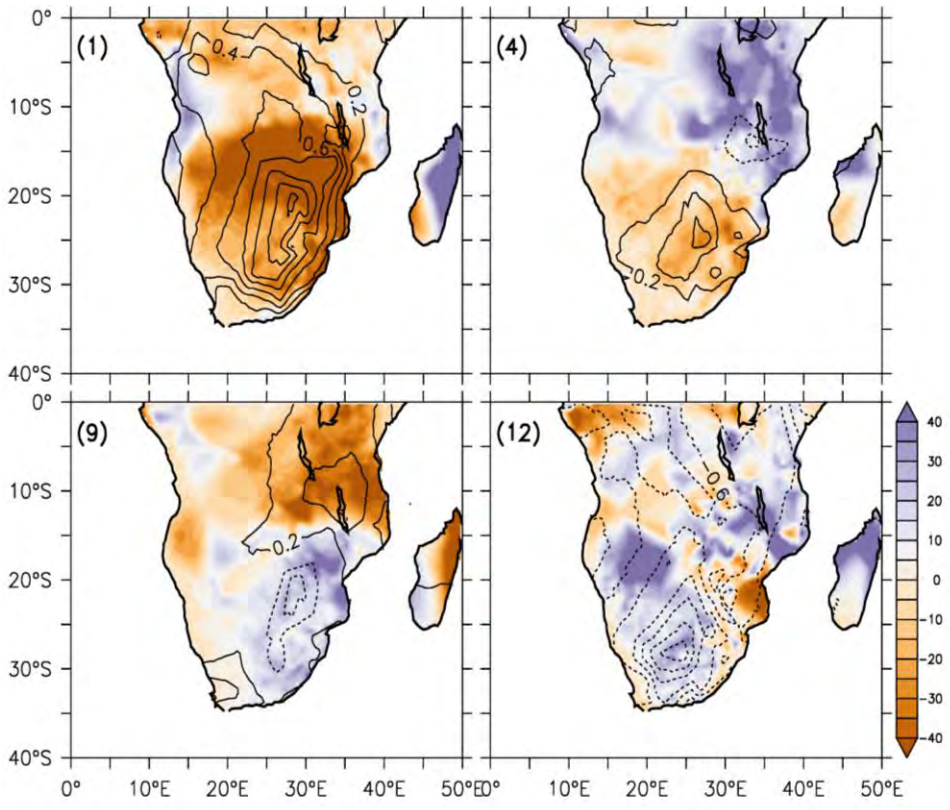

Figure 5.10: Composite of rainfall anomalies (colour; mm/month) and temperature anomalies (^{o}C) for the extremely different drought patterns [i.e. Nodes (1), (4), (9) and (12)] during summer (DJF) in 1950 -2013.

The pattern of vertical wind anomalies (Fig 5.11) for Node (1) is consistent with changes in the corresponding SST anomalies (shown in Fig. 5.9), except over the Atlantic Ocean. The pattern features an increase in convection over the warm SST areas (i.e. over the eastern and central Pacific Ocean and over the central Indian Ocean), but the maximum increase is over the central Pacific Ocean. It also features a decrease in convection over the cold SST areas (i.e. over the western Pacific Ocean), and shows no changes over the Atlantic Ocean despite the warm SST over the ocean. Most importantly, the vertical wind pattern shows a decrease in convection over Southern Africa, with a local maximum decrease at 0^{o} and at 20^{o}N. Fig. 5.11 shows that the decrease in convection is associated with a moisture flux divergence over the sub-continent. The subsidence is consistent with

the rainfall deficit and temperature increase, and hence with the dry conditions (SPEI <0) over the sub-continent.

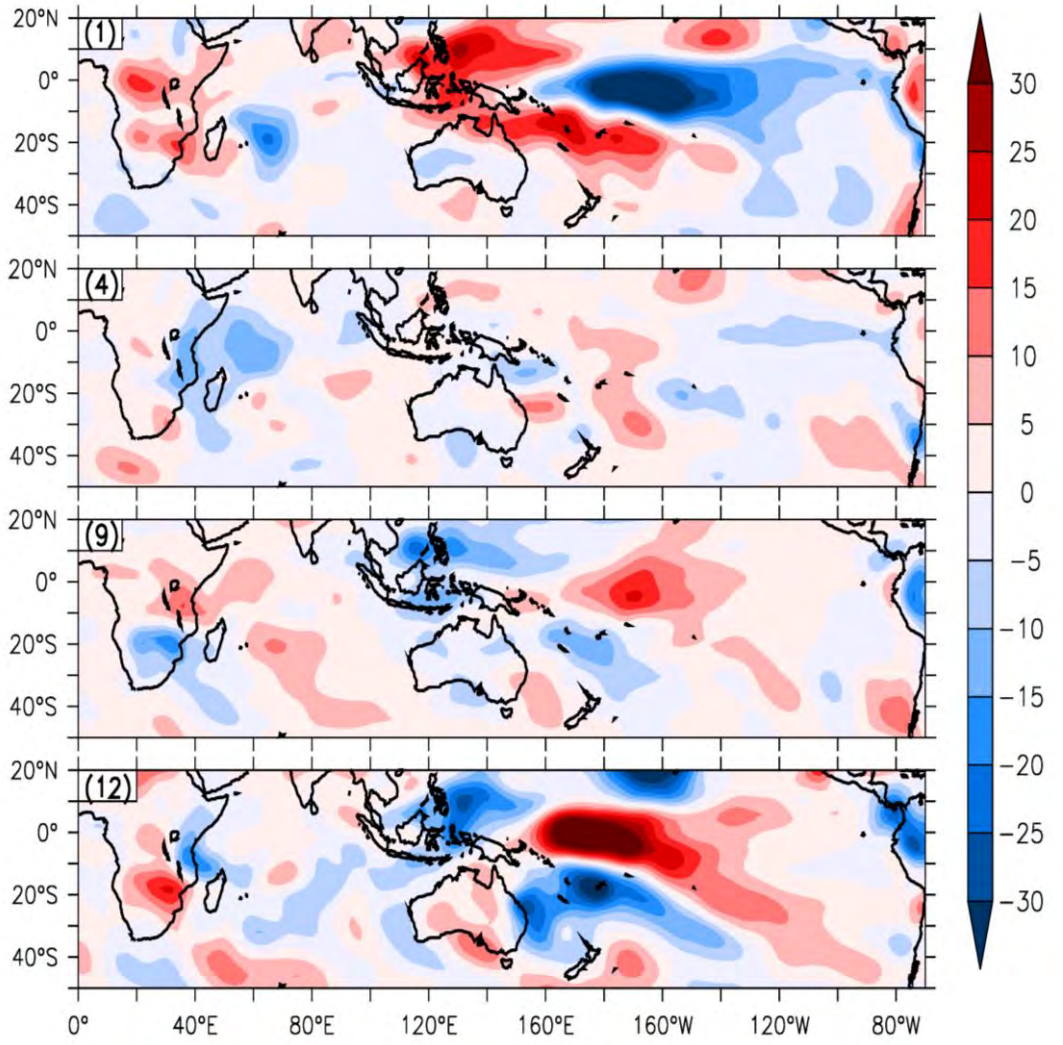

Figure 5.11: The composites of vertical wind (omega) anomalies (x 10^3 Pa s^{-1}) for the extremely different drought patterns (Nodes 1, 4, 9 and 12).

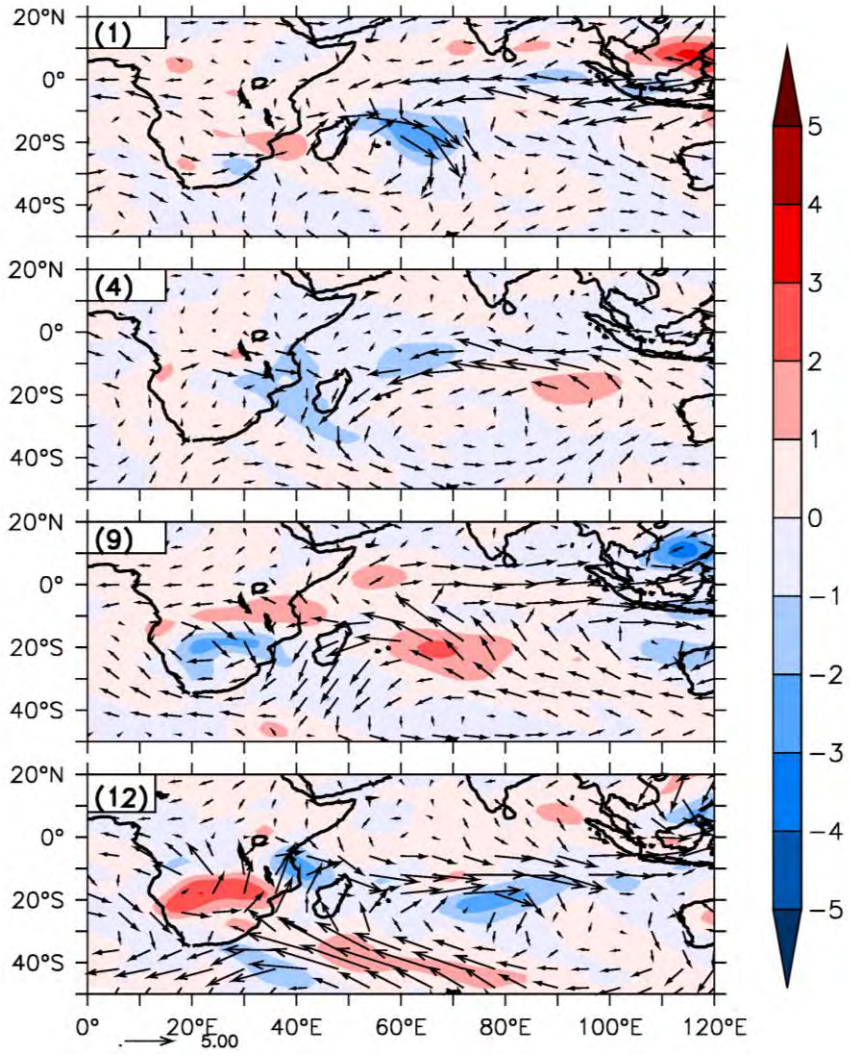

Figure 5.12: The composites of moisture flux (arrows; m s^{-1}) and moisture flux convergence (colour; x $10^{\wedge 6}$ s^{-1}) for the extremely different drought patterns (Nodes 1, 4, 9 and 12).

For Node (12), the vertical velocity pattern is almost a mirror image of Node (1) over the Pacific Ocean and Atlantic Ocean, but not over the Indian Ocean or over Southern Africa. The pattern shows an increased convection that extends from the central Indian Ocean to Southern Africa, and the maximum increase is over south Mozambique (Fig5.11). This is consistent with the maximum moisture flux convergence over the area (Fig5.12). Comparing Node (12) with (1), it seems that the increased convection in Node (12) only replaces the decreased convection at 0^{o} in Node (1) pattern, but not at 20^{o}S. Contrarily to expectation, Node (12) also features a maximum decreased convection at around 20^{o}N, as

in Node (1) pattern. The decreased convection is consistent with the moisture divergence over the area. Hence, there are only two major consistent changes in dynamics of Node (1) and (12), apart from the changes in vertical motion at 0^{o}N. First, the nodes have opposite patterns of vertical motion over the Pacific Ocean (in agreement different mode of ENSO); and second, they feature opposite regional temperature (warm and cool, respectively) over Southern Africa and over the surrounding oceans (i.e. both Indian and Atlantic Oceans). The link between these two dynamic changes is not clear and remains a subject of future study.

For Node (9), over the Pacific Ocean, the vertical wind pattern resembles that of Node (12) though with a lower magnitude. But, over the Indian Ocean and Southern Africa, it is a mirror image of that of Node (12). For instance, in contrast to Node (12), the Node (9) pattern features a decreased convection that extends from the Indian Ocean to Mozambique, and increased convection that extends from south of 20^{o}S over the continent to the Indian Ocean. The pattern is consistent with the location of moisture flux convergence (Fig5.12), rainfall surplus, cooling (Fig.5.10), and wet condition (SPEI >0; Fig.5.1) south of 20^{o}S over the sub-continent. It is also consistent with the location of the moisture flux divergence (Fig5.12), rainfall deficit, warming (Fig.5.10), and wet condition (SPEI >0; Fig5.1) north of 20^{o}S.

For Node (4), the magnitude of the vertical wind changes is weak over the Pacific Ocean, especially when compared with those of other nodes (Fig5.11). The weak magnitude is not consistent with the corresponding SST pattern which shows a strong Canonical El Niño pattern (Fig.5.9). Nevertheless, the magnitude is higher over the Indian Ocean and Southern Africa than over the Pacific Oceans (Fig5.11). In the vertical wind pattern, an enhanced convection extends from 30^{o}S to 5^{o}N and covers the Eastern Africa and western topical Indian Ocean, but convection is suppressed south of 20^{o}N over the sub-continent. The associated moisture flux field (Fig.5.12) shows a strong moisture flux convergence supporting the enhanced convection, and a weak moisture flux divergence in the area of the suppressed convection. However, the location of the enhanced convection is consistent with the cooling and rainfall surplus over the wet areas (i.e., SPEI > 0),

while the location of the suppressed convection is consistent with the warming and rainfall deficit over the dry areas (SPEI < 0).

5.8 Summary

In this chapter, we have studied the characteristics of Southern African droughts and examined the roles of SST and atmospheric teleconnections on the drought patterns. We used the two drought indices (SPEI and SPI) to identify drought patterns. In drought identification, SPI uses only rainfall data while SPEI uses rainfall and temperature data. For comparison, we computed the drought patterns using datasets (observed rainfall and temperature) from two sources: CRU (1950 – 2013) and UDEL (1950 – 2010), and employed the SOM to categorize drought patterns into 12 major patterns. The atmospheric teleconnections (ENSO, AAO, IOD, and BEN, SASD, SIOD) were characterized using their corresponding climate indices. The results of our analysis can be summarised as follows:

- The 12 drought patterns can be broadly categorized into 3 groups. The first group (all-dry patterns) features a dry condition over the entire Southern Africa, the second (all-wet patterns) shows a wet condition over the whole region, but the third group (dipole patterns) shows both wet and dry conditions over the region.
- A comparison with a previous study (Ujeneza and Abiodun, 2014) reveals the classification of Southern African drought patterns using SOM gives a broader and more robust classification than using PCA.
- Although the drought patterns can occur in any season, some drought patterns have preference for seasons.
- While some drought patterns persist from season to season, others easily transit to another pattern in the following season.
- The decadal variability of SPEI drought patterns suggests a general shift in the Southern Africa drought, from “all-wet” condition in 1950s-1970s to “all-dry”

condition in 1990s – 2010s, possibly due to the global warming; but, the shift is missing in the decadal variability of SPI drought patterns.

- Only 20% of the drought patterns are induced solely by El Niño Southern Oscillation Index (ENSO), other drought patterns are caused by complex interactions among the atmospheric teleconnections.

6 : Simulating Southern African drought patterns with CORDEX Models

This chapter examines the capability of RCMs in simulating drought patterns over Southern Africa as described in the previous chapter. We aggregated the SPEI values from the 10 CORDEX RCMs with those from the observations and Reanalysis data creating one big array. The SOM algorithm was used to classify the 3-month SPEI values into 12 drought patterns. Composite analyses of sea surface temperatures, precipitation and temperature associated with each drought pattern were generated for all RCMs.

6.1 The drought patterns in Southern Africa

Figure (6.1) shows that the classification of observed and simulated drought patterns into 12 nodes by SOMs can be broadly categorized into three groups. In the first group (hereafter ADP: nodes 1, 5, and 6), the patterns feature negative SPEI values (dry conditions) over much of Southern Africa. In contrast, the second group (hereafter AWP: nodes, 7,8,11 and 12), the drought patterns feature positive SPEI values (wet conditions) over a bulk of Southern Africa. In the third group (hereafter AMP: nodes, 2,3,4,9 and 10), the SPEI values exhibit a dipole pattern, with positive values dominating one portion of the region and negative SPEI values dominating the other side. For instance, the SPEI values in node (4) are negative over the north-eastern portion of Southern Africa and positive south of 25˚S. This implies that while one portion of Southern Africa is under wet conditions the other portion is experiencing dry conditions. These drought patterns are essentially identical to those obtained in previous chapter but with some notable differences. For example, the negative (positive) SPEI values in node 12(1) displayed in this chapter do not cover much of north of 10˚S as shown in chapter 5. These differences are inevitable since the two chapters use two different periods and the drought patterns presented here not only include observations as in chapter 5 but also model outputs.

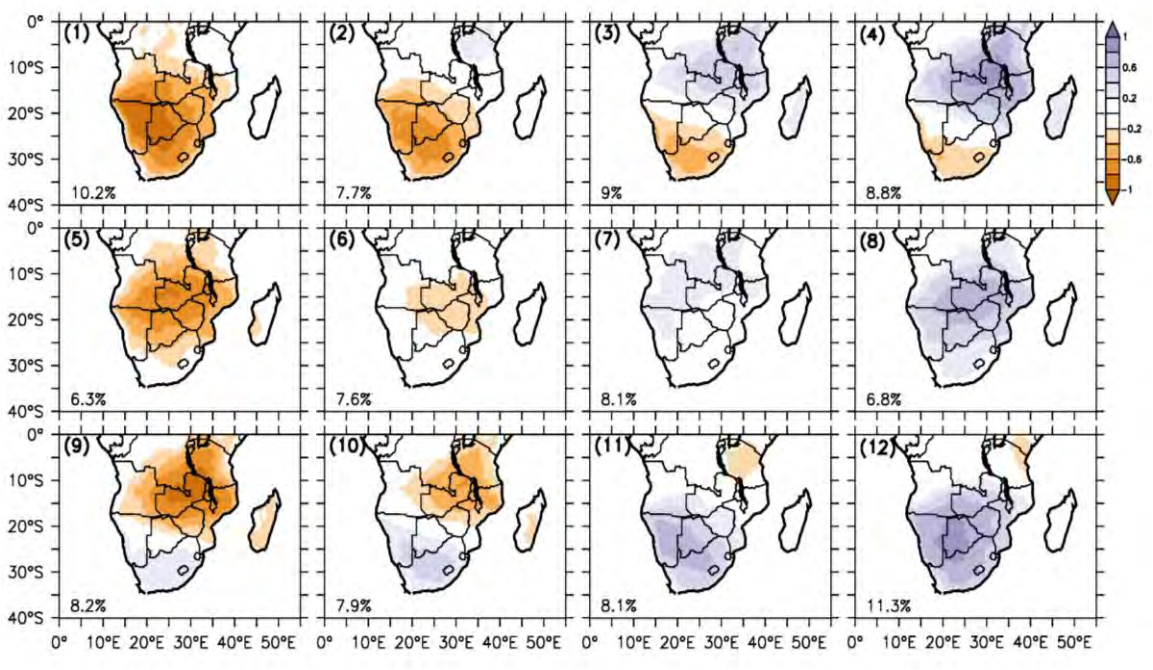

Figure 6.1: Drought regimes generated by a 3X4 SOM array using combined SPEI values from 12 datasets (observations, reanalysis and 10 CORDEX RCMs). The regime number is shown on the top left corner of each panel and the frequency of the regime is shown on the lower left corner.

6.2 Seasonal distribution of the drought patterns in Southern Africa

There are some discrepancies between observations and reanalysis datasets in terms of seasonal distribution of the drought patterns (Fig.6.2). In the observations, pattern 3 is the most frequent (11 events) followed by pattern 12 (10 events), while in the reanalysis dataset, pattern 12 is the most recurrent (11 events) followed by pattern 1 (10 events). Furthermore, in the CRU dataset, patterns 8 and 9 never occurred during the austral summer period and patterns 3, 11 and 12 are most frequent patterns during this period of the year, contributing 16.7% each. In the reanalysis dataset, all the patterns were reported in all the seasons, with patterns 7 and 12 being the most common during the austral summer. Differences can also be spotted in the models simulation of the patterns. PRECIS is the only model reporting high frequency of pattern 3 as in the observation, though the model underestimates the number of events. During the austral summer period, only ARPEGE and RAMCO models capture the absence of patterns 8 and 9.

Some models (i.e., HIRHAM and WRF) simulate the absence of drought pattern 8 while others (REMO, PRECIS, REGCM and CRCM) capture the non-occurrence of pattern 9.

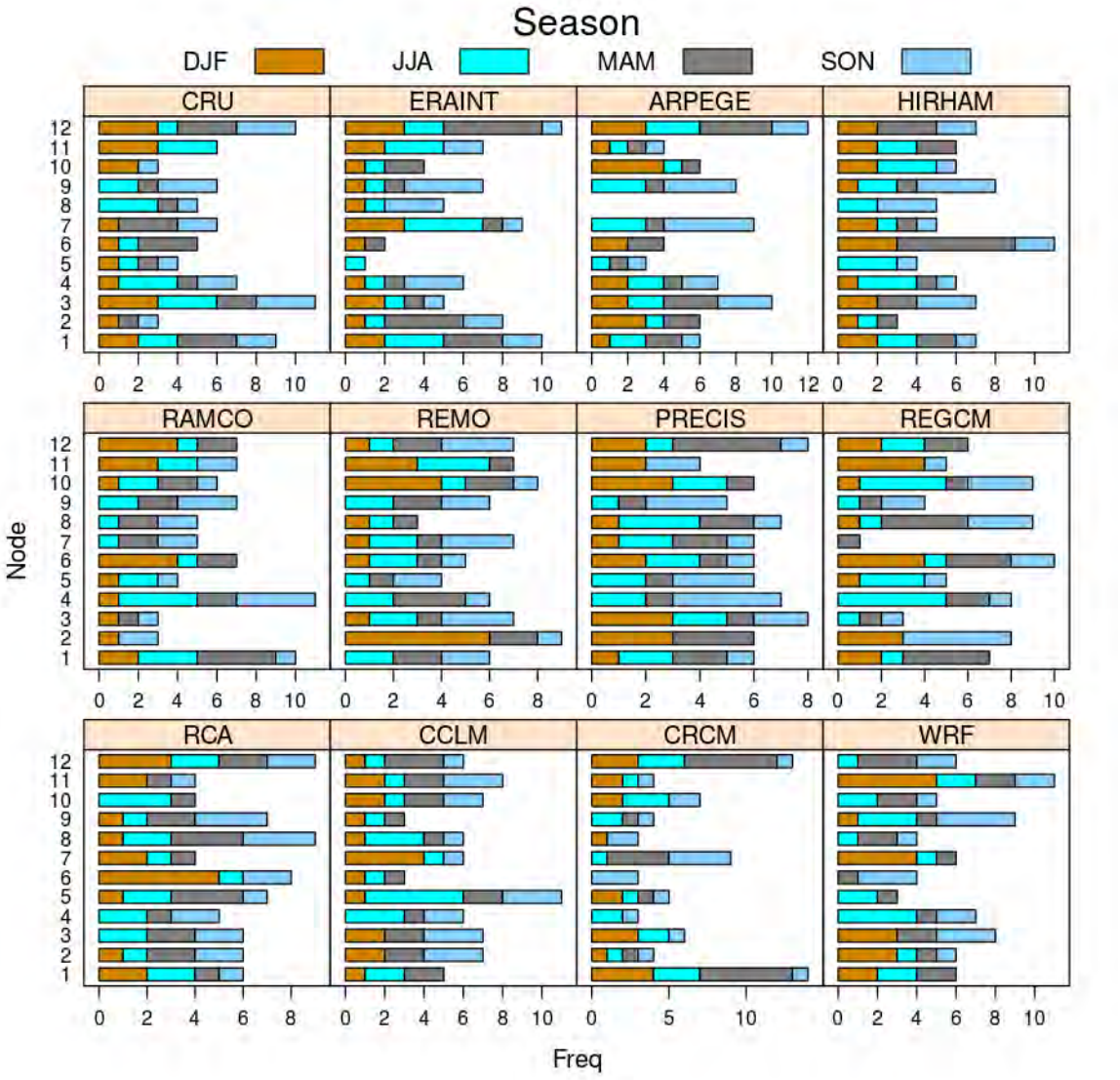

Figure 6.2 : Seasonal frequency of each node (drought pattern) for all the ten 10 CORDEX RCMs, ERAINT reanalysis data and CRU during the 1990-2008 period.

A very skilful RCM is expected to reproduce the drought patterns as in the observation. This means that ideally the frequency of occurrence of the patterns in the RCM is expected to match the one from the observations. Averaging the SPEI values over the

entire domain of study, suggests that the ARPEGE model is more in agreement with the observation than any other RCM in the study (Fig.6.3). It has the highest correlation coefficient (r=0.58) with the observations and possesses the lowest (α≈0.75) root-mean-square-error (RMSE). The model outperforms the reanalysis dataset (ERAINT), which shows a lower correlation coefficient (r=0.52) with the observations. Previous studies (e.g., Kalognomou et al., 2013 and Shongwe et al., 2014) have also reported the good performance of ARPEGE over Southern Africa. Conversely, HIRHAM model has the weakest correlation (r=0.21) with the reference data (CRU), followed by the RCA model, which has a correlation coefficient of 0.25. Overall, the normalized standard deviation of all the models varies from approximately 0.5 to 0.75. REMO model seems to exhibit the lowest amplitude of SPEI values while CCLM and RCA show the highest amplitude.

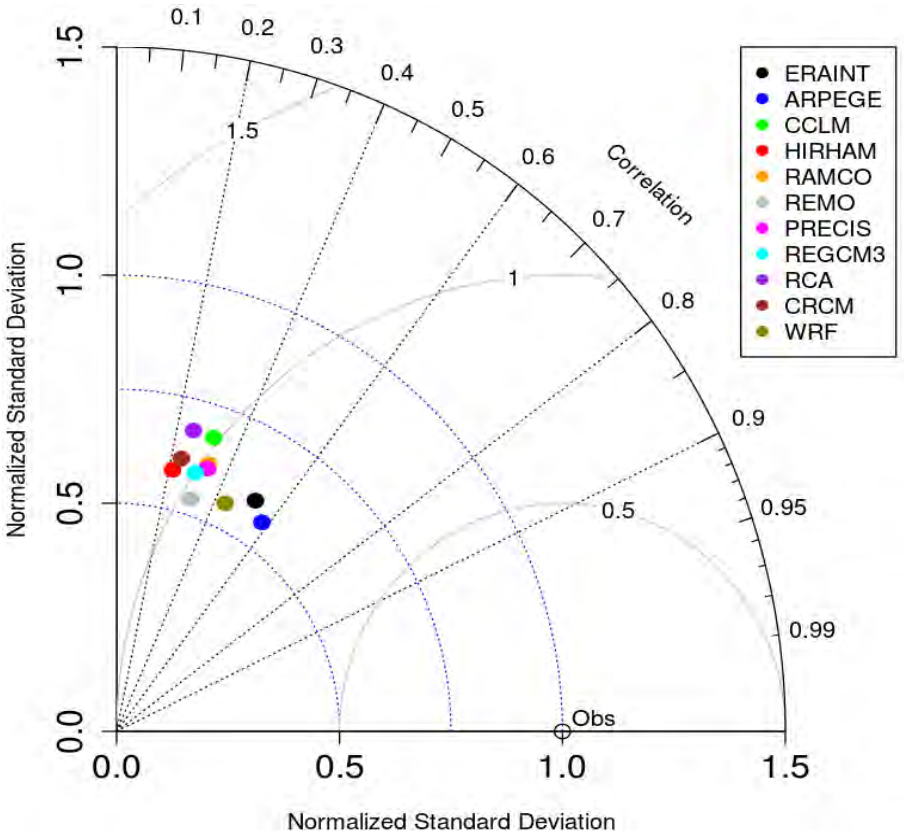

Figure 6.3: Taylor Diagram for area-average monthly SPEI values over the entire Southern Africa during the period 1990-2008. The SPEI values from CRU (open circle along the x-axis) are used as the reference data.

To further understand the performance of the RCMs in reproducing the drought patterns, we computed the correlation between the frequency of occurrence of the drought patterns in the models and observation (see Cassano et al. 2007 and Finnis et al., 2009). The results from the correlation analysis are shown in Table 6.1. The correlation coefficients vary from model to model and from season to season, with some models having positive correlation with the observations while others have negative. The REMO models exhibits the highest correlation (r=0.77) during the austral spring, whereas RCA and CRCM models possess the weakest correlation (r=-0.26) with the observation during autumn and spring, respectively. Overall, there is a poor correlation between models and observation during the austral winter period, which is the dry season over the Southern Africa region with the exception of the Southwestern tip of the region, which experiences a Mediterranean climate (Reason and Jagadheesha,2005; Philippon et al., 2011). It seems that CRCM and RAMCO are the best RCMs for simulating the summer drought patterns, whereas RCA models shows difficulties in simulating drought patterns during this time of the year. CRCM model also performs well during the autumn in conjunction with HIRHAM and ARPEGE models.

The RCM errors during the austral summer are presented in Fig.6.4. The errors were calculated by subtracting node frequencies from the RCM with those from the observation. Generally, the frequency of occurrence of the ADP drought patterns (patterns 1, 5, 6) is well captured by the RCMs than the one from the AWP drought patterns (patterns 7,8,11 and 12). For instance, 50% of the RCMs simulate well pattern 1 and 40% of the models capture pattern 5. On the other hand, only 20% of the models can accurately simulate the frequency of occurrence of pattern 12 and 30% of the CORDEX RCMs reproduce the frequency of pattern 11. Overall, about 60% of the models simulate correctly the frequency of occurrence of pattern 9, while only 20% of the models show the ability to simulate patterns 4, 6, 7. 70% of the CORDEX RCMs grossly underestimate the frequency of occurrence of pattern 3, which is one of the most common patterns in summer. For instance, REGCM and RCA underestimate 17% of the time that the pattern occurs while ARPEGE, HIRHAM and CCLM models underestimate about 6% of the time.

Table 6.1: Correlation coefficients between node frequencies in observation, Reanalysis and the 10 CORDEX RCMs. Bold values represent significant correlation at 90% confidence level.

Model	DJF	MAM	JJA	SON
ERAINT	**0.53**	0.37	-0.06	0.29
ARPEGE	0.49	**0.59**	-0.04	**0.72**
HIRHAM	**0.53**	**0.61**	0.15	0.51
RAMCO	**0.60**	**0.52**	0.31	0.13
REMO	0.19	-0.13	**0.54**	**0.77**
PRECIS	**0.56**	0.49	0.14	0.27
REGCM	0.27	0.48	0.02	-0.42
RCA	0.05	-0.26	-0.06	0.24
CCLM	0.16	-0.1	0.20	-0.23
CRCM	**0.71**	**0.69**	-0.04	-0.26
WRF	0.37	0.10	0.26	0.25

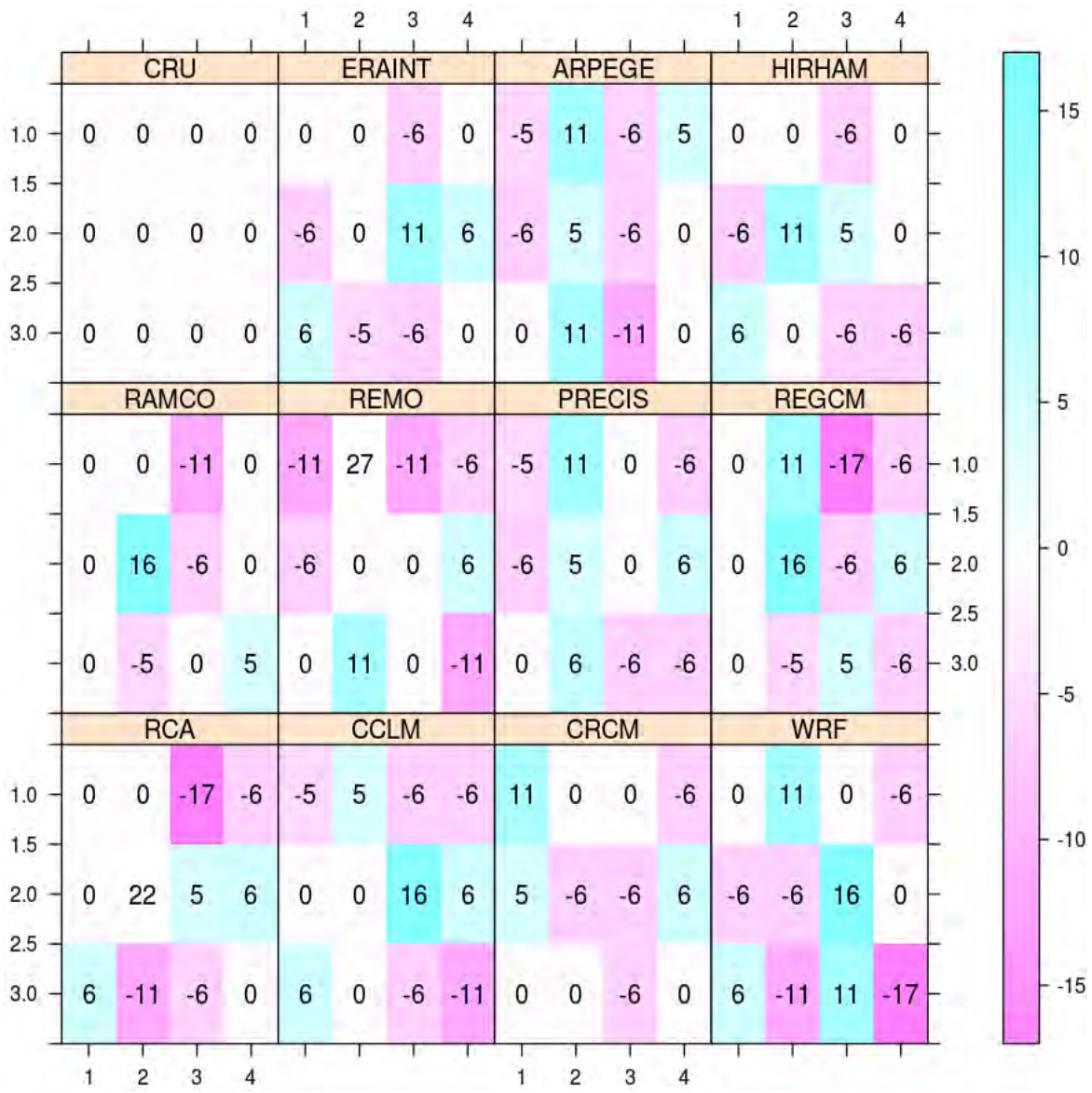

Figure 6.4: Difference (%) in node frequency between the CORDEX models and CRU dataset during the austral summer period. Negative values imply that the model underestimate the frequency of occurrence of a node while a positive value means that the RCM overestimates the frequency of occurrence of the node.

6.3 The persistence and transition of the drought patterns in the models and observation

Some drought patterns can persist from one season to another while others never do (Fig.6.5). For instance, drought pattern (1) has the highest probability of persisting in the following season whenever it occurs. This pattern has persisted for 3 times, which represents more than 30% of its occurrence. Conversely, patterns (2), (5) and (11) are short-lived patterns; they never persisted during the entire period of the study. The drought patterns also show a preference for patterns in which they can transit to. In this regard, drought pattern 11 has an equal probability (P=33%) of transiting to either pattern (4) or (12) in the CRU dataset. Same probability is also observed for the transition of node (9) to (12). The reanalysis dataset (Fig.6.5b) shows a comparable feature with the CRU dataset (Fig6.5a). The two datasets depict the major dry and wet events in Southern Africa. For example, they are in agreement that during the 1991/92 severe drought event, Southern Africa was under the effect of drought pattern (1), which represents dry conditions across the entire region. Unanimously, CRU and Reanalysis data show that this pattern persisted for two consecutive seasons (austral summer and autumn) during the 1991/92 season, affecting the entire growing season in Southern Africa. Furthermore, the two datasets collectively reveal that drought pattern (1) has the highest probability of persisting in the following season whenever it occurs. Obviously, there are some discrepancies between the datasets. For instance, the two datasets disagree on the number of transient drought patterns. While CRU reports only 3 patterns (2, 5 and 11), ERAINT shows 8 (patterns 3, 4,5,6,8,9,10 and 11), which are completely different from those in the CRU dataset.

The probability of a drought pattern to persist or transit to a different pattern varies considerably in the CORDEX models (Fig.6.6 and Fig.6.7). The ARPEGE model is the only model presenting similar results with CRU and ERAINT reanalysis dataset. The model depicts the major wet and dry seasons in Southern Africa. It also captures the occurrence of drought pattern (1) during the 1991/92 drought event and shows high probability of persistence of this pattern. However, the model fails to simulate properly the transition of the drought patterns. Apart from the ARPEGE model, PRECIS is the other model showing high probability of pattern (1) persisting whenever it is observed.

Other RCMs show persistence of different patterns ranging from dry patterns (e.g., CCLM) to wet patterns (e.g., CRCM). With respect to transition of the dry patterns, no single model is in agreement with the observation. All the RCMs (including the Reanalysis dataset) show a multitude of transitions. These differences between the models and observation might be related to the poor phase synchronization (Fig.6.8). No single model shows synchronization above 50%. The ARPEGE model possesses the highest synchronization (η=46.7%) among all the models (including the reanalysis dataset) while RegCM3 has the worst (η=10.75). Despite the relatively weak phase synchronization, some models are capable of simulating the general wet and dry pattern as in the observation. For instance, during the 1996/97 season, CRU dataset shows a persistence of drought pattern 12 during the austral summer and autumn whereas REMO model shows a persistence of drought pattern 11 during the same period. Given the fact that pattern 11 is also markedly a wet node we can infer that the model captured the event.

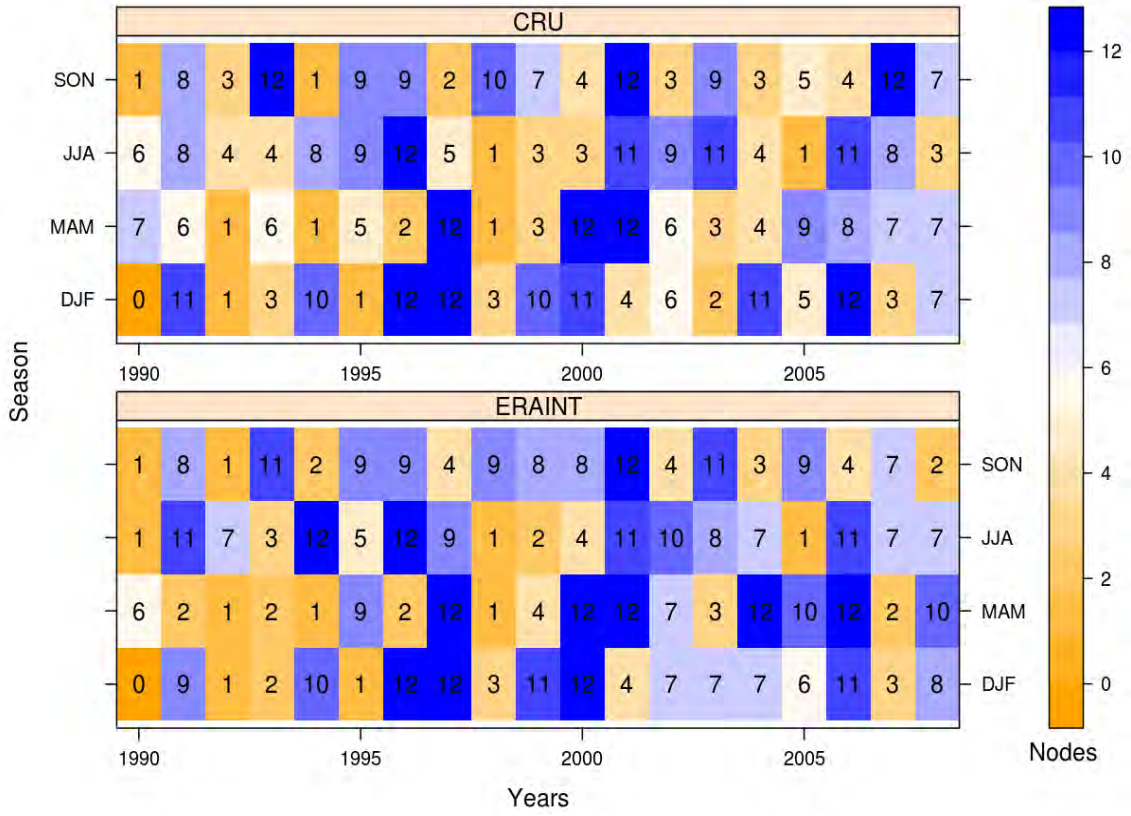

Figure 6.5: Inter-annual variation of the drought patterns in observation and reanalysis data.

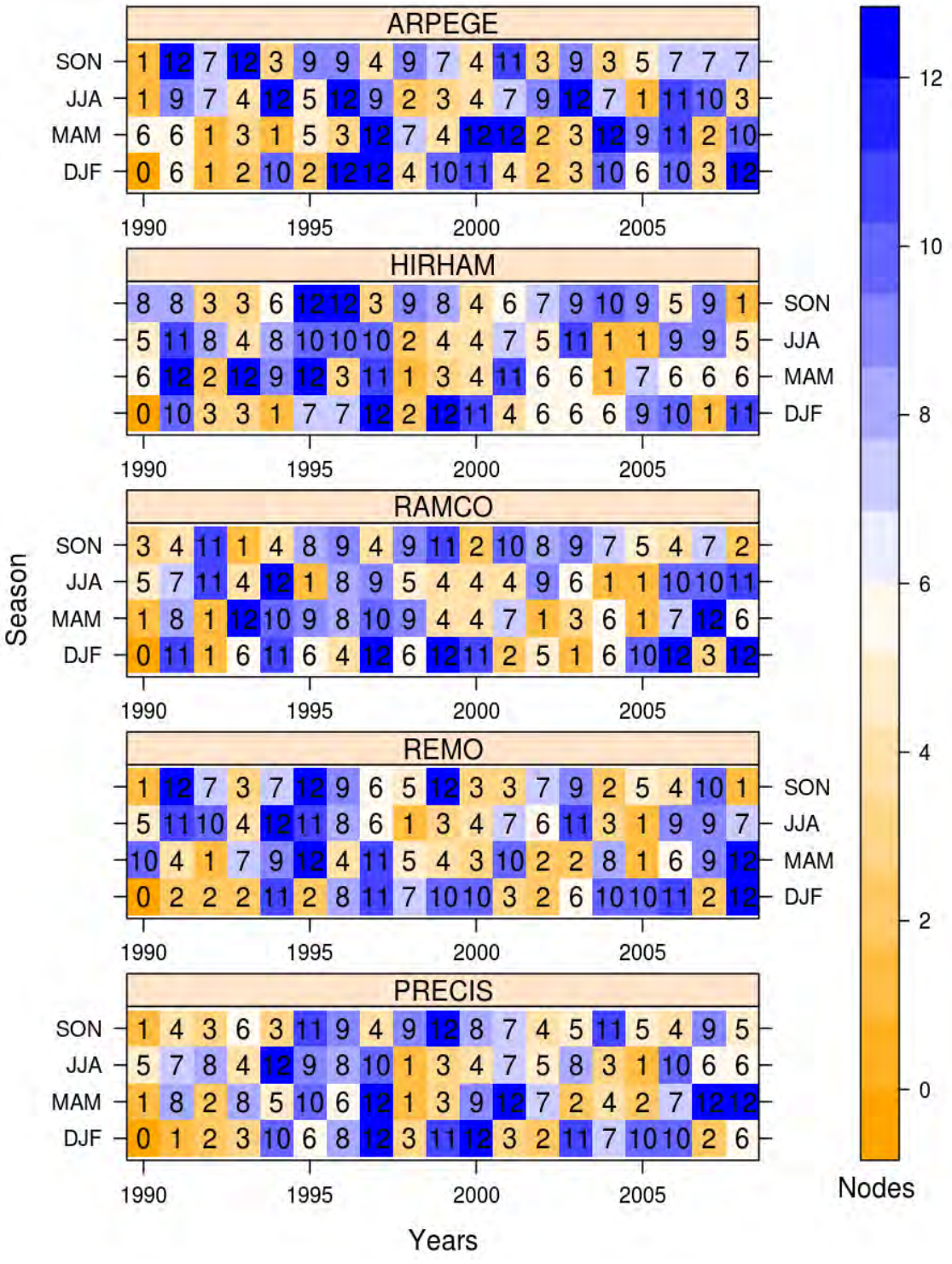

Figure 6.6: Inter-annual variation of the drought patterns in ARPEGE, HIRHAM, RAMCO, REMO and PRECIS models.

.

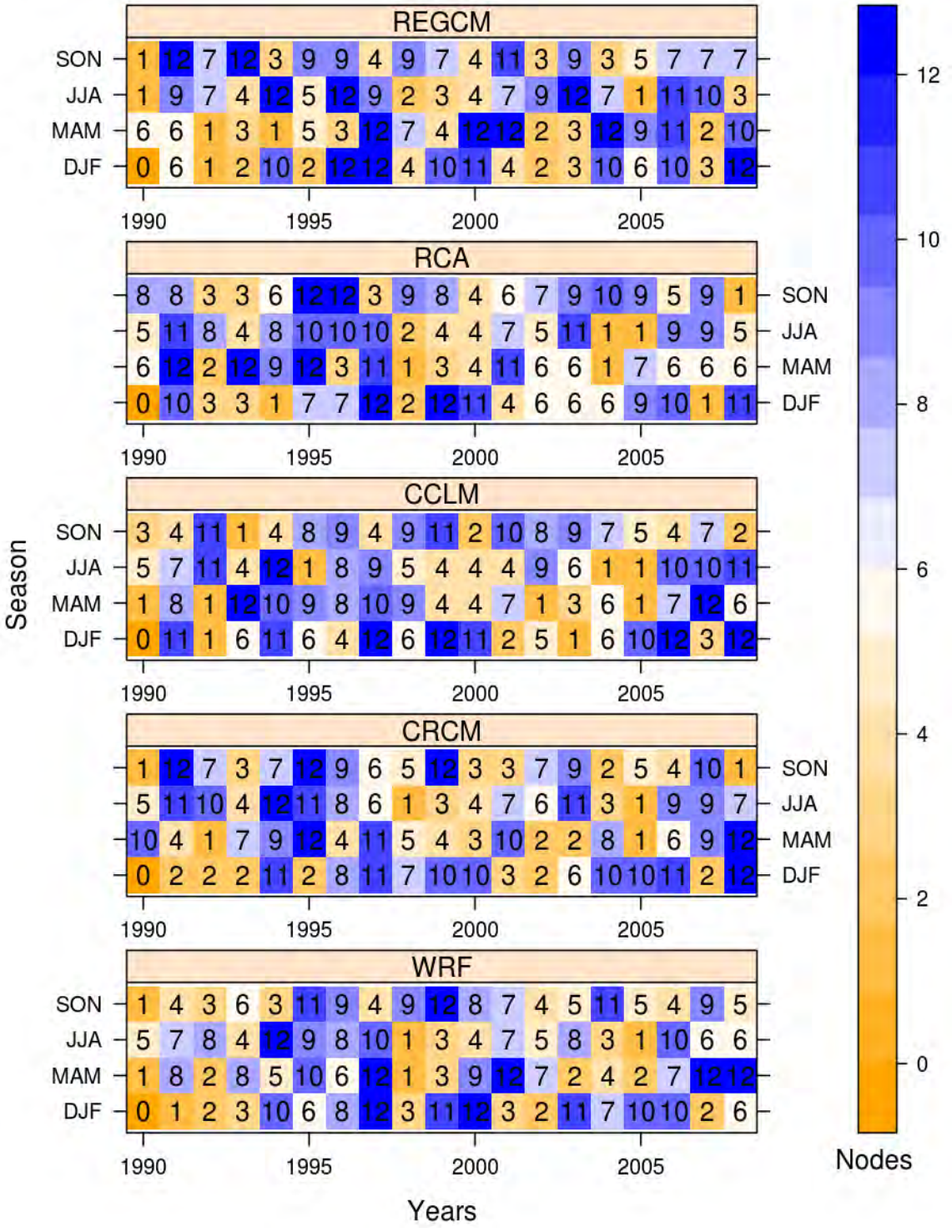

Figure 6.7: Inter-annual variation of the drought patterns simulated by REGCM, RCA, CCLM, CRCM and WRF models.

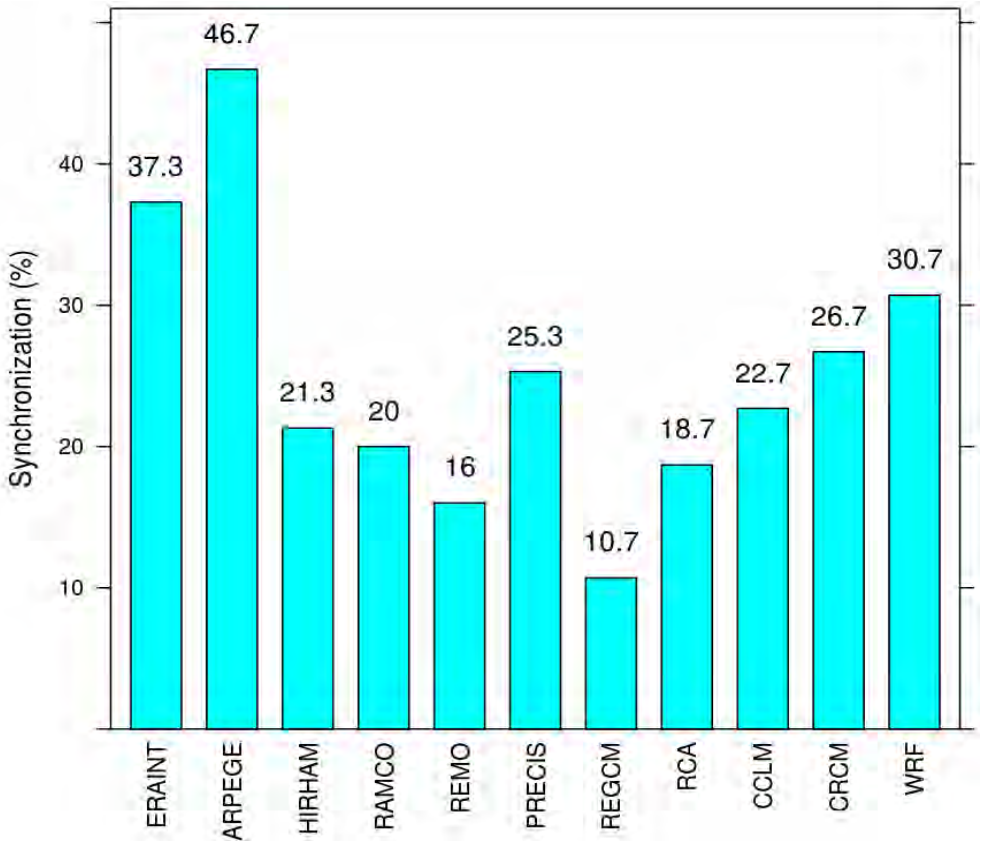

Figure 6.8: Phase synchronization (%) of node occurrence between the CORDEX models and CRU observation.

6.4 Composite anomalies of sea surface temperatures, precipitation and temperature

In this section we investigate how well the models simulate the SST, precipitation and temperature anomalies associated with each drought pattern. For brevity, we only show anomalies of patterns 1 and 12 during the austral summer. We chose these two patterns because of their high frequency of occurrence.

6.4.1 Sea Surface Temperatures

The composited SST anomalies for patterns 1 and 12 show opposite SST patterns in the Pacific Ocean (Fig.6.9 and Fig.6.10). In pattern 1, the SSTs are anomalously warm over the central and eastern Equatorial Pacific. This is a typical characteristic of the so-called

El Niño type 3 (EN3, Johnson et al. 2013; Hoell et al., 2014). Conversely, the SST anomalies during the occurrence of drought pattern 12 are negative over the equatorial eastern Pacific, resembling the La Niña type 4 (LN4) conditions described in Hoell et al. (2014). The SSTs anomalies in pattern 1 and 12 are also different over the Indian Ocean. In pattern 1, the SSTs show warm anomalies over the Western Australia and cold anomalies over the southern Madagascar. This feature of SST anomalies in the Indian Ocean corresponds to the negative phase of the so-called Subtropical Indian Ocean Dipole (SIOD, Behera and Yamagata 2001, Reason 2001, Hansingo and Reason 2009, Morioka et al, 2010).

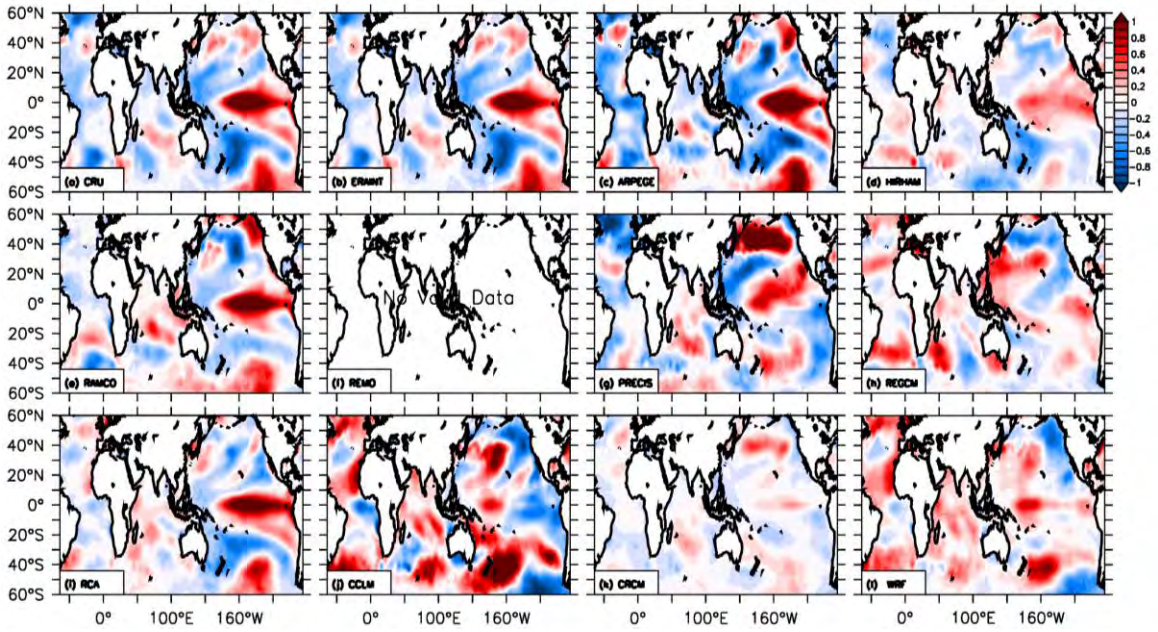

Figure 6.9: Composite of sea surface temperature anomalies (˚C) for nodes 01 during austral summer (December-January-February) period.

In pattern 12, the feature of the SST anomalies is reversed, with cold waters off the coast of Australia and warm waters over the southern Madagascar, which is typical of a positive phase of the SIOD. In the Atlantic Ocean, SSTs in pattern 1 are characterized by slightly positive values off the coast of Southern Africa and negative values on the western side of South Atlantic. These conditions are usually present during the negative phase of the South Atlantic Subtropical Dipole (SASD, Venegas et al. 1997, Fauchereau

et.al 2003, Hermes and Reason 2005, Morioka et al. 2011, Morioka et al. 2012). In pattern 12, the SST anomalies are a mirror image of pattern 1, with negative SST anomalies off the coast of Southern Africa and positive over the western South Atlantic. This feature of SST in the Southern Atlantic Ocean is commonly known as positive phase of the SASD.

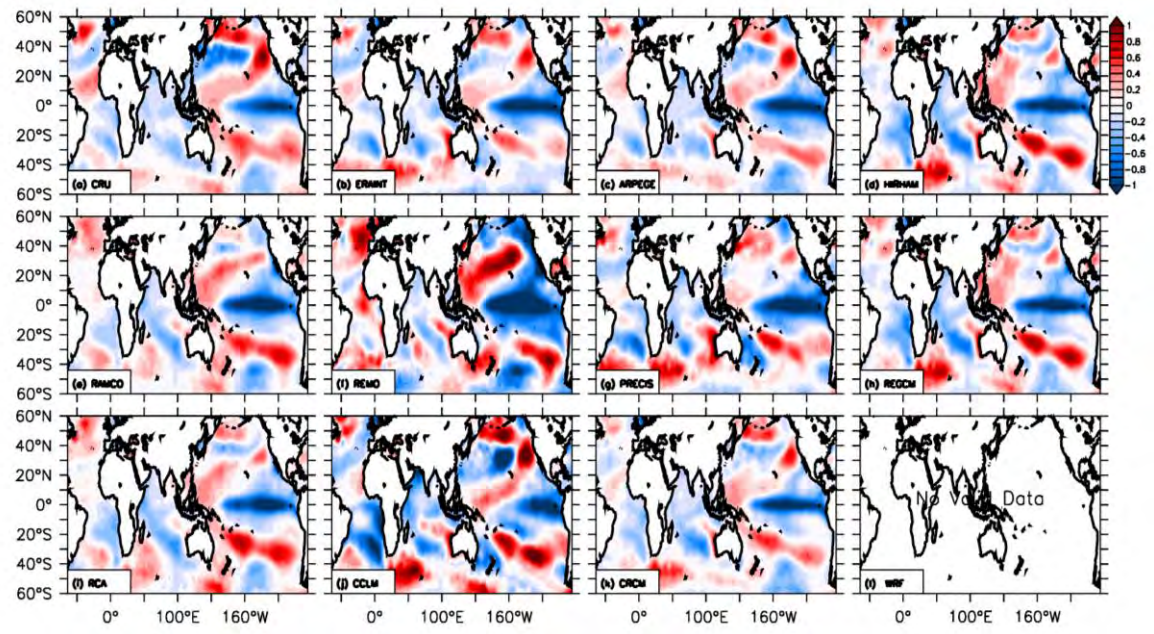

Figure 6.10: Composite of sea surface temperature anomalies (˚C) for nodes 12 during austral summer period**.**

The general SST anomalies configuration in pattern 1 is captured by 80% of the RCMs. However, the ARPEGE, RAMCO and RCA seem to best portray the El Niño conditions associated with pattern 1, while the SST feature is weak in the HIRHAM, REGCM and CRCM models. REMO model does not capture drought pattern 1, therefore the model is not able of simulating the El Niño conditions associated with this pattern. The SST feature in the CCLM model is closer to La Niña situation instead of El Niño. Results suggest that the RCMs have difficulties in simulating the correct SST structure in the Indian and Atlantic Oceans. The subtropical dipoles in these two oceans are well defined

in RAMCO, PRECIS and REGCM, whereas in the remaining set of models, the dipole-like structure is fading or even non-existent. There is also a good agreement amongst the 10 RCMs regarding the simulation of the SST anomalies associated with drought patterns. Nine RCMs accurately simulate the la Niña configuration in pattern 12. WRF is the only model not capturing this pattern. Compared to pattern 1, the dipole structures in the Atlantic and Indian Oceans are much better portrayed in pattern 12.

6.4.2 Precipitation

The drought patterns 1 and 12 create two distinct impacts on precipitation over Southern Africa. Drought pattern 1 is associated with below normal rainfall conditions across the entire region, with the exception of the northeast portion of the region, where patches of positive anomalies can be observed (Fig.6.11). This is an expected feature as the El Niño conditions are associated with the weakening of the walker Circulation limb over Southern Africa, hence suppression of rainfall (Mulenga et al., 2003). Furthermore, the negative phase of SIOD is associated with the weakening of the Mascarene high pressure centre in the Indian Ocean, which in turn decreases the onshore moisture flux and consequently increases the likelihood of the dry conditions over Southern Africa (Morioka et al., 2012). As opposed to pattern 1, pattern 12 shows a clear dipole pattern in rains over Southern Africa, with wet conditions dominating south of 20˚S and dry conditions above the same latitude (Fig.6.12). This is also a typical La Niña pattern, which is associated with the strengthening of the Angola low and consequent creation of rain-bearing clouds called Tropical Temperate Troughs (TTT, Harrison 1984; Todd and Washington, 1999; Washington and Todd, 1999; Todd et al., 2004, Fauchereau et al., 2009; Pohl et al., 2009; Manhique et al., 2011, Hart 2012). The positive SIOD is also known to increase the likelihood of above wet conditions over a bulk of Southern Africa. These results are in agreement with previous studies, which suggested that in general El Niño conditions favour dry conditions while the opposite occurs during La Niña events. In general, all the RCMs reproduce the rainfall patterns associated with drought patterns 1 and 12, with exception of REMO and PRECIS, which do not capture patterns 1 and 12, respectively.

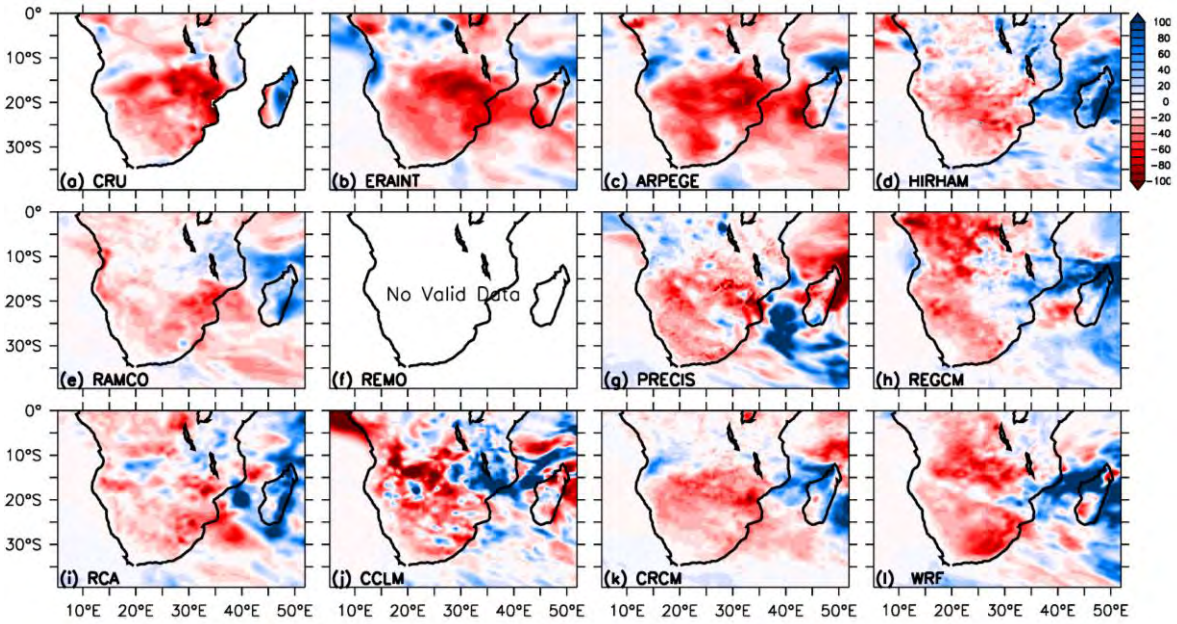

Figure 6.11: Composite of precipitation (mm) for node 1 during austral summer period.

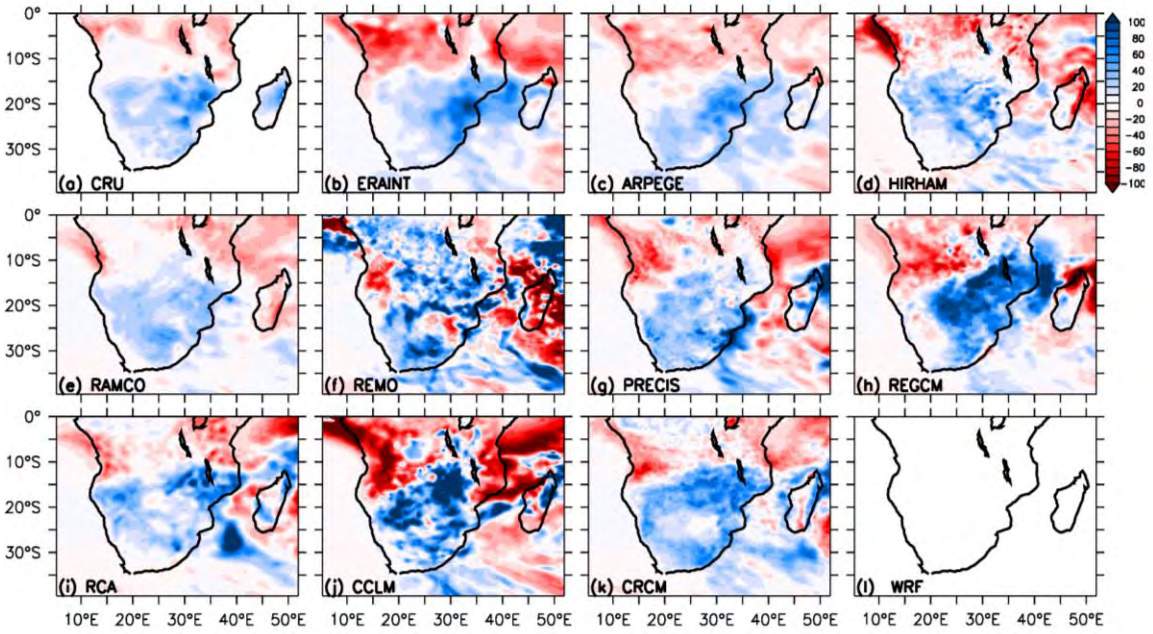

Figure 6.12: Composite of precipitation (mm) for node 12 during austral summer period

6.4.3 Temperature

Both drought patterns 1 and 2 also produce opposed effects on the temperature over the subcontinent. The temperature anomalies associated with drought pattern 1 show a dipole pattern, with warmer temperatures over a large area of Southern Africa and cooler temperatures over the north-eastern side of our study domain (Fig.6.13). This is in agreement with previous studies (e.g., Reason and Jagadheesha, 2005; and Lyon, 2009). El Niño conditions have been linked to above normal temperatures and likelihood of heat waves, mainly due to the high pressure centre anchored over the region. High pressure centre is associated with subsidence, hence suppression of rainfall over the region. Broadly speaking, all the RCM models capture this pattern, with the exception of REMO, which never simulates the pattern and CCLM model where the positive anomalies are confined over Botswana and parts of Namibia. REGCM also shows negative anomalies over Zimbabwe, western Mozambique and portions of Limpopo. On the contrary, temperature anomalies in pattern 12 are negative over a great area of Southern Africa and positive around Tanzania and Democratic Republic of Congo (Fig.6.14). With regards to the RCMs, WRF model doesn't capture this pattern while the remaining set of the CORDEX models simulate the pattern. However, in some cases the anomalies are overestimated. For instance, CCLM shows extremely positive anomalies over Angola and northern Mozambique and negative anomalies elsewhere in our study domain.

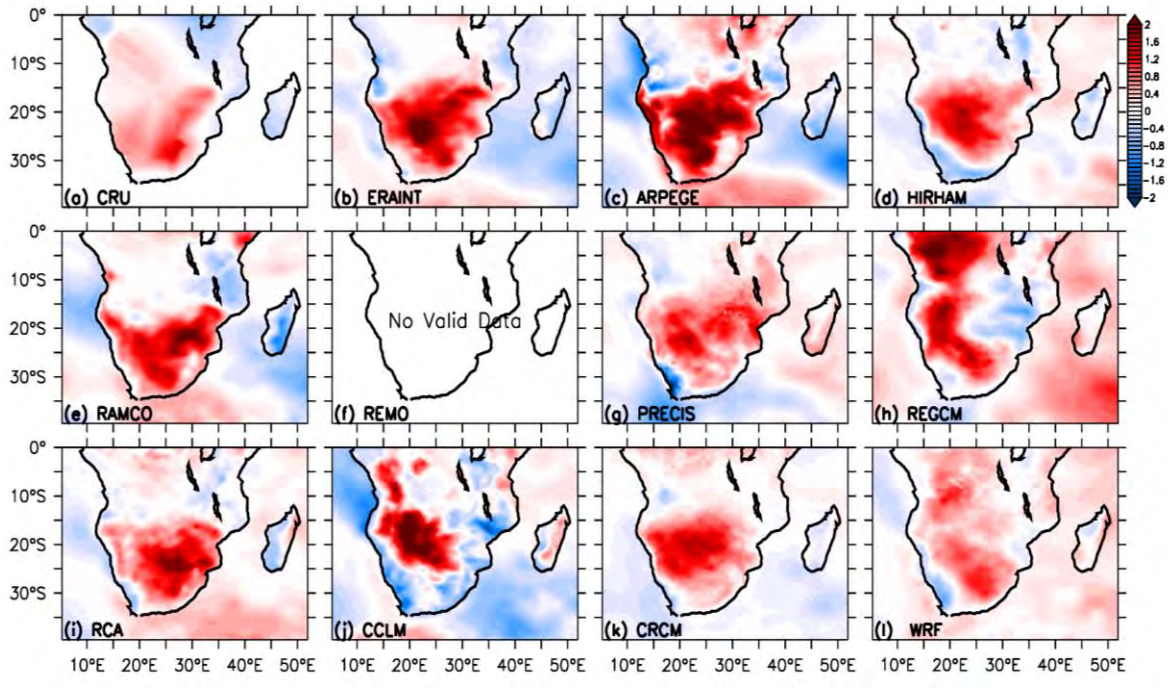

Figure 6.13: Composite of temperature (˚C) for node 1.

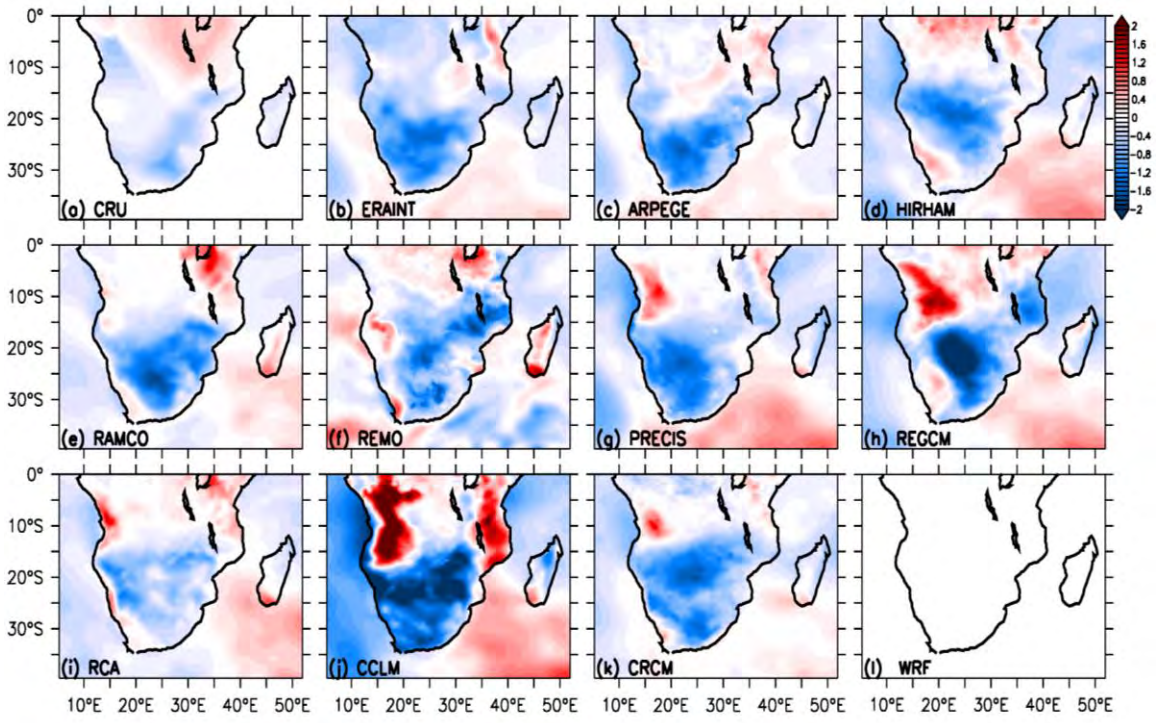

Figure 6.14: Composite of temperature (˚C) for node 12.

6.5 Sensitivity of the simulated drought patterns to different lateral boundary conditions

Our analyses so far in this chapter were based on RCMs driven by ERAINT reanalysis data, which are considered "perfect" lateral boundary conditions. However, for climate change studies RCMs are generally driven by different GCMs. Therefore, it is important to examine how the ability of the RCMs in simulating drought pattern is impacted when subjecting the RCMs to different lateral boundary conditions. It is equally important to investigate how well the RCMs capture the positive trend in decadal frequency of the all-dry drought patterns suggested in chapter 5. This section attempts to answer the above questions.

As in Chapter 4, the RCA model was chosen for the sensitivity tests. The experiment setup is the same as in chapter 4(section 4.4), though the period of simulations is different. In Chapter 4, we used the 1989-2005 period while in this section the 1950 - 2005 period was chosen. We created a new SPEI array composed of the CRU dataset, the RCA outputs forced with 7 different GCMs and the Ensemble mean of the 7 RCA simulations for the 1950-2005 period. This SPEI array was subjected to SOM algorithm and the results are given in figures 6.15 and 6.16.

There is a good resemblance between the drought patterns from the new SPEI array (Fig.6.15) with those generated in chapter 5 using only CRU observation. However, the new drought patterns are swapped. For example, node 9 in this new SOMs arrangement corresponds to node 1 in the SOM arrangement using only CRU data, while node 4 corresponds to node 12. This new orientation of the nodes is normal to SOMs algorithm owing to its random nature. The new drought patterns can also be classified into three groups, namely all-dry patterns, all-wet patterns and the dipole patterns. Similar to drought pattern from previous chapter, the wettest pattern is one of the most common nodes.

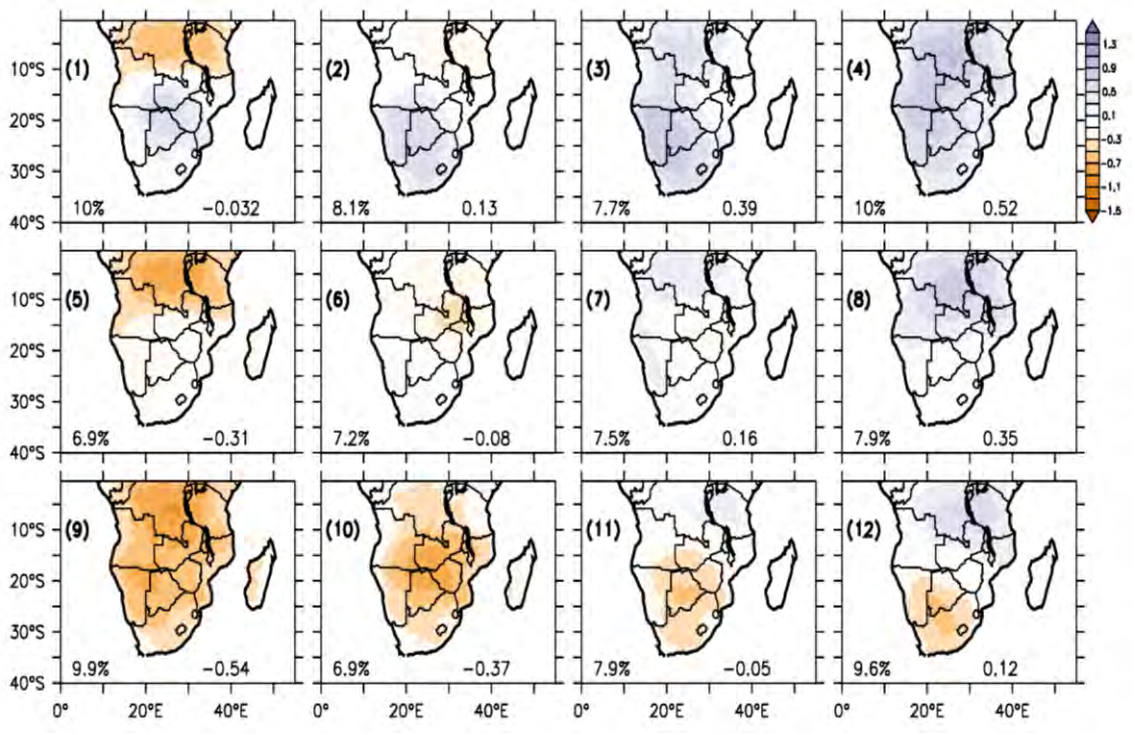

Figure 6.15: The SOM array (3 x 4 nodes) of the seasonal SPEI (3-month scale). Each node represents a drought pattern over Southern Africa in 1950 - 2005. Negative SPEI corresponds to a dry condition while the positive values correspond to a wet condition. In each panel, the node tag is on the upper left corner of the panel, the frequency of occurrence (%) of the node is on the lower left corner, and the mean SPEI (over Southern Africa) is on the lower right corner.

There is also a good agreement between the decadal frequency from the new SPEI values and the one in chapter 5. As in chapter 5, the decadal frequency of the drought patterns in the new SPEI values shows a general shift in the Southern African drought pattern from all-wet pattern in the past (prior to 1980s) to well-dry patterns in recent decades (since 1990s). For example, node (1), which represents the most dry conditions with mean SPEI=-0.54, has its peak during the 1990s, whereas node 4, the wettest node with mean SPEI=0.52, recorded its peak in 1960s and it is in decline since ever. The good performance of the RCA simulation must be related to the inclusion of the observed dataset and Ensemble mean in the SPEI array. The Ensemble mean has the ability of cancelling the errors from individual simulation of the RCA model.

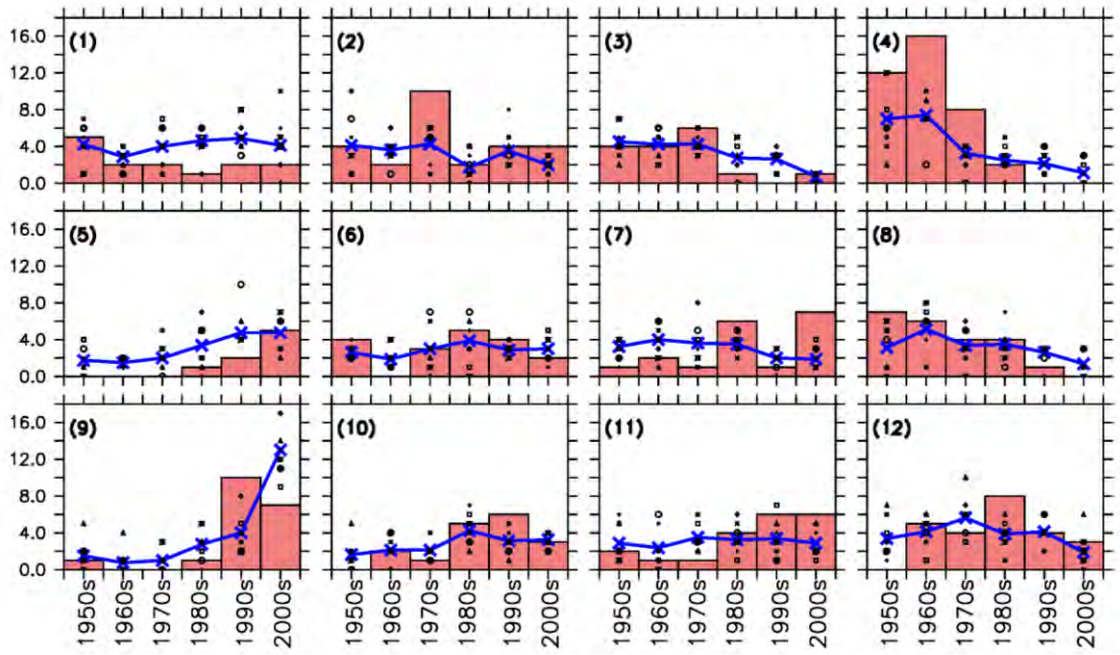

Figure 6.16: The decadal variation of the drought patterns (shown in Fig 6.13).

6.6 Summary

In this chapter, we investigated the ability of 10 Regional Climate Models (RCMs) in simulating drought regimes in Southern Africa. The RCMs were taken from the Coordinated Regional Climate Downscaling Experiment (CORDEX) project and the observation dataset were obtained from Climate Research Unit (CRU) of University of East Anglia. All the RCMs were driven by the European Centre for Medium-Range Weather Forecast interim reanalysis data (ERAINT). We employed the Standardized Precipitation-Evapotranspiration (SPEI) to identify droughts and Self organizing Maps (SOM) algorithm to cluster droughts into different groups. Composite analyses of Sea Surface Temperatures (SST), precipitation and temperature associated with each drought pattern were generated for all RCMs. This investigation revealed that:

- The drought patterns can be roughly clustered into three main groups. In the first group (all dry patterns), the patterns are characterized by negative SPEI values

(dry conditions) over much of Southern Africa. As opposed to patterns in the first group, drought patterns belonging to the second group (all wet patterns) are characterized by positive SPEI values (wet conditions) over a bulk of Southern Africa. Finally, the drought patterns in the third group (dipole patterns) are characterized by a dipole pattern in the SPEI values showing a co-occurrence of wet and dry conditions in Southern Africa.

- CORDEX models show difficulties in simulating the drought patterns over Southern Africa. This is mainly due to the poor phase synchronization between models and observations. However, ARPEGE model outperforms the remaining models in the CORDEX project models. The model has the highest correlation coefficient ($r=0.58$) with the observations and possesses the lowest ($\alpha \approx 0.75$) root-mean-square-error (RMSE). Furthermore, it shows the best phase synchronization ($\eta=46.7$) with the observations.

- At inter-annual scale, dry and wet patterns alternate throughout our study period. Drought pattern 1 was responsible for the 1991/92 severe drought and has the highest probability ($P>30\%$) of persisting for at least one season whenever it is observed. Conversely, patterns 2, 5 and 11 are ephemeral patterns- they hardly ever persist. Only ARPEGE and PRECIS models were able to depict the high persistence of drought pattern 1 and none of the models simulated the transition of drought patterns.

- The two most common drought patterns (1 and 12) are ENSO-related. Pattern 1 is linked to El Niño type 3 conditions while pattern 12 is associated with La Niña type 4 conditions in the Pacific Ocean. All the RCMs capture the SST conditions associated with drought regime 1, with the exception of the REMO which never simulated these conditions. In a similar way, WRF is the only model failing to capture the SST conditions tied to drought pattern 12. Overall, the RCMs seem to perform better under La Niña than El Niño conditions.

7 : Conclusions and Recommendations

7.1 Conclusions

Drought remains a threat to socio-economic activities in Southern Africa. This study uses the Standardized Precipitation-Evapotranspiration Index (SPEI, computed using rainfall and temperature data) to identify 3-month drought over Southern Africa, and compares the observed and simulated drought patterns. The observation data are from the Climate Research Unit (CRU) and University of Delaware (UDEL), while the simulation data are from 10 RCMs (ARPEGE, CCLM, HIRHAM, RACMO, REMO, PRECIS, RegCM3, RCA, WRF, and CRCM) that participated in the Regional Climate Downscaling Experiment (CORDEX) project. We used the 1950-2013 period to identify the major drought patterns in the observations. However, for the evaluation of the RCMs, a common period (1989-2008) was used. Our main focus was on the austral summer (December-January-February) as it represents the core rainy season and any rainfall deficit during this period can cause crop failure. We used the correlation analysis to investigate the link between ENSO and drought patterns in Southern Africa, whereas the Self Organizing Map (SOM) algorithm was used to classify drought patterns into 12 most important patterns.

The results from the study can be summarized as follows:

- There is a strong link between ENSO and droughts (SPEI) over Southern Africa. The link is owing to the influence of ENSO on both rainfall and temperature fields, but the correlation between ENSO and temperature is stronger than the correlation between ENSO and rainfall. Hence, using only rainfall to monitor droughts in Southern Africa may underestimate the influence of ENSO on the droughts;

- Only few CORDEX RCMs simulate the influence of ENSO on Southern African drought as observed. In this regard, the ARPEGE model shows the best

simulation. The differences in the performance may be due to their lateral boundary conditions. The ARPEGE model is variable-resolution model. This stretching capability would allow a better interaction between large and small scale features in the ARPEGE model, and consequently a better representation of the rain producing systems in Southern Africa;

- The RCA-simulated link between ENSO and Southern African droughts is sensitive to the global dataset used as the lateral boundary conditions. In some cases, using RCA to downscale GCM simulations adds value to the simulated link between ENSO and the droughts, but in other cases the downscaling adds no value to the link. The added value of RCA to the simulated link decreases as the capability of the GCM to simulate the link increases. This study suggests that downscaling GCM simulations with RCMs over Southern Africa may improve or depreciate the simulated ENSO-drought link over the region;

- The 12 dominant drought patterns in Southern Africa can be broadly categorized into 3 groups. The first group (all-dry patterns) features a dry condition over the entire Southern Africa, the second (all-wet patterns) shows a wet condition over the whole region, but the third group (dipole patterns) shows both wet and dry conditions over the region;

- Only about 20% of the droughts patterns are induced solely by El Niño Southern Oscillation Index (ENSO), other drought patterns are caused by complex interactions among the atmospheric teleconnections;

- The decadal variability of SPEI drought patterns suggests a general shift in the Southern Africa drought, from "all-wet" condition in 1950s-1970s to "all-dry" condition in 1990s – 2010s, possibly due to the global warming ;

- CORDEX models show difficulties in simulating the drought patterns over Southern Africa. This is mainly due to the poor phase synchronization between models and observations. However, ARPEGE model outperforms the remaining

models in the CORDEX project models. The model has the highest correlation coefficient (r=0.58) with the observations and possesses the lowest (α≈0.75) root-mean-square-error (RMSE). Furthermore, it shows the best phase synchronization (η=46.7) with the observations;

- The two most common drought patterns (1 and 12) are ENSO-related. Pattern 1, which represents dry conditions across Southern Africa, is linked to El Niño type 3 conditions (positive SST anomalies encompassing both central and eastern Pacific Ocean) while pattern 12, which represents wet conditions over the bulk of Southern Africa, is associated with La Niña type 4 conditions in the Pacific Ocean. The connection of droughts in Southern Africa with El Niño Modoki was not evident in this study. All the RCMs capture the SST conditions associated with drought regime 1, with the exception of the REMO which never simulated these conditions. In a similar way, WRF is the only model failing to capture the SST conditions associated with drought pattern 12. Overall, the RCMs seem to perform better under La Niña than El Niño conditions.

7.2 Limitations and Recommendations

As any research project, the present study is far from perfect. We have identified some limitations that need to be addressed and largely improve our knowledge of drought in Southern Africa:

- Our focus in this study was on the meteorological drought at a seasonal timescale. For more robust conclusions it would be important to include other types of droughts, such as agricultural and hydrological droughts. In addition to that, other seasons (e.g., winter, autumn and spring) should also deserve a thorough assessment as we did with the austral summer. Furthermore, more long-term droughts using 12-month and 24-months SPEI should also be considered in order to have a full picture of drought evolution in Southern Africa.
- The period of study for observations (1950-2013) and model (1989-2008) is relatively short. Using datasets with a longer time period (i.e., Paleo-Climate

dataset) may give better information on whether the disappearance of the all-wet drought pattern is due to the global warming, or it is a part of natural climate variability. However, the study has indicated that the Southern Africa drought pattern is generally shifting from all-wet condition to all-dry condition and the shifting can only be recognized with a drought index that include temperature in monitoring the drought.

- The investigation on the sensitivity of regional climate models to lateral boundary conditions was carried out using only one RCM. It would be ideal to include other RCMs for a more comprehensive study. This can now easily be done as more and more data from the CORDEX project becomes available.

We have also identified several avenues for future research:

- Drought prediction is a crucial component of an effective Early Warning System. As we write this thesis, the Climate Experts from the Southern African Development Community (SADC) are gathered in Kinshasa, in Democratic Republic of Congo, preparing the seasonal rainfall forecast for the forthcoming rainy season. This Forum of Climate Experts takes place every year. With this in mind, future research should focus on investigating the predictability of the twelve drought patterns identified in this PhD thesis. This would be of great importance in the water management sector within the SADC member states as the countries have some trans-boundary rivers.

- The climate of Southern Africa shows already a high degree of variability with frequent floods, droughts and tropical cyclones. Under the projected climate change conditions the situation is expect to worsen, therefore, it will be important to understand how the twelve drought patterns identified in the present work will evolve in the future under these projected conditions. This type of study would definitely aid governments in the region in the process of elaboration of their long-term development plans.

- Results from this study show that further research is still needed in order to improve the performance of both global and regional climate models in simulating first rainfall and temperature, which in turn will improve the model's ability in accurately simulating drought characteristics over Southern Africa. We think that the twelve drought patterns identified in this study can be used for climate model development in Southern Africa. For instance, it is important to investigate which parameterization schemes or other model physics reproduce best the drought patterns.

8 References

Abiodun BJ, Prusa JM and Gutowski WJ (2008): Implementation of a nonhydrostatic, adaptive-grid dynamic core in CAM3. Part I: comparison of dynamics cores in aqua-planet simulations, *Clim. Dyn.* **31**, 7-8, 795-810, DOI: 10.1007/s00382-008-0381-y.

Abiodun BJ, Gutowski WJ, Abatan AA and Prusa JM (2011): CAM-EULAG: A Non-Hydrostatic Atmospheric Climate Model with Grid Stretching. Acta Geophysica. vol. 59, no. 6, 1158-1167. DOI: 10.2478/s11600-011-0032-2

Abiodun BJ, Lawal KA, Salami TA and Abatan AA (2012): Potential influences of global warming on future climate and extreme events in Nigeria. Reg. Environ. Change. 13:477-491.

Abiodun BJ, Lawal, KA, Salami, AT, and Abatan, AA (2013): Potential influences of global warming on future climate and extreme events in Nigeria. Regional Environmental Change, 13(3), 477-491.

Abiodun BJ, Abba Omar S, Lennard C and Jack C (2015): Using regional climate models to simulate extreme rainfall events in the Western Cape, South Africa. *Int. J. Climatol.*DOI: 10.1002/joc.4376

Abramowitz M and Stegun IA (1965): Handbook of Mathematical Functions, with Formulas, Graphs, and Mathematical Tables. Dover Publications: New York, U.S.; 1046.

Andreadis KM, Clark EA, Wood AM, Hamlet AF and Letternmaier DP (2005): Twentieth-Century Drought in the Conterminous United States. J. Hydrometeorology, 6,985-1001

Agarwal P and Skupin A (2008): Self-Organising Maps: Applications in Geographic information Science, John Wiley & Sons, Ltd, England

Aggarwal CC and Reddy CK (2014): Data clustering: Algorithms and Applications. Chapman & Hall. 648pp

Ahmad MI, Sinclair CD and Werrity (1988): Log-logistic flood frequency analysis. Journal of Hydrology 98,205-224.

Alley WM (1984): The Palmer Drought Severity Index: Limitations and assumptions. Journal of Climate and Applied Meteorology 23:1100–1109.

Andrews ED, Antweiler RC, Neiman PJ, Ralph FM (2004): Influence of ENSO on flood frequency along the California Coast. J. Climate, **17**: 337-348.

Anyamba A, Tucker CJ, Mahoney R (2002) From El Niño to La Niña: Vegetation Response Patterns over East and Southern Africa during the 1997–2000 Period. Journal of Climate, **15**, 3096-3103.

Araujo JA, Abiodun BJ and Crespo O (2014) Impacts of drought on grape yields in Western Cape, South Africa. Theor Appl Climatol DOI 10.1007/s00704-014-1336-3

Ash KD and Mtyas CJ (2012): The influences of ENSO and the Subtropical Indian Ocean Dipole on the tropical cyclone trajectories in the southwestern Indian Ocean. Int.J.Climatol, 32:41-56.

Ashok K, Behera SK, Rao SA, Weng H, Yamagata T (2007) El Niño Modoki and its possible teleconnection. J Geophys Res 112 (C11): C11, 007. doi:10.1029

Ashok K and Yamagata T (2009): The El Niño with a difference. Nature,vol 481

Barry RG and Chorley RJ (2003): Atmosphere, Weather and Climate.8th edn. Routledge.

Begueria S, Vicente-Serrano SM, Reigb F and Latorre B (2013): Standardized precipitation evapotranspiration index (SPEI) revisited: parameter fitting, evapotranspiration models, tools, datasets and drought monitoring. Int. J. Climatol. DOI: 10.1002/joc.3887

Behera SK, P. S. Salvekar, and T. Yamagata, 2000: Simulation of interannual SST variability in the tropical Indian Ocean. J. Climate, 13, 3487–3499.

Behera SK, Krishnan R and Yamagata T (1999): Unusual ocean–atmosphere conditions in the tropical Indian Ocean during 1994. Geophys. Res. Lett., 26, 3001–3004, doi: 10.1029/1999GL010434.

Behera, S. K., and T. Yamagata, 2001: Subtropical SST dipole events in the southern Indian Ocean. Geophys. Res. Lett., 28, 327–330, doi:10.1029/2000GL011451.

Benages JRC (2014): Drought variability and change across the Iberian Peninsula. PhD Thesis. Universitat Rovira I Virgili.

Benestad R E (2008): Empirical-Statistical Downscaling. Singapore: World Scientific Publishing Co. Pte.Ltd.

Benson C and Clay E (1998): The impact of Drought on Sub-Saharan African Economies. A preliminary Examination. World Bank Technical Paper No.401.

Bezeau P, Sharp M and Gascon G (2014): Variability in summer anticyclonic circulation over the Canadian Artic Archipelago and west Greenland in the late 20th/early 21st centuries and its effect on glacier mass balance. Int. J. Climatol.DOI: 10.1002/joc.4000

Blamey R, Reason CJC (2007): Relationships between Antarctic sea-ice and South African winter rainfall. *Climate Research* 33: 183–193.

Boterill LC and Cockfield G (2013): Drought, Risk Management, and Policy Making under Uncertainty. CRC Press.

Boken VJ, Cracknell A, Heathcote R (2005): Monitoring and predicting Agricultural Drought: A Global Study. Oxford University Press, 495pp

Boulard D, Pohl B, Cretat B, Vigaud N, Pham-Xuan T (2013): Downscaling large-scale climate variability using a regional climate model: the case of ENSO over Southern Africa. Clim Dyn. 40, pp 1141-1168.

Bridgman HA and Oliver JE (2006): The Global Climate System: Patterns, Processes, and Teleconnections. Cambridge University Press, 359pp

Brown JR, Jako C, Hayenes JM (2010): An Evaluation of Rainfall Frequency and Intensity over the Australian Region in a Global Climate Model. Journal of Climate, 23: 6504-6525

Burke EJ, Brown SJ and Christidis N (2006): Modeling the Recent Evolution of Global Drought and Projections for the Twenty-First Century with the Hadley Centre Climate Model. J. of Hydromet. 7, 1113:1125

Calzi DL (2013): Dams, Drought and Energy-Water Interdependencies.178pp, Nova Publishers. New York.

Calliham, D. M., Eriksen, J. H., & Herrick, A. B. (1994) Famine averted: The United States government response to the 1991/92 Southern Africa drought. Evaluation Synthesis Report. Washington: Management Systems International.

Calow RC, MacDonald AM, Nicol AL and Robins NS (2010): Ground Water Security and Drought in Africa: Linking Availability, Access, and Demand. GROUND WATER, Vol. 48:246:256

Camberlin P, Janicot S, Poccard I (2001): Seasonality and Atmospheric dynamics of the teleconnection between African rainfall and Tropical Sea-Surface Temperature: Atlantic vs. ENSO. *Int. J. Climatol*. **21**: 973–1005.

Cassano JJ, Lynch A and Uotila P (2007): Predicted changes in synoptic forcing of net precipitation in large Arctic River basins during the 21st century. Journal of Geophysical Research-Biogeosciences **112**:G04S49; DOI: 10.1029/2006JG000332.

Caviedes C (2001): El Niño in History: Storming through the ages. University Press of Florida. 296pp

Cavos T (1999): Large-Scale Circulation Anomalies Conducive to Extreme Precipitation Events and Derivation of Daily Rainfall in Northeastern Mexico and Southeastern Texas. Journal of Climate, **12**, 1506-1523.

Chambers D, Tapley B, and Stewart R (1999): Anomalous warming in the Indian Ocean coincident with El Niño. J. Geophys. Res., 104, 3035–3047, doi: 10.1029/1998JC900085.

Codron F (2005): Realation between annular modes and the mean state: Southern Hemisphere summer. J. Climate,18,320-330.

Coiffier J (2011): Fundamentals of Numerical Weather Prediction. Cambridge University Press, 363pp

Compo GP, et al.. (2011): The Twentieth Century Reanalysis Project, Q. J. R. Meteorol. Soc., 137(654), 1–28, doi:10.1002/qj.776.

Cook KH (2000): The South Indian Convergence Zone and interannual rainfall variability over Southern Africa. J Clim 13:3789–3804

Cretat J, Pohl B, Richard Y and Drobinski P (2012): Uncertainties in simulating regional climate of Southern Africa: Sensitivity to physical parameterizations using WRF. Clim Dyn, 38:613–634

Cretat J, Pohl B, Smith CC, Vigaud N and Richard Y (2015): An original way to evaluate daily rainfall variability simulated by a regional climate model: the case of South African austral summer rainfall. Int.J.Climatol.35:2485-2502.

Dahan A (2010): Putting the Earth System in a numerical box? The evolution from climate modeling toward global change. Studies in History and Philosophy of Modern Physics ,41,282-292

Dai A (2011): Drought under global warming: a review. WIREs Clim. Change 2:45–65.

Dai A (2013): Increasing drought under global warming in observations and models. Nat. Climate Change, 3, 52–58, doi: 10.1038/nclimate1633.

Dee DP, Uppala SM, Simmons AJ, Berrisford P, Poli P, Kobayashi S, Andrae U, Balmaseda MA, Balsamo G, Bauer P, Bechtold P, Beljaars ACM, van de Berg L, Bidlot J, Bormann N, Delsol C, Dragani R, Fuentes M, Geer AJ, Haimberger L, Healy SB, Hersbach H, Holm EV, Isaksen L, Kallberg P, Kohler M, Matricardi M, McNally AP, Monge-Sanz BM, Morcrette J–J, Park B-K, Peubey C, de Rosnay P, Tavolato C, Thepaut J-N, Vitart F (2011): The ERA-Interim reanalysis: configuration and performance of the data assimilation system. Q J R Meteorol Soc **137**:553–597. doi:10.1002/qj.828

Denis B, Laprise R, Caya D and Cote J (2002): Downscaling ability of one-way regional climate models: the Big-Bother Experiment Climate Dynamics (2002) 18: 627–646.

Diallo I, Giorgi F, Sukumaran S, Stordal F and Giuliani G (2014): Evaluation of RegCM4 driven by CAM4 over Southern Africa: mean climatology, interannual variability and daily extremes of
wet season temperature and precipitation. Theor Appl Climatol DOI 10.1007/s00704-014-1260-6

Di Luca A, R de Elia, Laprise R (2013): Potential for small scale added value of RCM's downscaled climate change signal. Clim Dyn **40**, 601–618.

Di Luca A, de Elia R, Laprise R (2012) Potential for added value in precipitation simulated by high-resolution nested regional climate models and observations. Clim Dyn **38**:1229–1247. doi: 10.1007/s00382-011-1068-3.

Dommenget D and Latif M (2002): Acautionary note on the interpretation of EOFs. J. Climate, 15, 216–225, doi: 10.1175/1520-0442

Dommenget D (2007): Evaluating EOF modes against a stochastic null hypothesis. Climate Dyn., 28, 517–531, doi:10.1007/ s00382-006-0195-8.

Dommenget D (2011): An objective analysis of the observed spatial structure of the tropical Indian Ocean SST variability. Climate Dyn., 36, 2129–2145, doi:10.1007/s00382-010-0787-1.

Dosio A, and Panitz H-J (2015): Dynamically downscaling of CMPI5 CGMs over CORDEX-Africa with COSMO-CLM: analysis of the climate change signal and differences with the driving GCMs. Clim Dyn. doi:10.1007/s00382-015-2664-4

Dosio A, Panitz H-J, Schubert-Frisius M and Luethi D (2015): Dynamical downscalingofCMIP5global circulation models over CORDEX-Africawith COSMO-CLM: evaluation over the present climateand analysis of the added value.Clim Dyn 44:2637–2661.doi:10.1007/s00382-014-2262-x

Dube LT and JURY MR (2000) : The nature of climate variability and impacts of drought over KwaZulu/Natal, South Africa. S. Afr. Geograp. J. 82 (2) 44-53.

Dutra E, Di Giuseppe F., Wetterhall F and Pappenberger F (2013): Seasonal forecasts of droughts in African basins using the Standardized Precipitation Index, Hydrol. Earth Syst. Sci., 17, 2359– 2373, doi: 10.5194/hess-17-2359-2013, 2013.

Dutra E., Pozzi W., Wetterhall F., Di Giuseppe F., Magnusson, L., Naumann G., Barbosa P., Vogt J. and Pappenberger, F. (2014): Global meteorological drought – Part 2: Seasonal forecasts, Hydrol.Earth Syst. Sci. Discuss., 11, 919–944, doi: 10.5194/hessd11-919-2014.

ECA (2008): Africa Review Report on Drought and Desertification. Available at: www.uneca.org

Edossa DC, Woyessa YE and Welderufael WA (2014): Analysis of Droughts in the Central Region of South Africa and their Association with SST Anomalies. Hindawi Publishing Corporation International Journal of Atmospheric Sciences. http://dx.doi.org/10.1155/2014/508953

Endris HS, Lennard C, Hewitson B, Dosio A, Nikulin G, Panitz H (2015): Teleconnection responses in multi-GCM driven CORDEX RCMs over Eastern Africa. Clim DynDOI 10.1007/s00382-015-2734-7

Engelbrecht FA, de Rautenbach CJW, McGregor JL, Katzfey JJ (2002): January and July climate simulations over the SADC region using the limited area model DARLAM. Water SA 28:361–373.

Engelbrecht FA, McGregor JL, Engelbrecht CJ (2009): Dynamics of the Conformal-Cubic Atmospheric Model projected climate-change signal over southern Africa. *International Journal of Climatology* **29**:1013–1033.

Engelbrecht, C. J., Engelbrecht, F. A. and Dyson, L. L. (2013): High-resolution model-projected changes in mid-tropospheric closed-lows and extreme rainfall events over southern Africa. Int. J. Climatol., 33: 173–187.

Engelbrecht CJ, Landman WA, Engelbrecht FA and Malherbe J (2015): A synoptic decomposition of rainfall over the Cape south coast of South Africa. Clim Dyn, 44:2589–2607 DOI 10.1007/s00382-014-2230-5

Everitt B, Landau S, Leese M and Stahl D (2011) Cluster Analysis. 5th Edition. John Wiley & Sons, Ltd, United Kingdom.

FAO (2004): Drought impact mitigation and prevention in the Limpopo River basin, Rome. Available at http://www.fao.org/docrep/008/y5744e/y5744e00.htm#Contents. Visited on 30/12/2014.

Fauchereau, N., Trzaska S, Richard Y, Roucou P, and Camberlin P (2003): Sea-surface temperature co-variability in the southern Atlantic and Indian Oceans and its connections with the atmospheric circulation in the Southern Hemisphere. Int. J. Climatol., 23, 663–677, doi:10.1002/joc.905

Fauchereau N, Pohl B, Reason CJC, Rouault M, Richard Y (2009): Recurrent daily OLR patterns in the Southern Africa/Southwest Indian Ocean region, implications for South African rainfall and teleconnections. Clim Dyn 32:575–59.

Favre A, Philippon N, Pohl B, Kalognomou E, Lennard C, Hewitson BC, Nikulin G, Dosio A, Panitz and Cerezo-Mota R (2015): Spatial distribution of precipitation annual cycles over South Africa in 10 CORDEX regional climate model present-day simulations. Clim Dyn DOI 10.1007/s00382-015-2677-z

Finnis J, Cassano J, Hollnad M, Serreze M and Uotila P (2009): Synoptically forced hydroclimatology of major Arctic watersheds in general circulation models; Part 1: the Mackenzie River Basin. Int. J. Climatol. **29**: 1226–1243.DOI: 10.1002/joc.1753

Florenchie P, Lutjeharms JRE, Reason CJC, Masson S and Rouault M (2003): The source of Benguela niños in the South Atlantic Ocean. Geophysical Research Letter **30**: DOI: 10.1029/2003GLO17172.

Florenchie P, Reason CJC, Lutjeharms JRE, Rouault M, Roy C, Masson S. (2004): Evolution of interannual warm and cold events in the Southeast Atlantic Ocean. Journal of Climate **17**: 2318–2334.

Fuchs BA, Svoboda MD,Wihlite AD and Hayes MJ (2014): Drought indices for Drought Risk Assessment in a changing Climate. In Eslamina S (2014): Handbook of Engineering Hydrology: Modeling, Climate Change, and Variability. CRC Press, 634pp.

GAR (2011): Global assessment report on Disaster Risk Reduction: Revealing Risk, Redefining Development. Accessed via www.preventionweb.net/gar

Gibbs WJ and Maher JV (1967): Rainfall deciles as drought indicators. Bureau of Meteorology Bulletin . No. 48, Commonwealth of Australia, Melbourne.

Giorgi F (1990): On the simulation of regional climate using a limited area model nested in a general circulation model. J.Clim.3, 941-963

Giorgi F, Mearns LO (1999): Introduction to special section: Regional climate modelling revisited. *J Geophys Res*, 104:6335–6352.

Glantz MH (2001) Currents of change: Impacts of El Niño and La Niña on Climate and Society. 2nd Edition. Cambridge University Press, Cambridge, UK.

Grimm AM and Reason CJC (2010): Does the South American Monsoon Influence African Rainfall? J. Climate, 24, 1226-1238. DOI: 10.1175/2010JCLI3722.1

Grist J, Nicholson SE and Mpolokang A (1997): On the use of NDVI for estimating rainfall fields in the Kalahari of Botswana. Journal of Arid Environments. 35: 195–214

Guo F, Liu Q, Sun S and Yang J (2015): Three types of Indian Ocean Dipoles. J. Climate,28,30-73-3092

Haensler A, Hagemann S, Jacob D (2011): Dynamical downscaling of ERA40 reanalysis data over Southern Africa: added value in the simulation of seasonal rainfall characteristics. Int J.Climatol. **31**: 2338-2349

Haile AT and Rientjes T (2015): Evaluation of regional climate model simulations of rainfall over the Upper Blue Nile basin. Atmos. Research,161-162.

Hallack-Alegria J, Ramirez-Hernandez J, Watkins Jr DW (2012): ENSO-conditioned rainfall drought frequency analysis in northwest Baja California, Mexico. Int. J. Climatol. **32**: 831–842

Hansingo K and Reason CJC (2009): Modelling the atmospheric response over southern Africa to SST forcing in the southeast tropical Atlantic and southwest subtropical Indian Oceans Int. J. Climatol. 29: 1001–1012

Hart N C G, Reason CJC, and Fauchereau N (2010): Tropical–extratropical interactions over southern Africa: Three cases of heavy summer season rainfall. Mon. Wea. Rev., 138, 2608–
2623.

Harris I, Jones PD, Osborn TJ, Lister DH (2014) Updated high-resolution grids of monthly climatic observations - the CRU TS3.10 Dataset. Int. J. Climatol., 34: 623-642. doi: 10.1002/joc.3711

Harrison M (1984): A generalised classification of southern African summer rain-bearing synoptic systems. J Climatol **4**:547–560.

Hayes M, Svoboda M, Wall N, Widhalm M (2011): The Lincoln declaration on drought indices: Universal meteorological drought index recommended. Bull. Amer. Meteor. Soc., **92:** 485–488.

Heim RR (2002): A review of twentieth-century drought indices used in the United States. Bull. Amer. Meteor. Soc., 83, 1149–1165.

Hermes JC and Reason CJC (2005): Ocean model diagnosis of interannual coevolving SST variability in the south Indian and South Atlantic Oceans. J. Climate, 18, 2864–2882, doi:10.1175/JCLI3422.1.

Hernandez-Diaz L, Laprise R, Sushama S, Martynov A, Winger K Dugas B (2013): Climate Simulation Over CORDEX Africa Domain using the fifth-generation Canadian Regional Climate Model (CRCM5). Clim Dyn, **40**: 1415-1433.

Hewiston BC, Crane RG (1996) Climate downscaling: Techniques and application. Clim Res, 7: 85-95.

Hewitson B.C., and Crane RG, 2002: Self-organizing maps: Applications to synoptic climatology. Climate Res., 22, 13–26.

Hewitson BC, Daron J, Crane RG, Zermoglio MF and Jack C (2014): Interrogating empirical-statistical downscaling. Climatic Change.122:539–554. DOI 10.1007/s10584-013-1021-z

Hoell A, Funk C, Magadzire T, Zinke J, Husak G (2014) El Niño–Southern Oscillation diversity and Southern Africa teleconnections during Austral Summer. Clim Dyn DOI 10.1007/s00382-014-2414-z

Hudson DA, Jones RG (2002): Regional climate model simulations of present-day and future climates of southern Africa. Hadley Centre Technical Note N 39, 42 pp.

IPCC: Climate Change 2007: The Physical Science Basis. Contribution of Working Group I to the Fourth Assessment, in: Report of the Intergovernmental Panel on Climate Change, edited by:

Solomon, S., Qin, D., Manning, M., Chen, Z., Marquis, M., Averyt, K. B., Tignor, M., and Miller, H. L., Cambridge University Press, Cambridge, UK and New York, NY, USA, 996 pp., 2007.

IPCC, 2013: Climate Change 2013: The Physical Science Basis. Contribution of Working Group I to the Fifth Assessment Report of the Intergovernmental Panel on Climate Change [Stocker, T.F., D. Qin, G.-K. Plattner, M. Tignor, S.K. Allen, J. Boschung, A. Nauels, Y. Xia, V. Bex and P.M. Midgley(eds.)]. Cambridge University Press, Cambridge, United Kingdom and New York, NY, USA, 1535 pp.

Jacobson MZ (2005): Fundamentals of Atmospheric Modeling. Cambridge University Press. 829pp

Jain SK, Agarwal PK and Singh VP (2007): Hydrology of water resources of India. Water Science and Technology library,vol.57, Springer,1277pp

Johnson NC (2013) How many ENSO flavors can we distinguish? J Clim 26(13):4816–4827. doi:10.1175/JCLI-D-12-00649.1

Jolliffe IT (2002): Principal Component Analysis, 2nd edition. Springer,519pp

Jones C, Giorgi F and Asrar G (2011): The coordinated regional downscaling experiment: CORDEX, an international downscaling link to CMIP5. CLIVAR Exch 56:34–40

Jones PG and Thornton PK (2013): Generating downscaled weather data from a suite of climate models for agricultural modelling applications. Agric. Systems, 114:1-5

Joubert AM and Hewitson BC (1997): Simulating present and future climate changes of southern Africa using general circulation models. Prog. Phys. Geogr. **21**: 51–78.

Joubert AM (1994): Simulations of southern African climatic change by early-generation general circulation models, Water SA, 20, 315–322.

Joubert A M. (1995): Simulations of southern African climate by early-generation general circulation models, SA, 91, 85–91.

Joubert AM, Mason SJ (1996): Drought over Southern Africa in a doubled-CO2 Climate. Int. J. Climatol, **16**: 1149-1156.

Joubert AM (1997): Simulations by the Atmospheric Model Intercomparison project of Atmospheric circulation over Southern Africa. Int. J. Climatol, 17, 1129-1154

Joubert AM and Tyson PD (1996): Equilibrium and Coupled GCM simulations of future Southern African Climate. S Afr. J. Science,92,471-484

Joubert AM, Katzfey JJ, McGregor JL, Nguyan KC (1999): Simulating midsummer climate over southern Africa using a nested regional climate model. J. Geophys. Res., **104**: 19015–19025

Jury MR (1996): Regional Teleconnection patterns associated with summer rainfall over South Africa, Namibia, and Zimbabwe. Int. J. Climatol, 16,135-153.

Jury MR (1998): Statistical Analysis and Prediction of KwaZulu-Natal Climate. Theor. Appl. Climatol. 60, 1-10

Jury MR, Mulenga HM and Mason SJ (1999): Exploratory Long-Range Models to Estimate Summer Climate Variability over Southern Africa. J. Climate, 12, 1892-1899

Jury MR and Mwafulirwa ND (2002): Climate variability in Malawi, part 1: Dry summers, statistical associations and predictability. Int. J. Climatol. 22: 1289–1302.

Kalnay E (2003): Atmospheric modeling, data assimilation and predictability. Cambridge University Press. 369pp

Kalognomou E, Lennard C, Shongwe M, Pinto I, Favre A, Kent M, Hewitson B, Dosio A, Nikulin G, Panitz H, Büchner M (2013): A diagnostic evaluation of precipitation in CORDEX models over southern Africa. J. Climate, **26**:9477-9506. doi:10.1175/JCLI-D-12-00703.1

Kao HY, Yu JY (2009) Contrasting eastern-pacific and central-pacific types of ENSO. J Clim 22(3):615–632. doi:10.1175/2008J CLI2309.1

Karl, T. R., and A. J. Koscielny (1982): Drought in the United States: 1895– 1981, J. Climatol., 2, 313– 329, doi:10.1002/joc.3370020402

Kataoka,T., Tozuka T, Masumoto Y and Yamagata T (2012): The Indian Ocean subtropical dipole mode simulated in the CMIP3 models. Climate Dyn., 39, 1385–1399, doi:10.1007s/00382-011-1271-2.

Kgatuke MM, Landman WA, Beraki A, Mbedzi MP (2008): The internal variability of the RegCM3 over South Africa. Int J Clim **28**:505–520.

Kim J, Waliser DE, Matttmann CA, Goodale CE, Hart AF, Zimdars PA, Crichton DJ, Jones, C, Nikulin G, Hewitson B, Jack C, Lennard C, Favre A (2014): Evaluation of the CORDEX-Africa multi-RCM hindcast: systematic model errors. Clim Dyn, 42:1189–1202DOI 10.1007/s00382-013-1751-7

Klutse N.A.B, Sylla MB, Diallo I, Sarr A, Dosio A, Diedhiou A, Kamga A, Lamptey B, Ali A, Gbobaniyi EO, Owusu K, Lennard C, Hewitson B, Nikulin G, Panitz H-J, Bucher M (2014): Daily characteristics of West African summer monsoon precipitation in CORDEX simulations. Theor Appl Climatol. DOI 10.1007/s00704-014-1352-3

Klutse N.A.B, Abiodun BJ, Hewitson BC, Gutowski WJ and Tadross MA (2015): Evaluation of two GCMs in simulating rainfall inter-annual variability over Southern Africa. Theor Appl Climatol. DOI 10.1007/s00704-014-1356-z

Kohonen T, Hynninen J, Kangas J and Laaksonen J (1995) SOM_PAK, The self-organizing map program package version 3.1. Laboratory of Computer and Information Science, Helsinki University of Technology, Finland, 27 pp

Kohonen T., 2001: Self-Organizing Maps. 3rd edition. Springer, 501 pp.

Kruger AC. 1999: The influence of the decadal-scale variability of summer rainfall on the impact of El Niño and La Niña eventsin South Africa. International Journal of Climatology **19**: 59–68.

Kug JS, Jin FF, and An SI (2009): Two types of El Niño events: cold tongue El Niño and warm pool El Niño. J Clim 22(6):1499–1515. doi:10.1 175/2008JCLI2624.1

Kuleshov Y (2012): Southern Hemisphere Tropical Cyclone Climatology. In Modern Climatology by Wang S and Gillies RR. Janeza Trdine.

Lake PS (2011): Drought and Aquatic Ecosystems: Effects and Responses, 402pp. Willey-Blackwell

Landman W and Mason SJ (1999): Change in the association between Indian Ocean Sea-surface temperatures and summer rainfall over South Africa and Namibia. Int. J. Climatol.19:1477:1492

Landman WA, Kgatuke M-J, Mbedzi M, Breaki A and Piesanie A (2009): Performance comparison of some dynamical and empirical downscaling methods for South Africa from a seasonal climate modelling perspective. Int. J. Climatol. **29**: 1535–1549. DOI: 10.1002/joc.1766

Landman, WA and Beraki A (2012): Multi-model forecast skill for mid-summer rainfall over southern Africa. Int. J. Climatol., 32: 303–314.

Landman WA, DeWitt D, Lee D-E, Braki A and Lotter D (2012): Seasonal Rainfall Prediction Skill over South Africa: One-versus Two-Tiered Forecasting Systems. Weather Forec. 27, 489:501.

Laprise R, Hernandez-Diaz L, Tete K, Sushuma L, Separovic L, Martynov A, Winger K Valin M (2012): Climate projection over the CORDEX Africa domain using the fifth-generation Canadian Regional Climate Model (CRCM5). Climate Dynamics 41, 3219-3246

Larkin NK and Harrison DE (2005): On the definition of El Niño and associated seasonal average US weather anomalies. Geophys Res Lett 32(13):L13,705. doi:10.1029/2005GL022738

Legates DR, Willmott CJ (1990): Mean seasonal and spatial variability in gauge-corrected, global precipitation. Int J Climatol 10:111–127.

Liu L, Xie S-P, Zheng X-T, Li T, Du Y, Huang G and Yu W-D (2014): Indian Ocean variability in the CMIP5 multi-model ensemble: the zonal dipole mode. Clim Dyn 43:1715–1730DOI 10.1007/s00382-013-2000-9

Lobo VJAS (2009) Application of Self-organizing Maps to the Maritime Environment. In V.V. Popovich et al., (eds.), Information Fusion and Geographic Information Systems, Lecture Notes in Geoinformation and Cartography. DOI: 10.1007/978-3-642-00304-2_2, Springer-Verlag Berlin Heidelberg 2009.

Lorentz DJ and Hartman DL (2001): Eddy-zonal flow feedback in the Southern Hemisphere.J.Atmos.Sci,58,3312-3327.

Lyon B (2004): The strength of El Niño and the spatial extent of tropical drought. Geophys. Res. Lett., 31, L21204, doi: 10.1029/2004GL020901.

Lyon B (2009): Southern Africa Summer Drought and Heat Waves: Observations and Coupled Model Behavior. *J. Climate*, **22**, 6033–6046.

Lyon B and Barnston AG (2005): ENSO and the spatial extent of interannual precipitation extremes in tropical land areas. J. Climate, **18**: 5095–5109.

Ma M, Ren L, Yuan F, JiangS, Liu Y, Kong H and Gong L (2013): A new standardized Palmer drought index for hydro-meteorological use. Hydrol. Process. DOI: 10.1002/hyp.10063.

Mackellar N, Tadross M, Hewiston B (2010) Synoptic-based evaluation of climatic response to vegetation change over southern Africa. Int. J. Climatol. **30**: 774–789

Macron C, Pohl B, Richard Y and Bessafi M (2014): How do Tropical Temperate Troughs Form and Develop over Southern Africa? J. Climate. DOI: 10.1175/JCLI-D-13-00175.1

Mainguet M (1999): Aridity and Human Development. Springer-Verlag Berlin, 209pp

Makarau A and Jury MR (1997): Predictability of Zimbabwe Summer Rainfall. Int. J. Climatol, 17,1421-1432

Malherbe J, Landman WA and Engelbrecht (2013): The bi-decadal rainfall cycle, Southern Annular Mode and tropical cyclones over the Limpopo River Basin, southern Africa. Clim Dyn
DOI 10.1007/s00382-013-2027-y

Manatsa D, Chingombe W, Matsikwa H, Matarira CH (2008): The superior influence of Darwin Sea level pressure anomalies over ENSO as a simple drought predictor for Southern Africa. Theor. Appl. Climatol. **92**, 1–14

Manatsa D, Mukwada G, Siziba E, Chinyanganya T (2010): Analysis of multidimensional aspects of agricultural droughts in Zimbabwe using the Standardized Precipitation Index (SPI). Theor Appl Climatol (2010) 102:287–305 DOI 10.1007/s00704-010-0262-2.

Manatsa D and Mukwada G (2012): Rainfall Mechanisms for the Dominant Rainfall Mode over Zimbabwe Relative to ENSO and/or IODZM. The Scientific World Journal,Volume 2012, doi:10.1100/2012/92631

Manatsa D, Mushore T and Lenouo A: Improved predictability of droughts over southern Africa using the standardized precipitation evapotranspiration index and ENSO. Theor Appl Climatol DOI 10.1007/s00704-015-1632-6

Manhique A J, Reason CJC, Rydberg L, and Fauchereau N (2011): ENSO and Indian sea surface temperatures with tropical temperate troughs over Mozambique and the southwest Indian Ocean. Int. J. Climatol., 31, 1–13.

Manhique AJ, Reason CJC, Silinto B, Zucula J, Raiva I, Congolo F and Mavume AF (2015): Extreme rainfall and floods in southern Africa in January 2013 and associated circulation patterns. Nat Hazards DOI 10.1007/s11069-015-1616-y

Masih I, Maskey S, Mussa FEF and Trambeur P (2014) : A review of droughts on the African continent: a geospatial and long-term perspective. Hydrol. Earth Syst. Sci., 18, 3635–3649. doi:10.5194/hess-18-3635-2014

Mason SJ and Joubert AM (1997): Simulated Changes in Extreme Rainfallover Suthern Africa. Int. J. Climatol. , 17, 291–301

Mason SJ (2001): El Niño, climate change and Southern African climate. Environmetrics **12**: 327–345.

Maure GA (2013): Effects of Biomass-Burning Aerosol loadings on Southern Africa Climate. PhD Thesis, University of Cape Town (UCT), Cape Town, South Africa

Maxwell JT, Ortegren JT, Knapp PA and Soule PT (2013): Tropical Cyclones and Drought Amelioration in the Gulf and Southeastern Coastal United States. J. Climate, 26, 8440:8452

McEvoy D, Huntington J, Abatzoghou J, Edward L (2012): An Evaluation of Multiscalar Drought Indices in Nevada and Eastern California. Earth Interactions**, 16,** paper 1-18.

McHugh MJ and Rogers JC (2000): North Atlantic Oscillation Influence on Precipitation Variability around the Southeast African Convergence Zone. J. Climate, 14: 3631-3642.

McGregor JL (1997): Regional Climate Modelling. Meteorol.Atmo.Phys. 63,105-117

McKee TB, Doesken NJ, Kleist J (1993): The relationship of drought frequency and duration to time scale. Preprints, Eighth Conf. on Applied Climatology, Anaheim, CA, Amer. Meteor. Soc., 179–184.

Meadows M (2006): Global Change and Southern Africa. Geographical Research. 44(2), 135–145

Meehl GA, Covey C, Delworth T, Latif M, McAvaney B, Mitchell JFB, Stouffer RJ and Taylor KE (2007): The WCRP CMIP3 multimodel dataset: a new era in climate change research. Bull Am. Meteorol Soc 88:1383–1394

Mishra A Singh V, Desai V (2009): Drought characterization: a probabilistic approach. Stoch Environ Res Risk Assess 23, 41–55.

Mishra AK and Singh VP (2010): A review of drought concepts, J. Hydrol., 391(1–2), 202–216, doi: doi:10.1016/j.jhydrol.2010.07.012.

Misra J (1991): Phase synchronization. Info Process Lett 38:101–105

Moeletsi ME and Walker S (2012): Assessment of agricultural drought using a simple water balance model in the Free State Province of South Africa Theor Appl Climatol, 108:425–450. DOI 10.1007/s00704-011-0540-7.

Mounkaila MS, Abiodun BJ and Omotosho JB (2015): Assessing the capability of CORDEX models in simulating onset of rainfall in West Africa. Theor Appl Climatol 119:255–272. DOI 10.1007/s00704-014-1104-4

Morioka Y., Tozuka T, and Yamagata T. (2010): Climate variability in the southern Indian Ocean as revealed by self organizing maps. Climate Dyn., 35, 1059–1072, doi:10.1007/s00382-010-0843-x

Morioka Y, Tozuka T, and Yamagata T (2011): On the growth and decay of the subtropical dipole mode in the South Atlantic. J. Climate, 24, 5538–5554, doi:10.1175/2011JCLI4010.1.

Morioka Y, Tozuka T,Masson S, Terray P, Luo JJ, and Yamagata T (2012): Subtropical dipole modes simulated in a coupled general circulation model. J. Climate, 25, 4029–4047, doi:10.1175/JCLI-D-11-00396.1.

Mulenga HM, Rouault M, Reason CJC (2003): Dry summers over north-eastern South Africa and associated circulation. Clim Res, **25**: 29-41.

Naumann G, Garrote L, Iglesias A and Vogt J (2014): Exploring drought vulnerability in Africa: an indicator based analysis to be used in early warning systems. Hydrol. Earth Syst. Sci., 18, 1591–1604, 2014. doi:10.5194/hess-18-1591-2014

Nel W (2009): Rainfall trends in the Kwazulu-Natal Drakensberg region of South Africa during the twentieth century. Int.J. Climatol.29, 1634:1641.

Neelin JD (2011): Climate Change and Climate Modelling. Cambridge University Press. 300pp

Nicholson SE, Leposo D and Grist J (2001): The Relationship between El Niño and Drought over Botswana. J. Climate, 14,323-335

Nicholson SE (2011): Dryland Climatology. Cambridge University Press. 530pp.

Nikulin G, Jones C, Giorgi F, Asrar G, Büchner M, Cerezo-Mota R,Christensen OB, Déqué M, Fernandez J, Hänsler A, van Meijgaard E, Samuelsson P, Sylla MB, Sushamak L. (2012): Precipitation climatology in an ensemble of CORDEX-Africa regional climate simulations.
Journal of Climate **25**: 6057–6078.

Oettli P, Tozuka T, Izumo T, Engelbrecht FA and Yamagata T (2013):The self-organizing map, a new approach to apprehend the Madden–Julian Oscillation influence on the intraseasonal variability of rainfall in the southern African region. Clim Dyn DOI 10.1007/s00382-013-1985-4

Oliver JE (2005): Encyclopaedia of World Climatology. Springer, 874pp.

Palmer W.C. 1965: Meteorological drought. Research Paper No. 45, U.S. Department of Commerce Weather Bureau, Washington, D.C.

Panitz HJ, Dosio A, Büchner M, Lüthi D, Keuler K (2014): COSMO-CLM (CCLM) climate simulations over CORDEX-Africa domain: analysis of the ERA-Interim driven simulations at 0.44and 0.22 resolution. Clim Dyn 42(11–12):3015–3038

Philippon N, M Rouault, Richard Y and Favre A (2011): The influence of ENSO on winter rainfall in South Africa. Int. J. Climatol. DOI: 10.1002/joc.3403.

Philippon N, Martiny N, Camberlin P, Hoffman M and Gond V (2014): Timing and patterns of ENSO signal in Africa over the last 30 years: insights from Normalized Difference Vegetation Index data. J. Climate. doi:10.1175/JCLI-D-1300365.1,

Pohl B, Fauchereau N, Richard Y, Rouault M and Reason CJC (2009): Interactions between synoptic, intraseasonal and interannual convective variability over Southern Africa. Clim Dyn, 33:1033–1050DOI 10.1007/s00382-008-0485-4

Pohl B, Fauchereau N, Reason CJC and Rouault M (2010): Relationships between the Antarctic Oscillation, the Madden-Julian Oscillation and ENSO, and consequences for rainfall analysis. J.Climate, 23,238:254.

Potop V, Mozny M, Soukup J. (2012): Drought at various time scales in the lowland regions and their impact on vegetable crops in the Czech Republic. *Agric Forest Meteorol* **156**: 121–133.

Quiring S (2001): The detection and prediction of agricultural drought in the Canadian Prairies. Master of Arts dissertation. University of Manitoba.

Ratnam JV, Behera SK, Masumoto Y, Takahashi K and Yamagata T (2011): Anomalous climatic conditions associated with the El Niño Modoki during boreal winter of 2009. Climate Dyn., 39, 227–238, doi:10.1007/s00382-011-1108-z.

Ratnam JV, Behera SK, Mausmoto Y, Takahashi K and Yamagata T (2012): Anomalous climatic conditions associated with the El Niño Modoki during boreal winter of 2009. Clim Dyn. 39:227–238. DOI 10.1007/s00382-011-1108-z

Ratnam JV, Behera SK, Masumoto Y, Takahashi K, Yamagata T (2012): A simple regional coupled model experiment for summer-time climate simulation over southern Africa. Clim Dyn (2012) **39**: 2207–2217.

Ratnam JV, Behera SK, Ratna SB, De CJ, Rautenbach W, Lennard C, Luo J, Masumoto Y, Takahashi K, Yamagata T (2013): Dynamical Downscaling of Austral Summer Climate Forecasts over Southern Africa Using a Regional Coupled Model. J. Climate (2013) **26**: 6015-6032.

Ratnam JV, Behera SK, Masumoto Y and Yamagata T (2014): Remote Effects of El Niño and Modoki Events on the Austral Summer Precipitation of Southern Africa. J.Climate, 27, 3802-3815

Reason CJC, RJ Allan, JA Lindesay and TJ Ansell (2000): Enso and climatic signals across the Indian Ocean basin in the global context: part I, interannual composite patterns. Int. J. Climatol. 20: 1285–1327.

Reason CJC (2001): Subtropical Indian Ocean SST dipole events and southern African rainfall. Geophys. Res. Lett., 28, 2225–2227, doi:10.1029/2000GL012735

Reason CJC, Rouault M, Melice JL and Jagadheesha D (2002): Interannual winter rainfall variability in SW South Africa and large scale ocean-atmosphere interactions. Meteorol. Atmos. Phys., **80**: 19-29.

Reason CJC and D. Jagadheesha (2005): A model investigation of the recent ENSO impacts over Southern Africa. Meteor. Atmos. Phys., **89**: 181–205.

Reason CJC, Hachigonta S and Phaladi RF (2005): Interannual variability in rainy season characteristics over the Limpopo region of Southern Africa. Int J Climatol **25**:1835–1853.

Reason CJC, Rouault M (2005): Links between the Antarctic Oscillation and winter rainfall over western South Africa. Geophysical Research Letters 32: L07705.10.1029/2005GL022419.

Reason CJC, Landman W and Tennant W (2006): Seasonal to decadal prediction of southern African climate and its links with variability of the Atlantic Ocean. Bull. Amer. Meteor.Soc., 87, 941–955.

Rencher AC (2002): Methods of Multivariate Analysis. 2nd Edition. Wiley, 732pp.

Resta M (2012): Graph Mining based SOM: A tool to Analyze Economic Stability. In Applications of Self Organizing Maps, Edited by Magnus Johnsson.

Reynolds, Richard W., Thomas M. Smith, Chunying Liu, Dudley B. Chelton, Kenneth S. Casey, Michael G. Schlax (2007): Daily High-Resolution-Blended Analyses for Sea Surface Temperature. J. Climate, 20, 5473–5496.

Richard Y and Poccard I (1998): A statistical study of NDVI sensitivity to seasonal and interannual rainfall variations in Southern Africa, International Journal of Remote Sensing, 19:15, 2907-2920, DOI:10.1080/014311698214343

Richard Y., Trzaska S, Roucou P, and Rouault M (2000): Modification of the southern African rainfall variability/ENSO relationship since the late 1960s. Climate Dyn., 16, 883–895, doi:10.1007/s003820000086

Richard Y, Fauchereau N, Poccard I, Rouault M, Trzaska S (2001): XXth century droughts in southern Africa spatial and temporal variability, teleconnections with oceanic and atmospheric conditions, Int. J. Climatol. **21**: 873– 885.

Rocha A Simmons I (1997) Interannual variability of Southern African summer rainfall. Part I. Relationship with air-sea interaction processes. Int. J. of Climatol. 17:235-265

Rojas O., Vrieling A., Rembold F. (2011): Assessing drought probability for agricultural areas in Africa with coarse resolution remote sensing imagery. Remote Sensing of Environment 115: 343-352.

Ropelewski CF, Halpert MS (1987): Global and regional scale precipitation and temperature patterns associated with El Niño/Southern Oscillation. *Monthly Weather Review* **115**: 1606–1626.

Rosenzweigh C and Hillel D (2008): Climate Variability and the Global Harvest: Impacts of El Niño and other Oscillations on Agrosystems. Oxford University Press, 274pp

Rossi G, Vega and Bonaccorso B (2007): Methods and Tools for Drought Analysis and Management. Water Science and Technology Library. Vol. 62

Rouault M, Florenchie P, Fauchereau N, Reason CJC (2003): Southeast tropical Atlantic warm events and southern African rainfall. Geophysical Research Letter 30: 8009. DOI: 10.1029/2002GL014840.

Rouault M, Richard Y (2005): Intensity and spatial extent of droughts in southern Africa. Geophys. Research Letters vol. **32**: L15702.

Rouault M, Illig S, Barthlomae C, Reason CJC and Bentamy (2007): A Propagation and origin of warm anomalies in the Angola Benguela upwelling system in 2001. Journal of Marine Systems 68, 473–488

Rummukainen M (2010): State-of-the-art with regional climate models. WIRES Climate Change, 1, 82-96. DOI: 10.1002/wcc.008

Saji NH., Goswami BN., Vinayachandran PN and Yamagata T (1999): A dipole mode in the tropical Indian Ocean. Nature, 401, 360–363.

Samuelsson P., Jones C, Willen U, Ullerstig A, Gollvik S, Hansson U, Jansson C, Kjellstrom E, Nikulin G, Wysr K (2011): The Rossby Centre regional climate model RCA3: Model description and performance. Tellus, 63A, 4–23.

Sandeep S, Stordal F, Sardeshmukh PD and Compo GP (2014): Pacific Walker Circulation variability in coupled and uncoupled climate models. Clim Dyn, 43:103–117DOI 10.1007/s00382-014-2135-3

Santos JP, Portela MM and Polido-Curvo (2011): Regional Frequency Analysis of Drought in Portugal Water Resour Manage (2011) 25:3537–3558. DOI 10.1007/s11269-011-9869-z

Schuenemann, KC and Cassano JJ (2010), Changes in synoptic weather patterns and Greenland precipitation in the20th and 21st centuries: 2. Analysis of 21st century atmospheric changes using self-organizing maps, J. Geophys. Res., 115, D05108, doi: 10.1029/2009JD011706

Semenov MA, Barrow EM (2002). LARS-WG: a stochastic weather generator for use in climate impact studies (Version 3.0). http://www.rothamsted.bbsrc.ac.uk/mas-models/larswg.html. Accessed 14June 2015

Shannon LV, Boyd AJ, Brundrit GB, and Taunton-Clark J. (1986): On the existence of an El Niño-type phenomenon in the Benguela system. Journal of Marine Research **44**: 495–520

Sheffield J and Wood EF (2008): Projected changes in drought occurrence under future global warming from multi-model, multi-scenario, IPCC AR4 simulations. Climate Dyn., **13,** 79–105, doi:10.1007/s00382-007-0340-z.

Sheffield J and Wood EF (2011): Droughts: Past Problems and Future Scenarios. Earthscan

Sheridan SC and Lee CC (2011): The Self-organizing map in synoptic climatological research. Progress. Physic.Geogr,35(1)109-119.

Shongwe ME, Van Oldnborgh GJ, Van den Hurk BJJ, De Boer B, Coelho CA and Van Aalst MK (2009): Projected Changes in Mean and Extreme Precipitation in Africa under Global Warming. Part I: Southern Africa. J. Climate, 22, 3819-3837.

Shongwe ME, Kalognomou E-A, Ntsangwane L and Pinto I (2014): An evaluation of CORDEX regional climate models in simulating precipitation over Southern Africa. Atmos. Sci. Let. DOI: 10.1002/asl2.538

Smith, T.M., R.W. Reynolds, T.C. Peterson, and J. Lawrimore, 2008: Improvements NOAAs Historical Merged Land–Ocean Temp Analysis (1880–2006). *Journal of Climate*, **21**, 2283–2296

Skific, N., Francis JA and Cassano JJ (2009): Attribution of projected changes in atmospheric moisture transport in the Arctic: A self organizingmap perspective, J. Climate, 22, 4135–4153

Storch HV and Zwiers FW (1999): Statistical Analysis in Climate Research. Cambridge University Press, 495pp

Suzuki R., Behera SK, Iizuka S and Yamagata T (2004): Indian Ocean subtropical dipole simulated using a coupled general circulation model. J. Geophys. Res., 109, C09001, doi: 10.1029/2003JC001974

Tadross MA, Jack C, Hewitson BC (2005): On RCM-based projections of change in southern African summer climate. Geophys Res Lett **32**: L23713 doi: 10.1029/2005GL024460.

Tadross MA, Gutowski Jr, Hewitson BC, Jack C, New M (2006): MM5 simulations of interannual change and the diurnal cycle of southern African regional climate. Theor. Appl. Climatol. 86, 63–80 DOI 10.1007/s00704-005-0208-2

Taylor KE (2001): Summarizing multiple aspects of model performance in a single diagram. Journal of Geophysical Research 106:7183–7192

Taylor KE, Stouffer RJ, Meehl GA (2012): An overview of CMIP5 and the experiment design. Bull Am Meteorol Soc **93**:485–498. doi:10.1175/BAMS-D-11-00094.1

Tennant W (1999): Numerical forecasting of monthly climate in Southern Africa. Int. J. Climatol. **19**: 1319–1336.

Tennant W and Hewitson BC (2002): Intra-seasonal rainfall characteristics and their importance to the seasonal prediction problem. Int.J.Climatol.22, 1033-1048.

Tennant W (2003): An assessment of intraseasonal variability from 13-Yr GCM Simulations. Mon. Weather Review **131**: 1975-1991.

Tennant W and Reason CJC (2005): Associations between the Global Energy Cycle and Regional Rainfall in South Africa and Southwest Australia. J. Climate, 18, 3032-30-46

The World Bank (2005): Disaster Hotspots: A Global Risk Analysis. Disaster Risk Management series. No.5

Thompson SA (1999): Water use, management, and planning in the United States. Academic Press, 391pp.

Thompson DW and Wallace JM (2000): Annular modes in extratropical circulation. Part I: Month-to-month variability. J. Climate, 13, 1000-106.

Thornthwaite CW (1948): An approach toward a rational classification of climate. Geogr. Rev., 38:55–94.

Todd M and Washington R (1999): Circulation anomalies associated with tropical-temperate troughs in southern Africa and the southwest Indian Ocean. Climate Dyn., **15:** 937–951.

Todd MC, Washington R and Palmer PI (2004): Water vapour transport associated with tropical-temperate trough systems over southern Africa and the southwest Indian Ocean. J Clim **24**:555–568

Tozuka T, Abiodun BJ and Engelbrecht FA (2013): Impacts of convection schemes on simulating tropical-temperate troughs over southern Africa. Clim Dyn DOI 10.1007/s00382-013-1738-4

Trambauer P, Maskey S, Werner M, Pappenberger F, Van Beek LPH and Uhlenbook S (2014) : Identification and simulation of space–time variability of past hydrological drought events in the Limpopo River basin, southern Africa. Hydrol. Earth Syst. Sci., 18, 2925–2942

Trenberth KE, Shea D (2005) Relationships between precipitation and surface temperature. GEOPHYSICAL RESEARCH LETTERS, VOL. 32, L14703, doi:10.1029/2005GL022760

Trujillo AP and Thurman HV (2011): Essentials of Oceanography. Tenth Edition. Prentice Hall, 576pp.

Tumbo SD, Mpeta E, Tadross M,Kahimba FC, Mbillinyi BP and Mahoo HF (2010): Application of self-organizing maps technique in downscaling GCMs climate change projections for Same, Tanzania. Physics and Chemistry of Earth, 35, 68-617

Ujeneza E and Abiodun (2014): Drought regimes in Southern Africa and how well GCMs simulate them. Clim Dyn DOI 10.1007/s00382-014-2325-z.

Unganai LS, Kogan FN (1998): Drought Monitoring and Corn Yield Estimation in Southern Africa from AVHRR data,REMOTE SENS. ENVIRON.,63,219–232.

Unganai LS and Bandason T (2005): Monitoring Agricultural Drought in Southern Africa. In Monitoring and Predicting Agricultural Drought: A global study. Oxford University Press

Unganai LS Troni J, Manatsa D and Mukarakate D (2013): Tailoring seasonal climate forecasts for climate risk management in rainfed farming systems of southeast Zimbabwe, Climate and development, 5, 139-152, DOI: 10.1080/17565529.2013.801823

UNISDR, 2009: Drought Risk Reduction Framework and Practices: Contributing to the Implementation of the Hyogo Framework for Action. United Nations secretariat of the International Strategy for Disaster Reduction (UNISDR), Geneva, Switzerland, 213 pp.

USAID (2014): A review of downscaling methods for climate change projections.

Usman MT, Reason CJC (2004): Dry spell frequencies and their variability over southern Africa. Clim Res **26**:199–211.

Van Heerden J and Taljaard JJ, 1998: Africa and the surrounding waters. In Meteorology of the Southern Hemisphere, American Meteorological Society, Boston, MA, pp. 141–174.

Van den Dool (2007): Empirical Methods in Short-Term Climate Predictions. Oxford University Press,252pp.

Venegas SA, Mysak LA, and Straub DN, 1997: Atmosphere– ocean coupled variability in the South Atlantic. J. Climate, 10, 2904–2920.

Vicente-Serrano S, Beguería S, López-Moreno J (2010): A Multiscalar Drought Index Sensitive to Global Warming: The Standardized Precipitation Evapotranspiration Index. J. Climate, 23, 1696-1617

Vicente-Serrano S, López-Moreno J., Drumond A, Gimeno L, Nieto R, Morán-Tejeda E, Lorenzo-Lacruz J, Beguería S, Zabalza J. (2011): Effects of warming processes on droughts and water resources in the NW Iberian Peninsula (1930−2006). Clim Res, 48, 203-212.

Vidal JP, Martin E., Franchisteguy L., Habets F., Soubeyroux, JM., Blanchard M. and Baillon M. (2010): Multilevel and multiscale drought reanalysis over France with the Safran-Isba-Modcou hydrometeorological suite, Hydrol. Earth Syst. Sci., 14, 459–478,doi:10.5194/hess-14-459-2010.

Vigaud N, Pohl B, Cretat J (2012): Tropical Temperate interactions over Southern Africa simulated by a regional climate model. Clim Dyn, doi 10.1007/s00382-012-1314-3.

Vitart F, Anderson A and Stockdale T (2003): Seasonal forecasting of tropical cyclone landfall over Mozambique. J Clim 16:3932–3945.

Vogel CH and JH Drummond (1993): Dimensions of Drought: South African Case Studies

Wainer I, Prado LF, KhodriM and Otoo-Bliesner (2014): Reconstruction of the South Atlantic Subtropical Dipole index for the past 12,000 years from surface temperature proxy. Scientific Reports, 4: 5291, DOI: 10.1038/srep05291

Wang, L., Chen W and Zhou W, 2014: Assessment of future drought in Southwest China based on CMIP5 multimodel projections. Adv. Atmos. Sci., 31(5), 1035–1050, doi: 10.1007/s00376-014-3223-3.

Wardlow BD, Anderson MC ad Verdin JP (2012): Remote Sensing of Drought .Innovative Monitoring Approaches, 472pp.CRC Press.

Warner TT (2011): Numerical Weather Prediction. Cambridge University Press,550pp

Washington R and Todd M (1999): Tropical-temperate links in Southern Africa and Southwest Indian Ocean satellite-derived daily rainfall. Int J Climatol **19**:1601–1616.

Washington R and Preston A (2006): Extreme wet years over southern Africa: Role of Indian Ocean sea surface temperatures, J. Geophys. Res., 111, D15104, doi: 10.1029/2005JD006724.

Webster, PJ, Moore AM, Loschnigg JP and Leben RR (1999): Coupled ocean atmosphere dynamics in the Indian Ocean during1997–98, Nature, 401, 356–360.

Wehrens R (2011) Chemometrics with R: Multivariate Data Analysis in the Natural Sciences and Life Sciences. Springer-Verlag Berlin Heidelberg

Wells N., Goddard S, and Hayes MJ (2004): A self-calibrating Palmer Drought Severity Index, J. Clim., 17, 2335–2351, doi: 10.1175/1520-0442.

Weller E, Cai W, Du Y, and Min SK (2014): Differentiating flavors of the Indian Ocean Dipole using dominant modes in tropical Indian Ocean rainfall, Geophys. Res. Lett., 41, 8978–8986, doi: 10.1002/2014GL062459.

Wilby RL and Wigley TML (1997): Downscaling general circulation model output: A review of metjhods and limitations. Prog. Phys. Geogr, 21,530-548.

Wilby RL, Charles SP, Zorita E, Timbal B, Whetton P, Mearns LO (2004): Guidelines for use of Climate Scenarios Developed from Statistical Downscal-ing Methods. IPCC Report. Available at www.ipcc-data.org/guidelines/dgmno2v1092004.pdf

Wilhite DA (2005): Drought and Water Crises: Science, Technology, and Management Issues, 402pp. CRC Press

Williams CJR, Kniveton DR and Layberry R (2010): Assessment of a climate model to reproduce rainfall variability and extremes over Southern Africa. Theor Appl Climatol. 99:9–27. DOI 10.1007/s00704-009-0124-y

Wilks D (2010): Use of stochastic weather generators for precipitation downscaling. WIRES Climate Change, 1,898-907

Wilks DS (2011): Statistical Methods in Atmospheric Sciences 3rd ed. Int. Geophy. Series V.100, 688pp.

WMO 2006: Drought Monitoring and Early Warning: Concepts, progress and future challenges. Report No. 1006.

WMO 2014: Atlas of Mortality and Economic Losses from Weather, Climate and Water Extremes (1970-2012). Report No.1123

Wolter K, Timlin MS (2011): El Niño/Southern Oscillation behaviour since 1871 as diagnosed in an extended multivariate ENSO index (MEI.ext). Int. J. Climatology, **31**:1074-1087.

Yamagata T., Behera SK , Rao SA, Guan Z, Ashok K and Saji HN (2003): Comments on ''Dipoles, temperature gradients, and tropical climate anomalies.'' Bull. Amer. Meteor. Soc., 84, 1418–1422, doi:10.1175/BAMS-84-10-1418.

Yeh S, Kug J, Dweitte B, Kwon M, Kirtman B and Jin F (2009): El Niño in a changing Climate. Nature, 461, doi: 10.1038/nature08316

Yeh SW, Ham YG, and Lee JY (2012): Changes in the tropical pacific SST trend from CMIP3 to CMIP5 and its implication of ENSO. J Clim 25(21):7764–7771. doi:10.1175/JCLI-D-12-00304.1

Zhang Q, Kornich H and Holmgren K (2012): How well do reanalyses represent the southern African precipitation? Clim Dyn. DOI 10.1007/s00382-012-1423-z

Zhao T and Dai A (2015): The Magnitude and Causes of Global Drought Changes in the Twenty-First Century under a Low–Moderate Emissions Scenario. J. Climate, 28, 4490-4512, DOI: 10.1175/JCLI-D-14-00363.1

Zhao Y and Nigam S (2015): The Indian Ocean Dipole: A Monopole in SST. J Climate, 28, 3-19. DOI: 10.1175/JCLI-D-14-00047.1

Zhong Z, Wang X, Lu W and Hu Y (2010): Further study on the effect of buffer zone size on regional climate modelling. Clim Dyn, **35**: 1027-1038.